VOLUME 122 NUMBER 2

# THE ASTROPHYSICAL JOURNAL

AN INTERNATIONAL REVIEW OF SPECTROSCOPY AND ASTRONOMICAL PHYSICS

SEPTEMBER 1955

THE HYADES AND COMA BERENICES STAR CLUSTERS *H. L. Johnson and C. F. Knuckles* 209
LUMINOSITY FUNCTION AND SPACE MOTIONS OF G8-K1 STARS DERIVED FROM SPECTROSCOPIC PARALLAXES . . . . . *Ian Halliday* 222
ELECTRON DENSITIES IN THE ORION NEBULA . . . . . *Donald E. Osterbrock* 235
THE PHOTOELECTRIC PHOTOMETRY OF PLANETARY NEBULAE . *William Liller* 240
A STUDY OF RR LYRAE IN THREE COLORS . . . . . *Robert H. Hardie* 256
AXIAL ROTATION AND STELLAR EVOLUTION . . . . . *Allan R. Sandage* 263
STELLAR EVOLUTION AND THE SYNTHESIS OF THE ELEMENTS *W. A. Fowler, G. R. Burbidge, and E. Margaret Burbidge* 271
THE PULSATIONAL STABILITY OF MODELS FOR RED GIANT STARS *John Paul Cox* 286
HYDROMAGNETIC DYNAMO MODELS . . . . . *Eugene N. Parker* 293
HYDROMAGNETIC DISTURBANCES IN A FLUID OF FINITE CONDUCTIVITY *P. H. Roberts* 315
ON THE X- AND Y-FUNCTIONS OF S. CHANDRASEKHAR . . . . *I. W. Busbridge* 327
NOTES
AURORAL RAYS AS ELECTRIC-DISCHARGE PHENOMENA . . . . . *Joseph W. Chamberlain* 349
IS HELIUM A COMPONENT OF AURORAL PARTICLES? . . . . . *C. Y. Fan* 350
ON CERTAIN REGULARITIES IN THE STRUCTURE OF COMPLEX TERM SPECTRA . *David Layzer* 351
ON THE COLORS OF SUBDWARFS . . . . . *M. Schwarzschild, L. Searle, and R. Howard* 353
ON THE DETERMINATION OF THE MASS OF A SPHERICALLY SYMMETRIC CLUSTER *Mogens Rudkjøbing* 357
ANNOUNCEMENT
A MANUAL OF STYLE FOR THE ASTROPHYSICAL JOURNAL . . . . . 358
ERRATA . . . . . 358
ABSTRACTS OF ASTROPHYSICAL JOURNAL: SUPPLEMENT SERIES
STUDIES IN GALACTIC STRUCTURE. II. LUMINOSITY CLASSIFICATION FOR 1270 BLUE GIANT STARS *W. W. Morgan, A. D. Code, and A. E. Whitford* 359
STELLAR SPECTRA IN MILKY WAY REGIONS. III. A REGION IN CEPHEUS-LACERTA *S. W. McCuskey* 359
STELLAR SPECTRA AND COLORS IN A MILKY WAY REGION IN CASSIOPEIA *Alice H. Farnsworth* 360

THE UNIVERSITY OF CHICAGO PRESS
CHICAGO, ILLINOIS, U.S.A.

September 1955 Vol. 122, No. 2

# THE ASTROPHYSICAL JOURNAL

## AN INTERNATIONAL REVIEW OF SPECTROSCOPY AND ASTRONOMICAL PHYSICS

Founded in 1895 by George E. Hale and James E. Keeler

Published in Collaboration with the American Astronomical Society

S. CHANDRASEKHAR
*Managing Editor*

GERARD P. KUIPER
*Associate Editor*

Yerkes Observatory of the University of Chicago

EDITORIAL BOARD

LEO GOLDBERG (1953-59)
The Observatory of the University of Michigan

H. W. BABCOCK (1953-57)
Mount Wilson Observatory of the Carnegie Institution of Washington

MARTIN SCHWARZSCHILD (1954-58)
Princeton University Observatory

G. HERZBERG (1952-56)
National Research Council, Ottawa

C. D. SHANE (1952-55)
Lick Observatory, University of California

---

The Astrophysical Journal is published bimonthly by the University of Chicago at the University of Chicago Press, 5750 Ellis Avenue, Chicago 37, Illinois, during January, March, May, July, September, and November. ¶Two volumes are published per year, one beginning with the January issue and the other beginning with the July issue. On all orders from the United States and its possessions the subscription price is $7.50 per volume or $15.00 per year; the price of single copies is $3.50. ¶On all orders from Canada the subscription price is $8.00 per volume or $16.00 per year; the price of single copies is $3.65. On all orders from all other countries the subscription price is $8.25 per volume or $16.50 per year; the price of single copies is $3.75. (Orders for service of less than a volume will be charged at the single-copy rate.) ¶Subscriptions are payable in advance. Please make all remittances payable to The University of Chicago Press, in United States currency or its equivalent by postal or express money orders or bank drafts. (Exception: members of The American Astronomical Society must send their subscriptions and remittances to the Treasurer of the Society.)

The following is an authorized agent:

For the British Commonwealth, except North America and Australasia: The Cambridge University Press, Bentley House, 200 Euston Road, London, N.W. 1, England. Prices of yearly subscriptions and of single copies may be had on application.

Claims for missing numbers should be made within the month following the regular month of publication. The publishers expect to supply missing numbers free only when losses have been sustained in transit, and when the reserve stock will permit.

Business correspondence should be addressed to The University of Chicago Press, Chicago 37, Illinois.

Communications for the editors and manuscripts should be addressed to: S. Chandrasekhar, Editor of THE ASTROPHYSICAL JOURNAL, Yerkes Observatory, Williams Bay, Wisconsin.

Line drawings and photographs should be made by the author, and all marginal notes such as co-ordinates, wave lengths, etc., should be included in the cuts. It will not be possible to set up such material in type.

One copy of the corrected galley proof should be returned as soon as possible to the editor, Yerkes Observatory, Williams Bay, Wisconsin. Authors should take notice that the manuscript will not be sent to them with the proof.

The cable address is "Observatory, Williamsbay, Wisconsin."

The articles in this journal are indexed in the *International Index to Periodicals*, New York, N.Y.

Applications for permission to quote from this journal should be addressed to The University of Chicago Press, and will be freely granted.

Microfilms of complete journal volumes are available to regular subscribers only and may be obtained at the end of the year. Orders and inquiries should be addressed to University Microfilms, 313 North First Street, Ann Arbor, Michigan.

Notice to subscribers: If you change your address, please notify us and your local postmaster immediately.

Entered as second-class matter, July 31, 1940, at the Post-Office at Chicago, Ill., under the Act of March 3, 1879.
Acceptance for mailing at special rate of postage provided for in United States Postal Act of October 3, 1917, Section 1103, amended February 28, 1925.
Copyright 1955 by the University of Chicago.

[PRINTED IN U.S.A.]

THE ASTROPHYSICAL JOURNAL

AN INTERNATIONAL REVIEW OF SPECTROSCOPY AND ASTRONOMICAL PHYSICS

VOLUME 122 SEPTEMBER 1955 NUMBER 2

# THE HYADES AND COMA BERENICES STAR CLUSTERS*

H. L. JOHNSON AND C. F. KNUCKLES
Lowell Observatory
*Received April 6, 1955*

ABSTRACT

Three-color photoelectric observations, on the $U$, $B$, $V$ system, are given of members of the Hyades and Coma Berenices star clusters. A number of stars which may be subdwarf members of the Hyades cluster are identified. However, if these stars are cluster members, they occur in the outer regions of the cluster. A probably significant difference in the intensity of the ultraviolet radiation of the F- and G-type main-sequence stars in the Coma Berenices and Hyades clusters has been found. The main sequences of the Hyades and Praesepe clusters are nearly identical in shape. The Hyades main sequence agrees well in absolute magnitude with the near-by stars. Comparison of the Hyades-Praesepe main sequence with the Pleiades main sequence reveals a systematic difference in the direction and approximate size predicted by an evolutionary theory based on the generalized Cowling model.

## I. THE HYADES

During the months of December, 1954, and January, February, and March, 1955, three-color observations were made on most of the known members of the Hyades cluster. The observations were made with the same filters and 1P21 photomultiplier that were used for the original definition of the $U$, $B$, $V$ system (Johnson and Morgan 1953), and the observations reported here are on that system. The cluster observations were made in the manner described for Praesepe (Johnson 1952), using the two stars Nos. 71 ($\theta^1$ Tau) and 72 ($\theta^2$ Tau) as cluster standards. Special observations to tie the cluster observations into the fundamental system were made on fourteen different nights; in addition, many observations were made on $\epsilon$ Tau (No. 70) and $\eta$ Tau, for which standard values have been given by Johnson and Harris (1954) and Johnson and Morgan (1953). These observations of $\epsilon$ Tau and $\eta$ Tau provide an additional check of the cluster zero points. The estimated probable errors of the zero points are listed in Table 1*a*. The internal probable errors, relative to the two cluster standard stars, are listed in Table 1*b*. The observations on the cluster stars are listed in Table 2, which is divided into the same four groups as those used by van Bueren (1952) in his Table 2. It is therefore not necessary to list again the data he has compiled for these stars, since direct cross-reference between the two tables can be made.

* This research has been supported in part by the Office of Naval Research under Contract NR 046-744.

The data given in Table 2 are plotted in Figure 1, where the large spots designate the stars listed in Table 2*a* and the first four stars in Table 2*c;* the open circles, those in Table 2*b* and the rest of Table 2*c;* and the small spots, the stars in Table 2*d*. The crosses designate known binaries. The probability of cluster membership for the stars in the three groups may be judged from the following: *large spots:* both radial velocities and proper motions are in excellent agreement with those expected for cluster members; *open circles:* proper motions in excellent agreement with those expected, but no radial velocity available, or membership doubtful because of relatively large deviations from expected values of radial velocity and proper motion; *small spots:* fainter stars whose proper motions indicate cluster membership. Stars Nos. 136, 150, and 164 can be classified as nonmembers on the basis of the photometry.

The line fitting the Hyades main sequence was derived in the following manner: the best smooth curve was drawn by eye through the Hyades main sequence. The values so obtained are listed in Table 3, second column. Next, the same procedure was carried out

TABLE 1*a*

PROBABLE ERRORS (MAG.) OF TIE-IN OF HYADES STANDARDS WITH *U*, *B*, *V* SYSTEM

| *V* | *B*−*V* | *U*−*B* |
|---|---|---|
| ±0.008 | ±0.004 | ±0.008 |

TABLE 1*b*

PROBABLE ERRORS (MAG.) OF HYADES OBSERVATIONS WITH RESPECT TO CLUSTER STANDARDS FOR ONE OBSERVATION

| *V* | *B*−*V* | *U*−*B* | |
|---|---|---|---|
| ±0.006 | ±0.005 | ±0.010 | *V*<9.5 |
| ±0.011 | ±0.017 | ±0.025 | *V*>9.5 |

for Praesepe (Johnson 1952); the values for Praesepe are listed in the third column of Table 3. Praesepe was chosen as a comparison cluster because of the evident similarity of its color-magnitude diagram to that of the Hyades. The differences, Praesepe *minus* Hyades, are given in the fourth column of Table 3. It is evident that the shapes of the two main sequences are very similar and that the mean line drawn in Figure 1 is a very good fit to the Hyades observations, except possibly at the very faint end, where there are only a few stars known to be members of the Hyades cluster.

The relationship between $U-B$ and $B-V$ for the Hyades is shown in Figure 2. In this figure the crosses designate the four yellow giants, and the open circles the seventeen stars that fall considerably below the main sequence of Figure 1. One notes a significant systematic deviation of the "subdwarfs" from the main-sequence stars in the sense that the lower-luminosity stars have stronger ultraviolet. This is the same effect noticed earlier for a few near-by stars (Johnson and Morgan 1953) and clearly evident for the subdwarf HR 4550 (Johnson and Harris 1954). Miss Roman (1954) has also found this ultraviolet "excess" in a few high *Z*-velocity subdwarfs. This luminosity effect also is in the direction that would be expected from the observations in NGC 752 (Johnson 1953), in which a clear correlation between ultraviolet intensity and luminosity was found for stars on and above the main sequence.

The numbers of these "subdwarfs" are listed in Table 4. Four of these stars—Nos. 98, 125, 155, and 156—have accurately measured proper motions and radial velocities in excellent agreement with those to be expected for cluster members. Eight more—Nos. 113, 134, 139, 144, 147, 148, 172, and 188—have accurately measured proper motions (but no radial-velocity measures) that, again, agree well with those to be expected for cluster members. Furthermore, in Figure 1, most of the "subdwarfs" fall on a fairly well-defined sequence that runs approximately parallel with, and shows about the same scatter as, the cluster main sequence.

TABLE 2a

Magnitudes and Colors of Hyades Stars

| Star No. | V | B-V | U-B | n | Star No. | V | B-V | U-B | n |
|---|---|---|---|---|---|---|---|---|---|
| 1 | 7.40 | .566 | .118 | 4 | 62 | 7.38 | .537 | .076 | 3 |
| 2 | 7.78 | .617 | .159 | 4 | 63 | 8.06 | .632 | .169 | 2 |
| 3 | 8.35 | .751 | .325 | 4 | 64 | 8.12 | .657 | .202 | 2 |
| 4 | 8.88 | .848 | .537 | 3 | 65 | 7.42 | .535 | .060 | 3 |
| 5 | 9.36 | .920 | .699 | 4 | 66 | 7.51 | .555 | .052 | 2 |
| 6 | 5.97 | .341 | .001 | 3 | 67 | 5.72 | .271 | .100 | 3 |
| 7 | 8.98 | .896 | .627 | 3 | 68 | 5.90 | .320 | .057 | 3 |
| 8 | 6.37 | .419 | - .004 | 4 | 69 | 8.64 | .746 | .335 | 2 |
| 9 | 8.67 | .708 | .235 | 3 | 70 | 3.52 | 1.011 | .878 | 13 |
| 10 | 7.85 | .589 | .100 | 3 | 71 | 3.85 | .955 | .741 | std |
| 11 +12 | 6.01 | .396 | .024 | 3 | 72 | 3.41 | .179 | .132 | std |
| 13 | 6.62 | .420 | - .010 | 3 | 73 | 7.85 | .609 | .131 | 2 |
| 14 | 5.73 | .355 | - .004 | 3 | 74 | 5.03 | .228 | .120 | 3 |
| 15 | 8.09 | .658 | .204 | 3 | 75 | 6.59 | .531 | .060 | 2 |
| 16 | 7.06 | .419 | .011 | 3 | 76 | 9.20 | .759 | .401 | 2 |
| 17 | 8.46 | .696 | .243 | 3 | 77 | 7.05 | .502 | .041 | 2 |
| 18 | 8.06 | .638 | .167 | 3 | 78 | 6.92 | .453 | .000 | 2 |
| 19 | 7.14 | .512 | .045 | 3 | 79 | 8.96 | .831 | .489 | 2 |
| 20 | 6.32 | .399 | .016 | 2 | 80 | 5.58 | .319 | .099 | 3 |
| 21 | 9.15 | .816 | .467 | 4 | 81 | 7.10 | .470 | .006 | 2 |
| 22 | 8.34 | .771 | .333 | 2 | 82 | 4.78 | .173 | .126 | 3 |
| 23 | 7.54 | .679 | .239 | 2 | 83 | 5.48 | .259 | .097 | 3 |
| 24 | 5.65 | .275 | .076 | 3 | 84 | 5.40 | .262 | .091 | 3 |
| 25 | 9.60 | .987 | .807 | 2 | 85 | 6.51 | .426 | .009 | 3 |
| 26 | 8.63 | .743 | .332 | 2 | 86 | 7.05 | .463 | .001 | 2 |
| 27 | 8.46 | .715 | .305 | 2 | 87 | 8.58 | .743 | .352 | 2 |
| 28 | 3.66 | .993 | .813 | 2 | 88 | 7.78 | .539 | .059 | 3 |
| 29 | 6.88 | .561 | .088 | 2 | 89 | 6.02 | .335 | .037 | 3 |
| 30 | 5.59 | .278 | .083 | 2 | 90 | 6.40 | .413 | - .001 | 2 |
| 31 | 7.47 | .566 | .079 | 2 | 91 | 8.94 | .883 | .545 | 2 |
| 32 | 6.11 | .374 | .026 | 2 | 92 | 8.66 | .741 | .339 | 2 |
| 33 | 5.26 | .223 | .099 | 2 | 93 | 9.40 | .883 | .621 | 2 |
| 34 | 6.17 | .457 | .021 | 2 | 94 | 6.62 | .431 | - .005 | 3 |
| 35 | 6.80 | .436 | - .010 | 4 | 95 | 4.66 | .240 | .087 | 3 |
| 36 | 6.80 | .441 | - .001 | 2 | 96 | 8.51 | .841 | .487 | 2 |
| 37 | 6.61 | .405 | .000 | 2 | 97 | 7.94 | .634 | .146 | 2 |
| 38 | 5.72 | .320 | .102 | 2 | 98 | 9.23 | .448 | - .005 | 2 |
| 39 | 7.86 | .678 | .220 | 2 | 99 | 9.38 | .851 | .597 | 2 |
| 40 | 6.99 | .563 | .089 | 2 | 100 | 6.02 | .381 | .021 | 2 |
| 41 | 3.77 | .977 | .817 | 2 | 101 | 6.65 | .433 | .012 | 2 |
| 42 | 8.86 | .759 | .351 | 2 | 102 | 7.54 | .603 | .111 | 2 |
| 43 | 9.40 | .907 | .609 | 2 | 103 | 5.79 | .307 | .061 | 2 |
| 44 | 7.19 | .450 | .027 | 2 | 104 | 4.27 | .123 | .113 | 2 |
| 45 | 5.64 | .296 | .135 | 2 | 105 | 7.53 | .575 | .095 | 2 |
| 46 | 9.11 | .867 | .541 | 2 | 106 | 7.96 | .669 | .205 | 2 |
| 47 | 4.80 | .158 | .121 | 2 | 107 | 5.39 | .252 | .121 | 2 |
| 48 | 7.14 | .521 | .042 | 5 | 108 | 4.68 | .155 | .115 | 2 |
| 49 | 8.24 | .585 | .124 | 2 | 109 | 9.40 | .817 | .447 | 2 |
| 50 | 7.62 | .601 | .123 | 2 | 110 | 8.86 | .687 | .245 | 2 |
| 51 | 6.97 | .443 | .003 | 2 | 111 | 5.40 | .253 | .081 | 2 |
| 52 | 7.80 | .597 | .133 | 2 | 112 | 5.37 | .187 | .125 | 3 |
| 53 | 5.97 | .367 | .047 | 2 | 113 | 7.26 | .549 | .079 | 2 |
| 54 | 4.22 | .137 | .120 | 4 | 114 | 8.54 | .723 | .307 | 2 |
| 55 | 5.28 | .247 | .095 | 4 | 115 | 9.09 | .843 | .530 | 2 |
| 56 | 4.30 | .049 | .055 | 2 | 116 | 9.01 | .821 | .511 | 2 |
| 57 | 6.46 | .491 | .015 | 2 | 117 | 9.67 | 1.065 | .921 | 2 |
| 58 | 7.53 | .680 | .240 | 2 | 118 | 7.74 | .580 | .111 | 2 |
| 59 | 7.49 | .543 | .077 | 2 | 119 | 7.12 | .559 | .065 | 2 |
| 60 | 4.29 | .268 | .125 | 4 | 120 | 7.34 | .735 | .321 | 2 |
| 61 | 7.38 | .514 | .019 | 3 | 121 | 7.29 | .504 | .028 | 2 |

TABLE 2a cont'd

| Star No. | V | B-V | U-B | n | Star No. | V | B-V | U-B | n |
|---|---|---|---|---|---|---|---|---|---|
| 122 | 6.76 | .541 | .050 | 2 | 127 | 8.89 | .736 | .345 | 2 |
| 123 | 5.10 | .214 | .118 | 2 | 128 | 6.75 | .450 | - .005 | 2 |
| 124 | 6.27 | .497 | .059 | 2 | 129 | 4.64 | .145 | .135 | 2 |
| 125 | 9.31 | .489 | - .044 | 3 | 130 | 5.43 | .242 | .143 | 2 |
| 126 | 6.37 | .291 | .064 | 2 | 131 | 6.01 | .270 | .037 | 2 |
| | | | | | 132 | 8.54 | .665 | .251 | 2 |

TABLE 2b

| | | | | | | | | | |
|---|---|---|---|---|---|---|---|---|---|
| 133 | 9.67 | .611 | .057 | 4 | 143 | 7.90 | .525 | .059 | 2 |
| 134 | 10.04 | .651 | .162 | 3 | 144 | 9.09 | .507 | - .026 | 3 |
| 135 | 8.98 | .886 | .622 | 3 | 145 | 9.33 | .778 | .359 | 2 |
| 136 | 7.42 | 1.108 | .952 | 2 | 146 | 7.24 | .531 | .063 | 2 |
| 137 | 5.89 | .324 | .041 | 2 | 147 | 9.17 | .545 | .053 | 3 |
| 138 | 8.29 | .865 | .501 | 2 | 148 | 8.93 | .605 | .077 | 2 |
| 139 | 9.10 | .650 | .139 | 3 | 149 | 8.50 | .617 | .094 | 3 |
| 140 | 8.94 | .757 | .337 | 2 | 150 | 8.79 | 1.036 | .621 | 2 |
| 141 | 4.48 | .253 | .133 | 2 | 151 | 9.93 | .945 | .703 | 2 |
| 142 | 8.34 | .665 | .205 | 2 | 152 | 9.25 | .941 | .604 | 2 |

TABLE 2c

| Star No. | B.D. | V | B-V | U-B | n | Star No. | B.D. | V | B-V | U-B | n |
|---|---|---|---|---|---|---|---|---|---|---|---|
| 153 | 29° 503 | 8.91 | .859 | .570 | 3 | 163 | -1° 697 | 7.98 | .370 | .028 | 3 |
| 154 | 20° 480 | 5.80 | .409 | .009 | 3 | 164 | 18° 719 | 6.01 | 1.210 | 1.324 | 3 |
| 155 | 24° 846 | 9.48 | .529 | .071 | 2 | 165 | 23° 747 | 8.52 | .615 | .190 | 2 |
| 156 | 29° 936 | 10.38 | .724 | .317 | 2 | 166 | 17° 807 | 9.59 | .515 | .070 | 2 |
| 157 | 25° 373 | 5.79 | .443 | .036 | 3 | 167 | 28° 783 | 8.92 | .478 | .017 | 2 |
| 158 | 11° 456 | 8.03 | .609 | .134 | 3 | 168 | 16° 822 | 5.54 | .220 | .103 | 2 |
| 159 | 18° 514 | 8.74 | .516 | - .005 | 2 | 169 | 9° 1064 | 4.12 | .154 | .081 | 3 |
| 160 | 7° 592 | 5.46 | .363 | - .001 | 3 | | | | | | |
| 161 | 25° 674 | 9.05 | .843 | .527 | 2 | | | | | | |
| 162 | 20° 721 | 7.84 | .705 | .266 | 3 | | | | | | |

TABLE 2d

| | | | | | | | | | | |
|---|---|---|---|---|---|---|---|---|---|---|
| 170 | 23° 571 | 10.21 | 1.185 | 1.045 | 2 | 180 | 16° 609 | 9.10 | .853 | .580 | 2 |
| 171 | 14° 685 | 10.10 | .709 | .246 | 2 | 181 | 15° 634 | 10.32 | 1.167 | 1.079 | 4 |
| 172 | 13° 671 | 10.20 | .635 | .133 | 2 | 182 | 15° 638 | 8.93 | .844 | .487 | 3 |
| 173 | 15° 616 | 10.49 | 1.237 | 1.180 | 3 | 183 | 15° 650 | 9.69 | .910 | .680 | 3 |
| 174 | 17° 715 | 9.99 | 1.058 | .951 | 2 | 185 | 16° 640 | 9.48 | 1.105 | .922 | 2 |
| 175 | 16° 593 | 10.30 | 1.031 | .928 | 3 | 186 | 19° 754 | 9.98 | 1.402 | 1.256 | 3 |
| 176 | 17° 721 | 9.01 | .939 | .659 | 3 | 187 | 13° 783 | 8.97 | .761 | .374 | 2 |
| 177 | 13° 684 | 10.57 | 1.123 | 1.004 | 2 | 188 | Gron. 205 | 11.07 | .805 | .392 | 3 |
| 178 | 13° 685 | 9.00 | .837 | .529 | 2 | 189 | Gron. 215 | 11.13 | 1.368 | 1.242 | 3 |
| 179 | 14° 699 | 9.52 | .934 | .703 | 2 | 190 | Gron. 229 | 10.71 | 1.357 | 1.177 | 3 |
| | | | | | | 191 | Gron. 283 | 11.03 | 1.291 | 1.262 | 4 |

It would seem reasonable, on the basis of the foregoing arguments, to conclude that the existence of subdwarfs in the Hyades has been established. However, as Figure 3 shows clearly, the space distribution of these "subdwarfs" is very different from that of the cluster main-sequence stars: if these stars are cluster members, *they occur only in the outer regions of the cluster.* It is possible, of course, to assume that these "subdwarfs" are not actually cluster members but are, instead, main-sequence objects situated beyond

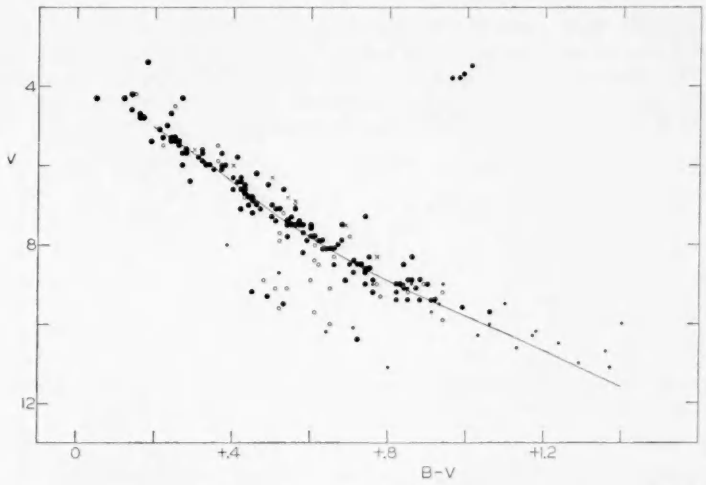


FIG. 1.—The color-magnitude diagram for the Hyades. *Large spots:* Proper motions and radial velocities indicate membership. *Open circles:* Proper motions indicate cluster membership, or proper motions and radial velocities indicate possible membership. *Small spots:* Fainter stars, possible cluster members. *Crosses:* double stars.

TABLE 3

MAIN SEQUENCES OF THE HYADES AND PRAESEPE CLUSTERS

| $B-V$ | $V$ | | Pr − Hy | Mean $M_v$* |
|---|---|---|---|---|
| | Hyades | Praesepe | | |
| +0.2 | 5.1 | 8.2 | +3.1 | 2.14 |
| +0.3 | 5.75 | 8.65 | +2.9 | 2.69 |
| +0.4 | 6.35 | 9.4 | +3.05 | 3.36 |
| +0.5 | 7.15 | 10.1 | +2.95 | 4.12 |
| +0.6 | 7.8 | 10.8 | +3.0 | 4.79 |
| +0.7 | 8.4 | 11.3 | +2.9 | 5.34 |
| +0.8 | 8.95 | 11.8 | +2.85 | 5.86 |
| +0.9 | 9.35 | 12.3 | +2.95 | 6.32 |
| +1.0 | ..... | 12.75 | ..... | 6.76 |
| +1.1 | ..... | 13.1 | ..... | 7.11 |
| +1.2 | ..... | 13.65 | ..... | 7.66 |
| +1.3 | ..... | 14.1 | ..... | 8.11 |
| +1.4 | ..... | 14.6 | ..... | 8.61 |
| Mean | ..... | ..... | +2.96 | ..... |

* Computed by using a distance modulus for the Hyades of 3.03 mag. (van Bueren 1952).

the cluster. This assumption leads, however, to the improbable circumstance in which we find a "cluster" of high-velocity (~110 km/sec) stars at about two and a half times the distance of the Hyades. This comes about because the proper motions of these stars and, in four cases, the radial velocities are in agreement with the motion of the Hyades cluster. The space velocity of the Hyades is about 44 km/sec and the proper motion about 0".1 per year.

## II. THE COMA BERENICES STAR CLUSTER

During the last three years (1953, 1954, 1955) occasional observations have been made, during the course of other work, on the members of the star cluster in Coma Berenices. The observations were made with the same equipment and in the same fashion as for the Hyades. The colors and magnitudes of the Coma Berenices stars are given in Table 5. The fifth column gives the number of observations on each star. Star No. 146

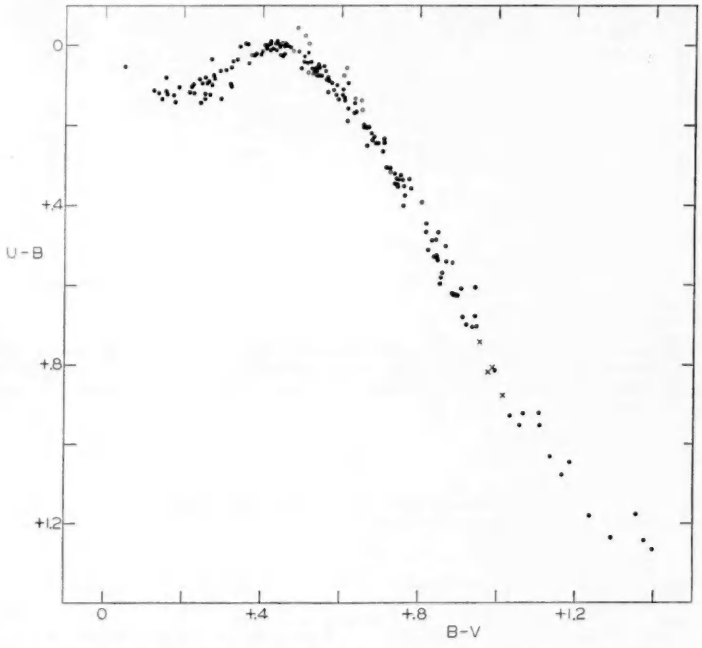


FIG. 2.—$U - B$ versus $B - V$ for the Hyades. *Open circles:* Stars below the main sequence in Fig. 1

TABLE 4

THE "SUBDWARFS" IN THE HYADES

| | | | | | |
|---|---|---|---|---|---|
| 98 | 147 | 166 | 134 | 156 | 172* |
| 125 | 148 | 167 | 139 | 159 | 188* |
| 133 | 155 | 171* | 144 | 163 | |

* No. 171 = Osvalds' (1954) No. 125, "probable member."
No. 172 = Osvalds' (1954) No. 197, "certain member."
No. 188 = Osvalds' (1954) No. 469, "certain member."

was used as the single standard star for the cluster. The probable errors of the zero points are listed in Table 6*a*, and the probable errors with respect to the cluster standard in Table 6*b*.

The color-magnitude diagram, $V$ versus $B-V$, for the Coma cluster is given in Figure 4, which shows no features not reported earlier by Weaver (1952), except for the addition of several faint stars that probably are cluster members.

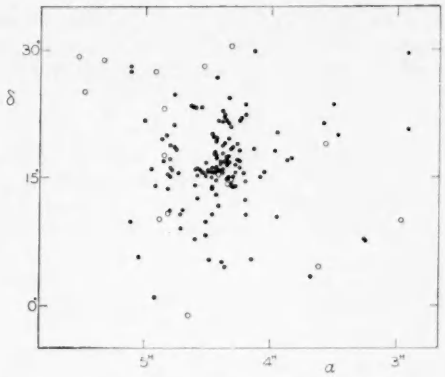


FIG. 3.—The position in the sky of the Hyades stars. *Open circles:* Stars below the main sequence in Fig. 1.

TABLE 5

MAGNITUDES AND COLORS OF STARS IN COMA BERENICES STAR CLUSTER

| Star No.* | $V$ | $B-V$ | $U-B$ | $n$ | Star No.* | $V$ | $B-V$ | $U-B$ | $n$ |
|---|---|---|---|---|---|---|---|---|---|
| 10 | 6.04 | +0.114 | +0.106 | 3 | 107 | 5.18 | +0.076 | +0.106 | 3 |
| 19 | 8.12 | + .397 | − .030 | 3 | 109 | 6.42 | + .266 | + .075 | 3 |
| 36 | 8.13 | + .407 | − .036 | 3 | 111 | 8.17 | + .518 | − .008 | 3 |
| 49 | 7.89 | + .353 | + .058 | 3 | 114 | 8.60 | + .453 | − .044 | 2 |
| 53 | 8.73 | + .525 | + .020 | 2 | 118 | 8.37 | + .449 | − .022 | 2 |
| 58 | 8.83 | + .510 | + .013 | 2 | 125 | 4.95 | + .273 | + .177 | 2 |
| 60 | 6.48 | + .181 | + .088 | 3 | 130 | 5.00 | + .081 | + .128 | 2 |
| 62 | 6.27 | + .167 | + .147 | 2 | 132 | 9.91 | + .679 | + .188 | 2 |
| 65 | 9.02 | + .566 | + .049 | 2 | 139 | 6.76 | + .163 | + .096 | 2 |
| 68 | 6.67 | + .177 | + .094 | 3 | 144 | 6.54 | + .179 | + .109 | 2 |
| 76 | 9.10 | + .547 | + .028 | 3 | 145 | 6.65 | + .207 | + .088 | 2 |
| 82 | 7.42 | + .275 | + .026 | 3 | 146 | 5.29 | − .049 | − .118 | Std |
| 85 | 9.34 | + .589 | + .062 | 2 | 150 | 9.78 | + .776 | + .314 | 2 |
| 86 | 8.55 | + .463 | − .019 | 2 | 160 | 5.46 | + .049 | + .104 | 5 |
| 90 | 8.56 | + .461 | − .044 | 2 | 162 | 8.61 | + .475 | − .044 | 2 |
| 91 | 4.83 | + .497 | + .264 | 3 | 183 | 6.29 | + .108 | + .096 | 2 |
| 92 | 8.61 | + .535 | + .002 | 2 | A3 | 10.81 | + .895 | + .572 | 3 |
| 97 | 9.12 | + .540 | + .011 | 2 | A13 | 10.51 | + .773 | + .384 | 3 |
| 101 | 8.42 | + .443 | − .024 | 2 | A14 | 10.00 | + .793 | + .332 | 3 |
| 102 | 9.36 | + .594 | + .080 | 3 | A21 | 10.38 | +0.834 | +0.422 | 3 |
| 104 | 6.73 | +0.237 | +0.050 | 2 | | | | | |

* Star numbers according to Trumpler (1938).

The relationship between the two color indices, $U-B$ versus $B-V$, is shown in Figure 5. Note that the two yellow-white giant stars in Figure 4 deviate from the main-sequence stars in the direction discussed earlier: the higher the luminosity of the star, the lower the intensity of ultraviolet radiation.

### III. COMPARISONS OF $U-B$ AMONG THE PRAESEPE, HYADES, AND COMA BERENICES CLUSTERS

The relationships between $U-B$ and $B-V$ for the three clusters—the Hyades, the Coma cluster, and Praesepe—are compared in Figure 6. The Hyades and Coma clusters are represented by the solid lines, while Praesepe is represented by the spots. It is evi-

TABLE 6*a*

PROBABLE ERRORS (MAG.) OF TIE-IN OF COMA BERENICES CLUSTER STANDARD WITH *U*, *B*, *V* SYSTEM

| $V$ | $B-V$ | $U-B$ |
|---|---|---|
| ±0.010 | ±0.005 | ±0.010 |

TABLE 6*b*

PROBABLE ERRORS (MAG.) OF COMA BERENICES CLUSTER OBSERVATIONS WITH RESPECT TO CLUSTER STANDARD, FOR ONE OBSERVATION

| $V$ | $B-V$ | $U-B$ | |
|---|---|---|---|
| ±0.006 | ±0.005 | ±0.010 | $V<9.5$ |
| ±0.011 | ±0.017 | ±0.025 | $V>9.5$ |

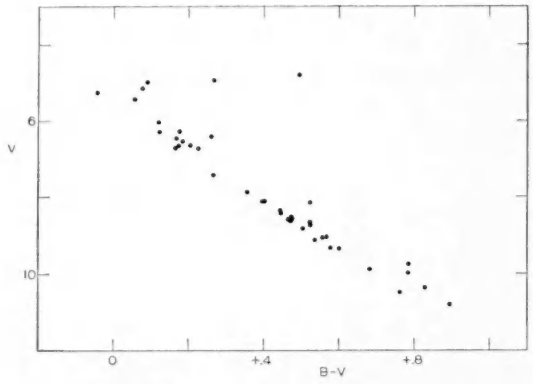


FIG. 4.—The color-magnitude diagram for the star cluster in Coma Berenices

dent that in the region of $B-V$ around +0.4 the Coma cluster stars have stronger ultraviolet radiation by about 0.035 mag. than do the stars of the other two clusters. This small difference is fairly well established (compare the probable errors of the zero points in Tables 1 and 5*a* and 5*b*) and has been checked by special intercluster transfers.

While the deviation of the Coma cluster stars from those of the Hyades is in the same sense as that for the "subdwarfs" in the Hyades, it is not reasonable to suppose that this comparison suggests that the Coma cluster main-sequence stars are subdwarfs, since the spectra of these stars indicate that they are normal main-sequence objects (Weaver 1952). A more reasonable explanation is in terms of Miss Roman's (1950) strong-line and weak-line stars. The Coma cluster stars might be expected to belong to her weak-line class, and the Hyades and Praesepe stars to her strong-line class. We see, therefore,

that, while there seem to be fairly well-defined correlations between $U-B$ and luminosity for the F and G stars in a given cluster, there probably are systematic differences between clusters, caused perhaps by differing chemical composition, that mask much of this luminosity effect. The near-by bright stars provide a heterogeneous sample of stars such as we might find in galactic clusters in general, and among such stars a considerable scatter in $U-B$ is found for F and G main-sequence stars (Johnson and Morgan 1953).

## IV. COMPARISON OF THE HYADES-PRAESEPE MAIN SEQUENCE WITH THAT OF THE PLEIADES

If we fit the Pleiades main sequence to the Hyades-Praesepe sequence in the range of $B-V = +0.5$ to $+0.6$ (the reddest that the Pleiades main sequence has been meas-

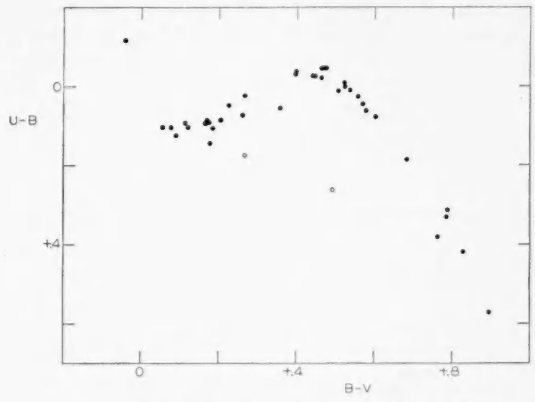


FIG. 5.—$U-B$ versus $B-V$ for the Coma Berenices star cluster. *Open circles:* The two yellow-white giants in Fig. 4.

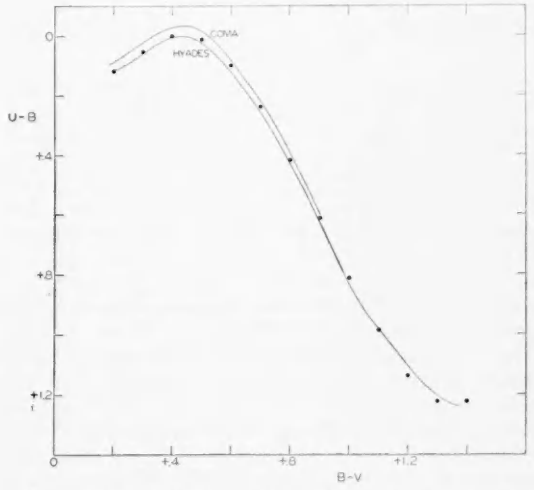


FIG. 6.—$U-B$ versus $B-V$ for three clusters, Coma, Hyades, and Praesepe (*spots*)

ured photoelectrically), we find, as is shown in Figure 7, that the blue end of the Pleiades main sequence falls below the Hyades-Praesepe main sequence. This deviation is in the direction we would expect from certain current theories of stellar evolution (Schönberg and Chandrasekhar 1942; Harrison 1944), since the Pleiades is a younger cluster than either the Hyades or Praesepe. If we assume that the age of a cluster can be computed from the absolute magnitudes and the masses of the stars in the region of the color-magnitude diagram where the cluster sequences deviate strongly from the main sequence

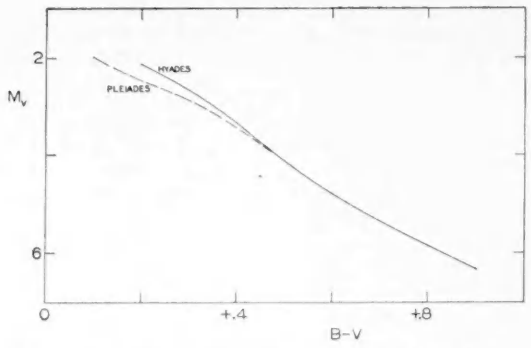


FIG. 7.—Comparison of the main sequences of the Hyades and the Pleiades

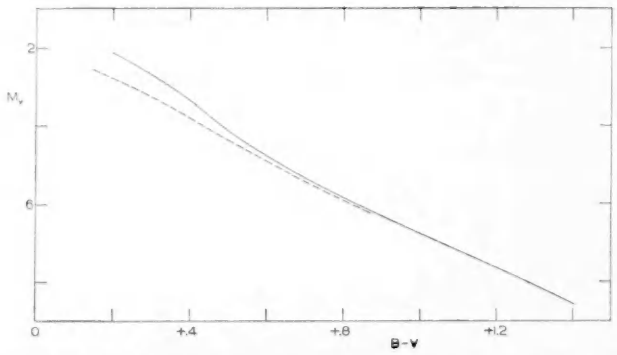


FIG. 8.—The "original" main sequence (*dotted line*) computed from the present Hyades-Praesepe main sequence (*solid line*).

(see eq. [24] of Strömgren 1952), the age of the Pleiades is about $2 \times 10^8$ years and that of the Hyades and Praesepe about $1 \times 10^9$ years.

The theory of the generalized Cowling model, as developed by Harrison (1944), enables us to compute from the observed sequence the "original" position of the Hyades-Praesepe main sequence, assuming that the age of the clusters is $1 \times 10^9$ years. The dotted line in Figure 8 represents this computed main sequence. Compare Figure 8 with Figure 7.

Figure 8 shows that when we fitted the Pleiades main sequence to the Hyades-Praesepe main sequence at $B-V = +0.5$ to $+0.6$, we placed the Pleiades main se-

quence about 0.2 mag. too high. This comes about because the Hyades-Praesepe stars at $B-V = +0.5$ to $+0.6$ have already evolved somewhat. Figure 9 shows a comparison between the main sequence for an age of $2 \times 10^8$ years (computed from the Hyades-Praesepe main sequence) and the observed Pleiades main sequence fitted to the *computed* main sequence at $B-V = +0.6$. The dotted line represents the Pleiades, while the spots represent the values computed from the Hyades-Praesepe main sequence. The agreement between the two is quite good; the computed values even suggest something of the observed shape of the Pleiades main sequence. This comparison of cluster observations with theory indicates that the evolutionary theory initiated by Schönberg and Chandrasekhar (1942) and developed further by Harrison (1944) may, in fact, describe rather closely the actual physical processes that take place in these stars.

The distance modulus for the Pleiades cluster that we obtain by the procedure above is about 5.3 mag. (corrected for interstellar absorption), corresponding to a distance of about 114 parsecs, compared with the previous value of 144 parsecs (Johnson and Morgan 1953). The new value is in closer agreement with the geometrically determined distance (Gratton 1938).

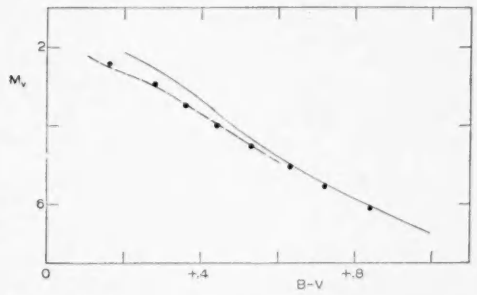


FIG. 9.—Comparison of the Pleiades main sequence (*dotted line*) with values (*spots*) computed from the Hyades-Praesepe main sequence (*solid line*).

## V. COMPARISONS OF THEORETICAL MAIN SEQUENCES OF DIFFERENT AGES WITH NEAR-BY STARS

The computed main sequences for various ages (starting from the observed Hyades-Praesepe main sequence at an age of $1 \times 10^9$ years) are compared in Figure 10 with near-by stars of luminosity class V, for which trigonometric parallaxes having probable errors smaller than 10 per cent have been measured (*spots*) and the mean absolute magnitudes determined from large groups of stars with measured trigonometric parallaxes (*open circles*). The individual stars (*spots*) were selected from Table 3 of Johnson and Morgan (1953); the trigonometric parallaxes for these stars were taken from the Yale *Catalogue of Stellar Parallaxes* (Jenkins 1952). The mean values (*open circles*) were taken from the calibrations given by Morgan and Keenan (Hynek 1951) for stars of luminosity class V, transformed to $V-B$ by means of the tabulated relationship between MK and $B-V$ given by Johnson and Morgan (1953). The open circles represent, therefore, the mean values for groups of stars. The lines labeled *0*, *1*, and *5* are the computed main sequences for 0, 1, and $5 \times 10^9$ years, respectively. (The $1 \times 10^9$-year line is, of course, the observed line for Hyades-Praesepe.)

Note, first, the close agreement of the computed main sequences with the near-by stars, especially the open circles, for $B-V > +0.8$. Remember that the Hyades-Praesepe line was fixed in absolute magnitude by the *geometrical* parallax of the Hyades cluster and that the Praesepe main sequence was used only as a sort of interpolation

formula for the Hyades that, as Figure 1 shows, fits the Hyades observations quite satisfactorily except possibly at the red end ($B-V > +1.2$), where very few Hyades were observed. This close agreement of cluster main sequence with near-by stars ($B-V > +0.8$), obtained by the use of *geometrical parallaxes only*, indicates, since the near-by stars may be assumed to be a heterogeneous mixture of stars of all ages, that the initial main sequence (age = 0) is quite narrow and well represented ($B-V > +0.8$) by our computed main sequence for age 0.

Let us next direct our attention to the bluer stars. Here we find that the lines for age = 0 and $5 \times 10^9$ years bound the region occupied by the near-by stars. This is precisely the result we would expect if the near-by stars were a heterogeneous mixture of stars of all ages from 0 to $5 \times 10^9$ years. We note that the calibration points of Keenan and Morgan (*open circles*) fall above the main sequence for age 0 (and in part of the diagram above the Hyades-Praesepe line), just as we would expect if the stars of luminosity class

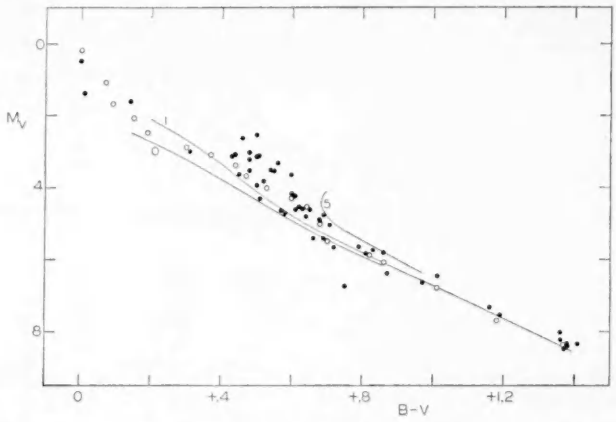


FIG. 10.—Comparison of the theoretical main sequences of age = 0, $1 \times 10^9$, and $5 \times 10^9$ years with near-by stars. *Spots:* Individual near-by stars. *Open circles:* Keenan and Morgan's calibration of luminosity class V.

V were a mixture of stars that had evolved various distances (with an arbitrary upper limit) from the original main sequence.

The later stages of stellar evolution had been discussed theoretically by Sandage and Schwarzschild (1952) and from the standpoint of observation by Johnson (1954).

## VI. CONCLUSION

We have presented three-color photoelectric observations of the Hyades and Coma Berenices star clusters. The Hyades main sequence is very similar to Praesepe's, and a mean line that represents the Hyades main sequence satisfactorily has been derived. The absolute-magnitude calibration for this line has been obtained from the geometrical parallax for the Hyades cluster given by van Bueren (1952).

A number of stars, probably cluster members according to their proper motions and (four stars) radial velocities, that fall about 2 mag. below the main sequence are found in the Hyades. If these stars are cluster members, they occur only in the outer regions of the cluster. It would be of considerable interest to investigate the proper motions of faint stars in the outer regions of Praesepe, to see whether this cluster also has a relatively

large population of subdwarfs at large distances from the cluster center. Four subdwarfs are already known in the Praesepe cluster.

Ultraviolet observations in the Coma Berenices star cluster show that its F- and G-type stars probably radiate about 0.035 mag. more ultraviolet than do similar stars in the Hyades.

A comparison of the Hyades-Praesepe main sequence with the observed Pleiades main sequence shows differences between the clusters that are in the same direction and approximately the amount predicted by the theory of the generalized Cowling model.

A comparison is made of the theoretical main sequences for different ages with near-by stars. All absolute-magnitude calibrations are geometrical, either trigonometric parallaxes (near-by stars) or the cluster parallax of the Hyades. This comparison indicates that the initial main sequence (age 0) is fairly narrow and that the oldest among the near-by stars may be around $5 \times 10^9$ years old. The agreement of theory with observation indicates that the theory of the generalized Cowling model may describe rather closely the actual physical processes taking place in the stars during the earlier stages of their evolution.

## REFERENCES


Bueren, H. G. van. 1952, *B.A.N.*, Vol. **11**, No. 432.
Gratton, L. 1938, *Zs. f. Ap.*, **15**, 48.
Harrison, M. Hall. 1944, *Ap. J.*, **100**, 343.
Hynek, J. A. (ed.), 1951, *Astrophysics* (New York: McGraw-Hill Book Co.).
Jenkins, L. F. 1952, *General Catalogue of Trigonometric Stellar Parallaxes* (New Haven: Yale University Observatory).
Johnson, H. L. 1952, *Ap. J.*, **116**, 640.
———. 1953, *ibid.*, **117**, 356.
———. 1954, *ibid.*, **120**, 325.
Johnson, H. L., and Harris, D. L. 1954, *Ap. J.*, **120**, 196.
Johnson, H. L., and Morgan, W. W. 1953, *Ap. J.*, **117**, 313.
Osvalds, V. V. 1954, *A.N.*, **281**, 193.
Roman, N. G. 1950, *Ap. J.*, **112**, 554.
———. 1954, *A.J.*, **59**, 307.
Sandage, A. R., and Schwarzschild, M. 1952, *Ap. J.*, **116**, 463.
Schönberg, M., and Chandrasekhar, S. 1942, *Ap. J.*, **96**, 161.
Strömgren, B. 1952, *A.J.*, **57**, 65.
Trumpler, R. J. 1938, *Lick Obs. Bull.*, **18**, 167.
Weaver, H. F. 1952, *Ap. J.*, **116**, 612.

# LUMINOSITY FUNCTION AND SPACE MOTIONS OF G8–K1 STARS DERIVED FROM SPECTROSCOPIC PARALLAXES*

IAN HALLIDAY†
David Dunlap Observatory
*Received March 31, 1955; revised May 20, 1955*

ABSTRACT

Visual MK classifications and luminosity measures made with the help of an oscilloscopic microphotometer have been determined for 227 stars in the spectral range G8–K1, from spectrograms with a dispersion of 33 A/mm. An analysis of the luminosities leads to a relative luminosity function which shows a distinct minimum in the region of the subgiants. Spectroscopic parallaxes and space motions are computed for all the stars. For 24 stars the component of the space motion in the galactic plane is 65 km/sec or more.

## INTRODUCTION

Recent theories of stellar evolution and galactic structure have indicated a need for more information on the distribution of stars in luminosity and on their motions in various parts of the Galaxy. A study of the luminosity function and space velocities of a group of stars of late spectral type within about 300 parsecs of the sun is reported here. The spectral range is bounded on the one side by the large increase in the frequency of giant stars at G8 and on the other by the complete disappearance of subgiant stars for types later than K1 (Roman 1952). The G8 and G9 stars are treated in one group, and the K0 and K1 stars in another.

Quite different luminosity functions for stars of this type have been published by Gratton (1933) and by Strömberg, whose results were converted to unit volume by Oort (1932). Gratton's function differs from Strömberg's in that it has a continuous increase in the frequency of stars between giants and dwarfs, while Strömberg's function has a pronounced minimum for the subgiants.

## OBSERVATIONAL MATERIAL

All suitable spectrograms of dispersion 33 A/mm which have been taken with the 74-inch telescope of the David Dunlap Observatory were employed. Most of these spectrograms had been obtained for radial-velocity determinations. Altogether, 453 stars in the range from G8 to K1 were classified visually on the MK system (Johnson and Morgan 1953) for both luminosity class and spectral type. Of these, 82 had been observed because of their known parallaxes, so these stars were not included in the study of the luminosity function.

First, an analysis was made of the visual classifications of the remaining 371 stars, in an attempt to establish whether the observations would agree with the function by Gratton or by Strömberg. This analysis was inconclusive because of the difficulty in determining the range in absolute magnitude covered by luminosity class III–IV. Since the standard spectra are all for integral classes, a tendency exists to put doubtful stars in the integral rather than the half-integral classes. Luminosity class III–IV, then, covers a smaller range in magnitude than does class III or class IV. The numerical evaluation of the range is difficult, and the luminosity function changes appreciably as successive assumptions are tried.

* *Communications from the David Dunlap Observatory*, No. 37.

† Now at the Dominion Observatory, Ottawa, Canada.

To eliminate this uncertainty, a more continuous variation in the luminosity parameter was needed so that the distribution could be treated statistically. At the time this problem arose, the oscilloscopic microphotometer designed and built by W. R. Hossack (1953) was being tested for luminosity-classification work. Because the method showed considerable promise for both speed and accuracy, the stars were reclassified with this microphotometer.

The microphotometer, the technique of measurement, and the method of reduction have been described by Hossack (1953, 1954). The calibration-curves from microphotometer readings to "luminosity number" (a decimal system of luminosity classes) were constructed, by a method described by Trumpler and Weaver (1953). The luminosity numbers may be taken to be on the MK system because a comparison of over one hundred visual classifications (to be published later) with those of Miss Roman (1952) had shown good agreement in both luminosity class and spectral type.

In general, four luminosity criteria were used, and the luminosity numbers derived from the separate calibration-curves were averaged without weights. The criteria used were: 4191/4196, 4202/4196, 4202/4215, 4250/4215. For the supergiants and bright giants, comprising about 2 per cent of the stars, the ratio 4233/4236 was used and given a larger weight than the other ratios. The ratio 4077/4071 was not used because of underexposure of many of the spectrograms in this region. The visual estimates of spectral type were retained.

The microphotometer requires spectrograms of more uniform quality than does the visual method of classification, and suitable spectrograms were available for 227 of the 371 stars which had been classified visually. The results are shown in Table 1.

The first column is the HD number of the star, and the second column is the luminosity number, $L$. The third column is the visual classification of the star for spectral type and luminosity class. The fourth is the apparent visual magnitude. Any magnitude given to a hundredth is the average of the value in a list published by Mrs. Payne-Gaposchkin (1937) and the value in the *Potsdam Generalkatalog* (Müller and Kempf 1907), with a zero-point correction of $-0.28$ mag. applied to the Potsdam values. Magnitudes given to a tenth of a magnitude are from the *Henry Draper Catalogue*.

Visual absolute magnitudes, $M$, are shown in the fifth column. These were determined for each spectral-type and luminosity-number combination from calibrations published by Miss Roman (1952) and by Keenan and Morgan (1951). Miss Roman's values for luminosity numbers 2.0, 2.5, and 3.0 were accepted, and Morgan's values for class 5.0. Linear interpolation was applied between these points, and values for spectral type G9 were interpolated between G8 and K0.

The spectroscopic parallaxes, $\pi_{sp}$, are shown in the sixth column. They were computed from the values of $m$ and $M$ by the relation

$$M = m + 5 + 5 \log \pi_{sp} .$$

No corrections for space absorption have been applied.

Only 22 stars in Table 1 have measured trigonometric parallaxes (Jenkins 1952). These parallaxes, $\pi_{tr}$, are shown in the seventh column. The agreement of the two parallaxes is reasonable, with a tendency for the larger spectroscopic values to exceed the trigonometric values. The spectroscopic parallaxes should have smaller percentage errors for the giants than for the dwarfs on account of the larger sample available for calibration purposes. The trigonometric parallaxes for giants are of little value, since they are generally comparable in size with their probable errors.

The last four columns of Table 1 show the position angle of the total proper motion, $\theta$; the tangential velocity, $T$; the radial velocity, $V$; and the total space velocity, $W$. These are discussed in a later section.

TABLE 1

SPECTRAL CLASSIFICATIONS, PARALLAXES, AND SPACE MOTIONS

| H.D. | $L$ | Visual | $m$ | $M$ | $\pi_{sp}$ | $\pi_{tr}$ | $\theta$ | $T$ | $V$ | $W$ |
|---|---|---|---|---|---|---|---|---|---|---|
| 166 | 5.0 | K0 V | 6.06 | +6.00 | 0.097 | 0.069 | 122 | 1 | − 3 | 3 |
| 167 | 3.2 | G9 III | 6.58 | +0.90 | .0073 | ..... | 276 | 46 | + 9 | 47 |
| 1419 | 2.9 | K0 III | 5.95 | +0.40 | .0078 | ..... | 254 | 42 | +11 | 43 |
| 1527 | 3.2 | K1 III | 6.14 | +1.34 | .0110 | ..... | 278 | 30 | −31 | 43 |
| 1605 | 4.0 | K1 IV | 7.47 | +3.50 | .0161 | ..... | 350 | 27 | +14 | 30 |
| 2767 | 3.7 | K1 III | 5.70 | +2.69 | .0250 | ..... | 300 | 11 | +15 | 19 |
| 2952 | 2.9 | K0 III | 5.86 | +0.40 | .0081 | ..... | 123 | 27 | −28 | 39 |
| 3856 | 2.9 | G9 III–IV | 5.68 | +0.10 | .0077 | ..... | 279 | 24 | + 7 | 25 |
| 4006 | 3.1 | G9 III–IV | 7.9 | +0.62 | .0035 | ..... | 204 | 57 | −18 | 60 |
| 4372 | 3.8 | K1 IV | 7.21 | +2.96 | .0141 | ..... | 249 | 25 | +17 | 30 |
| 4686 | 3.2 | G9 III | 7.12 | +0.90 | .0057 | ..... | 270 | 37 | + 1 | 37 |
| 4831 | 3.0 | G8 III | 7.23 | 0.00 | .0036 | ..... | 239 | 57 | −10 | 58 |
| 5449 | 3.3 | G9 III | 8.6 | +1.17 | .0033 | ..... | 295 | 24 | + 7 | 25 |
| 7229 | 3.1 | G8 III | 6.11 | +0.28 | .0068 | ..... | 209 | 13 | +37 | 39 |
| 7426 | 3.0 | G9 III | 8.7 | +0.35 | .0021 | ..... | 18 | 51 | + 3 | 51 |
| 7578 | 3.6 | K1 III | 5.95 | +2.42 | .0197 | ..... | 278 | 12 | + 8 | 14 |
| 8375 | 3.7 | G8 IV | 6.15 | +1.96 | .0145 | ..... | 45 | 82 | + 4 | 82 |
| 8747 | 3.7 | K0 III | 6.58 | +2.55 | .0156 | ..... | 256 | 18 | − 6 | 19 |
| 8949 | 3.2 | K1 III | 6.22 | +1.34 | .0106 | ..... | 73 | 36 | − 3 | 36 |
| 10588 | 3.3 | G8 III–IV | 6.28 | +0.84 | .0082 | ..... | 289 | 37 | − 5 | 37 |
| 11650 | 2.6 | G9 III | 7.59 | −0.65 | .0022 | ..... | 105 | 74 | − 5 | 74 |
| 11721 | 3.2 | G8 III–IV | 8.1 | +0.56 | .0031 | ..... | 33 | 47 | +28 | 55 |
| 12402 | 2.6 | K1 III | 6.49 | −0.48 | .0040 | ..... | 77 | 42 | +14 | 44 |
| 12638 | 2.9 | G8 III | 7.04 | −0.20 | .0036 | ..... | 39 | 26 | −22 | 34 |
| 12897 | 3.0 | K1 III | 7.20 | +0.80 | .0052 | ..... | 58 | 80 | − 3 | 80 |
| 13013 | 3.0 | G8 III | 6.28 | 0.00 | .0055 | ..... | 178 | 29 | +26 | 39 |
| 13747 | 3.2 | K0 III | 6.28 | +1.23 | .0098 | ..... | 120 | 75 | +15 | 76 |
| 13836 | 5.0 | G8 V | 8.2 | +5.60 | .030 | ..... | 101 | 37 | − 1 | 37 |
| 14067 | 2.9 | G9 III | 6.38 | +0.10 | .0055 | ..... | 255 | 57 | −17 | 60 |
| +26°392* | 3.0 | G9 III | 8.0 | +0.35 | .0030 | ..... | 262 | 138 | −68 | 154 |
| 15328 | 3.3 | K0 III | 6.36 | +1.49 | .0106 | ..... | 291 | 17 | + 9 | 19 |
| 15464 | 3.0 | K1 III | 6.15 | +0.80 | .0085 | ..... | 127 | 32 | + 5 | 32 |
| 16467 | 3.1 | G9 III | 6.16 | +0.62 | .0078 | ..... | 42 | 18 | − 7 | 19 |
| 17228 | 3.0 | G8 III | 6.18 | 0.00 | .0058 | ..... | 68 | 31 | +18 | 36 |
| 17382 | 4.6 | K1 V | 8.2 | +5.12 | .024 | 0.077 | 102 | 42 | + 6 | 42 |
| 18202 | 3.0 | G8 III | 6.42 | 0.00 | .0052 | ..... | 68 | 10 | +25 | 27 |
| 19066 | 3.5 | K0 III | 5.92 | +2.02 | .0166 | ..... | 299 | 30 | −36 | 47 |
| 19121 | 3.5 | K0 III | 5.97 | +2.02 | .0162 | ..... | 342 | 13 | −12 | 18 |
| 19525 | 3.5 | G9 III | 6.28 | +1.71 | .0122 | ..... | 334 | 47 | +28 | 55 |
| 23526 | 2.9 | G9 III | 5.84 | +0.10 | .0071 | ..... | 182 | 34 | −38 | 51 |
| 24154 | 3.0 | K0 III | 6.64 | +0.70 | .0065 | ..... | 117 | 2 | +54 | 54 |
| 24768 | 2.9 | G8 III | 7.50 | −0.20 | .0029 | ..... | 320 | 26 | − 2 | 26 |
| 25296 | 2.8 | G8 III | 7.20 | −0.40 | .0030 | ..... | 22 | 25 | −29 | 38 |
| 25602 | 3.1 | K0 III–IV | 6.18 | +0.96 | .0090 | ..... | 146 | 43 | − 8 | 44 |
| 25877 | 2.6 | G8 II | 6.16 | −0.80 | .0041 | ..... | 348 | 11 | −13 | 17 |
| 26076 | 3.3 | K1 III | 5.98 | +1.61 | .0134 | ..... | 347 | 8 | + 1 | 8 |
| 26605 | 3.2 | G9 III | 6.42 | +0.90 | .0079 | ..... | 294 | 47 | +24 | 53 |
| 28191 | 3.1 | K1 III | 6.13 | +1.07 | .0097 | ..... | 117 | 28 | + 7 | 29 |
| 28322 | 3.1 | G9 III | 6.08 | +0.62 | .0081 | ..... | 30 | 16 | +16 | 23 |
| 28505 | 3.2 | G8 III | 6.42 | +0.56 | 0.0067 | ..... | 210 | 33 | −76 | 83 |

TABLE 1—*Continued*

| H.D. | $L$ | Visual | $m$ | $M$ | $\pi_{sp}$ | $\pi_{tr}$ | $\theta$ | $T$ | $V$ | $W$ |
|---|---|---|---|---|---|---|---|---|---|---|
| 28930 | 2.9 | G8 III | 6.00 | −0.20 | 0.0058 | ..... | 225 | 31 | −40 | 51 |
| 30111 | 2.9 | G9 III | 6.98 | +0.10 | .0043 | ..... | 140 | 26 | +10 | 28 |
| 30138 | 2.9 | G9 III | 5.94 | +0.10 | .0068 | ..... | 243 | 5 | +29 | 29 |
| 30545 | 3.0 | K1 III | 5.86 | +0.80 | .0097 | ..... | 285 | 5 | −34 | 34 |
| 32518 | 3.2 | K1 III | 6.28 | +1.34 | .0103 | 0.006 | 106 | 28 | − 3 | 28 |
| 34810 | 2.7 | K0 III | 6.17 | −0.20 | .0053 | ..... | 259 | 9 | −12 | 15 |
| 35238 | 3.1 | K1 III | 6.20 | +1.07 | .0094 | ..... | 288 | 26 | +32 | 41 |
| 36040 | 3.2 | K1 III | 5.82 | +1.34 | .0127 | ..... | 277 | 9 | + 8 | 12 |
| 36041 | 3.1 | G9 III | 6.28 | +0.62 | .0074 | ..... | 126 | 15 | + 5 | 16 |
| 37329 | 3.3 | G9 III | 6.34 | +1.17 | .0092 | ..... | 45 | 13 | + 3 | 13 |
| 37956 | 3.0 | K1 III | 6.44 | +0.80 | .0074 | ..... | 288 | 10 | +17 | 20 |
| 38527 | 3.2 | G8 III | 5.76 | +0.56 | .0091 | ..... | 229 | 29 | −41 | 50 |
| 38645 | 2.9 | G9 III | 6.18 | +0.10 | .0061 | .003 | 135 | 16 | + 2 | 16 |
| 38765 | 3.8 | K1 III | 6.14 | +2.96 | .0231 | ..... | 71 | 35 | +23 | 42 |
| 39632 | 2.3 | G9 II | 6.04 | −1.58 | .0030 | ..... | 9 | 28 | − 1 | 28 |
| 39743 | 2.9 | G8 III | 6.26 | −0.20 | .0051 | ..... | 90 | 18 | − 6 | 19 |
| 40280 | 2.9 | G9 III | 6.43 | +0.10 | .0054 | ..... | 273 | 44 | − 8 | 45 |
| 40460 | 2.8 | G9 III | 6.52 | −0.15 | .0046 | ..... | 189 | 64 | +85 | 106 |
| 41467 | 2.7 | K0 III | 6.00 | −0.20 | .0058 | ..... | 128 | 10 | 0 | 10 |
| 41636 | 2.7 | G9 III | 6.28 | −0.40 | .0046 | ..... | 197 | 45 | −93 | 103 |
| 42351 | 2.9 | K1 II–III | 6.28 | +0.48 | .0069 | ..... | 180 | 24 | −16 | 29 |
| 42466 | 3.0 | K1 III | 5.92 | +0.80 | .0095 | ..... | 188 | 15 | + 8 | 17 |
| 44391 | 2.0 | G9 II | 7.46 | −2.60 | .00097 | ..... | 270 | 127 | −21 | 129 |
| 44780 | 3.0 | K1 III | 6.26 | +0.80 | .0081 | ..... | 25 | 10 | − 3 | 10 |
| 44867 | 3.1 | G9 III | 6.22 | +0.62 | .0076 | ..... | 118 | 32 | +60 | 68 |
| 45824 | 3.0 | G8 III | 8.0 | 0.00 | .0025 | ..... | 57 | 51 | −15† | 53 |
| 46277 | 2.6 | G9 III | 7.8 | −0.65 | .0020 | ..... | 311 | 25 | −13 | 28 |
| 46336 | 3.2 | G9 III | 8.0 | +0.90 | .0038 | ..... | 121 | 15 | +24 | 28 |
| 46509 | 2.7 | K0 III | 5.72 | −0.20 | .0065 | ..... | 39 | 26 | −20 | 33 |
| 47220 | 2.8 | K1 III | 6.16 | +0.16 | .0063 | ..... | 218 | 35 | −24 | 42 |
| 47270 | 3.0 | K1 III | 6.25 | +0.80 | .0081 | ..... | 65 | 25 | −35 | 43 |
| 47358 | 2.9 | G9 III | 6.14 | +0.10 | .0062 | ..... | 145 | 9 | −22 | 24 |
| 50371 | 3.3 | G9 III | 6.13 | +1.17 | .0102 | ..... | 169 | 48 | −48 | 68 |
| 51814 | 2.6 | G8 III | 5.82 | −0.80 | .0047 | ..... | 270 | 10 | + 1 | 10 |
| 53925 | 2.8 | K1 III | 6.15 | +0.16 | .0063 | ..... | 0 | 3 | + 3 | 4 |
| 54825 | 2.3 | K0 III | 6.62 | −1.52 | .0024 | ..... | 339 | 37 | +31 | 48 |
| 56989 | 2.9 | G9 III | 5.82 | +0.10 | .0072 | ..... | 171 | 4 | + 8 | 9 |
| 58683 | 2.7 | G8 III | 8.1 | −0.60 | .0018 | 0.014 | 212 | 291 | +46 | 295 |
| 59878 | 2.9 | G9 III | 6.32 | +0.10 | .0057 | ..... | 281 | 14 | +19 | 24 |
| 62141 | 2.6 | K0 III | 6.16 | −0.50 | .0047 | ..... | 324 | 33 | −14 | 36 |
| 62264 | 3.7 | K0 III | 6.10 | +2.55 | .0196 | ..... | 50 | 11 | − 7 | 13 |
| 63410 | 3.2 | G8 III | 6.76 | +0.56 | .0058 | ..... | 272 | 23 | +72 | 76 |
| 63799 | 3.1 | K1 III | 6.14 | +1.07 | .0097 | ..... | 100 | 33 | −62 | 70 |
| 64938 | 2.6 | G8 III | 6.08 | −0.80 | .0042 | ..... | 11 | 5 | + 2 | 5 |
| 65066 | 2.9 | K0 III | 5.98 | +0.40 | .0077 | ..... | 111 | 9 | −49 | 50 |
| 65735 | 3.2 | K1 III | 6.24 | +1.34 | .0105 | ..... | 49 | 10 | +17 | 20 |
| 65757 | 3.7 | K1 III–IV | 6.36 | +2.69 | .0184 | ..... | 11 | 8 | +16 | 18 |
| 67402 | 2.8 | G9 III | 6.88 | −0.15 | .0039 | ..... | 209 | 22 | + 2 | 22 |
| 68461‡ | 3.2 | K0 III | 5.94 | +1.23 | .0114 | ..... | 56 | 6 | −31 | 32 |
| 68776 | 3.2 | G8 III | 6.20 | +0.56 | 0.0074 | ..... | 256 | 5 | +14† | 15 |

TABLE 1—*Continued*

| H.D. | $L$ | Visual | $m$ | $M$ | $\pi_{so}$ | $\pi_{tr}$ | $\theta$ | $T$ | $V$ | $W$ |
|---|---|---|---|---|---|---|---|---|---|---|
| 69478 | 2.3 | G8 III | 6.14 | −1.64 | 0.0028 | ..... | 222 | 21 | +16 | 26 |
| 72908 | 2.4 | G9 III | 6.25 | −1.24 | .0032 | ..... | 355 | 16 | −19 | 25 |
| 73593 | 3.3 | G8 IV | 5.23 | +0.84 | .0132 | 0.014 | 25 | 52 | −38 | 64 |
| 73599 | 3.3 | K1 III | 6.34 | +1.61 | .0113 | ..... | 205 | 9 | + 5 | 10 |
| 74669 | 3.3 | K0 III | 7.22 | +1.49 | .0071 | ..... | 202 | 33 | +21 | 39 |
| 76508 | 2.8 | K1 III | 6.10 | +0.16 | .0065 | ..... | 247 | 24 | +10 | 26 |
| 76629 | 2.7 | G8 III | 6.10 | −0.60 | .0046 | ..... | 38 | 12 | −24 | 27 |
| 78633 | 3.1 | G8 III–IV | 6.38 | +0.28 | .0060 | ..... | 134 | 32 | +12 | 34 |
| 79517 | 3.0 | G8 III | 6.36 | 0.00 | .0053 | ..... | 201 | 51 | +62 | 80 |
| 85505 | 2.7 | G9 III | 6.20 | −0.40 | .0048 | ..... | 232 | 28 | +10 | 30 |
| 88476 | 3.2 | G8 III | 6.75 | +0.56 | .0058 | ..... | 270 | 12 | + 4 | 13 |
| 89268 | 3.3 | K1 III | 6.25 | +1.61 | .0118 | ..... | 101 | 8 | −19 | 21 |
| 95233 | 3.1 | G9 III | 6.35 | +0.62 | .0071 | ..... | 101 | 3 | + 5 | 6 |
| 100030 | 3.9 | G8 IV | 6.24 | +2.52 | .0180 | ..... | 105 | 38 | +45 | 59 |
| 100655 | 3.5 | G9 III | 6.31 | +1.71 | .0120 | ..... | 313 | 9 | − 5 | 10 |
| 101112 | 3.0 | K1 III | 6.14 | +0.80 | .0086 | ..... | 48 | 26 | +11 | 28 |
| 103736 | 3.2 | G8 III | 6.13 | +0.56 | .0077 | ..... | 180 | 22 | +26 | 34 |
| 103953 | 2.8 | K0 III | 6.56 | +0.10 | .0051 | ..... | 89 | 55 | −14 | 57 |
| 108471 | 3.1 | G8 III | 6.28 | +0.28 | .0063 | ..... | 87 | 33 | − 2 | 33 |
| 108861 | 3.3 | G8 III–IV | 5.96 | +0.84 | .0095 | ..... | 109 | 35 | − 7 | 36 |
| 109996 | 3.1 | K1 III | 6.30 | +1.07 | .0090 | ..... | 252 | 14 | −21 | 25 |
| 111591 | 2.8 | K0 III | 6.32 | +0.10 | .0057 | ..... | 108 | 38 | +13 | 40 |
| 112570 | 2.9 | G9 III | 5.94 | +0.10 | .0068 | ..... | 182 | 34 | +18 | 38 |
| 113847 | 3.2 | K1 III | 5.48 | +1.34 | .0149 | ..... | 41 | 15 | − 9 | 17 |
| 114724 | 2.8 | K1 III | 6.26 | +0.16 | .0060 | ..... | 182 | 19 | −15 | 24 |
| 114793 | 3.4 | G8 III | 6.34 | +1.12 | .0090 | ..... | 290 | 17 | −13 | 21 |
| 116594 | 2.9 | K0 III | 6.18 | +0.40 | .0070 | ..... | 10 | 37 | + 3 | 37 |
| 118266 | 2.7 | K1 III | 6.34 | −0.16 | .0050 | ..... | 119 | 100 | +42 | 108 |
| 118536 | 3.0 | K1 III | 6.24 | +0.80 | .0082 | ..... | 140 | 18 | + 3 | 18 |
| 122742 | 4.6 | G8 V | 6.14 | +4.48 | .047 | .061 | 132 | 34 | − 3 | 34 |
| 122744 | 3.0 | G9 III | 6.24 | +0.35 | .0066 | ..... | 265 | 16 | − 9 | 18 |
| 133485 | 3.2 | G8 III–IV | 6.38 | +0.56 | .0069 | ..... | 146 | 16 | − 9 | 18 |
| 134493 | 2.8 | K0 III | 6.14 | +0.10 | .0062 | ..... | 170 | 23 | −12 | 26 |
| 136274 | 5.0 | G8 V | 7.99 | +5.60 | .033 | .005 | 258 | 72 | −12 | 73 |
| 138085 | 3.1 | G8 III–IV | 6.35 | +0.28 | .0061 | ..... | 336 | 57 | +37 | 68 |
| 140438 | 3.7 | G8 III–IV | 6.37 | +1.96 | .0131 | ..... | 42 | 9 | + 6 | 11 |
| 144046 | 2.4 | G9 III | 6.04 | −1.24 | .0035 | ..... | 240 | 59 | −27 | 65 |
| 144287 | 5.0 | G9 V | 7.08 | +5.80 | .056 | .041 | 328 | 70 | −25 | 74 |
| 145457 | 3.4 | G9 III | 6.56 | +1.44 | .0095 | ..... | 359 | 24 | +13 | 27 |
| 146603 | 2.5 | G8 III | 6.06 | −1.00 | .0039 | ..... | 208 | 71 | + 6 | 71 |
| 152224 | 2.8 | K0 III | 6.12 | +0.10 | .0063 | ..... | 25 | 36 | −10† | 37 |
| 153226 | 4.3 | K0 IV | 6.26 | +4.14 | .038 | ..... | 335 | 15 | −11 | 19 |
| 153312 | 3.2 | K0 III | 6.18 | +1.23 | .0102 | ..... | 151 | 11 | − 2 | 11 |
| 154391 | 2.8 | K1 III | 6.00 | +0.16 | .0068 | ..... | 310 | 50 | + 1 | 50 |
| 154619 | 2.7 | G8 III–IV | 6.20 | −0.60 | .0044 | ..... | 64 | 57 | − 4 | 57 |
| 155500 | 3.4 | K0 III | 6.12 | +1.76 | .0134 | ..... | 51 | 16 | +14 | 21 |
| 159925 | 3.0 | G9 III | 6.02 | +0.35 | .0073 | ..... | 144 | 15 | +24 | 28 |
| 160822 | 3.0 | K0 III | 6.24 | +0.70 | .0078 | ..... | 223 | 63 | +15 | 65 |
| 161178 | 3.0 | G9 III | 5.72 | +0.35 | .0084 | −0.010 | 86 | 8 | +23 | 24 |
| 162468 | 3.5 | K1 III–IV | 6.02 | +2.15 | 0.0168 | ..... | 265 | 6 | +29 | 30 |

TABLE 1—*Continued*

| H.D. | $L$ | Visual | $m$ | $M$ | $\pi_{sp}$ | $\pi_{tr}$ | $\theta$ | $T$ | $V$ | $W$ |
|---|---|---|---|---|---|---|---|---|---|---|
| 162734 | 3.3 | K0 III | 6.30 | +1.49 | 0.0109 | ..... | 356 | 17 | −23 | 27 |
| 163993 | 2.6 | G8 III | 3.56 | −0.80 | .0134 | 0.018 | 102 | 30 | +18 | 35 |
| 165473 | 3.3 | G9 III | 7.6 | +1.17 | .0052 | ..... | 196 | 29 | +40 | 49 |
| 166207 | 2.9 | K0 III | 6.12 | +0.40 | .0072 | ..... | 356 | 62 | −38 | 73 |
| 167304 | 3.0 | K0 III | 6.12 | +0.70 | .0082 | ..... | 203 | 32 | −28 | 43 |
| 169221 | 2.7 | K1 III | 6.27 | −0.16 | .0052 | ..... | 315 | 19 | + 2 | 19 |
| 170619 | 3.5 | G8 IV | 7.7 | +1.40 | .0055 | ..... | 357 | 31 | − 5 | 31 |
| 170829 | 4.4 | G8 IV | 6.42 | +3.92 | .032 | .028 | 184 | 40 | −39 | 56 |
| 171994 | 4.0 | G8 IV | 6.20 | +2.80 | .0209 | ..... | 358 | 17 | −26 | 31 |
| 172424 | 4.0 | G8 III | 6.24 | +2.80 | .0205 | ..... | 214 | 3 | −22 | 22 |
| 173398 | 2.5 | K0 III | 5.88 | −0.80 | .0046 | ..... | 351 | 57 | − 9 | 58 |
| 174414 | 2.9 | K0 III | 6.76 | +0.40 | .0053 | ..... | 304 | 16 | +35 | 38 |
| 175679 | 2.5 | G8 III | 6.05 | −1.00 | .0039 | ..... | 162 | 4 | + 3 | 5 |
| 175743 | 3.1 | K1 III | 5.58 | +1.07 | .0125 | .003 | 200 | 62 | +64† | 89 |
| 176776 | 3.1 | K1 III | 6.26 | +1.07 | .0092 | ..... | 32 | 5 | − 8 | 9 |
| 177199 | 3.3 | K1 III | 5.98 | +1.61 | .0134 | ..... | 286 | 5 | +13 | 14 |
| 179094‡ | 3.5 | K1 IV | 5.89 | +2.15 | .0179 | .004 | 236 | 38 | +23 | 44 |
| 181122 | 2.7 | G9 III | 6.34 | −0.40 | .0045 | ..... | 194 | 35 | + 7 | 36 |
| 181597 | 3.3 | K1 III | 6.12 | +1.61 | .0125 | .002 | 342 | 15 | + 5 | 16 |
| 181655 | 5.0 | G8 V | 6.09 | +5.60 | .080 | ..... | 216 | 17 | +22 | 28 |
| 182272 | 2.8 | K0 III | 5.98 | +0.10 | .0067 | ..... | 189 | 24 | + 4 | 24 |
| 182488 | 5.0 | K0 V | 6.28 | +6.00 | .088 | .057 | 352 | 8 | 0 | 8 |
| 182617 | 3.4 | K0 III | 7.62 | +1.76 | .0067 | ..... | 225 | 13 | +30 | 33 |
| 182635 | 2.9 | K1 III | 6.32 | +0.48 | .0068 | ..... | 358 | 53 | −13 | 55 |
| 183399 | 2.7 | K0 III | 6.52 | −0.20 | .0045 | ..... | 229 | 31 | + 7 | 32 |
| 185264 | 3.4 | G9 III | 6.38 | +1.44 | .0103 | ..... | 311 | 19 | +27 | 33 |
| 185436 | 3.0 | K0 III | 6.30 | +0.70 | .0076 | ..... | 240 | 51 | +25 | 57 |
| 187614 | 2.7 | G8 III | 6.40 | −0.60 | .0040 | ..... | 79 | 18 | + 8 | 20 |
| 189671 | 2.3 | G8 II | 6.34 | −1.64 | .0025 | ..... | 312 | 30 | − 3 | 30 |
| 190252 | 3.0 | G8 III | 6.18 | 0.00 | .0058 | ..... | 29 | 47 | + 4 | 47 |
| 193094 | 2.9 | G9 III | 6.16 | +0.10 | .0063 | ..... | 323 | 37 | − 1 | 37 |
| 194220 | 2.9 | K0 III | 6.12 | +0.40 | .0072 | ..... | 44 | 31 | − 2 | 31 |
| 194616 | 2.7 | K0 III | 6.30 | −0.20 | .0050 | ..... | 56 | 14 | −12 | 18 |
| 194937 | 3.2 | G9 III | 6.02 | +0.90 | .0095 | ..... | 21 | 18 | + 6 | 19 |
| 194953 | 2.7 | G8 III | 6.25 | −0.60 | .0043 | ..... | 80 | 45 | − 6 | 45 |
| 195820 | 3.4 | K0 III | 6.06 | +1.76 | .0138 | ..... | 2 | 19 | + 7 | 20 |
| 196642 | 3.1 | K0 III | 6.00 | +0.96 | .0098 | ..... | 197 | 22 | −19 | 29 |
| 196787 | 2.4 | G9 III | 5.20 | −1.24 | .0051 | ..... | 66 | 11 | + 8 | 14 |
| 197249 | 3.2 | G8 III | 6.14 | +0.56 | .0077 | ..... | 1 | 33 | +15 | 36 |
| 198236 | 3.1 | G8 III | 6.29 | +0.28 | .0063 | .001 | 235 | 47 | + 6 | 47 |
| 200578 | 3.3 | G8 III | 6.76 | +0.84 | .0065 | ..... | 239 | 19 | − 9 | 21 |
| 201669 | 3.2 | G8 III | 7.8 | +0.56 | .0036 | ..... | 269 | 72 | +22 | 75 |
| 203358 | 4.5 | G8 IV–V | 6.32 | +4.20 | .038 | ..... | 260 | 10 | −12 | 16 |
| 203630 | 3.3 | K1 III | 5.98 | +1.61 | .0134 | ..... | 306 | 9 | − 9 | 13 |
| 203733 | 2.9 | K0 III | 8.0 | +0.40 | .0028 | ..... | 67 | 96 | +33 | 102 |
| 203886 | 2.8 | K0 III | 6.28 | +0.10 | .0058 | ..... | 66 | 15 | − 8 | 17 |
| 205688 | 2.9 | G8 III–IV | 6.26 | −0.20 | .0051 | ..... | 310 | 99 | − 5 | 99 |
| 206040 | 3.3 | K1 III | 6.00 | +1.61 | .0132 | ..... | 265 | 22 | +16 | 27 |
| 206374 | 4.9 | G8 V | 7.42 | +5.32 | .038 | 0.031 | 103 | 28 | −28 | 40 |
| 206509 | 3.3 | K0 III | 5.90 | +1.49 | 0.0131 | ..... | 259 | 14 | +19 | 24 |

TABLE 1—*Continued*

| H.D. | $L$ | Visual | $m$ | $M$ | $\pi_{sp}$ | $\pi_{tr}$ | $\theta$ | $T$ | $V$ | $W$ |
|---|---|---|---|---|---|---|---|---|---|---|
| 206731 | 2.1 | G8 II–III | 5.92 | −2.28 | 0.0023 | ..... | 236 | 9 | +11 | 14 |
| 207088 | 2.7 | G8 III | 6.27 | −0.60 | .0042 | ..... | 83 | 88 | +10 | 89 |
| 207740 | 4.6 | G8 V | 8.0 | +4.48 | .020 | ..... | 277 | 30 | +21 | 37 |
| 209813 | 2.5 | K0 III | 6.37 | −0.80 | .0037 | ..... | 46 | 78 | − 9 | 79 |
| 210026 | 2.9 | K0 III | 7.9 | +0.40 | .0032 | ..... | 294 | 27 | + 1 | 27 |
| 211555 | 2.8 | K0 III | 7.02 | +0.10 | .0041 | ..... | 18 | 44 | −12 | 46 |
| 212750 | 3.1 | K0 III | 7.12 | +0.96 | .0059 | ..... | 284 | 55 | +12 | 56 |
| 212943 | 2.7 | K1 III | 4.66 | −0.16 | .0109 | 0.021 | 174 | 123 | +62 | 138 |
| 213014 | 3.4 | G9 III | 7.32 | +1.44 | .0067 | ..... | 263 | 6 | −30 | 31 |
| 213025 | 3.2 | G8 III | 6.35 | +0.56 | .0069 | ..... | 256 | 46 | −31 | 55 |
| 213178 | 3.1 | K0 III | 7.02 | +0.96 | .0061 | ..... | 349 | 20 | + 3 | 20 |
| 214265 | 3.1 | K0 III | 7.00 | +0.96 | .0062 | ..... | 66 | 37 | − 7 | 38 |
| 215030 | 3.1 | G9 III | 5.77 | +0.62 | .0093 | .000 | 56 | 62 | − 2 | 62 |
| 217019 | 2.5 | K1 III | 6.16 | −0.80 | .0041 | ..... | 44 | 84 | +18 | 86 |
| 217673 | 2.7 | K1 III | 6.16 | −0.16 | .0054 | ..... | 248 | 24 | + 6 | 25 |
| 218103 | 2.5 | G9 III | 6.36 | −0.90 | .0035 | ..... | 130 | 31 | − 6 | 32 |
| 218416 | 2.5 | K0 III | 6.02 | −0.80 | .0043 | ..... | 317 | 17 | +16 | 23 |
| 218660 | 3.0 | K1 III | 6.46 | +0.80 | .0074 | ..... | 10 | 18 | +21 | 28 |
| 219736 | 3.5 | K1 III | 6.84 | +2.15 | .0115 | ..... | 255 | 39 | + 6 | 39 |
| 221113 | 2.8 | G9 III | 6.36 | −0.15 | .0050 | ..... | 215 | 97 | +27 | 101 |
| 221115 | 2.8 | G9 III | 4.38 | −0.15 | .0124 | .009 | 42 | 22 | −10 | 24 |
| 221364 | 3.0 | K0 III | 6.42 | +0.70 | .0072 | ..... | 260 | 7 | + 3 | 8 |
| 221861 | Ib | K0 Ib | 5.70 | −4.50 | .00091 | ..... | 333 | 12 | + 7 | 14 |
| 222618 | 3.0 | G8 III | 6.10 | 0.00 | .0060 | ..... | 288 | 18 | + 1 | 18 |
| 224085‡ | 4.9 | K0 V | 7.02 | +5.73 | .055 | 0.034 | 70 | 33 | −13 | 35 |
| 224895 | 3.2 | K1 III | 6.76 | +1.34 | .0082 | ..... | 234 | 44 | − 7 | 45 |
| 225292 | 3.1 | G9 III | 6.46 | +0.62 | 0.0068 | ..... | 81 | 31 | +18 | 36 |

* BD number, not in *Henry Draper Catalogue*.

† The radial velocity is variable, but no orbit has been computed. The value given is the average of all measures.

‡ The following stars have characteristics:
HD 68461: *H* lines strong, possibly composite spectrum. Spectroscopic binary.
179094: *Ca* H and K emission known. Spectroscopic binary.
224085: *Ca* H and K emission known, H lines very weak. Spectroscopic binary.

## DERIVATION OF LUMINOSITY FUNCTIONS

The distribution of the stars in Table 1 according to luminosity number is shown in Table 2. The G8 and G9 stars are combined in one group, and the K0 and K1 stars in another group. The tabular interval chosen is one-fifth of a luminosity class, as shown in the first column. The observed number of stars in each luminosity interval is given in the second and seventh columns, and in the third and eighth columns these distributions have been smoothed of minor fluctuations.

Before the smoothed frequency functions are converted to luminosity functions they must be corrected for the effects of error dispersion. The luminosity measures are subject to errors from (*a*) effects of the exposure density of the spectrograms, (*b*) matching the line intensities in making the readings, and (*c*) calibrating to luminosity numbers. As a result of these errors, the observed distributions can be expected to have less sharp maxima and minima than the true distributions.

An estimate of the probable error of the luminosity-number determinations was made in the following way. For each star four luminosity-number estimates were available, one from each of the spectral criteria used. From the internal agreement of these four

numbers, the estimated probable errors of the mean turned out to be $\pm 0.11$ luminosity class for the G8 and G9 stars and $\pm 0.14$ class for the K0 and K1 stars. This is in good agreement with the value of $\pm 0.16$ class obtained by Hossack (1954) from measuring three ratios on each of several spectrograms of a single star of similar spectral type. This indicates that there were no serious errors affecting all the measures on each spectrogram. If such errors existed, the internal agreement of the four ratios would have yielded a smaller probable error than would the comparison of the average luminosity numbers from different spectrograms. There were not sufficient spectrograms of good quality on the 33 A/mm dispersion to use the second method for the present material.

The smoothed frequency functions of the third and eighth columns of Table 2 were corrected by a numerical method for assumed probable errors of $\pm 0.11$ class for the third column and $\pm 0.14$ class for the eighth and a Gaussian distribution of the errors. The corrected distributions are shown in the fourth and ninth columns.

TABLE 2

LUMINOSITY FUNCTIONS FOR G8, G9, AND K0, K1 STARS

| $L$ | G8, G9 | | | | | K0, K1 | | | | |
|---|---|---|---|---|---|---|---|---|---|---|
| | Obs. | Smooth | Corrected | Final | Luminosity Function | Obs. | Smooth | Corrected | Final | Luminosity Function |
| 1.0, 2.1 | 2 | 1.2 | 0.94 | 0.94 | 0.035 | 1 | 0.6 | 0.27 | 0.27 | 0.009 |
| 2.2, 2.3 | 3 | 2.8 | 1.9 | 1.9 | 0.17 | 1 | 1.4 | 0.27 | 0.27 | 0.025 |
| 2.4, 2.5 | 6 | 7.0 | 5.8 | 5.8 | 1.4 | 4 | 4.0 | 1.7 | 1.7 | 0.45 |
| 2.6, 2.7 | 15 | 15.0 | 15.3 | 15.3 | 10 | 11 | 11.0 | 9.4 | 9.4 | 6.6 |
| 2.8, 2.9 | 22 | 22.0 | 23.1 | 23.1 | 29 | 23 | 23.0 | 26.9 | 26.9 | 45 |
| 3.0, 3.1 | 26 | 26.0 | 28.4 | 28.4 | 59 | 26 | 26.0 | 30.4 | 30.4 | 131 |
| 3.2, 3.3 | 24 | 24.0 | 28.3 | 28.3 | 120 | 21 | 21.0 | 23.9 | 23.9 | 225 |
| 3.4, 3.5 | 7 | 7.0 | 3.9 | 3.9 | 35 | 8 | 9.0 | 6.6 | 6.6 | 128 |
| 3.6, 3.7 | 2 | 2.2 | 0.54 | 0.54 | 10 | 5 | 4.0 | 2.2 | 2.2 | 91 |
| 3.8, 3.9 | 1 | 1.5 | 1.2 | 1.3 | 54 | 2 | 1.9 | 1.1 | 1.2 | 98 |
| 4.0, 4.1 | 2 | 1.2 | 1.1 | 1.3 | 110 | 1 | 1.0 | 0.60 | 0.77 | 139 |
| 4.2, 4.3 | 0 | 1.1 | 1.0 | 1.4 | 260 | 1 | 0.8 | 0.67 | 0.98 | 370 |
| 4.4, 4.5 | 2 | 1.2 | 1.1 | 1.6 | 650 | 0 | 0.7 | 0.61 | 1.1 | 860 |
| 4.6, 4.7 | 2 | 1.5 | 1.4 | 1.9 | 1700 | 1 | 0.8 | 0.71 | 1.2 | 2000 |
| 4.8, 4.9 | 1 | 2.0 | 1.9 | 2.5 | 4600 | 1 | 1.0 | 0.96 | 1.6 | 5400 |
| 5.0 | 4 | 3.3 | 4.6 | 5.2 | 20500 | 2 | 1.8 | 2.6 | 3.2 | 23000 |

Corrections to the frequencies of dwarf stars in Table 2 were required because there was a selection effect in the sample studied which involved the proper motions of the stars. About 65 per cent of the stars in the group were observed for radial velocity at the David Dunlap Observatory (Young 1945), in order to complete the list of radial velocities of northern stars in Schlesinger and Jenkins' (1940) *Catalogue of Bright Stars*. Since stars with large proper motions had been observed for radial velocity at an early date, the sample observed at the David Dunlap Observatory is deficient in high proper motions. Corrections for this selection effect are now considered.

An analysis of all those stars in the bright-star catalogue with northern declinations, spectral types between G5 and K5, and visual magnitudes from 5.8 to 7.0 indicated that the stars observed at the David Dunlap Observatory comprise an unbiased sample for proper motions less than $0''.21$ per year. For larger proper motions the deficiency of stars in the David Dunlap Observatory group is evident. The deficiency was evaluated for each of six ranges in proper motion. About 70 stars in the G8 and G9 group and another 70 in the K0 and K1 group are from the observing program affected by the selection effect. The corrections amount to a total of nearly 3 stars for each group.

The distribution of these corrections was converted from proper motion to absolute magnitude by assuming that the large proper motions correspond to tangential velocities of 50 km/sec. This rather large value for the tangential velocity insures that the correction is not underestimated for the brighter stars. The average apparent magnitude of the group is $m = 6.4$, so that proper motions of $0''.21$ per year or more correspond to absolute magnitudes of $M = +2.9$ or fainter. By means of the relation between luminosity numbers and absolute magnitudes, the corrections for the proper-motion selection effect were applied, and this gave the final corrected distributions of the fifth and tenth columns of Table 2. Only the last seven rows were affected by the correction.

The absolute magnitudes determine the relative volumes of space observed for each luminosity interval in Table 2. These ratios are independent of the apparent magnitudes of the stars if, as must be true for all but the most luminous stars in this survey, space absorption is negligible. The absolute magnitudes corresponding to the division points between successive rows in Table 2 were computed by averaging the values for the four spectral-type–luminosity-number combinations involved—e.g., G8, 2.9; G9, 2.9; G8, 3.0; and G9, 3.0—between the fifth and sixth rows. If the successive values of this average be indicated by $M_i$, then the relative volumes are proportional to the values of

$$(R_i)^3 - (R_{i+1})^3 ,$$

where

$$\log R_i = -0.2M_i .$$

When the relative volumes of space were computed, division of the frequencies in the fifth and tenth columns of Table 2 by the appropriate volume yielded the relative luminosity functions shown in the sixth and eleventh columns. These indicate the relative numbers of stars of different luminosities determined from a sample of stars, almost all of which are within 300 parsecs of the sun. No attempt has been made to convert to absolute luminosity functions in order to indicate the number of stars of each luminosity per cubic parsec. The stars used do not comprise a sufficiently homogeneous sample to permit ready determination of completeness factors, and the interesting features of the functions are shown just as well in the form of relative functions.

The final functions of Table 2 are plotted in Figure 1 for the G8 and G9 stars and in Figure 2 for the K0 and K1 stars. The luminosity scale has been converted here to absolute magnitude, and allowance has been made for the slight change in slope at class 3.0 of the linear relation between luminosity class and absolute magnitude. Only a limited region of the absolute-magnitude scale is shown. The frequency scales in the two figures are independent and do not give the relative frequencies of G8 and G9 giants compared to K0 and K1 giants. The dashed curves indicate the functions obtained if the error-dispersion correction is not applied.

The corrected and uncorrected curves cross one another in two places in the region of the giant stars. These are not symmetrically situated with respect to the maximum, because division by the relative volumes of space has greatly changed the shape of the original frequency functions. One point of intersection is evident in each figure, and the other point is in the wing of each curve between $M = 0$ and $M = -1$.

## DISCUSSION OF LUMINOSITY FUNCTIONS

The important result is the presence of a distinct frequency minimum for both groups of stars near luminosity number 3.6 or near absolute magnitude +2. These subgiant stars appear to be less numerous than either normal giants or dwarf stars in the spectral range from G8 to K1. This is in agreement with the results obtained by Strömberg. For bright giant stars the frequencies are less significant, since no account has been taken of galactic concentration for these stars.

To be sure of the reality of the frequency minimum near absolute magnitude +2, the

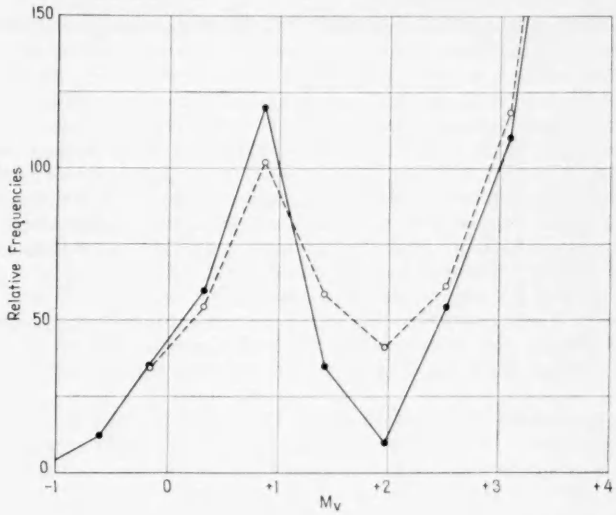


FIG. 1.—Relative frequencies of G8 and G9 stars as a function of visual absolute magnitude. The solid curve is the corrected function for a probable error of 0.11 luminosity class. The dashed curve is the uncorrected function.

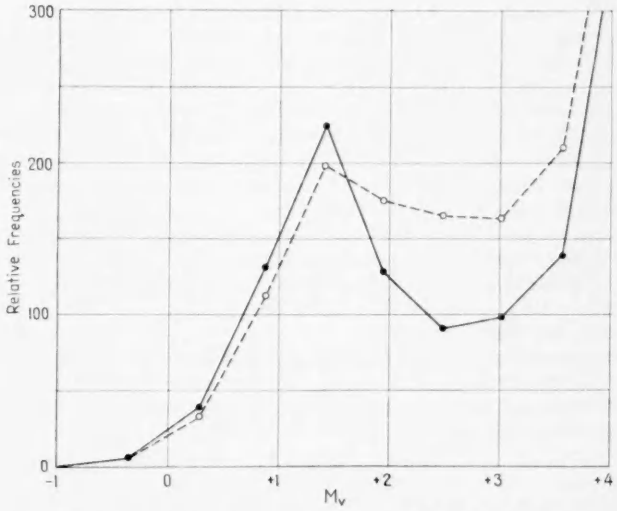


FIG. 2.—Relative frequencies of K0 and K1 stars as a function of visual absolute magnitude. The solid curve is the corrected function for a probable error of 0.14 luminosity class. The dashed curve is the uncorrected function.

assumptions which might affect it are now examined. In forming the calibration-curves to derive luminosity numbers from microphotometer readings (Trumpler and Weaver 1953), the sharp peak of the visual classifications at class III was diffused by assuming that one-quarter of these should be class III–IV and one-quarter should be class II–III. Many individual readings near class 3.5 result from this assumption, which tends to diffuse the final curve in this region rather than create an artificial minimum.

On the other hand, the error-dispersion correction tends to create a minimum; hence it is important not to overcorrect for this effect. The solid curves in the figures are based on the best available estimates of the errors involved, while the dashed curves are based on the assumption of no errors in the luminosity numbers, and they show that the minima exist even if the error-dispersion correction is omitted entirely.

The correction due to the proper-motion selection effect is small for stars as bright as the subgiants. The correction applied was based on a rather large assumed tangential velocity of 50 km/sec, which means that the corrections probably are too large for the brighter stars involved, again tending to decrease the prominence of the frequency minimum.

The frequency minimum could be strongly affected by the method of calibrating from luminosity numbers to absolute magnitude. Linear interpolation was applied between Miss Roman's values for class III and Morgan's values for class V. If Miss Roman's values for classes III–IV and IV had been used (which were derived from small samples), the minimum near class 3.6 would have been more pronounced, since the range in absolute magnitude from class III to class III–IV given by Miss Roman is smaller than that used here. The relative volumes of space in this range would then be smaller, which would give rise to a larger maximum near class 3.2, while a lower minimum near class 3.6 (or fainter) would result from the larger relative volumes associated with the correspondingly larger range in absolute magnitude. The effect would be further emphasized in converting from the luminosity-number intervals of Table 2 to the absolute-magnitude scales of Figures 1 and 2. The linear interpolation of absolute magnitude, then, also tends to decrease the extent of the minimum for subgiants.

Linear interpolation is probably the better procedure to adopt in any case, for any group of stars visually classified as class III–IV is likely to be closer to class III in its properties than to class IV. This is because there is an unavoidable error in the classifications and a great preponderance of stars near class III in the entire group, so that more stars near class III than near class IV will be classified as III–IV. While the definition of class III–IV could be based on some such group of stars, it would be more meaningful to have a uniform change of both spectral characteristics and absolute magnitude with the luminosity designation.

If the relation between luminosity number and absolute magnitude is not unique, so that there is a slight scatter in the absolute magnitudes of stars for which the correct luminosity numbers are identical, then the true luminosity function will have slightly more pronounced maxima and minima than the one derived here on the assumption of a unique relation between $L$ and $M$.

All the assumptions which might affect the reality of the frequency minimum for subgiants in the luminosity function are, therefore, such as to decrease its size. Its presence in the final functions and its general similarity in the two spectral groups leave little doubt that the effect is real.

## SPACE MOTIONS

Space motions were computed for each star, the procedure being as follows. The GC proper motions were first corrected by the systematic corrections given in the N30 catalogue (H. R. Morgan 1952). For some of the fainter stars the proper motions from the Yale catalogue (Barney 1953) were used. The spectroscopic parallax values were used to remove the parallactic component due to solar motion from each proper-motion

component. A solar motion of 20 km/sec toward an apex at $\alpha = 18^h04^m$, $\delta = +28°$ was assumed. The position angles, $\theta$, of the total proper motions are given in the eighth column of Table 1. Total proper motions were computed and converted to kilometers per second to give the tangential velocities, $T$, shown in the ninth column. The radial velocities, $V$ (corrected for the same solar motion), are shown in the tenth column. The velocities were derived from those in *Publications of the David Dunlap Observatory*, Volume 1, Nos. 3, 13, and 16, and from an additional list soon to be published. The space velocity, $W$, in the eleventh column is the vector sum of $T$ and $V$ and is then the velocity of the star relative to the local standard of rest.

The probable errors of the space velocities are very different from star to star and depend on the apparent magnitude, the absolute magnitude, and the relative sizes of the components $V$ and $T$. With individual probable errors of 0.4 mag. for $M$, 0".008 per year for the proper motion, and 2 km/sec for $V$, the probable errors for $W$ for a sixth-magnitude star with $V = 15$ km/sec and $T = 25$ km/sec are: 16 km/sec for luminosity number 2.0, 5 km/sec for 3.0, and 4 km/sec for 5.0. If the space motion is large, the probable error in $W$ will be large if $T$ is much larger than $V$, while the error in $W$ is always small if $V$ is much larger than $T$. The errors will be larger for fainter stars because of the proper-motion errors.

TABLE 3

SUSPECTED HIGH-VELOCITY STARS

| H.D. | $L$ | $G$ | Long. | H.D. | $L$ | $G$ | Long. |
|---|---|---|---|---|---|---|---|
| 11650 | 2.6 | 74 | 198 | 118266 | 2.7 | 108 | 332 |
| 13747 | 3.2 | 74 | 196 | 136274 | 5.0 | 68 | 212 |
| +26°392* | 3.0 | 151 | 345 | 144046 | 2.4 | 65 | 216 |
| 28505 | 3.2 | 83 | 322 | 144287 | 5.0 | 72 | 146 |
| 40460 | 2.8 | 100 | 180 | 166207 | 2.9 | 73 | 170 |
| 41636 | 2.7 | 91 | 298 | 175743 | 3.1 | 89 | 334 |
| 44867 | 3.1 | 65 | 186 | 203733 | 2.9 | 93 | 121 |
| 50371 | 3.5 | 65 | 306 | 207088 | 2.7 | 75 | 144 |
| 58683 | 2.7 | 213 | 213 | 209813 | 2.5 | 78 | 159 |
| 63410 | 3.2 | 75 | 155 | 212943 | 2.7 | 80 | 290 |
| 63799 | 3.1 | 70 | 347 | 217019 | 2.5 | 86 | 122 |
| 79517 | 3.0 | 67 | 152 | 221113 | 2.8 | 84 | 329 |

* BD number, not in *Henry Draper Catalogue*.

The space velocities in Table 1 reveal a number of high-velocity stars. Spectral differences between such stars and normal stars have been described by other investigators (Roman 1952; Keenan and Keller 1953) but were not apparent on the spectrograms used for this investigation. Some of the differences are best seen with lower dispersion, and others depend on criteria which are outside the region of good exposure density of the spectrograms.

A list of the suspected members of the high-velocity group is of value. A total of 32 stars have space velocities of 65 km/sec or larger. For each of these stars the component in the galactic plane was computed, with the galactic pole taken as $\alpha = 12^h40^m$, $\delta = +28°$. Table 3 lists the 24 stars for which this component is 65 km/sec or more. Successive columns give the HD number; the luminosity number, $L$; the component of $W$ in the galactic plane, $G$; and the galactic longitude toward which the component is directed.

None of the 24 stars in Table 3 has its velocity vector $G$ directed between galactic longitudes 347° and 121°, i.e., none is within 66° of galactic longitude 55°, the direction of galactic rotation in the solar neighborhood. This is in accord with the known avoidance of this direction by high-velocity stars. Two of the stars in Table 3, HD 144287 and HD 212943, have been listed previously as high-velocity stars (Miczaika 1940).

## CONCLUSIONS

Relative luminosity functions and individual space motions have been deduced from spectroscopic parallax data for 227 stars, obtained with the help of an oscilloscopic microphotometer. The luminosity functions have a pronounced minimum in the region of the subgiants, and an examination of all pertinent assumptions has shown that the effect must be real. It should be emphasized that the results apply to the narrow range in spectral type from G8 to K1.

A comparison of the luminosity function for the late G stars with the curve for the early K stars suggests that the frequency minimum is more pronounced for the late G stars. This conclusion is strongly dependent on the calibration which has been adopted to convert from luminosity numbers to absolute magnitude. This difference may have considerable evolutionary significance.

The determination of space velocities has revealed a number of suspected high-velocity stars which are listed in Table 3. While the accuracy of the space-velocity calculations is not sufficient to insure that all the stars of Table 3 are high-velocity stars (or that some other stars in Table 1 are not high-velocity stars), the magnitudes and directions of the motions in Table 3 indicate that a high proportion of these stars must be members of the high-velocity group. As such, their spectra deserve further study.

The writer wishes to express his thanks to Dr. W. W. Morgan and Dr. Daniel L. Harris III, of the Yerkes Observatory, for valuable suggestions on the classification criteria and the luminosity-function problem and for advice on the sources of apparent magnitude. He would also like to thank Dr. W. R. Hossack for his co-operation on the program with the oscilloscopic microphotometer and Dr. Donald A. MacRae for advice on the statistical methods employed. Finally, the author is indebted to Dr. John F. Heard for his helpful suggestions on all phases of the problem and for his general supervision of the research.

## REFERENCES

Barney, I. 1953, *Yale Trans.*, Vol. **24.**
Gratton, L. 1933, *B.A.N.*, **7,** 85.
Hossack, W. R. 1953, *J.R.A.S. Canada*, **47,** 195.
———. 1954, *Ap. J.*, **119,** 613.
Jenkins, L. F. 1952, *General Catalogue of Trigonometric Stellar Parallaxes* (New Haven: Yale University Observatory).
Johnson, H. L., and Morgan, W. W. 1953, *Ap. J.*, **117,** 313.
Keenan, P. C., and Keller, G. 1953, *Ap. J.*, **117,** 241.
Keenan, P. C., and Morgan, W. W. 1951, *Astrophysics*, ed. J. A. Hynek (New York: McGraw-Hill Book Co.), p. 23.
Miczaika, G. 1940, *A.N.*, **270,** 249.
Morgan, H. R. 1952, *Astronomical Papers American Ephemeris and Nautical Almanac*, Vol. **13,** Part III.
Müller, G., and Kempf, P. 1907, *Pub. ap. Obs. Potsdam*, Vol. **17.**
Oort, J. H. 1932, *B.A.N.*, **6,** 289.
Payne-Gaposchkin, C. 1937, *Harvard Mimeograms*, Ser. III, No. 1.
Roman, N. G. 1952, *Ap. J.*, **116,** 122.
Schlesinger, F., and Jenkins, L. F. 1940, *Catalogue of Bright Stars* (2d ed.; New Haven: Yale University Observatory).
Trumpler, R. J., and Weaver, H. F. 1953, *Statistical Astronomy* (Berkeley: University of California Press), p. 155.
Young, R. K. 1945, *Pub. David Dunlap Obs.*, **1,** 309.

# ELECTRON DENSITIES IN THE ORION NEBULA

DONALD E. OSTERBROCK
Mount Wilson and Palomar Observatories
Carnegie Institution of Washington, California Institute of Technology
*Received May 16, 1955*

## ABSTRACT

Measurements of the intensity ratio of the two components of the [*O* II] λ 3727 emission line at various points in the Orion Nebula are given. Since the variation of density in the nebula is indicated by the variation in surface brightness, the measurements are used to test the prediction of Seaton that the intensity ratio should vary with electron density. The conclusion is that the observations fit the theory well. The densities derived range from a high of $3 \times 10^4$ electrons/cm$^3$ at a point near the Trapezium to a low of $3 \times 10^2$ electrons/cm$^3$ at some of the faintest points observed in this investigation.

## I. INTRODUCTION

Seaton (1954*a*) has recently calculated the intensity ratio of the two components of the [*O* II] λ 3727 emission line as a function of electron density. Therefore, the measurement of this intensity ratio in a nebula, together with the use of his theoretical calculation, immediately gives the electron density in that nebula. This is a very simple and powerful method for determining the density in emission objects and will have wide application. However, the method is new, and the theoretical calculation of the variation of the intensity ratio with electron density should be checked in any way possible.

The present paper is concerned with such a check, made by observing the λ 3727 intensity ratio at many points in the Orion Nebula. It is well known that in this nebula there is a very steep decrease of surface brightness from the Trapezium outward, and it is therefore quite clear that the density falls sharply outward. Thus, although the absolute densities are not known, the qualitative run of densities is known, and therefore the way in which the intensity ratio should change going outward is known. Besides this check, a calculation is made of the electron densities at various points in the nebula for which there are observed values of the λ 3727 intensity ratio.

## II. THEORY

The [*O* II] line λ 3727 consists of the two components λ 3726.05 and λ 3728.80 (Bowen 1955), arising from transitions from the upper $^2D_{3/2}$ and $^2D_{5/2}$ states, respectively, to the ground $^4S_{3/2}$ state. In emission nebulae the *O* II ions are excited from the ground state to the upper states by collisions with electrons, and so the excitation conditions and therefore the ratio of intensities of the two components depend on the electron density. At very low densities the time between collisions is very long, and every ion that reaches an excited state by a collision is almost certain to lose its energy by radiating a photon before it has another collision. Under these circumstances the ratio of intensities of the two components is proportional to the ratio of excitation cross-sections and is λ 3729/λ 3726 = 1.5. (This fractional symbol will be used throughout the present paper to mean the ratio of the intensity of λ 3728.80 to the intensity of λ 3726.05.) On the other hand, at very high densities the time between collisions is very short, and an ion enters and leaves the excited state by collisions many times before it radiates a photon. Under these circumstances the ratio of intensities of the two components is the same as in thermodynamic equilibrium and is λ 3729/λ 3726 = 0.47. At intermediate

densities the intensity ratio varies between these limits. The detailed form of the variation, according to Seaton (1954*a*), is

$$\frac{\lambda\,3729}{\lambda\,3726} = 1.5\,\frac{1+3.3x}{1+10.5x}, \tag{1}$$

where $x = 10^{-2}N_e/T^{1/2}$, in terms of the electron density $N_e$ and temperature $T$.

The foregoing expression was derived by using numerical values of the transition probabilities computed by Garstang (1952) and a numerical value of the $^4S$–$^2D$ excitation cross-section computed by Seaton (1953). The cross-section for the $^2D_{3/2}$–$^2D_{5/2}$ process, which also enters the formula for the intensity ratio, was not computed, but instead an estimated value was used. An improved value of this cross-section may be expected to alter somewhat the relation between intensity ratio and electron density but will not change its general form.

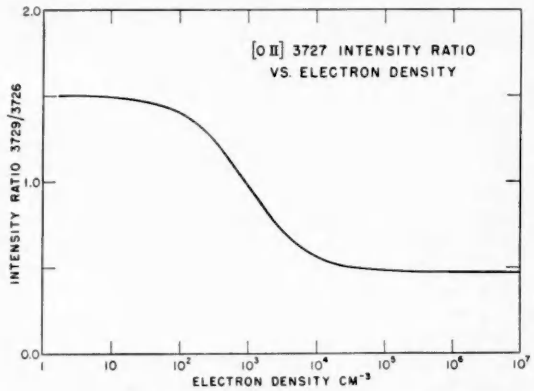


FIG. 1. Variation of λ 3729/λ 3726 intensity ratio with electron temperature at 10,000° K

A conventional value of the temperature of 10,000° will be used in the present paper for computing densities from intensity ratios by expression (1). The theoretical calculations summarized by Spitzer (1954) show that the temperature in an *H* II region must be in the general neighborhood of this value. In addition, there is a determination of the temperature in the Orion Nebula from a comparison of the intensities of the [*O* III] nebular and auroral lines. This calculation was first made by Aller (1946), who obtained a value of 10,500° by using the older computations of the excitation cross-sections; it was repeated by Seaton (1954*b*), who, attempting a correction for interstellar obscuration and using the newer values of the cross-sections, obtained a value of 13,000°. Both authors used the intensity measures of Wyse (1942), which refer to a bright region near the Trapezium. Thus the use of a value of 10,000° for the temperature seems safe, particularly as the percentage error in the electron density is only half the percentage error in the temperature.

Figure 1 shows the variation of the λ 3729/λ 3726 intensity ratio with electron density, calculated from equation (1) with an assumed temperature of 10,000°. According to this curve, the intensity ratio should be the smallest, but not less than 0.47, in the central, brightest, densest regions of the Orion Nebula and should increase in the outer, fainter, less dense regions, but not to a value greater than 1.5.

The previous photometric work on the λ 3729/λ 3726 intensity ratio was done by Aller, Ufford, and Van Vleck (1949). They observed a number of bright planetary nebulae, which are relatively high-density objects, and the λ 3729/λ 3727 intensity ratios clustered near 0.5, in agreement with the theoretical expectation. The intensity ratios measured for the two objects, NGC 40 and IC 4593 were 0.84 and 0.67, respectively, significantly larger than the mean; these objects, as Aller *et al.* (1949) pointed out, are two of the three objects of lowest surface brightness (and hence statistically of lowest density) in their list.

No observations of the [*O* II] λ 3729/λ 3726 intensity ratio larger than 0.84 have previously been published. However, *S* II has an electronic structure similar to that of *O* II, except that the sulphur ion has one more closed shell, and Seaton's (1954*a*) calculations predict that the intensity ratio of the red [*S* II] lines λ 6717 and λ 6731 changes with density in a fashion similar to that of the intensity ratio of the [*O* II] lines λ 3729 and λ 3726. Published data show this effect in *S* II, for in bright planetaries, which are relatively high-density objects, λ 6731, analogous to λ 3726 of *O* II, is stronger (Wyse 1942), while in *H* II regions, which are relatively low-density objects, λ 6717, analogous to λ 3729 of *O* II, is stronger (Johnson 1953).

## III. OBSERVATIONS

The observations of the present paper were made with the Newtonian-focus spectrograph of the 100-inch telescope. The plates were taken in the fifth-order ultraviolet with an *F*/1.5 camera, giving a dispersion of approximately 66 A/mm at λ 3727. The slit was opened so that its projected width on the plate corresponded to about 1.8 A, in order to make the line profile as flat-topped as possible. All the exposures were taken on Kodak IIa-O plates, with exposure times ranging from 50 seconds to 90 minutes.

The photometric calibration was provided by step-strip plates, taken with the calibration optics of the 100-inch telescope coudé spectrograph. Each calibration plate was taken from the same box as the nebular plate with which it was used, exposed for a time not different by more than a factor of 3 from the exposure time of the nebular plate, and developed with it. The plates were traced with the recording microphotometer of the California Institute of Technology at a magnification of either nine hundred or eighteen hundred times. The peak intensities of the two components were measured to get the λ 3729/λ 3726 intensity ratios. Tracings of comparison lines and also calculations according to the formula of van Cittert (Unsöld 1938) agreed in showing that the intensity of one component at this point is not appreciably affected by the wing of the other component.

Observations were made at the sixteen points identified in Table 1. In this table the first column gives the letter identifying the point; the second column gives a reference star; the third and fourth columns give the co-ordinates of the center of the slit in minutes of arc, measured north and east, respectively, from this star; and the fifth column gives the position angle of the slit. These slit positions are shown marked on three different direct exposures of the Orion Nebula in Figure 2. The slit length was 3 mm or 48″ in all cases, but at points *A*, *B*, *D*, and *F* the structure of the nebula is so patchy that a length of only about 20″ was measured on the plate. At points *T*, *V*, *W*, *X*, and *Y* the slit was trailed back and forth over a length of about 90″ during the exposure, and the measured value of the λ 3729/λ 3726 ratio refers to an average value over this length, while at the other points the slit was held fixed with respect to the nebula.

The sixth column of Table 1 gives the mean value of the measured λ 3729/λ 3726 ratio for each point; the seventh column gives the average deviation, without regard to sign, of a single plate from this mean; and the eighth column gives the number of plates measured. Finally, the last column gives the approximate distance of the point from the center of the Trapezium.

## IV. INTERPRETATION

Table 1 shows that there is good correlation of the λ 3729/λ 3726 intensity ratio with distance from the Trapezium, and a comparison of Table 1 and Figure 2 shows that this is at the same time a correlation of the intensity ratio with surface brightness. The smallest λ 3729/λ 3726 intensity ratio measured is 0.50, a little larger than the theoretical lower limit of 0.47, while the largest ratios measured are 1.24 and 1.26, well below the upper limit of 1.50. Point *P* deviates from the relationship between λ 3729/λ 3726 and surface brightnesss; but this is obviously due to the fact that it is in a region of extremely heavy absorption. Point *Z* has an intensity ratio somewhat smaller than either its surface brightness or its distance from the Trapezium would suggest; it is a point along the front which bounds NGC 1976 to the north and which may thus be a thin region of higher density.

TABLE 1

λ 3729/λ 3726 INTENSITY RATIOS IN THE ORION NEBULA

| POINT | REFERENCE STAR | SLIT | | P.A. | $\frac{\lambda\ 3729}{\lambda\ 3726}$ | A.D. | $n$ | DISTANCE FROM TRAPEZIUM |
|---|---|---|---|---|---|---|---|---|
| | | North | East | | | | | |
| *A* | $\theta_1$ Ori B | −0′.5 | −0′.4 | 140°.7 | 0.50 | 0.02 | 3 | 0′.6 |
| *B* | $\theta_2$ Ori A | +0.5 | −0.1 | 33.0 | 0.61 | .03 | 3 | 1.9 |
| *D* | −5°1318 | +0.4 | +0.7 | 90.0 | 0.77 | .02 | 3 | 2.6 |
| *F* | −5°1318 | −0.1 | +1.1 | 90.0 | 0.76 | .04 | 2 | 2.6 |
| *H* | Bond 335 | +0.1 | +0.8 | 0.0 | 1.24 | .03 | 3 | 14.0 |
| *J* | Bond 449 | −0.4 | 0.0 | 90.0 | 1.17 | .00 | 3 | 9.3 |
| *K* | Bond 363 | +3.0 | 0.0 | 90.0 | 1.05 | .03 | 4 | 13.5 |
| *M* | Bond 335 | −2.4 | −0.8 | 90.0 | 1.26 | .05 | 3 | 16.3 |
| *P* | −5°1326 | +2.9 | +0.6 | 90.0 | 0.92 | .02 | 2 | 3.3 |
| *R* | −5°1325 | −0.3 | −0.7 | 90.0 | 0.96 | .02 | 2 | 7.6 |
| *T* | −5°1326 | +1.2 | −0.3 | 90.0 | 0.90 | .02 | 2 | 3.5 |
| *V* | $\theta_2$ Ori A | +1.1 | −0.5 | 90.0 | 0.64 | .02 | 2 | 1.1 |
| *W* | $\theta_1$ Ori B | −0.4 | −0.6 | 90.0 | 0.55 | .02 | 2 | 0.7 |
| *X* | $\theta_1$ Ori B | +0.5 | −0.6 | 90.0 | 0.58 | .00 | 2 | 1.0 |
| *Y* | Bond 635 | +0.4 | −0.5 | 90.0 | 0.74 | .00 | 2 | 1.9 |
| *Z* | Bond 423 | −2.3 | 0.0 | 90.0 | 0.96 | 0.03 | 2 | 14.2 |

The highest density found from these λ 3729/λ 3726 ratios is a value of approximately $3 \times 10^4$ electrons/cm$^3$ at point *A*. Strömgren (1951) has determined a density of between $10^3$ and $10^4$ hydrogen atoms/cm$^3$ at the center of the Orion Nebula by measuring the absolute intensity of *Hβ*. His measurement refers to an average over a diameter of 1′.3 and thus is probably roughly comparable with the point *W*, for which the density of $1 \times 10^4$ electrons/cm$^3$ is found in the present investigation. The lowest density found from the λ 3729/λ 3726 ratios in the Orion Nebula is approximately $3 \times 10^2$ electrons/cm$^3$ at points *H* and *M*. It should not be concluded from Table 1 that the λ 3729/λ 3726 ratio does not become larger than 1.26; the outermost, faintest, least dense parts of the Orion Nebula were not observed in the present investigation. On the contrary, observations to be reported in detail later show the λ 3729/λ 3726 intensity ratios in *H* II regions such as NGC 281 and NGC 7000 to be much closer to the theoretical low-density limit of 1.50.

The conclusion may be drawn that the observations of the λ 3729/λ 3726 intensity ratio in the Orion Nebula fit the theory of Seaton (1954*a*) well. The densities derived

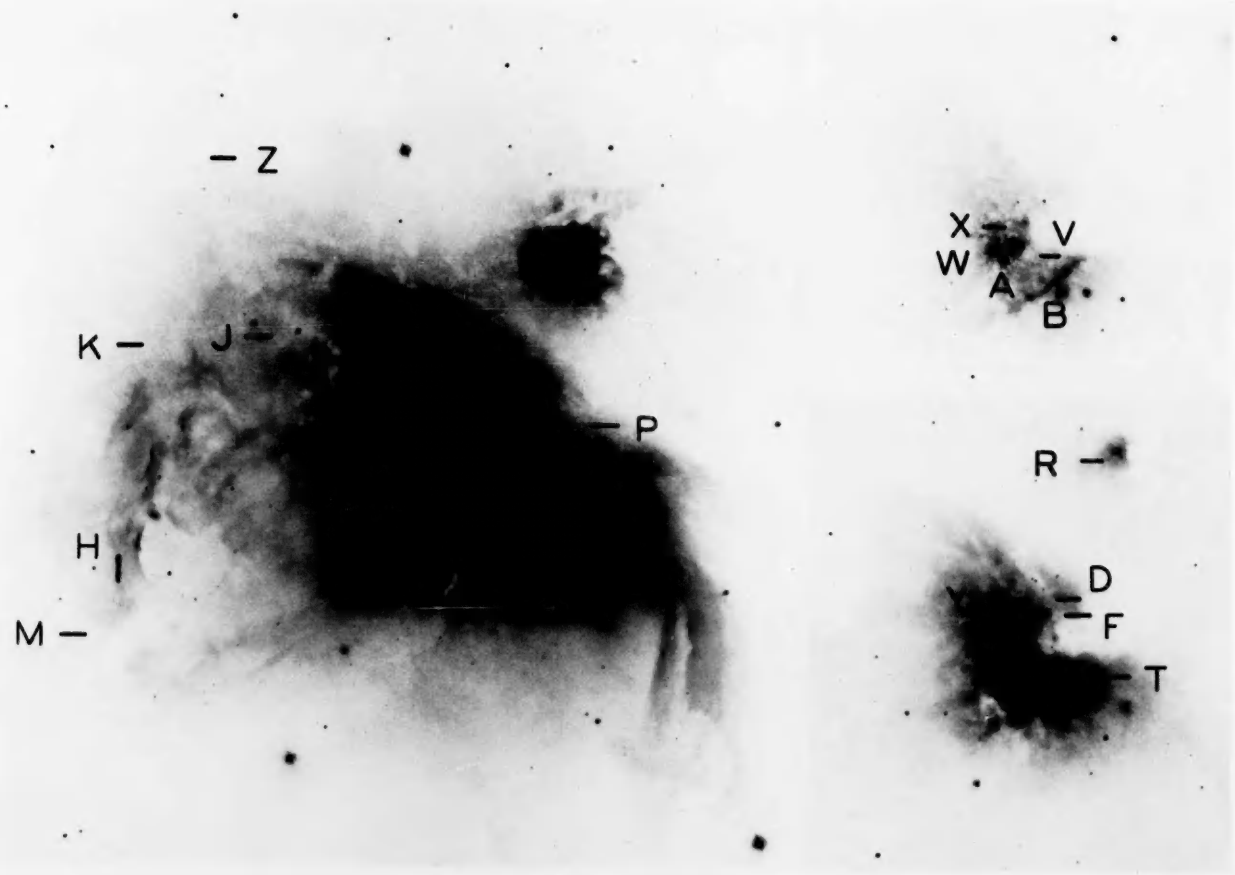


FIG. 2.—Three exposures of the Orion Nebula with slit positions marked. (Scale 15″ per mm)

from it range from a high of $3 \times 10^4$ electrons/cm$^3$ at a point near the Trapezium to a low of $3 \times 10^2$ electrons/cm$^3$ at some of the faintest points observed in this investigation.

## REFERENCES

Aller, L. H. 1946, *Pub. A.S.P.*, **58**, 165.
Aller, L. H., Ufford, C. W., and Van Vleck, J. H. 1949, *Ap. J.*, **109**, 42.
Bowen, I. S. 1955, *Ap. J.*, **121**, 306.
Garstang, R. H. 1952, *Ap. J.*, **115**, 506.
Johnson, H. M. 1953, *Ap. J.*, **118**, 370.
Seaton, M. J. 1953, *Proc. R. Soc. London, A*, **218**, 400.
———. 1954*a*, *Ann. d'ap.*, **17**, 74.
———. 1954*b*, *M.N.*, **114**, 154.
Spitzer, L. 1954, *Ap. J.*, **120**, 1.
Strömgren, B. 1951, *Problems of Cosmical Aerodynamics* (Dayton: Central Air Documents Office), p. 7.
Unsöld, A. 1938, *Physik der Sternatmosphären* (Berlin: J. Springer), p. 210.

# THE PHOTOELECTRIC PHOTOMETRY OF PLANETARY NEBULAE*

WILLIAM LILLER
The Observatory, University of Michigan, Ann Arbor, Michigan
*Received November 20, 1954; revised April 1, 1955*

## ABSTRACT

The surface brightnesses of fourteen planetary nebulae and the lower limits of the magnitudes of their exciting stars have been determined photoelectrically. Both narrow-band interference filters as well as conventional glass and gelatin filters were used to sort out the desired nebular and central-star radiations. The nebular surface brightnesses are in excellent accord with the results of Liller and Aller, but all indications are that the photographic magnitudes compiled by Berman are systematically too bright. However, the central-star magnitudes listed by Berman are generally in accord with the photoelectric observations reported here.

## I. INTRODUCTION

Photographic determinations of the brightnesses of planetary nebulae, both of the intensities of single monochromatic emissions and of the integrated magnitudes of the objects on the International system, have never been completely satisfactory. Because the photographic technique is not well suited to the measurement of the integrated brightness of an extended object, accurate intensities of planetary nebulae can be achieved only through tedious reductions of many microphotometer tracings. Furthermore, the presence of a central star can introduce an additional source of error unless care is taken. The magnitudes of the central stars themselves are difficult to measure photographically, because the stellar image is usually imbedded in the nebula, and abnormally high background density produced by the nebula makes intercomparison between the central star and other stars of known magnitude rather difficult.

The photoelectric photometer, with its ability to compare accurately the intensity of an extended object with that of a star, should be able to measure the nebular and central-star brightnesses more quickly and with higher precision than photographic techniques can. Instead of measuring the visual or photographic magnitude of the nebula, it seems preferable to determine the intensity of the nebula in the light of one or more of the stronger monochromatic radiations. Since the relative intensities of the nebular lines have been measured by a number of investigators (Plaskett 1928; Bowen and Wyse 1939; Aller 1941, 1951; Wyse 1942; Liller and Aller 1954; Bowen, Minkowski, and Aller 1955; Minkowski and Aller 1955), the brightnesses of all the lines can then be expressed in the same units, or, if preferred, the magnitudes of the nebulae can be computed.

Of all the nebular emissions from the planetaries, the [*O* III] pair at λ 4959 and λ 5007 is usually the brightest. Initial calculations made with approximate color response-curves for photomultipliers indicated that for most planetaries one should expect the greatest deflection from these oxygen lines. To isolate the green nebular radiations, either filters or a spectrograph can be used. A filter, besides eliminating the problem of overlapping images in slitless spectra, is small and simple to use. A narrow pass band is to be preferred, so that as few as possible of the neighboring radiations may be admitted to the photocell. Furthermore, a narrow-band filter will admit less continuous radiation from both the central star and the nebula.

Since the relative intensities of the emission lines and of the continuous radiation (Page 1936, 1942; Minkowski and Aller 1955) are known for most of the brighter planetaries, it is an easy matter to correct for the unwanted nebular radiations. But the rela-

* This paper is based in part on the author's thesis of the same title (Ann Arbor: University of Michigan Microfilms, 1953).

tive strength of the star's radiation with respect to the nebular radiation is not known accurately. Because of the small size of the majority of planetaries, there is little possibility of using a very small diaphragm to eliminate the light from the nebula and to measure the radiation from the star alone. It is possible, however, to measure the radiation of the star over a rather large spectral interval to the long-wave-length side of the [*O* III] pair, for there are usually no strong nebular radiations between λ 5007 and *Hα* at λ 6563. Then, knowing the approximate temperatures of the central stars and the amount of interstellar reddening, one should be able to calculate the brightness of the central star as seen through the interference filter.

## II. THE EQUIPMENT

The photometer that was used in this investigation was designed by the author and was constructed by Mr. Frank Ferris and the author in the Observatory shop. It employs a single lens just behind the filters to image the telescope objective on the cathode of an RCA 1P21 photomultiplier. The phototube output is fed into a d.c. amplifier, similar to the one described by Valley and Wallman (1948) but modified slightly by H. L. Johnson and A. E. Whitford. The amplified signal is relayed to a Brown recording potentiometer. To insure that an equal response was received from every point in the field of view, tracings were frequently made of a star drifting slowly across the largest of the circular diaphragms employed.

TABLE 1

FILTER COMBINATIONS AND OBSERVED RADIATIONS

| λ-Region | Source of Radiation | Filters |
|---|---|---|
| 4900–5050 A | Nebular [*O* III] lines | S-1392<br>Wratten 40<br>Schott GG7, 2 mm |
| 5100–6000 A | Central star | Wratten 40<br>Wratten 15 |

Dr. Robert R. McMath kindly made available the Francis C. McMath 24-inch Cassegrain reflector for this work. Its 600-inch focal length (*f*/25) provides an ideal scale of 14″/mm at the focus.

## III. SPECTRAL CHARACTERISTICS OF THE FILTERS AND PHOTOMULTIPLIER

The wave-length regions chosen for this investigation, the radiations that were measured there, and the filter combinations selected to isolate each spectral band are listed in Table 1. The S-1392 filter, loaned by Dr. A. F. Turner, of the Bausch and Lomb Optical Company, is an all-dielectric, multilayer interference filter with a half-width of only 35 A and with a maximum transmission of 81 per cent at λ 4985. The wave length of maximum transmission is almost exactly halfway between the two oxygen lines, and some light of only one other strong line—*Hβ* at λ 4861—is transmitted. As in all interference filters, there are other regions of high transmission. However, they are far enough from the narrow transmission band that conventional glass and gelatin filters can be used to eliminate them.

The transmission-curves of both the filter combinations were obtained with a Littrow prism spectrometer temporarily mounted in the 70-foot McGregor Tower of the McMath-Hulbert Observatory. The sun was used both as a light-source and as a wave-length standard. The spectrometer gave a dispersion of approximately 3 A/mm at

5000 A, and it was possible to set within 0.2 or 0.3 A of a desired wave length. It was necessary to use this high-dispersion equipment because of the extremely steep slope of the transmission-curve of the green interference filter. The transmission-curve was determined shortly after the beginning of the program. After the observations were completed, several points on the curve were remeasured, to make certain that no change in the physical properties of the filter had taken place. The two sets of measurements agreed, on the average, with an accuracy of 1 per cent of the measured values, corresponding to 0.01 mag.

Because of the steepness of the transmission-curve of the green interference filter in the vicinity of the wave lengths of the green nebular lines of oxygen ($1\frac{1}{2}$ per cent per angstrom), the Doppler shifts produced by the high velocities of the planetary nebulae relative to the earth are often large enough to shift the positions of the green oxygen lines to wave lengths where the transmission values of this filter differ appreciably from the transmission values at the normal wave lengths of the [*O* III] lines. Indeed, the line displacements caused by the motion of the earth around the sun are at times large enough to be of importance. The necessary wave-length corrections were derived from the radial velocities of the planetary nebulae determined by Campbell and Moore (1918) and by O. C. Wilson (1950).

Actually, the velocities of expansion of the nebular shells and the turbulent motions within the nebulae usually are sufficiently large to produce significant wave-length shifts. Since there is no way to correct for these motions, we must assume that the high transparency of these objects in the visible regions of the spectrum allows us to see to all parts of the nebulae and that the various velocity components of the material will average out as a whole.

To determine the spectral response-curve of the photomultiplier plus the transmission properties of the telescope and photometer optics, the spectrum of Vega was traced at varying zenith distances with the photometer mounted in its usual position at the focus of the 24-inch Cassegrain. The dispersion was provided by a 4-inch, 12° prism which was clamped to the upper end of the 24-inch tube. The transmission-curve of this prism was kindly provided by the Perkin-Elmer Corporation. The resulting spectrum had a dispersion of approximately 14 A/mm at $H\beta$, and the resolving power was sufficient to resolve the Balmer lines in the spectrum of Vega to $H\theta$. The spectral response-curve was then derived by comparing these tracings with the spectral intensity-curve of Vega measured photographically by Williams (1939).

The color response of the photometer plus telescope was determined on three nights during the time the observations were being made. The first two nights were separated by nearly two months; the last pair of nights were one month apart. The average probable error of a relative response value was calculated for each of the nights; they were, respectively, $\pm 0.019$, $\pm 0.040$, and $\pm 0.024$ mag. These are internal probable errors and do not include the errors in the determination of either the prism transmission or the intensity-curve of the spectrum of Vega.

There was a significant systematic shift in photometer response toward the blue during this time. Compared to the sensitivity at $\lambda$ 5000, the response at $\lambda$ 4040 increased at an average rate of 0.10 mag. per month. The sensitivity redward of $\lambda$ 5000 decreased accordingly. A shift of this type was observed by Stebbins, Whitford, and Johnson (1950). Their phototube likewise became more blue-sensitive, but at a slower rate than the phototube used here.

With both the filter transmission-curves and the relative response-curves of the photometer known, it is possible to calculate the relative sensitivities of the two color systems at any wave length. These curves are, of course, a function of time also.

Figure 1 shows the final response-curves of the spectral regions investigated, together with the relative line intensities of the planetary nebula NGC 2392, as measured by Minkowski and Aller (1955). A third pass band in the violet, which was used in an attempt to measure the colors of the central stars, is also shown (see Sec. X).

## IV. THE COMPARISON STARS

Ambarzumian (1933) has described a method by which the observed brightness of a monochromatic nebular image can be converted into suitable units of intensity. Briefly, it involves observing the spectrum of a planetary nebula with a wide-slit spectrograph (or narrow-band filter) and comparing the intensity of a monochromatic image with that of 1 A of the spectrum of a solar-type star at the same wave length.

Ideally, the spectral type and luminosity of all the comparison stars should be identical with that of the sun, namely, G2 V (Morgan, Keenan, and Kellman 1943). However, it is not always possible to fulfil these requirements, especially since the narrowness of the green interference filter makes it necessary to have bright comparison stars. It was decided to choose stars with spectral types within the range G0–G4 and with class V luminosities. Since all the comparison stars which were eventually selected are brighter than the eighth magnitude, it is certain that any effects of interstellar reddening are negligible.

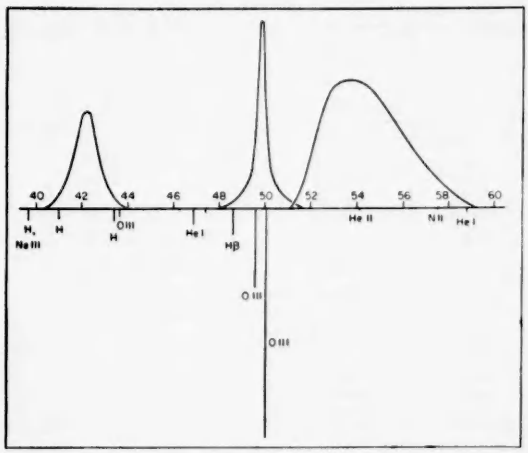


FIG. 1.—The relative instrumental response with the three filter combinations. The lower part of the diagram gives the relative nebular line intensities of NGC 2392 (Minkowski and Aller 1955).

A total of thirteen comparison stars was chosen. The magnitudes and colors of five of these have been determined photoelectrically by Johnson and Morgan (1953). The magnitudes and colors of the remaining stars have been measured only photographically. Therefore, it was necessary to observe photoelectrically these nine comparison stars, so that accurate photometry would be possible. The filters that were used in this two-color photometry were Schott filters BG12, 2 mm thick, for the blue, and GG7, 2 mm thick, for the yellow. These filters are the same as those used by Stebbins, Whitford, and Johnson (1950) in their work on three selected areas, except that the blue filter used here is twice as thick. The three brightest stars in SA 61 and the five Johnson and Morgan stars served as standards, all colors and magnitudes being reduced to the International ($P$, $V$) system. All the two-color photometry of the comparison stars was carried out during one night. Table 2 lists the comparison stars, their positions, spectral types, and the values of $P$ and $P - V$. The spectral types are those listed by Morgan, Keenan, and Kellman (1943), McCuskey (1949), McCuskey and Seyfert (1950), Roman (1950), and Wilson and Joy (1950). The average probable error of a value of $P$ is close to $\pm 0.03$, while that of a $P - V$ value is $\pm 0.01$.

In addition to this two-color photometry, the comparison stars were observed in the green at the time the nebular observations were being made. Since we are interested in the relative intensities of these stars and of the sun primarily in this spectral region, a green magnitude was defined for each of the comparison stars such that

$$G = \tfrac{1}{2}(P+V)\,. \tag{1}$$

These magnitudes were found to be quite consistent with the green deflections of the comparison stars. The use of green magnitudes rather than of $P$ or $V$ values in the final reductions should minimize the errors arising from the use of G-type stars having slightly different colors. Column 7 of Table 2 gives the values of $G$ for the comparison stars.

The magnitudes of three of the comparison stars were based entirely upon their green deflections. The $P$ and the $P - V$ values of these three stars are omitted from Table 2.

TABLE 2

THE COMPARISON STARS

| Star (1) | R.A. (1950) (2) | Dec. (1950) (3) | Sp. (4) | $P$ (5) | $P - V$ (6) | $G$ (7) |
|---|---|---|---|---|---|---|
| HR 3750 | 9h25m | − 5°8 | dG2 | ..... | ..... | 5.80 |
| λ Ser* | 15 44 | + 7.7 | dG2 | 4.91 | 0.48 | 4.67 |
| 72 Her* | 17 19 | +32.5 | dG2 | 5.89 | .50 | 5.64 |
| 26 Dra* | 17 35 | +62.0 | dG2 | 5.72 | .49 | 5.47 |
| HD 171746 | 18 34 | +16.9 | dG0 | 6.67 | .42 | 6.46 |
| HD 176377 | 18 57 | +30.1 | dG0 | 7.29 | .45 | 7.06 |
| HD 179957*† | 19 11 | +49.8 | dG5 | 6.44 | .54 | 6.17 |
| 179958*† | | | dG3 | | | |
| HD 182407 | 19 22 | + 5.4 | dG0 | ..... | ..... | 7.99 |
| HD 185269 | 19 35 | +28.4 | dG2 | ..... | ..... | 6.93 |
| HD 197488 | 20 41 | +45.6 | dG2 | 8.09 | .46 | 7.86 |
| HD 208704 | 21 56 | −12.9 | dG2 | 7.77 | .48 | 7.53 |
| 51 Peg* | 22 55 | +20.5 | dG0 | 6.10 | .57 | 5.82 |
| HD 218209 | 23 03 | +68.2 | dG3 | 8.01 | 0.51 | 7.75 |

* Standard star.

† Both stars measured together.

The apparent visual magnitude of the sun was taken as −26.87, which is the mean of the determinations by Kuiper (1938) and by de Vaucouleurs (1949). If we assume from its spectral type that $P - V = +0.50$ for the sun, the green magnitude of the sun will be −26.62.

## V. CONTRIBUTIONS OF THE CENTRAL STARS

As we have already pointed out, we must in some way determine the approximate color of the central star of each nebula measured with a base line defined by the effective wave lengths of the green and yellow sensitivity systems. Since there has been little published on the observed energy distributions of these objects, it remains to calculate the relative emergent fluxes of each central star at these two effective wave lengths and to estimate the effects of interstellar reddening.

In the calculation of the emergent fluxes, which will be described elsewhere, I assumed that the effective temperatures of the stars were equal to the Zanstra (1931) temperatures as determined by Berman (1937), except for those stars for which the temperature has been estimated from their spectra (Aller 1948; Aller and Wilson 1954). A model atmosphere and the resulting emergent flux were computed for one star, following the work

of Underhill (1951). The two parameters necessary for this calculation—the surface temperature and the logarithm of the surface gravity—were taken to be 35,000° K and 5.000, respectively. The latter value was found by Aller (1948) to be typical of planetary nuclei. The net integrated flux of this model star corresponds to 44,900° K, but the color temperature in the photovisual region of the spectrum is close to 57,000° K. In other words, for this particular star the color temperature is 1.27 times greater than the effective temperature. This relation between the two types of temperatures was used to find the color temperatures of all the central stars.

Two methods have been used by other investigators to estimate the amount of interstellar reddening. Berman (1936), assuming that interstellar reddening varied as $\lambda^{-2.2}$, deduced the color excesses for many of the planetaries from their distances, which he also derived (Berman 1937). Aller (1951) compared the theoretical and the observed Balmer decrements for several of the planetary nebulae and, assuming the absorption proportional to $\lambda^{-1}$, evaluated the quantity $C$, defined by the equation

$$\log \frac{I_n}{I_4} = \log \frac{I_n^0}{I_4^0} - C\left(\frac{1}{\lambda_n} - \frac{1}{0.4681}\right), \tag{2}$$

where $I_n/I_4$ is the observed intensity of the $n$th Balmer line with respect to $H\beta$ and $I_n^0/I_4^0$ is the intrinsic value of this quantity. Berman's values of interstellar reddening

TABLE 3

ADOPTED VALUES OF INTERSTELLAR REDDENING

| Nebula | $C$ | Nebula | $C$ |
|---|---|---|---|
| NGC 40 | 0.24 | NGC 6720 | 0.10 |
| NGC 2392 | .05 | BD+30°3639 | .50 |
| NGC 3242 | .11 | NGC 6818 | .19 |
| IC 4593 | .09 | NGC 6826 | .10 |
| NGC 6210 | .12 | NGC 7009 | .10 |
| NGC 6543 | .12 | NGC 7027 | .48 |
| NGC 6572 | 0.16 | NGC 7662 | 0.18 |

seem to be impaired by the use of an incorrect absorption law and of poorly known distances. However, he has determined the relative Balmer line intensities from the available spectrographic plates in the Lick Observatory collection. From his 1938–39 observations Aller has underestimated the intensities of the fainter images and has arrived at values of interstellar reddening that appear to be systematically too large.

For the present purpose I evaluated the quantity $C$ by the method employed by Aller but used observed Balmer line strengths published by Berman (1936). These values, calculated with the aid of equation (2) for the fourteen planetary nebulae that were ultimately chosen for study, are listed in Table 3.

Finally, it is necessary to know the effective wave length of the two color systems. For the green region it is clear, because of the narrowness of the interference-filter pass band, that the value of $\lambda_{\text{eff}}$ is very near $\lambda$ 4985, the wave length of maximum transmission. However, the broadness of the yellow filter combination makes it necessary to calculate the effective wave length from the relation given by Seares and Joyner (1943),

$$\lambda_{\text{eff}} = \frac{\Sigma \lambda s y}{\Sigma s y}, \tag{3}$$

where $s$ is the sensitivity of the system and $y$ is the relative intensity of the source at $\lambda$. The effective wave length was calculated with four different sets of values for $y$. The first two correspond to black-body sources with temperatures of 20,000° and 80,000° K. Then these two sources were "reddened" by an amount defined by equation (2) with the parameter $C = 0.50$. Both the temperatures and the values of $C$ (0.50 and 0.00) bracket the extremes of color temperature and space reddening of most of the central stars of the planetary nebulae on the observing list. Table 4 shows the effective wave lengths of the yellow sensitivity system for the four artificial sources. The small change in $\lambda_{eff}$ indicates clearly that the energy-curves of very hot objects, such as planetary nuclei, do not differ

TABLE 4

EFFECTIVE WAVE LENGTHS OF YELLOW SENSITIVITY SYSTEM

| $T_c$ (° K) | $C$ | $\lambda_{eff}$ (A) | $T_c$ (° K) | $C$ | $\lambda_{eff}$ (A) |
|---|---|---|---|---|---|
| 20,000..... | 0.00 | 5431 | 20,000..... | 0.50 | 5438 |
| 80,000..... | 0.00 | 5433 | 80,000..... | 0.50 | 5440 |

TABLE 5

EFFECTIVE AND COLOR TEMPERATURES OF THE CENTRAL STARS

| Nebula | $T_e$/1000 | $T_c$/1000 | $I_0/I_y$ |
|---|---|---|---|
| NGC 40..... | 35 | 45 | 1.25 |
| NGC 2392..... | 34* | 44 | 1.35 |
| NGC 3242..... | 35 | 45 | 1.32 |
| IC 4593..... | 33.4* | 42 | 1.32 |
| NGC 6210..... | 32† | 40 | 1.31 |
| NGC 6543..... | 35 | 45 | 1.32 |
| NGC 6572..... | 45 | 57 | 1.30 |
| NGC 6720..... | 70 | 89 | 1.34 |
| BD+30°3639..... | 25 | 32 | 1.12 |
| NGC 6818..... | 70 | 89 | 1.29 |
| NGC 6826..... | 32† | 40 | 1.32 |
| NGC 7009..... | 50 | 63 | 1.34 |
| NGC 7027..... | 80 | 101 | 1.16 |
| NGC 7662..... | 55 | 70 | 1.30 |

* Temperature determined by Aller (1948).
† Temperature determined by Aller and Wilson (1954).

greatly in the visual region, even over large temperature ranges. Therefore, a mean value of 5435 A for the effective wave length of the yellow sensitivity-curve was adopted. Table 4 lists the effective wave lengths to the nearest angstrom. Equation (3) certainly cannot be expected to give this precision, but the wave-length differences of Table 4 are of the right order of magnitude.

Having color temperatures and color excesses for all the central stars, one can easily compute the relative intensities of these objects at the effective wave lengths of the two color systems. In Table 5 are listed the adopted values of the effective temperatures, the computed color temperatures, and, lastly, the ratios of the intensities of the central stars at the effective wave lengths of the two spectral regions. The effective temperatures are those given by Berman (1937), except when marked by an asterisk or a dagger.

## VI. METHOD OF REDUCTION

We should now be able to derive from the observations of each planetary the intensities of the [*O* III] emissions at λ 4959 and λ 5007. We should also be able to determine the brightness of the central star in the two colors. These data, coupled with the observations of the solar-type comparison stars in the green, will allow us to express the intensities of these sources of radiation in convenient absolute units, since the energy distribution in the solar spectrum—and, therefore, in the spectrum of any star of identical spectral type and luminosity—is well known.

The method used to reduce the photoelectric deflections can be best described by developing the equations appropriate to the observations. The following set of symbols will be used:

$D_\lambda$ = The value of a raw deflection in the wave-length region λ;

$I_\lambda$ = The intensity at a wave length λ (per unit wave length if a continous emission);

$s_\lambda$ = The sensitivity of the equipment at a wave length λ.

The objects observed will be denoted by

$n$ = Nebula,

$*$ = Central star,

$G$ = Solar-type comparison star.

The kind of nebular radiation will be designated by

$m$ = Monochromatic,

$c$ = Continuous.

The observed deflections from the planetary nebulae in both the colors will consist of contributions from both the nebula and the central star; thus

$$D_\lambda = D_\lambda(n, m) + D_\lambda(n, c) + D_\lambda(*). \tag{4}$$

This relation can be expanded as follows:

$$D_\lambda = a\Sigma I_\lambda(n, m)\, s_\lambda + a\int I_\lambda(n, c)\, s_\lambda d\lambda + b\int I_\lambda(*)\, s_\lambda dy, \tag{5}$$

where $a$ and $b$ are constants which must be determined for each planetary. The first two terms of equation (5) represent the contributions from the monochromatic and continuous nebular radiations, respectively; the last term takes account of the continuous radiation from the central star. Since the energy-curves of the central stars are generally smooth and the absorption and emission lines weak and since the green and yellow sensitivity-curves are nearly symmetrical, it is permissible, with little loss of accuracy, to write

$$\int I_\lambda(*)\, s_\lambda d\lambda = A_\lambda \bar{I}_\lambda(*). \tag{6}$$

Here $A_\lambda$ is the total area underneath the sensitivity-curve, and $\bar{I}_\lambda(*)$ is the value of $I_\lambda(*)$ at the effective wave length of the color system under consideration.

For each planetary, $D_\lambda$ is observed in each of the two colors. Therefore, equation (5) represents two independent equations. All the quantities on the right-hand side of this equation are known, and it is, in theory, a simple matter to calculate what the deflection would be from each individual source of radiation. The values of $I_\lambda(n)$ expressed in terms of the intensity of $H\beta$ were taken from Liller and Aller (1954) whenever possible,

since their work was done photoelectrically. Also, the results of Page (1936, 1942), Aller (1941, 1951), Bowen, Minkowski, and Aller (1955), and Minkowski and Aller (1955) were used. The values of the other terms have already been discussed.

Unfortunately, insufficient attention has been given to the photovisual spectra of most planetary nebulae, and accurate line intensities are available in this region of the spectrum for only five of the nebulae: NGC 40, 2392, and 7662 (Minkowski and Aller 1955); NGC 7027 (Bowen, Minkowski, and Aller 1955); and NGC 7009 (Aller 1941). The procedure for perhaps getting a more reliable set of intensities for each of the nine poorly observed objects was as follows: There is a fair correlation between the intensities of the yellow lines of each well-observed planetary and the intensities of the lines in the blue-violet spectrum produced by the same ion. Hence, by comparing the blue-violet spectrum of each of the poorly observed objects with the well-observed nebulae, it was possible to deduce the approximate intensities of each yellow line. This approximation should have little effect on the intensity measurements of the green nebular lines, but the accuracy of any calculations of the brightnesses of the central stars will be seriously impaired.

Measurements of the continuous spectra have been made by Page (1936, 1942) on all but four of the fourteen planetaries in the far violet, and the continuous radiation has been measured as far to the red as $\lambda$ 4800 for NGC 7662, 6572, and 7027. Minkowski and Aller (1955) have determined the relative intensities of the continua for NGC 40, 2392, 7027, and 7662 far into the red and have found that the intensity distribution of this source of radiation varies from nebula to nebula. However, the intensity variations with wave length are not too large. It was assumed that, for those planetary nebulae for which no data exist on the continuous spectra in the yellow, the continuum in this region of the spectrum was as bright as the mean intensity of the blue and violet continua. For those nebulae for which there is no information at all on their continuous spectra, the missing data were supplied by matching the monochromatic spectra as before. Again these approximations have a negligible effect on the intensity measurements of the green [*O* III] lines of most of the planetaries, but any brightness estimates for the central stars are further impaired.

In addition, we need to know the deflection from 1 A of the spectrum of the comparison star at the wave lengths of the green nebular lines. Knowing the energy-curve of the sun, we can calculate this quantity from the equation of proportionality:

$$D^1_\lambda (G) = \frac{D_\lambda (G)\ I_\lambda (G)\ s_\lambda\, \Delta\lambda}{\int I_\lambda (G)\ s_\lambda d\lambda}, \tag{7}$$

where $\Delta\lambda = 1$ A. The integral in this relation is carried out over the region of the spectrum admitted by the appropriate filter combination. All the foregoing equations apply, of course, to the deflections after the appropriate atmospheric corrections have been made.

## VII. THE OBSERVATIONS

Because of the faintness of even the brightest planetaries and since the central stars are even fainter, it was possible to include in the observing list only the brightest planetaries. In Berman's (1937) listing of the magnitudes of the nebulae and the central stars, there are eighteen objects north of declination $-35°$ with photographic magnitudes brighter than 10.0. Of these, thirteen were selected for their favorable location in the sky, for the absence of stars within the area covered by the nebulae, and for the existence of good data on the relative strengths of the nebular radiations. The remaining planetary, IC 4593, was selected because of its reportedly bright central star and because it is one of the brightest low-excitation nebulae.

All the observations were made during the spring and summer of 1952. Only the very best nights were used. Except for one planetary, NGC 6720, all deflections for any one

nebula and its comparison star were made with the same-sized diaphragm. So that there would be no possibility of cutting off some of the light from a nebula, photometer diaphragms were used which had diameters at least 10″ larger than the greatest nebular dimension quoted by Curtis (1918). Because of the faintness of the inner regions of NGC 6720 and its large angular diameter, it was possible to diaphragm out nearly all the nebular radiations and to measure the central-star brightness directly. For this nebula the comparison star was measured with both a large and a small diaphragm.

The use of a very narrow-band interference filter simplifies the atmospheric extinction corrections that must be applied to the observations. Because the effective wave length of this green filter can never change by more than a few angstroms—even with the wide variety of energy sources encountered in this program—it was not necessary to include terms in the extinction-correction equations which depended directly upon the color of the object. This simplification in the green was justified by the extinction-curves determined for three objects: HD 149881, an early B star; 72 Herculis, one of the G-type comparison stars; and NGC 6210.

In the yellow the filter combination half-width is much larger than in the green, but because the calculations of the nebular deflections in the yellow were not of high precision, the color of the nebula again was not included in the extinction equation. Except for these two simplifications, the atmospheric extinction was determined in the usual manner.

It is of interest to note that for NGC 6543, 6572, 6818, and 7662, the computed yellow deflection from the *nebula* was larger than the observed total deflection by an appreciable amount (more than 15 per cent). Although the yellow deflections were never large, the average deviations of these deflections were quite small. It seems, therefore, that the relative intensities of either the monochromatic emissions or the continuum as measured photographically are in error by at least 15 per cent. The contributions of the nebular continua to the yellow deflections of these nebulae were calculated to be several times larger than the contributions of the monochromatic radiations. Therefore, the source of this discrepancy seems to lie in the continuum intensity measurements, which are those of Page (1936, 1942). However, Page determined the continuum intensity on two different occasions in the far violet for NGC 7662, and the results are in fair agreement (13 per cent). Nevertheless, we must conclude that the continuum intensities listed by Page for these nebulae are in error and that they are too high by at least 15 per cent.

Even though there are no accurate data on the monochromatic and continuous radiation intensities for NGC 6720—the Ring Nebula in Lyra—the observations should be regarded as quite good. The relative intensities of the three lines included in the green deflection were taken as follows: $N_1 = 80$, $N_2 = 27$, $H\beta = 10$.

The photoelectric observations of BD + 30°3639, Campbell's shell star, are of interest. The monochromatic nebular intensities listed by Aller (1941) for this planetary were used in the green. The brightness of the continuum in the green and the intensities of both the monochromatic and the continuous radiations in the yellow were taken to be the same as NGC 40. The resulting value of $a$ (see eq. [5]) was negative, however, meaning that the calculated intensity of the nebula in the green is negative. This result clearly points out the need for more complete spectrophotometry of planetary nebulae. Furthermore, strong emission lines, which are much brighter than those of the nebula, are numerous in the spectrum of the central star, and until accurate spectrophotometry of these radiations is available, there is not too much information which can be derived from the present photoelectric observations.

## VIII. SURFACE BRIGHTNESSES OF THE NEBULAE

In deriving the surface brightnesses of the nebulae by Ambarzumian's method, I have taken from the work of Pettit (1940) the values of the emission of the sun per square sec-

ond of arc per angstrom unit at the wave lengths of the green nebular lines. Henceforth, the term "surface brightness," $S_\lambda$, will be used to designate the flux in ergs per square centimeter per second at the outer boundary of the nebula.

In Table 6 are listed the thirteen nebulae for which surface brightnesses were derived. Listed in addition are the surface brightnesses of four planetary nebulae which were measured photoelectrically by Liller and Aller (1954), who used a different technique. Column 2 gives the angular radii of the nebulae in seconds of arc, taken from the work of Curtis (1918). Column 3 tabulates the logarithms of the sums of the surface brightnesses of the $N_1$ and $N_2$ lines of [*O* III], and, for comparison, column 4 gives the values of this quantity which were found by Liller and Aller (1954), again photoelectrically. The next column lists the adopted values of log $(S_1 + S_2)$. The results of Liller and Aller are given half the weight of the present results, since their values of log $(S_1 + S_2)$ were derived with a less reliable method. Columns 6 and 7 list the logarithms of the surface

TABLE 6

SURFACE BRIGHTNESSES OF THE PLANETARY NEBULAE

| Nebula | $A$ | Liller log $(S_1+S_2)$ | Liller and Aller log $(S_1+S_2)$ | Adopted log $(S_1+S_2)$ | log $S_1$ | log $S_2$ | Liller log $S\beta$ | Menzel and Aller log $S\beta$ | Page and Greenstein log $S\beta$ |
|---|---|---|---|---|---|---|---|---|---|
| (1) | (2) | (3) | (4) | (5) | (6) | (7) | (8) | (9) | (10) |
| NGC 40 | 18″ | −2.87 | ..... | −2.87 | −3.03 | −3.39 | −2.52 | −0.84 | −1.40 |
| NGC 2392 | 23 | −1.38 | ..... | −1.38 | −1.43 | −1.96 | −2.47 | ..... | ..... |
| NGC 3242 | 10 | +0.10 | ..... | +0.10 | −0.06 | −0.42 | −1.19 | ..... | ..... |
| IC 4593 | 5 | −0.44 | ..... | −0.44 | −0.56 | −1.06 | −1.29 | ..... | ..... |
| NGC 6210 | 4 | +0.57 | +0.55 | +0.56 | +0.43 | −0.04 | −0.62 | ..... | ..... |
| NGC 6543 | 10 | +0.03 | − .05 | 0.00 | −0.13 | −0.61 | −0.95 | − .14 | −0.70 |
| NGC 6572 | 7 | +0.32 | + .38 | +0.34 | +0.22 | −0.27 | −0.85 | − .14 | −0.70 |
| NGC 6720 | 35 | −1.41 | ..... | −1.41 | −1.54 | −1.98 | −2.44 | ..... | ..... |
| NGC 6818 | 9 | −0.35 | − .35 | −0.35 | −0.47 | −0.95 | −1.41 | ..... | ..... |
| NGC 6826 | 13 | −0.54 | − .57 | −0.55 | −0.67 | −1.17 | −1.52 | − .65 | −1.21 |
| NGC 7009 | 9 | +0.11 | + .22 | +0.15 | +0.01 | −0.42 | −1.06 | + .10 | −0.46 |
| NGC 7027 | 5 | +0.42 | + .36 | +0.40 | +0.28 | −0.20 | −0.90 | − .20 | −0.76 |
| NGC 7662 | 8 | +0.07 | + .15 | +0.09 | −0.03 | −0.51 | −1.17 | + .12 | −0.44 |
| NGC 1535 | 9 | ..... | − .45 | −0.45 | −0.58 | −1.05 | −1.64 | − .75 | −1.31 |
| IC 418 | 6 | ..... | − .18 | −0.18 | −0.29 | −0.82 | −0.43 | −0.46 | −1.02 |
| IC 2149 | 6 | ..... | − .68 | −0.68 | −0.81 | −1.27 | −1.42 | ..... | ..... |
| NGC 6803 | 2.5 | ..... | −0.16 | −0.16 | −0.29 | −0.74 | −1.32 | ..... | ..... |

brightnesses in the light of the $N_1$ and $N_2$ lines, respectively, as determined from column 5. The logarithm of the surface brightness of each nebula in the light of $H\beta$, derived from the adopted surface brightness in the light of [*O* III], is tabulated in column 8. Here again the photoelectric determinations of the relative intensities of the [*O* III] lines and $H\beta$ were used when possible, because of their much higher accuracy. Finally, the last two columns tabulated the logs of the surface brightnesses in the $H\beta$ line derived from the data listed by Menzel and Aller (1941) and the adjusted values of this quantity given by Page and Greenstein (1951).

It should be emphasized that the surface brightnesses of Table 6 were calculated by assuming that the nebulae were all uniform disks having diameters equal to the quantity $A$, tabulated in column 2 of this table. Thus ring-shaped nebulae like NGC 6720 are actually brighter per unit area than the listed value.

The two completely independent photoelectric determinations of the surface brightnesses agree excellently. The average probable error found from a comparison of these results is $\pm 2.8$ per cent or $\pm 0.070$ mag.; it should be emphasized that this is the external probable error.

The surface brightnesses of the planetary nebulae derived by Menzel and Aller (1941) were admittedly approximate, since they were calculated from the magnitudes for these objects given by Berman (1937). At the time their paper was published, there were no better data, and the comparison of the two sets of values in Table 6 is made only to show that the electron densities calculated by Menzel and Aller are too high in every case but one (IC 418).

Page and Greenstein (1951) arbitrarily adjusted the values of the surface brightnesses derived by Menzel and Aller, because the original values were, in five cases, too large to satisfy the inequality

$$4\pi R^2 S_L < L_{SB} \ , \tag{8}$$

where $S_L$ is the total surface brightness of the nebula of radius $R$ and $L_{SB}$ is the bolometric luminosity of the central star. Page and Greenstein simply decreased the logarithms of the surface brightnesses by 0.56, so that inequality (9) would be satisfied. The photoelectric investigations show that their empirical adjustment was in the right direction but still was not large enough. Their discussion made it evident that further observational work was acutely needed.

Ambarzumian (1933) has evaluated the logarithms of the surface brightnesses, in the light of $H\beta$, of two of the nebulae included in the present investigation, NGC 6572 and 7027. His results were $-0.50$ and $-0.67$, respectively. The agreement is fair and is probably as good as could be expected, since Ambarzumian's measures were made photographically.

## IX. PHOTOGRAPHIC MAGNITUDES OF THE NEBULAE

Having the sensitivity-curve of the International photographic system, one can calculate the magnitudes of the nebulae, since the relative intensities of the nebular lines and of the continua are available and since the surface brightness of at least one of these radiations is known. The procedure is to sum the product of the relative intensity of each line and the sensitivity of the International system at the wave length of that line and to add to this sum the integrated product of the continuum intensity and the sensitivity. In addition, the integrated product of the energy-curve of the sun and of the International sensitivity must be calculated. As the relative intensities of one of the green oxygen lines and of 1 A of the spectrum of the standard G-type star at the same wave length are known, the magnitudes of the standard star and the nebula can be reduced to the same scale, and the International photographic magnitude can be determined. A similar procedure would yield the photovisual magnitudes of the nebulae.

Since, as we have seen, accurate information about the line intensities of planetary nebulae in the yellow is meager, photographic magnitudes should be more reliable than photovisual magnitudes. The sensitivity-curve of the International photographic system was taken from the work of Seares and Joyner (1943). The resulting International photographic magnitudes of the planetaries which have been observed photoelectrically, either here or by Liller and Aller (1954), are given in Table 7, column 2. These values are compared in column 4 with the photographic magnitudes of planetary nebulae tabulated by Berman (1937). These latter values were taken mainly from the work of Vorontsov-Velyamino (1934).

It should be emphasized that the sensitivity-curves of the plates that were used by Vorontsov-Velyaminov (1934) in his determination of nebular magnitudes is not known. Furthermore, the spectral sensitivity of most blue-sensitive emulsions is changing rapidly at the wave lengths of the green oxygen lines. To indicate the effect of different emulsions, I have also derived magnitudes for the nebulae by using the sensitivity of the Seed 23 plate given by Yü (1926). According to Yü and also to Seares and Joyner (1943), the Seed 23 plate is considerably less sensitive at λ 5000 than is the International system. The Seed 23 magnitudes are tabulated in column 3 of Table 7.

The earlier magnitudes clearly are systematically brighter than either the photoelectrically determined Seed 23 or the International photographic magnitudes. The average differences are, respectively, −0.7 and −0.4 mag. It may be, of course, that the plates from which the earlier magnitudes were derived were even more sensitive to the λ 5000 region than either the Seed 23 plate or the International response-curve. There would still remain, nevertheless, a considerable scatter.

The magnitudes derived here should not be given high weight, since they depend rather critically on the earlier photographic spectrophotometry of these nebulae. Their astrophysical value is small, and they are included only to indicate that the earlier measures of nebular magnitudes should be regarded with suspicion.

### X. MAGNITUDES, COLORS, AND TEMPERATURES OF THE CENTRAL STARS

It was originally hoped that reliable magnitudes for the nebular nuclei would come out of this work. Had adequate information on nebular intensities in the yellow been avail-

TABLE 7

PHOTOGRAPHIC MAGNITUDES OF THE NEBULAE

| Nebula (1) | Liller − International (2) | Liller − Seed 23 (3) | Berman (4) | Nebula (1) | Liller − International (2) | Liller − Seed 23 (3) | Berman (4) |
|---|---|---|---|---|---|---|---|
| NGC 40 | 10.7 | 10.5 | 9.5 | NGC 6572 | 9.0 | 9.4 | 9.2 |
| NGC 1535 | 10.4 | 10.9 | 9.9 | NGC 6720 | 9.7 | 10.1 | 9.0 |
| IC 418 | 9.4 | 9.3 | 10.6 | NGC 6803 | 12.4 | 12.7 | 11.3 |
| IC 2149 | 11.2 | 11.4 | 10.5 | NGC 6818 | 10.0 | 10.3 | 9.6 |
| NGC 2392 | 10.4 | 10.7 | 8.5 | NGC 6826 | 9.8 | 10.2 | 9.2 |
| NGC 3242 | 8.8 | 9.1 | 9.7 | NGC 7009 | 8.9 | 9.3 | 7.9 |
| IC 4593 | 11.4 | 11.7 | 11.1 | NGC 7027 | 9.6 | 10.1 | 9.8 |
| NGC 6210 | 9.7 | 10.1 | 10.0 | NGC 7662 | 9.2 | 9.5 | 8.7 |
| NGC 6543 | 8.8 | 9.2 | 8.7 | | | | |

able, this would have been possible for all but a few of the fainter objects. However, as was stated in Section VI, the computed yellow deflection from the nebula was larger than the observed total deflection for four nebulae. The luminosity of a fifth central star, NGC 7027, came out far too bright, according to the observation of Baade, who was not able to find a central star for this planetary brighter than the eighteenth magnitude (reported in a letter from Dr. Minkowski to Dr. Aller). It seems extremely doubtful whether magnitudes for any of the other central stars could be trusted, except for NGC 6720, the Ring Nebula in Lyra, where the magnitude was measured directly. However, it is possible to find an upper limit to the brightnesses of the planetary nuclei by assuming that the yellow deflections are due entirely to the central stars and that there are no nebular radiations in this part of the spectrum. Since the yellow sensitivity-curve corresponds quite closely to that of the International photovisual system, I assumed that the yellow deflections gave directly the relative intensities on this system. The solar-type stars were used as comparison stars. These calculated upper limits to brightness, expressed in photovisual magnitudes, are listed in column 2 of Table 8. These values are compared in column 3 with the photographic magnitudes of the nuclei published by Berman (1937). In making a comparison of the two sets of magnitudes, it should be remembered that although all these objects are reddened to some extent by interstellar dust, their color indices are probably all slightly negative, with the exception of BD+30°3639, NGC 7027, and possibly NGC 40 (see Tables 3 and 5).

All Berman's central-star magnitudes are fainter than the lower (brighter) limit set by the photoelectric observations, except that of IC 4593. It seems that for this central star Berman was certainly in error. Perhaps this difference is the result of a typographical error.

For the one central star for which it was possible to measure the star directly, NGC 6720, the photovisual magnitude derived from the photoelectric observations is 14.2, which is in fair accord with the photographic magnitude of 14.4 listed by Berman.

The precision of the upper limits of central-star brightnesses averages close to a tenth of a magnitude (probable error); the primary source of error arises from the small size of the yellow deflections.

During the time the observations were being made, I attempted to measure the intensities of the brighter central stars in the violet region of the spectrum, in order to determine photoelectric colors for these stars. Deflections were made of the light passing through a metallic interference filter which had a half-width of 130 A and whose maximum transmission was halfway between $H\gamma$ and $H\delta$. This region of the spectrum is freer from nebular radiations than any other wave-length interval of reasonable size,

TABLE 8

MAGNITUDES OF THE CENTRAL STARS

| Nebula (1) | Liller $m_{pv}$ Lower Limit (2) | Berman $m_{pg}$ (3) | Nebula (1) | Liller $m_{pv}$ Lower Limit (2) | Berman $m_{pg}$ (3) |
|---|---|---|---|---|---|
| NGC 40 | 11.0 | 11.3 | BD+30°3639 | 10.1 | 10.3 |
| NGC 2392 | 10.4 | 10.5 | NGC 6818 | 12.0 | 15.0 |
| NGC 3242 | 11.3 | 11.9 | NGC 6826 | 9.9 | 10.7 |
| IC 4593 | 10.9 | 10.2 | NGC 7009 | 10.9 | 11.9 |
| NGC 6210 | 11.3 | 11.7 | NGC 7027 | 11.3 | 15.6 |
| NGC 6543 | 10.3 | 11.2 | NGC 7662 | 11.1 | 12.7 |
| NGC 6572 | 11.0 | 12 | | | |

except the yellow portion of the spectrum. Unfortunately, this investigation was not entirely successful. Because of the faintness of even the brightest central stars, as much of the light had to be admitted to the photocell as possible, and consequently the radiation from the central star was badly contaminated with the light from nebular $H\gamma$ and $H\delta$. More precise determinations of the relative intensities of the nebular radiations are needed than are now available, in order to sift out the light passing through this violet interference filter.

With these new photoelectric data it is possible to calculate new temperatures for the central stars by using, for instance, one of the methods of Zanstra (1931*a*, *b*), which compares the luminosity of the exciting star with that of the surrounding nebula. However, until central-star magnitudes of the precision of the new nebular brightnesses become available, there would be no real gain in precision. The same can be said about the calculation of the rate of energy emitted by a unit volume of each nebula. This datum is obtainable only with a knowledge of the distance of the planetary. Since the distances of these objects have never been determined satisfactorily, no attempt will be made to calculate this quantity in this paper.

## XI. SUMMARY

The nebular surface brightnesses which have been derived are sharply discordant with earlier photographic results. Since the values reported here are in excellent agreement

with those found photoelectrically by Liller and Aller (1954), we must conclude that the photographic determinations of surface brightnesses are in error and that their use should be avoided. Furthermore, the inadvisability of extracting surface brightnesses from nebular magnitudes is emphasized, particularly for radiations whose wave lengths lie in regions of the spectrum where the sensitivity of the receiver is changing rapidly. It should be clear, then, that nebular magnitudes are of little practical value. In deriving surface brightnesses, strong evidence has accumulated that the continuum intensities measured by Page (1936, 1942) are, at least for some planetaries, in error by more than 15 per cent.

Until better continuum intensities are available, there seems to be little hope of deriving central-star magnitudes of photoelectric precision with the method described here. However, the observations do allow the reasonably precise calculation of lower (brighter) limits of magnitudes for these stars. With one exception (IC 4593), the magnitudes listed by Berman (1937) lie above this limit, indicating that there are no serious errors in his tabulation.

The success of this program has encouraged the writer and Professor Aller to continue the work to fainter planetaries with the larger telescopes at Mount Wilson. We hope that soon there will be available reliable surface brightnesses for nearly all the nebulae for which Aller (1941, 1951) has measured the relative intensities of the monochromatic radiations.

A list of all the names of those who have assisted me in this work would be embarrassingly long. However, special mention should be made of Dr. Lawrence H. Aller, who emphasized the poor quality of the existing data on nebular surface brightnesses and discussed with me in some detail the problems connected with the photometry of planetary nebulae. I would like to thank Dr. Freeman D. Miller, at whose instance the writer undertook the design and construction of a photoelectric photometer. A grant by the Rackham School of Graduate Studies to Dr. Miller for the purchase of the Brown Recorder made the entire project possible. The equipment that was used at the McMath-Hulbert Observatory was placed at the writer's disposal by Dr. Robert R. McMath, and Drs. Mohler and Pierce of that observatory gave me many helpful suggestions. Grateful acknowledgment is made to Dr. H. Zanstra for his critical reading of the manuscript. Finally, Dr. Stanley P. Wyatt gave me many helpful observing hints, for which I am very grateful.

## REFERENCES

Aller, L. H. 1941, *Ap. J.*, **93**, 236.
———. 1948, *ibid.*, **108**, 462.
———. 1951, *ibid.*, **113**, 125.
Aller, L. H., Bowen, I. S., and Minkowski, R., 1955, *Ap. J.*, **122**, 62.
Aller, L. H., and Wilson, O. C. 1954, *Ap. J.*, **119**, 243.
Ambarzumian, V. A. 1933, *Zs. f. Ap.*, **6**, 107.
Berman, L. 1936, *M.N.*, **96**, 892.
———. 1937, *Lick Obs. Bull.*, **18**, 73.
Bowen, I. S., and Wyse, A. B. 1939, *Lick Obs. Bull.*, **19**, 1.
Campbell, W. W., and Moore, J. H. 1918, *Lick Obs. Bull.*, **13**, 75.
Curtis, H. D. 1918, *Lick Obs. Bull.*, **13**, 55.
Johnson, H. L., and Morgan, W. W. 1953, *Ap. J.*, **117**, 313.
Kuiper, G. P. 1938, *Ap. J.*, **88**, 429.
Liller, W., and Aller, L. H. 1954, *Ap. J.*, **120**, 48.
McCuskey, S. W. 1949, *Ap. J.*, **109**, 426.
Menzel, D. H., and Aller, L. H. 1941, *Ap. J.*, **93**, 200.
Minkowski, R., and Aller, L. H. 1955 (in press).
Morgan, W. W., Keenan, P. C., and Kellman, E. 1943, *An Atlas of Stellar Spectra* (Chicago: University of Chicago Press).

Page, T. L. 1936, *M.N.*, **96**, 604.
———. 1942, *Ap. J.*, **96**, 78.
Page, T. L., and Greenstein, J. L. 1951, *Ap. J.*, **114**, 98.
Pettit, Edison, 1940, *Ap. J.*, **91**, 159.
Plaskett, H. H. 1928, *Pub. Dom. Ap. Obs. Victoria*, **4**, 187.
Roman, Nancy, 1950, *Ap. J.*, **112**, 554.
Seares, F. H., and Joyner, M. C. 1943, *Ap. J.*, **98**, 312.
Stebbins, J., Whitford, A. E., and Johnson, H. L. 1950, *Ap. J.*, **112**, 469.
Underhill, A. B. 1951, *Pub. Dom. Ap. Obs. Victoria*, **8**, 357.
Valley, G. E., and Wallman, H. 1948, *Vacuum Tube Amplifiers* (New York: McGraw-Hill Book Co.), p. 480.
Vaucouleurs, G. de. 1949, *Ann. d'ap.*, **12**, 287.
Vorontsov-Velyaminov, B. A., 1934, *Russ. A.J.*, **11**, 54.
Williams, R. C. 1939, *Pub. Obs. U. Michigan*, **7**, 93.
Wilson, O. C. 1950, *Ap. J.*, **111**, 279.
Wilson, O. C., and Joy, A. H. 1950, *Ap. J.*, **111**, 221.
Wyse, A. B. 1942, *Ap. J.*, **95**, 356.
Yü, C. 1926, *Lick Obs. Bull.*, **12**, 104.
Zanstra, H. 1931*a*, *Pub. Dom. Ap. Obs. Victoria*, **4**, 209.
———. 1931*b*, *Zs. f. Ap.*, **2**, 1.

# A STUDY OF RR LYRAE IN THREE COLORS

ROBERT H. HARDIE
Lowell Observatory
*Received March 24, 1955; revised April 25, 1955*

ABSTRACT

Photometric observations in three colors, numbering 1048, are presented for the variable star RR Lyrae. The variations throughout the cycle and among the cycles are noted. A short-lived ultraviolet excess is found.

The variable star RR Lyrae (HD 182989; 1950 $\alpha = 19^h23^m$, $\delta = +42°41$) has been studied photoelectrically several times in recent years (Gordon and Kron 1947; Walraven 1949; Stebbins 1953). The first of these studies was made over parts of seven different cycles in one color. The results were used to investigate the periodic terms given by Detre (1943). A similar but lengthier study made by Walraven covered a 200-day interval, also in a single color, although this included all wave lengths from the ultraviolet to the near red because his apparatus comprised a reflector and a 1P21 photomultiplier used without filters. Since his work included many cycles, he was able to carry out a more thorough study of the components of period and to demonstrate some remarkable changes in the shape of the light-curve. The work of Stebbins was done in six colors and comprises some nine observations in each color made on four nights. From these, six representative colors at different phases were obtained, and, combining these data with Sanford's radial-velocity-curves (1935, 1949), he was able to separate temperature and radius changes, thus obtaining estimates of the luminosity and size of the star.

The work reported here consists of observations made during some twelve different cycles in the summer of 1953 covering a period of 45 days. The Lowell 20-inch reflector, which had just been completed, was used with the filters and 1P21 photocell which had been used to define the $V$, $B$, $U$ system of Morgan and Johnson (1953). The three colors are reduced to the $V$, $B$, $U$ system. Some portions of seven rising branches were obtained, five of which fell within an interval of 14 days and the other two of which followed after a 3-week interval of cloudy weather. Thus the observations are not well distributed with regard to the 41-day variation. About 350 observations in each color were secured, using as comparisons the stars BD42°3325 ($V = 7.01$, $B - V = +0.01$, $U - B = -0.12$) and BD42°3331 ($V = 8.62$, $B - V = +0.44$, $U - B = +0.11$).

Each observation in each color consisted of two deflections on the object separated by one on the sky, taking, altogether, somewhat over 1 minute. In general, six sets of three-color observations were obtained for the variable for each set of a comparison; hence a comparison star would be referred to only once every half-hour. Thus, at a slight cost in precision, the rapid variations were covered about as fully as was practicable, without resorting to a simultaneous multicolor technique. From intercomparison of the two comparison stars, the probable error of any single yellow or blue observation is 0.004 mag. and of any single ultraviolet observation is about 0.006 mag.

The observations are listed in Table 1 as one magnitude and two color indices for each time of observation; these three quantities have been adjusted to coincide in time. The times are heliocentric and are given as cycles and decimals computed from the epoch JD 2414856.408, with a period of 0.56683735 day (Walraven). The first observation was made on June 17.271 U.T., 1953. The ephemeris corrections, as developed by Walraven, appear to be inadequate when extrapolated from 1947 to 1953, the 1953 cycles being about 0.1 period earlier than predicted by his formula. Thus the present group of light-

TABLE I

| Cycle | V | B-V | U-B | Cycle | V | B-V | U-B | Cycle | V | B-V | U-B |
|---|---|---|---|---|---|---|---|---|---|---|---|
| 34735.476 | 7.792 | 0.378 | 0.042 | 34746.133 | 7.414 | 0.241 | 0.077 | 34753.221 | 7.346 | 0.231 | 0.085 |
| .490 | 7.786 | .425 | .019 | .138 | 7.388 | .225 | .088 | .235 | 7.382 | .232 | .088 |
| .506 | 7.793 | .436 | .013 | .145 | 7.359 | .206 | .105 | .242 | 7.394 | .239 | .104 |
| .520 | 7.819 | .425 | .029 | .157 | 7.319 | .205 | .107 | .247 | 7.405 | .243 | .111 |
| .534 | 7.820 | .442 | .011 | .164 | 7.308 | .204 | .107 | .254 | 7.431 | .241 | .111 |
| .546 | 7.843 | .435 | .022 | .170 | 7.304 | .197 | .111 | .293 | 7.490 | .272 | .100 |
| .562 | 7.848 | .442 | .023 | .177 | 7.304 | .196 | .104 | .300 | 7.498 | .285 | .094 |
| .575 | 7.875 | .430 | .028 | .182 | 7.306 | .196 | .099 | .307 | 7.523 | .274 | .094 |
| .590 | 7.887 | .429 | .038 | .191 | 7.305 | .210 | .097 | .313 | 7.525 | .288 | .092 |
| .606 | 7.895 | .442 | .022 | .205 | 7.327 | .207 | .107 | .318 | 7.534 | .293 | .081 |
| .620 | 7.913 | .431 | .027 | .212 | 7.339 | .215 | .111 | .322 | 7.548 | .305 | .084 |
| .636 | 7.918 | .437 | .027 | .219 | 7.355 | .216 | .111 | .336 | 7.579 | .309 | .070 |
| .649 | 7.941 | .434 | .011 | .224 | 7.370 | .225 | .... | .343 | 7.585 | .318 | .078 |
| .666 | 7.935 | .445 | .015 | .251 | 7.416 | .236 | .103 | .348 | 7.603 | .317 | .075 |
| .680 | 7.954 | .434 | .015 | .258 | 7.422 | .248 | .101 | .355 | 7.625 | .314 | .067 |
| .701 | 7.944 | .457 | .009 | .263 | 7.424 | .255 | .106 | .362 | 7.625 | .320 | .074 |
| .714 | 7.959 | .440 | .028 | .268 | 7.435 | .261 | .103 | .367 | 7.631 | .327 | .077 |
| .728 | 7.960 | .441 | .013 | 34749.500 | 7.780 | .396 | .056 | 34760.050 | 7.935 | .397 | -.027 |
| .742 | 7.973 | .439 | .011 | .507 | 7.801 | .401 | .039 | .057 | 7.878 | .385 | -.030 |
| .756 | 7.966 | .438 | .037 | .514 | 7.806 | .420 | .034 | .062 | 7.816 | .368 | -.048 |
| .770 | 7.975 | .432 | .032 | .530 | 7.838 | .406 | .035 | .069 | 7.735 | .360 | -.047 |
| .786 | 7.971 | .452 | .005 | .537 | 7.844 | .413 | .027 | .074 | 7.682 | .332 | -.046 |
| .800 | 7.988 | .419 | .025 | .544 | 7.851 | .418 | .040 | .080 | 7.632 | .297 | -.012 |
| .814 | 7.974 | .443 | .029 | .553 | 7.860 | .413 | .040 | .092 | 7.541 | .290 | .018 |
| 34738.903 | 8.011 | .422 | .073 | .559 | 7.858 | .428 | .034 | .097 | 7.509 | .271 | .024 |
| .914 | 8.040 | .431 | .047 | .576 | 7.882 | .425 | .034 | .103 | 7.468 | .270 | .029 |
| .930 | 8.069 | .431 | .051 | .582 | 7.890 | .432 | .043 | .110 | 7.425 | .241 | .054 |
| .944 | 8.094 | .438 | .050 | .590 | 7.892 | .436 | .036 | .115 | 7.382 | .223 | .073 |
| 34739.000 | 8.122 | .440 | .042 | .597 | 7.899 | .436 | .032 | .122 | 7.341 | .187 | .099 |
| .016 | 8.083 | .438 | .021 | .604 | 7.911 | .435 | .033 | .142 | 7.259 | .181 | .122 |
| .036 | 8.030 | .403 | .001 | .611 | 7.923 | .431 | .039 | .149 | 7.245 | .181 | .099 |
| .154 | 7.360 | .211 | .089 | .625 | 7.926 | .443 | .039 | .154 | 7.234 | .181 | .101 |
| .172 | 7.336 | .212 | .091 | .632 | 7.933 | .447 | .047 | .161 | 7.233 | .182 | .106 |
| .189 | 7.343 | .208 | .101 | .639 | 7.941 | .444 | .052 | .170 | 7.248 | .178 | .103 |
| .205 | 7.363 | .216 | .094 | .646 | 7.944 | .441 | .045 | .177 | 7.259 | .192 | .095 |
| .224 | 7.399 | .225 | .098 | .655 | 7.947 | .445 | .041 | .191 | 7.293 | .190 | .099 |
| .242 | 7.432 | .226 | .093 | .662 | 7.962 | .433 | .050 | .196 | 7.310 | .196 | .109 |
| .262 | 7.464 | .256 | .086 | .678 | 7.964 | .440 | .054 | .202 | 7.328 | .199 | .107 |
| .279 | 7.488 | .264 | .101 | .683 | 7.972 | .440 | .051 | .210 | 7.341 | .209 | .106 |
| .295 | 7.530 | .272 | .086 | .693 | 7.977 | .436 | .059 | .217 | 7.359 | .224 | .106 |
| .313 | 7.549 | .300 | .... | .697 | 7.983 | .434 | .064 | .224 | 7.369 | .236 | .091 |
| .328 | 7.584 | .316 | .055 | .703 | 7.979 | .445 | .061 | .341 | 7.593 | .317 | .072 |
| .341 | 7.596 | .339 | .054 | .711 | 7.985 | .439 | .052 | .348 | 7.606 | .320 | .082 |
| 34742.505 | 7.813 | .403 | .025 | .725 | 7.990 | .438 | .047 | .353 | 7.616 | .324 | .081 |
| .523 | 7.817 | .419 | .032 | .731 | 7.996 | .432 | .059 | .360 | 7.618 | .339 | .074 |
| .554 | 7.861 | .417 | .040 | .738 | 8.001 | .435 | .055 | .367 | 7.633 | .339 | .067 |
| .572 | 7.874 | .429 | .035 | .745 | 8.009 | .431 | .050 | .372 | 7.643 | .349 | .061 |
| .588 | 7.901 | .423 | .046 | .752 | 8.004 | .439 | .046 | .392 | 7.669 | .358 | .058 |
| .688 | 7.963 | .446 | .029 | .759 | 8.004 | .439 | .044 | .401 | 7.679 | .360 | .065 |
| .706 | 7.973 | .444 | .037 | 34753.029 | 8.085 | .427 | -.002 | .406 | 7.690 | .361 | .068 |
| .724 | 7.976 | .446 | .036 | .034 | 8.055 | .429 | .014 | .413 | 7.695 | .365 | .079 |
| .743 | 7.989 | .442 | .039 | .053 | 7.939 | .403 | -.007 | .420 | 7.702 | .370 | .075 |
| .773 | 7.997 | .443 | .042 | .059 | 7.897 | .389 | -.024 | 34761.820 | 8.034 | .445 | .034 |
| .789 | 8.001 | .444 | .041 | .062 | 7.834 | .379 | -.035 | .826 | 8.025 | .456 | .025 |
| .807 | 8.003 | .445 | .030 | .068 | 7.775 | .354 | -.042 | .833 | 8.024 | .453 | .029 |
| .824 | 8.002 | .448 | .028 | .074 | 7.704 | .339 | -.035 | .847 | 8.026 | .440 | .031 |
| .840 | 8.001 | .443 | .027 | .082 | 7.659 | .304 | -.040 | .854 | 8.026 | .438 | .022 |
| .860 | 7.995 | .431 | .039 | .094 | 7.590 | .300 | .016 | .861 | 8.011 | .441 | .023 |
| 34745.918 | 8.037 | .438 | .030 | .101 | 7.564 | .284 | .005 | .875 | 8.007 | .430 | .027 |
| .932 | 8.051 | .439 | .022 | .106 | 7.530 | .268 | .034 | .882 | 8.006 | .431 | .028 |
| .946 | 8.076 | .439 | .030 | .113 | 7.486 | .255 | .051 | .923 | 8.039 | .430 | .034 |
| 34746.050 | 7.957 | .407 | .006 | .119 | 7.446 | .238 | .063 | .928 | 8.039 | .436 | .040 |
| .055 | 7.907 | .393 | -.010 | .133 | 7.345 | .220 | .085 | .935 | 8.055 | .428 | .041 |
| .060 | 7.854 | .369 | -.004 | .140 | 7.323 | .200 | .094 | .942 | 8.063 | .430 | .037 |
| .073 | 7.735 | .337 | -.041 | .145 | 7.285 | .202 | .097 | .948 | 8.076 | .427 | .030 |
| .078 | 7.674 | .327 | -.032 | .154 | 7.272 | .195 | .095 | .955 | 8.076 | .439 | .027 |
| .083 | 7.641 | .311 | -.020 | .161 | 7.259 | .199 | .090 | .969 | 8.094 | .435 | .046 |
| .090 | 7.614 | .295 | .003 | .166 | 7.252 | .205 | .091 | .974 | 8.099 | .438 | .048 |
| .095 | 7.601 | .279 | .016 | .182 | 7.273 | .197 | .100 | .981 | 8.106 | .442 | .042 |
| .103 | 7.570 | .281 | .049 | .191 | 7.285 | .198 | .102 | .988 | 8.114 | .439 | .043 |
| .115 | 7.520 | .259 | .055 | .200 | 7.303 | .200 | .106 | .995 | 8.114 | .446 | .034 |
| .122 | 7.483 | .246 | .081 | .207 | 7.316 | .210 | .101 | 34762.002 | 8.114 | .439 | .025 |
| .126 | 7.460 | .237 | .074 | .214 | 7.335 | .214 | .095 | .014 | 8.106 | .438 | .020 |

TABLE I cont'd

| Cycle | V | B-V | U-B | Cycle | V | B-V | U-B | Cycle | V | B-V | U-B |
|---|---|---|---|---|---|---|---|---|---|---|---|
| 34762.022 | 8.100 | 0.432 | 0.020 | 34798.990 | 8.116 | 0.436 | 0.017 | 34800.860 | 7.974 | 0.435 | 0.035 |
| .027 | 8.083 | .428 | .020 | .999 | 8.110 | .435 | .009 | .866 | 7.989 | .427 | .033 |
| .032 | 8.067 | .421 | .018 | 34799.006 | 8.103 | .432 | .006 | .871 | 7.993 | .434 | .016 |
| .038 | 8.030 | .425 | .004 | .013 | 8.080 | .440 | -.001 | .985 | 8.116 | .435 | .022 |
| .043 | 7.993 | .395 | .001 | .020 | 8.045 | .415 | .001 | .992 | 8.108 | .445 | .020 |
| .053 | 7.908 | .383 | -.009 | .034 | 7.955 | .401 | .014 | .997 | 8.110 | .431 | .025 |
| .059 | 7.849 | .371 | -.030 | .039 | 7.891 | .383 | .007 | 34801.004 | 8.089 | .439 | .021 |
| .066 | 7.789 | .354 | -.038 | .046 | 7.840 | .344 | -.026 | .011 | 8.077 | .429 | .021 |
| .071 | 7.714 | .341 | -.041 | .053 | 7.726 | .317 | -.002 | .016 | 8.051 | .422 | .022 |
| .076 | 7.657 | .319 | -.028 | .060 | 7.640 | .265 | .025 | .031 | 7.958 | .408 | .017 |
| .082 | 7.604 | .278 | .006 | .068 | 7.568 | .282 | -.003 | .038 | 7.897 | .390 | -.018 |
| .094 | 7.520 | .266 | .040 | 34800.554 | 7.875 | .444 | .064 | .043 | 7.828 | .370 | -.018 |
| .097 | 7.490 | .253 | .034 | .563 | 7.884 | .433 | .069 | .050 | 7.760 | .352 | -.030 |
| .104 | 7.436 | .249 | .045 | .570 | 7.894 | .433 | .061 | .057 | 7.684 | .313 | .003 |
| .110 | 7.401 | .222 | .068 | .577 | 7.894 | .445 | .043 | .073 | 7.541 | .289 | .028 |
| .115 | 7.360 | .215 | .071 | .586 | 7.914 | .440 | .032 | .078 | 7.515 | .256 | .030 |
| .122 | 7.318 | .194 | .088 | .593 | 7.912 | .446 | .026 | .092 | 7.461 | .245 | .059 |
| .133 | 7.272 | .180 | .101 | .609 | 7.919 | .453 | .033 | .099 | 7.445 | .231 | .053 |
| .138 | 7.246 | .182 | .096 | .618 | 7.926 | .451 | .037 | .104 | 7.419 | .237 | .056 |
| .145 | 7.234 | .181 | .098 | .625 | 7.928 | .456 | .031 | 34820.210 | 7.349 | .220 | .110 |
| .150 | 7.230 | .181 | .095 | .632 | 7.932 | .449 | .034 | .216 | 7.363 | .228 | .101 |
| .156 | 7.234 | .174 | .097 | .639 | 7.937 | .451 | .034 | .223 | 7.380 | .233 | .102 |
| .161 | 7.232 | .178 | .102 | .646 | 7.939 | .458 | .029 | .230 | 7.394 | .239 | .097 |
| .166 | 7.239 | .179 | .108 | .664 | 7.955 | .449 | .031 | .235 | 7.406 | .242 | .094 |
| .173 | 7.250 | .178 | .105 | .671 | 7.948 | .455 | .041 | .242 | 7.420 | .250 | .093 |
| 34795.427 | 7.749 | .389 | .066 | .680 | 7.955 | .451 | .053 | .260 | 7.450 | .253 | .097 |
| .434 | 7.758 | .389 | .064 | .687 | 7.960 | .456 | .037 | .267 | 7.462 | .258 | .100 |
| .440 | 7.762 | .393 | .060 | .695 | 7.959 | .455 | .040 | .274 | 7.480 | .261 | .096 |
| .447 | 7.773 | .395 | .054 | .702 | 7.967 | .445 | .050 | .281 | 7.497 | .264 | .097 |
| .452 | 7.780 | .398 | .056 | .729 | 7.964 | .450 | .047 | .288 | 7.507 | .270 | .095 |
| .482 | 7.812 | .407 | .047 | .736 | 7.968 | .444 | .043 | .295 | 7.523 | .279 | .089 |
| .491 | 7.819 | .408 | .050 | .745 | 7.968 | .445 | .034 | .311 | 7.552 | .283 | .083 |
| .498 | 7.831 | .409 | .050 | .754 | 7.973 | .446 | .038 | .318 | 7.562 | .290 | .087 |
| .505 | 7.836 | .417 | .044 | .762 | 7.971 | .448 | .034 | .327 | 7.569 | .307 | .081 |
| .512 | 7.845 | .414 | .045 | .771 | 7.980 | .437 | .028 | .334 | 7.582 | .317 | .062 |
| .519 | 7.853 | .413 | .045 | .785 | 7.980 | .441 | .023 | .341 | 7.585 | .330 | .062 |
| 34798.923 | 8.057 | .429 | .038 | .792 | 7.977 | .444 | .025 | .348 | 7.602 | .335 | .065 |
| .928 | 8.065 | .424 | .035 | .800 | 7.980 | .436 | .027 | .364 | 7.624 | .344 | .052 |
| .935 | 8.065 | .427 | .041 | .808 | 7.974 | .438 | .030 | .371 | 7.639 | .347 | .055 |
| .942 | 8.067 | .436 | .043 | .815 | 7.979 | .431 | .031 | .378 | 7.645 | .354 | .057 |
| .951 | 8.079 | .438 | .043 | .821 | 7.978 | .427 | .041 | .387 | 7.660 | .344 | .055 |
| .958 | 8.091 | .436 | .045 | .836 | 7.970 | .433 | .040 | .392 | 7.663 | .353 | .050 |
| .974 | 8.113 | .434 | .030 | .841 | 7.972 | .431 | .038 | .401 | 7.680 | .352 | .048 |
| .981 | 8.110 | .442 | .026 | .850 | 7.975 | .428 | .037 | | | | |

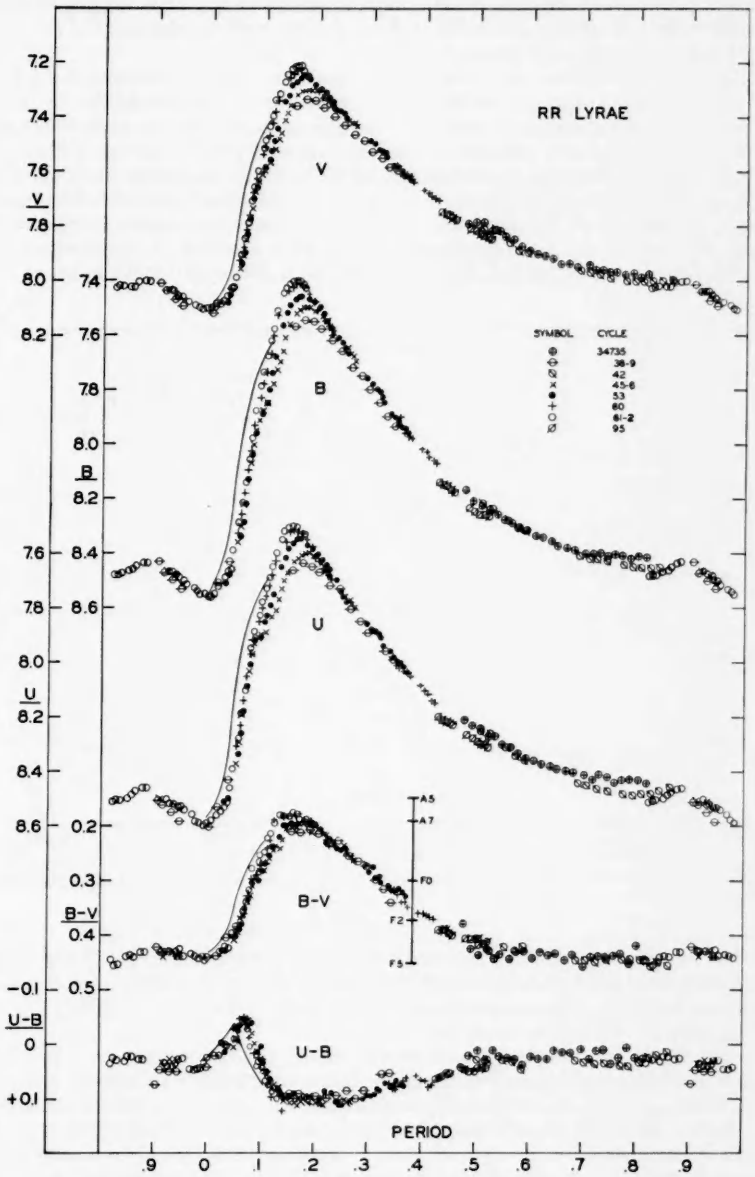


FIG. 1.—The full-line curves represent cycles 34798–34799 and 34800–34801. The spectral types attached to the $B - V$-curve are for unreddened main-sequence stars. For the sake of clarity, some observations are not plotted.

curves is at minimum at about phase 0.0, and phase 0.06 corresponds roughly to the part of the curve which Walraven labels $\Delta m = 0$; according to his development of the periodic terms, the phase should be 0.15 for this time.

The forms of the light-curves obtained are shown in Figure 1. The well-known variation of the maxima is common to each color studied and during these few cycles takes the form of a progressive rising of the maxima. However, it is of interest to note that the portions of the light-curves between phases 0 and 0.08 appear to be substantially common to the cycles 34746, 34753, 34760, and 34762 and that they differ only after phase 0.08 in a systematic way. This behavior is illustrated in Figure 2, in which the ultraviolet data are presented on an enlarged scale; the effect is most pronounced in this color and suggests that during light-increase some form of absorption occurs whose effect diminishes with the successive cycles. The cycles 34795, 34799, and 34800 all appear to be

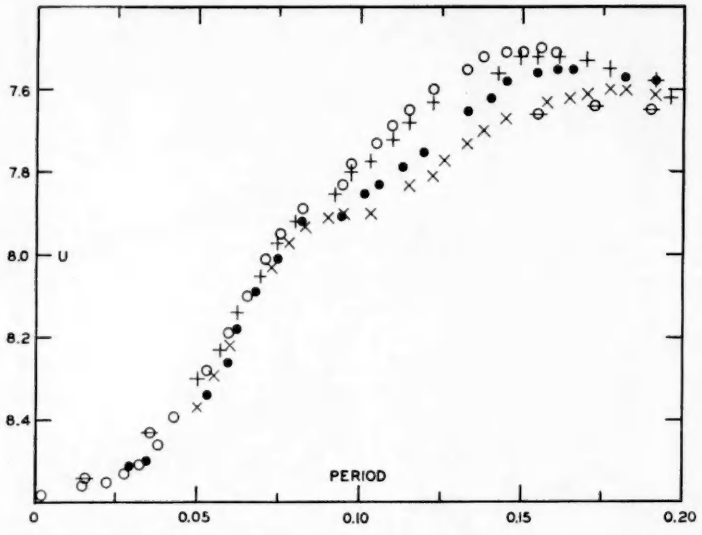


FIG. 2.—An enlarged portion of the ultraviolet light-curve showing a common rise to phase 0.08 and departures thereafter for several cycles.

about 0.02 period ahead of the corresponding observations in the earlier group, although a few observations taken in a somewhat later cycle, 34820, do not show such a discrepancy in phase. No phase differences are apparent at maximum or minimum light among the different light-curves for the same cycle.

The changes in the color indices are also illustrated, and it can be seen that the range in $B - V$ corresponds very well to the range found by Stebbins and to the estimates of spectral class based on the hydrogen lines to which he refers. Any appreciable reddening in RR Lyrae has been considered unlikely by Münch and Terrazas (1946), and this seems to be confirmed by the data on such B stars as there are in the direction of RR Lyrae, as contained in the list of 1332 B stars of Stebbins, Huffer, and Whitford (1940). It may be noted that the bluest color attained in the cycles appears to vary with the height of the maximum; in general, the higher the maximum, the bluer the color. Thus it may be that some slight variation in spectral type accompanies this phenomenon.The $U - B$ index between phases 0.15 and 1.0 is characteristic of the giants within this

spectral range, having about 0.05 mag. less ultraviolet than main-sequence stars of the same range. This is more evident in Figure 3, a $U - B$ versus $B - V$ diagram, where the main sequence is shown along with the positions of a few giants and RR Lyrae is represented by the points forming a loop.

It is interesting to note the brief excursions made in this diagram into the region above the main sequence characterized by strong ultraviolet radiation. This phenomenon is well marked in all the cycles covered; but, since the action is so rapid and the relative increase in the ultraviolet is about 10 per cent superimposed on an absolute increase of about 200 per cent, the individual cycles show considerable scatter around the schematic curve illustrated. Added to this scatter of an accidental nature is the influence of considerable systematic differences among the loops for various cycles. So far as can be noted from the data available, it appears that the phase of maximum ultraviolet excess

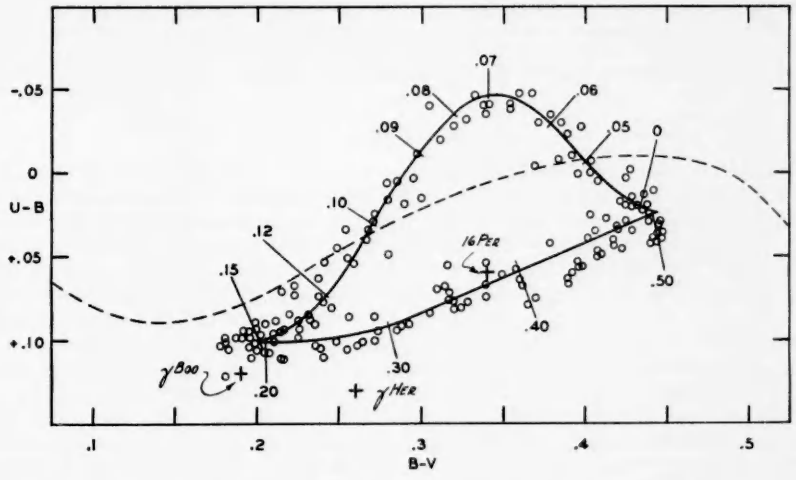


FIG. 3.—The dotted curve represents the main sequence. The numbers on the loop correspond to the phase in Fig. 1. For the sake of clarity, many observations are not plotted, particularly between phases 0.5 and 1.0 periods.

coincides with the phase where the individual light-curves depart from a common rising branch in the case of those cycles sharing the common portion.

Interest in this behavior of RR Lyrae induced Dr. Helmut Abt to obtain spectra with the McDonald coudé spectrograph during the rising branch of two cycles in 1954 (July 3.3 and 6.3 U.T.). (The author wishes to express his gratitude to Dr. Abt for the use of his unpublished data.) An inspection of the plates seemed to show a large and short-lived decrease in the strength of the hydrogen lines about the time of the ultraviolet excess. The equivalent widths of $H8$ and $H12$ were measured on thirteen plates and were found to undergo a decrease of about 12 per cent at this time. This effect may be sufficient to explain part of the ultraviolet excess.

It is at the same phase that the remarkable changes in the hydrogen-line structure occur as noted by Struve (1948) and Sanford (1949). A thorough study of this behavior in cycles characterized by maximum as well as minimum amplitudes would be of considerable interest, as would be intensive photoelectric observations made over a wide color range and including a measure of the Balmer discontinuity.

## REFERENCES

Detre, L. 1943, *Mitt. d. Sternw. Budapest-Svábhegy*, No. 17.
Gordon, C., and Kron, G. 1947, *Ap. J.*, **106**, 318.
Morgan, W. W., and Johnson, H. L. 1953, *Ap. J.*, **117**, 313.
Münch, G., and Terrazas, L. 1946, *Ap. J.*, **103**, 371.
Sanford, R. 1935, *Ap. J.*, **81**, 150.
———. 1949, *ibid.*, **109**, 211.
Stebbins, J. 1953, *Pub. A.S.P.*, **65**, 118.
Stebbins, J., Huffer, C., and Whitford, A. 1940, *Ap. J.*, **91**, 20.
Struve, O. 1948, *A.J.*, **53**, 108.
Walraven, T. 1949, *B.A.N.*, **11**, 17.

# AXIAL ROTATION AND STELLAR EVOLUTION

ALLAN R. SANDAGE
Mount Wilson and Palomar Observatories
Carnegie Institution of Washington, California Institute of Technology
*Received April 6, 1955*

ABSTRACT

Some of the current ideas of stellar evolution are tested by using Arne Slettebak's homogeneous data on the rotational velocities of stars. The values of $V \sin i$ for stars not now on the main sequence are shown to be consistent with the idea that these stars were once main-sequence objects but have moved into the giant and supergiant region of the $M_{bol}$, log $T_e$ plane by an evolutionary process. In particular, the data are entirely consistent with the evolutionary tracks computed by M. Schwarzschild and his collaborators.

## I. SCOPE OF THE PROBLEM

According to current ideas of stellar evolution, stars now in the giant and supergiant region of the $M_{bol}$, log $T_e$ diagram were once on the main sequence. They have moved to their present positions because of changes of internal structure due to a chemical in homogeneity in the deep interior. The details of this process have been studied theoretically by a number of workers (Oke and Schwarzschild 1952; Roy 1952; Sandage and Schwarzschild 1952; Taylor 1954). These investigations give the evolutionary tracks followed by idealized stars as they move from the main sequence.

There are several ways to test observationally the general content of these ideas of stellar evolution. The study of color-magnitude diagrams of star clusters is one powerful test method, and progress has recently been made in exploiting this approach (Johnson 1954; Miczaika 1954; Sandage 1954; Johnson and Sandage 1955). Another method, which is dynamical in character, is a comparison of the rotational velocities of main-sequence stars with those of giant and supergiant stars. The assumption of the conservation of angular momentum is made. With this approach, we ask whether the observed rotational velocities of all stars not now on the main sequence are consistent with the hypothesis that each star has moved from the main sequence to its present position along the tracks of evolution we wish to test.

This problem has recently been studied in a fundamental paper by Oke and Greenstein (1954). These authors analyze the rotational velocities of thirty-four stars. Their sample was very small and unfortunately excluded several stars which were known to have rapid rotation. This occurred because their plates were taken for another purpose. The conclusion of Oke and Greenstein was that the evolutionary picture was consistent with their data. However, owing to the smallness of their sample and to its statistical bias, questions as to the generality of their results arise.

Adequately to exploit this approach, rotational velocities for a large number of stars well distributed over the $M_{bol}$, log $T_e$ plane must be available. Furthermore, the position of each star in this plane must be known, so that the proposed evolutionary tracks may be used to predict the point along the main sequence from which each star came. Fortunately for this problem, several large investigations of the rotational velocities of stars have recently been completed. Among these, the work of Huang (1953), Herbig and Spalding (1955), and particularly Slettebak (1949, 1954, 1955) and Slettebak and Howard (1955) should be mentioned. Slettebak's extensive investigations are especially valuable, since they cover the entire relevant range of spectral types from B3 to G0 and

include the most accurate two-dimensional spectral classifications on the revised MK system (Johnson and Morgan 1953) that are now available for the stars studied. This is important, since it permits $M_{bol}$ and log $T_e$ to be determined for each star in question. Furthermore, Slettebak's data are statistically unbiased because of his method of selection. Consequently, Slettebak's data will be used in this paper to test the compatibility of the observed $V$ sin $i$ with the theoretical evolutionary tracks. The tracks chosen for the test are those computed by Sandage and Schwarzschild. It should be pointed out that the results are rather insensitive to the exact details of the assumed tracks. Consistency of the data with the evolutionary picture would not necessarily imply that the assumed evolutionary models are correct in detail but only that the mapping of stars from the main sequence into the giant region along tracks of nearly constant luminosity would seem to work in a general way.

The validity of using these particular tracks in the present case may be questioned, since the evolutionary models were computed for the case of no mixing between the exhausted core and the virgin envelope. If rotation strongly affects mixing, then tracks for unmixed models cannot be applied. Recent theoretical work (Mestel 1953) indicates, however, that rotation has an almost negligible effect on mixing, if the angular velocity is nearly constant throughout the star, even for stars near dynamical instability. Consequently, there appears to be no contradiction in applying unmixed models to the present study.

## II. METHODS OF ANALYSIS

There are three possible methods of treating the data. These methods differ in the severity of the analysis and in the amount of data needed to make the analysis. The first method asks the question: Are there any giant and supergiant stars rotating *faster* than would be expected from the fastest-rotating star now on the main sequence in the relevant spectral range? This is the method of Oke and Greenstein. A second and more comprehensive method tests not just the maximum rotational velocity but the entire distribution function of $V$ sin $i$. Each star in the giant and supergiant region is projected back onto the main sequence, using the evolutionary tracks. From the observed $V$ sin $i$ and the known ratio of the present radius to the radius which the star had on the main sequence, $R/R_0$, the main-sequence value of $V$ sin $i$ may be computed. The distribution function of these "recovered" values of $V$ sin $i$ can then be compared with that of stars now on the main sequence. The second method requires many more data than the first method but is a more severe test. The third method is a still more comprehensive test. If data were available for a sufficient number of giants and supergiants, the distribution function of $V$ sin $i$ at several points along any given evolutionary track could be found and compared with the distribution predicted from the theoretical tracks. The number of data required for this test is so great that it cannot be used in the present case. The application of these three methods requires, of course, the assumption that the distribution function of $V$ sin $i$ along the main sequence has not changed in the last $10^8$–$10^9$ years.

The first and second methods are applied here to Slettebak's data. Each star of luminosity class other than V was plotted in the $M_{bol}$, log $T_e$ plane by using Keenan and Morgan's (1951) calibration of the MK system as revised by Keenan (1955). A track of evolution was put through each star and carried back to the main sequence. The star's original spectral class and $R/R_0$ could then be determined. The rotational velocity of any star will decrease as $R/R_0$ increases, if angular momentum is conserved. The exact manner of the decrease will depend upon the distribution of the rotational velocities within the star. If the star rotates as a rigid body, the change of the moment of inertia, $I$, must be known as a function of $R/R_0$. For the theoretical models under consideration the moment of inertia may be found at each point of the evolutionary track, since the density distribution within the star is known at seven points corresponding to the seven computed models (Sandage and Schwarzschild 1952.) Hence $I$ may be found as a func-

tion of $R/R_0$, and consequently the relation $(V \sin i)_0 = f(R/R_0)(V \sin i)_{now}$ obtained. The computations of the moments of inertia have been made by Oke and Greenstein (1955), and the results are taken from their paper. Following these authors, this case of rigid-body rotation is called "case A." At the other extreme we may consider the case where every infinitesimal spherical shell maintains its own angular momentum during the expansion. Here $(V \sin i)_0 = R/R_0(V \sin i)_{now}$. Oke and Greenstein call this "case B." The true situation may be expected to lie somewhere between case A and case B.

## III. RESULTS

To facilitate the tests, the data were divided into the four spectral intervals B0–B9, A0–A3, A4–F0, and F1–G0. These particular intervals were chosen because the distribution of $V \sin i$ along the main sequence seemed to be similar within each range. Applica-

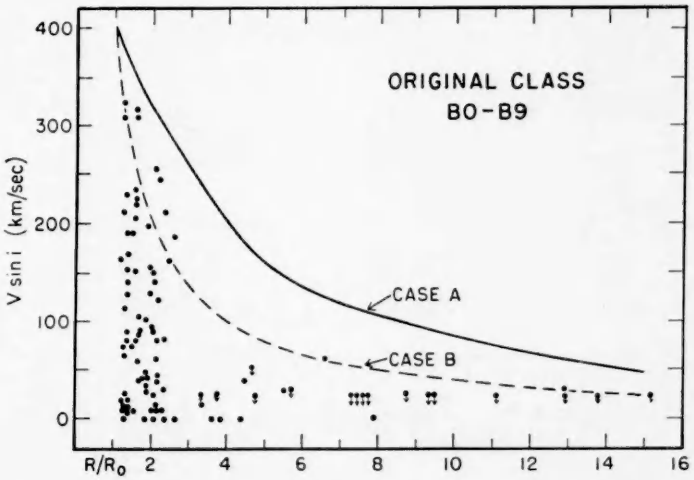


FIG. 1.—Observed $V \sin i$ for stars not now of luminosity class V plotted against the ratio of their present radius to their radius on the main sequence. Stars whose original spectral class was B0–B9 are plotted. The solid line, case A, shows how $V \sin i$ changes for a star rotating as a rigid body if it follows the Sandage-Schwarzschild evolutionary models. Case B is for stars in complete differential rotation.

tion of the first test method requires that the maximum value of $V \sin i$ be known for stars now along the main sequence. Histograms of the $V \sin i$ distributions for stars in Slettebak's lists of present luminosity class V were constructed for each of the four intervals, and the maximum $V \sin i$ was determined (see Figs. 3 and 4). These maximum $V \sin i$ are for B0–B9, 400 km/sec; for A0–A3, 360 km/sec; for A4–F0, 280 km/sec; and for F1–G0, 120 km/sec. These values represent the upper limits for the stars studied. Although the lists are completely homogeneous and statistically unbiased, there are stars not included in the present material, such as $\phi$ Per (B2, $V \sin i \approx 500$ km/sec) and HR 2142 (B2 IV, V; $V \sin i = 450$ km/sec) with higher rotations than the maxima given. The adopted maxima refer only to those stars in the present material whose luminosity class is known. These values must be used to keep the sample statistically unbiased.

Figures 1 and 2 show how the $V \sin i$ of a star rotating at the maximum permissible value for $R/R_0 = 1$ will change with increasing $R/R_0$. Cases A and B are shown. The observed values of $V \sin i$ are plotted at the $R/R_0$ appropriate for each star considered.

If any star is rotating faster than is consistent with the evolutionary hypothesis, it would lie above the limiting line of case A in Figures 1 and 2. These figures show that, to within the error of measurement, no stars for which the necessary data are available in Slettebak's lists are rotating faster than would be expected from the evolutionary tracks. The six rapidly rotating stars excluded by Oke and Greenstein are included in the present study and have no higher $V \sin i$ values than would be expected. There are, however, several rapidly rotating stars contained in Slettebak's list of B2–A2 stars which are excluded from Figures 1 and 2. These are stars for which estimates of the luminosity

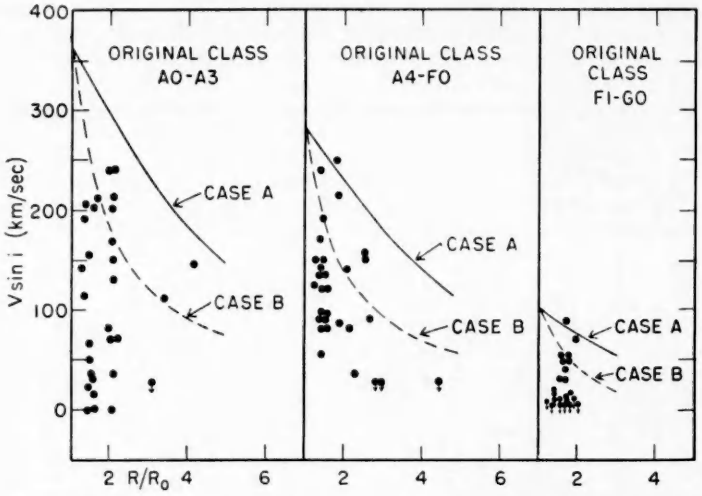


FIG. 2.—Same as Fig. 1 for original spectral types A0–A3, A4–F0, and F1–G0

TABLE 1

STARS WITH NO LUMINOSITY CLASS AVAILABLE

| Star | Sp. | $V \sin i$ (Km/Sec) | $R/R_\odot$* | Star | Sp. | $V \sin i$ (Km/Sec) | $R/R_\odot$* |
|---|---|---|---|---|---|---|---|
| $\psi$ Per | B5e | 390 | 1.39 | 7 Cep | B7 | 300 | 1.56 |
| 120 Tau | Bp | 280 | (1.4) | HR 8731 | B2pe | 340 | 1.21 |
| HR 2142 | B2 IV, V | 450 | 1.21 | o And | B6pe | 330 | 1.51 |
| $\kappa$ Dra | B7p1 | 250 | 1.56 | $\beta$ Psc | B5pe | 145 | 1.39 |
| $\theta$ Cr B | B7nne | 400 | 1.56 | $\psi$ Cyg | A3 IV, V | 300 | 1.33 |
| 48 Lib | Bpe | 400 | (1.4) | | | | |

* Computed by assuming stars are of luminosity class IV.

class were impossible because of the large rotational broadening of the lines. In most cases it is probable that the luminosity class is either IV or V, but a closer decision is not possible. Table 1 lists these excluded stars.The fourth column of this table gives $R/R_\odot$ on the assumption that the luminosity class is IV. We may test, therefore, whether the rotations of these stars are also consistent with the evolutionary hypothesis, even if $R/R_\odot > 1$. Three of the stars listed do exceed the criterion lines of case A by values

which are significant. These are HR 2142 (B2 IV, V), $\theta$ Cr B (B7nne), and 48 Lib (Bpe). However, there is as good a chance that these stars are of class V as of class IV. Consequently, the high $V$ sin $i$ cannot be regarded as objectionable to the theory. Four stars in Slettebak's list of A3–G0 stars (1955) had indefinite luminosity classes for the same reason. They were $\alpha$ Aql (A7 IV, V), $\psi$ Cyg (A3 IV, V), 33 Cyg (A3 IV, V), and $\alpha$ Cep (A7 IV, V). Here a decision on the correct luminosity class was possible for three of these from trigonometric parallaxes: $\alpha$ Aql is of class V, while 33 Cyg and $\alpha$ Cep are of class IV. These last two stars are plotted in Figure 2. The luminosity class of $\psi$ Cyg is still unknown. This star is listed in Table 1. The conclusion from the results of the first test method is that all data are consistent with the evolutionary hypothesis.

The results of the second test method are shown in Figures 3 and 4. Values of $(V \sin i)_0$ were computed for each star from the known value of $R/R_0$ according to case A or case B. The distribution function of these recovered $V$ sin $i$ is compared with the distribution

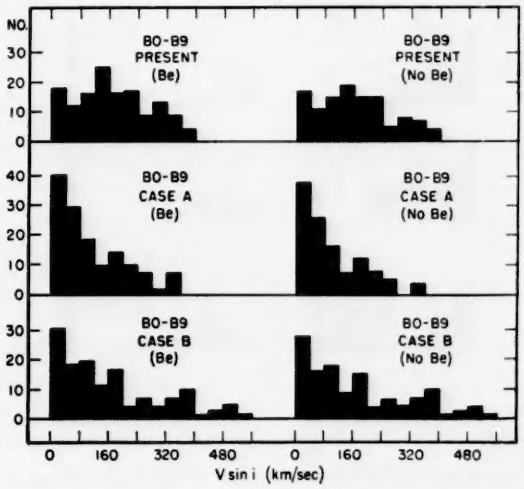


FIG. 3.—Histogram of the velocity distribution B0–B9 stars. Top diagrams are for stars currently on the main sequence. Distributions with and without Be stars are given. The middle histograms are the recovered distribution functions for case A. The bottom histograms are the recovered functions for case B.

function of stars of present luminosity class V. In Figures 3 and 4 the histograms of the recovered distribution for cases A and B have been normalized to the same total number as class V stars. Two cases are treated in Figure 3, one including and one excluding the Be stars.

Visual inspection is adequate in Figure 3 to see that the recovered B0–B9 distribution functions for both cases A and B contain more stars with small $V$ sin $i$ than they should. The observed values of $V$ sin $i$ for the giants and supergiants which originated as B0 V–B9 V stars are not high enough. A partial explanation for this apparent anomaly lies in the method of treating the data. Many of the giant and supergiant stars have observed values of $V$ sin $i$ which are tabulated as less than 25 km/sec. This value is the lower limit of detection with Slettebak's technique. The recovered $(V \sin i)_0$ on the main sequence is then known only to less than $R/R_0 \times 25$ for case B, with a similar situation for case A. For large $R/R_0$ this upper-limit value of $(V \sin i)_0$ can be quite

high. The data were statistically treated as if the true velocity were half the upper-limit value. This may not be the case. If the stars with large $R/R_0$ have true $V \sin i$ near the upper limit, part of the low-velocity portion of the distribution function will move to higher $(V \sin i)_0$. This will explain part, but not all, of the discrepancy. If the remaining discrepancy is statistically significant, speculation concerning a possible change in the velocity distribution along the B0–B9 portion of the main sequence in the last $10^7$–$10^8$ years, or, what is more likely, a loss of mass of these stars as they expand is possible. The data are too scarce, however, to make this venture profitable.

Comparison of the distribution function in the A0–G0 interval is shown in Figure 4. Case B seems definitely not to fit the data. This may also be seen from Figures 1 and 2, where many stars violate the case B upper line. Case B therefore seems unrealistic. The stars must rotate more nearly as rigid bodies than as stars in complete differential rotation.

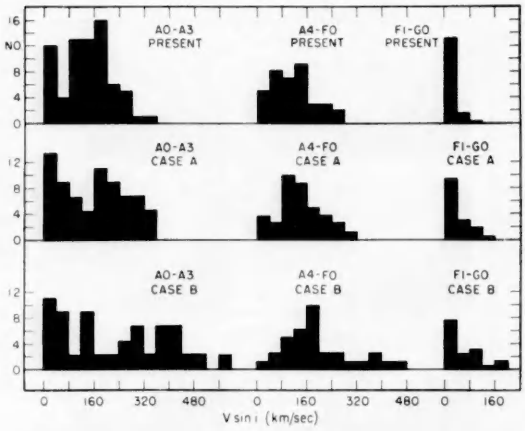


FIG. 4.—Same as Fig. 3 for the original spectral types A0–A3, A4–F0, and F1–G0

The distribution functions for case A and for the present main sequence in this spectral interval are very similar. Statistical methods of comparison are needed, since the functions are so similar. Table 2 lists the relevant characteristics for these two distributions. Given are the mean values of $V \sin i$, the square of the standard deviation of the distribution, the total sample number $n$, twice the standard deviation for the distribution of the differences in the mean $V \sin i$ if repeated samples could be taken, and the difference in the mean $V \sin i$ between the distributions.

The mean values of $V \sin i$ differ between the distributions by about 20 km/sec. Is this difference statistically significant? Following the standard treatment (e.g., Hoel 1947), we let $(\overline{V \sin i})_V$ and $(\overline{V \sin i})_A$ be the means of the two distribution functions whose comparability we wish to test. These two means may be considered as the first pair of samples taken from a large population in repeated sampling, i.e., they may be treated as variables for which one pair of values is available. If the number of individual stars $n$ is sufficiently large, the distribution functions of $(\overline{V \sin i})_V$ and $(\overline{V \sin i})_A$ which would be obtained from repeated sampling of the entire population will be normally distributed. If this is the case, it can be shown that the *differences* in the means are normally distributed, with a standard deviation given by

$$\sigma_{(\overline{V \sin i})_V - (\overline{V \sin i})_A} = \left( \frac{\sigma_V^2}{n_V} + \frac{\sigma_A^2}{n_A} \right)^{1/2}.$$

The statistical significance of the difference of the $\overline{V \sin i}$ between the two distributions may now be tested. We place the confidence limits of the statistical test at 0.05. This means that a difference of $2\sigma_{V-A}$ is just statistically significant. This value is tabulated in Table 2. For the A0–A3 and A4–F0 cases, the difference of $V \sin i$ between the distributions is not significant. Therefore, both distributions could have come from the same statistical population. The case F1–G0 is just significant, which indicates that the two means are farther apart than is expected if the true distributions are indeed the same. This case, however, does not represent the true situation, since nearly half the stars in this group have only upper limits to $V \sin i$, i.e., the tabulated $V \sin i$ are $< 25$ km/sec. The true statistics of the distribution are therefore not known.

The conclusion from the second test method is that the recovered velocity distribution in the range A0–G0, case A, is sufficiently like the present main-sequence distribution to be in agreement with the evolutionary hypothesis. The lack of agreement in the

TABLE 2

STATISTICS OF THE DISTRIBUTION FUNCTIONS

| | A0–A3 | | A4–F0 | | F1–G0 | |
|---|---|---|---|---|---|---|
| | Present V | Case A | Present V | Case A | Present V | Case A |
| $\overline{V \sin i}$ (km/sec) | 137 | 159 | 115 | 139 | 21 | 42 |
| $\sigma^2$ | $6.00\times10^3$ | $1.09\times10^4$ | $4.55\times10^3$ | $5.13\times10^3$ | $3.7\times10^2$ | $1.3\times10^3$ |
| $n$ | 71 | 32 | 37 | 30 | 38 | 24 |
| $2\sigma_{V-A}$ | 41 | | 34 | | 16 | |
| $(\overline{V \sin i})_A - (\overline{V \sin i})_V$ (km/sec) | 22 | | 24 | | 21 | |

B0–B9 range is not considered serious because of the unknown values of $(V \sin i)_0$ for stars of large $R/R_0$ with $V \sin i > 25$ km/sec. The first and second test methods therefore lead to the conclusion that the general evolutionary picture is tenable on the basis of the rotational-velocity data.

It is a real pleasure to acknowledge several discussions with Arne Slettebak concerning the observational aspects of this problem and to thank him for the privilege of using his data before the final list of rotational velocities was published.

REFERENCES

Herbig, G. H., and Spalding, J. F. 1955, *Ap. J.*, **121**, 119.
Hoel, P. G. 1947, *Introduction to Mathematical Statistics* (New York: John Wiley & Sons, Inc.).
Huang, S. S. 1953, *Ap. J.*, **118**, 285.
Johnson, H. L. 1954, *Ap. J.*, **120**, 325.
Johnson, H. L., and Morgan, W. W. 1953, *Ap. J.*, **117**, 313.
Johnson, H. L., and Sandage, A. R. 1955, *Ap. J.*, **121**, 616.
Keenan, P. G. 1955, private communication.
Keenan, P. G., and Morgan, W. W. 1951, *Astrophysics*, ed. Hynek (New York: McGraw-Hill Book Co., Inc.), chap. 1.

Mestel, L. 1953, *M.N.*, **113**, 716.
Miczaika, G. R. 1954, *Les Processus nucléaires dans les astres* (Louvain: Imprimerie Ceuterick), pp. 275–282.
Oke, J. B., and Greenstein, J. L. 1954, *Ap. J.*, **120**, 384.
Oke, J. B., and Schwarzschild, M. 1952, *Ap. J.*, **116**, 317.
Roy, A. E. 1952, *M.N.*, **112**, 484.
Sandage, A. R. 1954, *Les Processus nucléaires dans les astres* (Louvain: Imprimerie Ceuterick), pp. 254–274.
Sandage, A. R., and Schwarzschild, M. 1952, *Ap. J.*, **116**, 463.
Slettebak, A. 1949, *Ap. J.*, **110**, 498.
———. 1954, *ibid.*, **119**, 146.
———. 1955, *ibid.*, **121**, 653.
Slettebak, A., and Howard, R. F. 1955, *Ap. J.*, **121**, 102.
Taylor, R. J. 1954, *Ap. J.*, **120**, 332.

# STELLAR EVOLUTION AND THE SYNTHESIS OF THE ELEMENTS

W. A. FOWLER,* G. R. BURBIDGE
Cavendish Laboratory, University of Cambridge

AND

E. MARGARET BURBIDGE
Cambridge

*Received March 7, 1955; revised April 7, 1955*

## ABSTRACT

The production of neutrons in stellar interiors will occur through exoergic $(\alpha, n)$ reactions on $O^{17}$, $Ne^{21}$, $Mg^{25}$, and $Mg^{26}$ as well as on $C^{13}$, as first suggested by Cameron. With these reactions as possible neutron sources, an attempt is made to indicate a general, but still qualitative, basis for the synthesis of the elements in stars. The importance of successive stages of interaction of the light nuclei with hydrogen and helium is stressed. In particular, the reaction $Ne^{20}(p, \gamma)Na^{21}(\beta^+)Ne^{21}$, followed by $Ne^{21}(\alpha, n)Mg^{24}$, is taken as the basis for alterations and modifications of the mechanisms of Hoyle and Cameron for the synthesis of the intermediate and heavy elements, respectively. The use of this reaction obviates some of the difficulties encountered in processes in which a small proportion of hydrogen must be mixed into the stellar core at temperatures at which it will be very rapidly consumed.

A possible evolutionary scheme which is consistent with these element-building processes is outlined. It is supposed that the synthesis of the heavy elements will take place in stars which have reached the cool giant stage in their evolutionary path. The M as well as the S stars may be important in this connection. A rough estimate, based on the observed frequency of S stars, suggests that the rate of element synthesis in these stars is sufficient to produce the observed heavy-element abundances. Differences in chemical composition between population I, population II, and intermediate groups of stars are briefly discussed.

## I. INTRODUCTION

Recent work of Salpeter (1952), Hoyle (1954), and Cameron (1954, 1955) has indicated that the stable elements will be synthesized from hydrogen in the interior of evolving stars. In this paper we wish to clarify certain aspects of the nuclear reactions involved in the element synthesis, with the object of establishing a more general basis for the production of the elements in stellar interiors. Further, we wish to propose that such a process of continuous synthesis as stars evolve must now be seriously considered as the source of the observed universal astrophysical abundances of all the elements up to the naturally radioactive alpha-emitters. It is not possible at our present stage of knowledge to choose between a primeval and a continuous synthesis,[1] but the latter process now stands at least equal to the former in providing a rational basis for the production of the elements. In point of fact, it may be somewhat superior from a nuclear standpoint, in that it avoids the well-known difficulties of the primeval synthesis at masses 5 and 8. On the other hand, deuterium, *Li*, *Be*, and *B* cannot be synthesized permanently in stellar interiors. Their possible synthesis in high-energy nuclear reations on stellar surfaces will be discussed by us in a forthcoming publication. It must be emphasized that an ultimate decision will rest on further nuclear research, elucidated in part in what follows, and in an increasing accumulation of the astrophysical details of stellar evolution.

## II. NUCLEAR CONSIDERATIONS

### A. SYNTHESIS OF $C^{12}$, $O^{16}$, $Ne^{20}$, AND $Mg^{24}$

In the core of a star in which hydrogen has been transformed into helium by the *pp*-chain or the *CN*-cycle, contraction and the release of gravitational energy will occur until

* Fulbright scholar on leave of absence from the California Institute of Technology.

[1] We are not concerned here with the question of the primeval or continuous creation of matter. Our remarks are directed only to problems involved in the synthesis of the heavier elements from hydrogen.

the density ($\rho \sim 10^3$ gm/cc) and temperature ($T \sim 1.4 \times 10^{8}$°) are great enough for nuclear reactions involving helium to take place. These reactions, as discussed by Salpeter and Hoyle, produce $C^{12}$, $O^{16}$, $Ne^{20}$, and possibly $Mg^{24}$. New experimental information on these reactions has been analyzed by one of us (W. A. F.) and is in preparation for publication. There still do not exist direct experimental data on the cross-sections, and thus the abundance ratios in which the nuclei mentioned will be produced cannot be determined solely from nuclear data. The best estimates at present would indicate that the helium will be converted predominantly into $O^{16}$ and $Ne^{20}$; but, in view of the large uncertainties, it cannot be concluded that the nuclear data are inconsistent with the astrophysical abundance ratios $1:3:2:\frac{1}{10}$ for $C^{12}:O^{16}:Ne^{20}:Mg^{24}$. This point has previously been emphasized by Hoyle and assumes that not too large a fraction of these nuclei (half or less) has been destroyed subsequent to their formation.

### B. SYNTHESIS OF THE LIGHT ELEMENTS

The new elements produced in helium-burning will be introduced into interstellar and intergalactic gas by explosive or steady ejection from the core of an evolving star (Hoyle 1954). In some cases the core material may be ejected into the hydrogen atmosphere of the surrounding envelope. This will lead to modification of the $C^{12}$, $O^{16}$, $Ne^{20}$, and $Mg^{24}$ by hydrogen-burning. That fraction of these elements which does escape into interstellar gas, which is mainly hydrogen, may recondense into stars and also undergo modification by hydrogen-burning and even further helium-burning. In spite of the great complexity of the astrophysical processes here envisaged, these considerations do indicate a straightforward source of the other isotopes of the light nuclei.

Any $C^{12}$ from the helium core of a star introduced into the star's hydrogen envelope or, by condensation, into the material of a new star burning hydrogen will react to produce $C^{13}$, $N^{14}$, and $N^{15}$ in the equilibrium abundances determined by the temperature of interaction and by the cross-sections of the $CN$-cycle reactions. These reactions are cyclic and catalytic, and the total number of carbon-nitrogen nuclei remains unchanged. (The small leakage of $O^{16}$ by the capture reaction in $N^{15}$ is returned, as will become clear in what follows.) The nucleus $O^{16}$ introduced into hydrogen undergoes a radiative capture reaction and beta decay to $O^{17}$, which, in turn, undergoes an exoergic $(p, \alpha)$ reaction resulting in the production of $N^{14}$ and thus essentially of the equilibrium mixture of the carbon and nitrogen isotopes. Any small amount of $O^{18}$ produced by proton capture by $O^{17}$ also undergoes a $(p, \alpha)$ reaction, resulting in $N^{15}$ and thus a return to carbon and nitrogen. Thus $C^{12}$ and $O^{16}$ produce $C^{13}$, $N^{14}$, $N^{15}$, and $O^{17}$ in hydrogen-burning. It is an interesting point, already noted by Hoyle, that the equilibrium ratio (Fowler 1954) of $C^{13}$ to $N^{14}$ in the $CN$-cycle is about 1:50 at the temperatures at which hydrogen burns in stars ($\sim 2 \times 10^{7}$°). Thus, if enough $C^{13}$ is produced in this way to give the terrestrial ratio to $C^{12}$ of 1:90, then the universal abundance of $C^{12}$ and $N^{14}$ ought to be about equal. This is approximately what is observed. In fact, the cosmic abundances $C^{12}:N^{14}:O^{16} = 1:2:3$ indicate that a considerable fraction (one-third) of the original $C^{12}$ and $O^{16}$ has gone into $N^{14}$ and a small amount of $C^{13}$. Probably most of the $N^{14}$ and $C^{13}$ came from $C^{12}$, in which case two-thirds of the $C^{12}$ produced in helium-burning has been transformed in subsequent hydrogen-burning. On the other hand, the large observed cross-section of the $N^{15}(p, \alpha)$ process, 2800 times that observed for $N^{14}(p, \gamma)$, means that only 10 per cent of the $N^{15}$ in the observed ratio of $N^{15}:N^{14} = 1:270$ can be produced in the $CN$-cycle. However, the cross-section of the $N^{14}(p, \gamma)$ reaction in the range of stellar energies may be higher than that estimated from low-energy measurements by a factor of 10, and then this discrepancy would not exist (cf. discussion by Fowler 1954). A slight lowering of the hydrogen-burning temperature to $10^{7}$° would restore the agreement in the carbon and nitrogen isotope ratios noted earlier. This is probably a reasonable temperature for the conditions under which the ratios "freeze in" in stellar envelopes.

The rate of the $O^{17}(p, \alpha)$ reaction has been estimated (Salpeter 1955) to be $\sim$1000 times

that of the $O^{16}(p, \gamma)\, F^{17}(\beta^+)\, O^{17}$ process. Thus the ratio of $O^{17}$ to $O^{16}$ in oxygen which has entered into, but not been entirely consumed in, hydrogen ought to be $\sim$1:1000, since the $O^{17}$ abundance will rapidly build up to and follow this ratio. The observed abundance ratio $O^{17}:O^{16} = 1:2500$ is not unreasonable if this is the source of the $O^{17}$.

At this point it is well to emphasize that large amounts of $O^{16}$ introduced into the hydrogen envelope of a star cannot be entirely transformed into carbon and nitrogen. This is because these products of the oxygen and hydrogen processes react with the hydrogen very rapidly to convert it into helium, and thus the hydrogen will be consumed before all the oxygen is converted. This point is almost certainly of importance in connection with carbon- and nitrogen-rich stars. Either $C^{12}$ or $O^{16}$ ejected into the envelope of such stars will result in the occurrence of carbon, nitrogen, and oxygen isotopes in these envelopes. However, the element ratios will depend in a complicated way on the initial ratio of $C^{12}$ to $O^{16}$ and on the temperature at which the material reaching the stellar surface has last reacted. The isotopic ratios should be independent of these factors, and the observations of McKellar (1949) that $C^{12}:C^{13} = 3.4:1$ in R stars is in agreement with the predicted ratio of $4.3 \pm 1.6$ from cross-section measurements (Fowler 1954).

The nucleus $Ne^{20}$ introduced into hydrogen reacts to produce $Ne^{21}$, $Ne^{22}$, and $Na^{23}$ in a catalytic set of reactions similar to those involving the carbon and nitrogen isotopes. From the cross-section estimates made by Salpeter (1955) and the experimental results of Broström *et al.* (1947), neglecting possible low-lying resonances, the equilibrium abundance ratios of the three product nuclei should be of the order of 1 per cent of that of $Ne^{20}$. Only the natural abundance ratio $Ne^{22}:Ne^{20} = 1:10$ seems to be in disagreement with this, and we shall discuss this point in more detail in what follows. The leakage through to $Mg^{24}$ may be considerable in this case.

We conclude this section by noting that, as indicated by Hoyle, the small amounts of $O^{18}$ and $F^{19}$ found in nature can be produced by $(\alpha, \gamma)$ processes in helium interactions of $N^{14}$ and $N^{15}$. Hoyle also proposed that $O^{17}$ and $Ne^{21}$ could be produced in the reactions $C^{13}(\alpha, \gamma)$ and $O^{17}(\alpha, \gamma)$, but we shall see that more rapid competing reactions preclude this. We have already proposed alternative possibilities. The over-all conclusion is that helium-burning, with subsequent hydrogen-burning of a substantial fraction, approximately half, of the products, is capable of synthesizing all the stable isotopes from $C^{12}$ to $Mg^{24}$.

### C. SYNTHESIS OF THE INTERMEDIATE AND HEAVY ELEMENTS

Following the depletion of the helium with the production of $C^{12}$, $O^{16}$, $Ne^{20}$, and $Mg^{24}$, further contraction and increase of density and temperature in those stars with stable cores will result in reactions between these nuclei. These will eventually lead, in processes discussed in detail by Hoyle (1954), to the production of many of the nuclei up to and including the metals, the most stable nuclei at the minimum of the packing fraction-curve. Production of elements beyond the minimum by interactions of charged particles is not to be expected except at densities and temperatures far in excess of those presently indicated for stellar interiors on astrophysical grounds. Some nuclear data at high energy are available on reactions between $N^{14}$ and $O^{16}$ and other such light nuclei (Chackett *et al.* 1954), but it will be some time until reasonable extrapolations to energies corresponding to stellar temperatures can be made.

The production of heavy elements in stellar interiors has recently been shown by Cameron (1954) to be possible by the discovery of a mechanism which results in the production of neutrons by reactions between charged particles. It is suggested that unburned hydrogen interacting with the $C^{12}$ in a helium-reacting core will produce $C^{13}$ by capture and the decay of $N^{13}$, and thence neutrons by the exoergic reaction,

$$C^{13}\,(\alpha, n)\, O^{16} + 2.20 \text{ mev}\,. \tag{1}$$

In a star condensed originally from pure hydrogen, this process would only expedite the

conversion of $C^{12}$ into $O^{16}$. However, in a star condensed from material in which the metal peak in the abundance-curve had previously been produced as discussed earlier, the heavy elements up to the naturally radioactive alpha-emitters would now be synthesized by successive captures of neutrons by the originally metallic nuclei. The neutrons will first be thermalized to energies of the order of 10 kev. The product—cosmic abundance *times* capture cross-section—for the metals exceeds that of all lighter elements, with the possible exception of $N^{14}$. Thus a substantial part of the total number of neutrons produced will be captured by the metals. At least 20 neutrons must be supplied per metal atom to yield the anomalous heavy-element abundances apparently observed in S stars (Cameron 1955) and also to produce the heavy elements from $A \sim 100$ to $A = 209$ in approximately equal amounts (see Sec. III), with some excess for those particularly stable nuclei with a "magic" number (50, 82, 126) of neutrons or protons.

The time scale ($10^5$–$10^7$ years, as discussed in Sec. III) will be well suited to allow beta-decay between successive captures by the stable nuclei. This has always been a problem in the rapid primeval synthesis of heavy elements by neutron capture. The time scale will be too long, however, to permit synthesis beyond the first rapidly decaying alpha-emitter, $Po^{210}$, which has a half-life of only 138 days. We shall not discuss the synthesis of the naturally radioactive elements in this paper. The production of heavy nuclei by neutron capture will result naturally in the observed isotopic abundances in which the neutron-rich or heavy isotopes are the most abundant. Similarly, the production of the light nuclei by charged-particle reactions has naturally resulted in a greater abundance of the lighter isotopes among those nuclei. The isotopic abundances of the intermediate nuclei also show the effects of neutron-capture processes. This point is discussed in detail in Section IIE.

Section IIA indicates that $O^{16}$ and $Ne^{20}$ and perhaps even $Mg^{24}$ are more abundant, or at least exist over a longer time scale, than $C^{12}$ in a helium-reacting core. We wish to point out, however, that neutron production will still occur. The interaction of unburned hydrogen in the expanding core or hydrogen from the stellar envelope mixed with $O^{16}$, $Ne^{20}$, and $Mg^{24}$ will produce $O^{17}$, $Ne^{21}$, and $Mg^{25}$ by radiative capture and subsequent rapid beta-decay. The temperature of the helium-reacting core will lead to rapid proton-capture reactions for these nuclei. All these nuclei have exoergic $(\alpha, n)$ reactions, i.e.,

$$O^{17}(\alpha, n)\, Ne^{20} + 0.60 \text{ mev}, \tag{2}$$

$$Ne^{21}(\alpha, n)\, Mg^{24} + 2.58 \text{ mev}, \tag{3}$$

$$Mg^{25}(\alpha, n)\, Si^{28} + 2.67 \text{ mev}, \tag{4}$$

in which neutrons will be produced. It is to be noted that this is a general property of those nuclei with mass number $A$ given by $4n + 1$, with $n$ an integer, because of the marked four-structure periodicity in the binding energies of the light nuclei. For heavier nuclei—$Si^{29}$, $S^{33}$, $A^{37}$, etc.—the $(\alpha, n)$ reaction becomes endoergic as the four-structure becomes less pronounced. In passing, we note that the following reaction is also exoergic:

$$Mg^{26}(\alpha, n)\, Si^{29} + 0.04 \text{ mev}. \tag{5}$$

In the neutron-producing mechanisms involving reactions (1) and (2) there is one difficulty. In the production of $C^{13}$ some $N^{14}$ will also be produced by $C^{13}(p, \gamma)N^{14}$, and this nucleus readily converts neutrons into hydrogen by the reaction $N^{14}(n, p)C^{14}(\beta^-)N^{14}$ without destroying itself except on a very short time scale ($\sim$8000 years mean lifetime). Thus sufficient neutrons may not be available for heavy-element building if too much $N^{14}$ is produced. In the production of $O^{17}$, some $N^{14}$ will also be produced by the $O^{17}(p, \alpha)N^{14}$ reaction. The $F^{18}$, $Na^{22}$, and $Al^{26}$ produced in the other relevant capture reactions are radioactive and do not constitute a source of difficulty. Thus reactions (3) and perhaps

(4) may be the most effective sources of neutrons. Since $Ne^{20}$ has a greater chance than $Mg^{24}$ of being produced in quantity before the helium is consumed, mechanisms involving reaction (3) may be the most promising. It may be true that hydrogen can be introduced into the core under such circumstances that the $N^{14}$ difficulty involving reactions (1) and (2) does not occur. In fact, residual hydrogen remaining as helium-burning replaces hydrogen-burning will certainly be consumed by $C^{12}$ capture, leading to reaction (1), rather than by $O^{16}$ or $Ne^{20}$. The amount so remaining should be quite small, however, since hydrogen reacts so rapidly at $10^{8}°$. The essential point made here is that neutron production follows any building of heavier nuclei by helium as long as hydrogen can be introduced into the core by some mixing process or by the growth of the core before the hydrogen is completely consumed.

### D. AN ALTERNATIVE MODE OF HEAVY-ELEMENT PRODUCTION

The last point mentioned in the preceding paragraph actually constitutes a serious difficulty in the mechanisms for the production of neutrons discussed here. It is very improbable that any hydrogen can survive until the temperature ($T \simeq 1.4 \times 10^{8}°$) and density ($\rho \simeq 10^{3}$ gm/cc) necessary for the conversion of helium into carbon are reached. In the presence of the normal abundance of the carbon and nitrogen isotopes ($\sim 10^{-3}$ by atom), the mean lifetime of hydrogen is a few years even at $T = 0.5 \times 10^{8}°$ and only a few days at $T = 10^{8}°$. Very much smaller amounts of carbon and nitrogen will suffice to remove the hydrogen in the time scales actually involved. It is also difficult to see how large quantities of hydrogen from the relatively cool envelope of a star could be introduced into the hot core, where carbon, oxygen, or neon is being produced. On the same grounds as just noted, the hydrogen will be consumed before it reaches the region of helium-burning.

The difficulties, both nuclear and astrophysical, with the mixing of hydrogen into regions of helium-burning lead to a consideration of other possible sources of the nuclei $C^{13}$, $O^{17}$, $Ne^{21}$, or $Mg^{25}$, which produce neutrons for heavy-element building in helium-burning. Since the metallic elements are necessary in their normal cosmic abundances in the process, it is reasonable to assume that the light nuclei are also present in their normal abundances in the material from which a star producing heavy elements has originally condensed. In Table 1 we list these abundances relative to the metals as given by Urey (1952), using the isotopic abundances of Bainbridge (1953).

As noted previously, about 20 neutrons must be supplied per metal atom to produce the heavy-element abundances which are relatively constant above $A = 100$. Cameron has already noted that the abundance of the $C^{13}$ left over in the core from the $CN$-cycle is insufficient to produce this number of neutrons. At equilibrium in the $CN$-cycle, $C^{12}:C^{13} = 4.3:1$; so that, from Table 1, we see that about 2.4 $C^{13}$ nuclei are available per metal nucleus. (Here we have neglected the conversion of some $O^{16}$ into carbon and nitrogen, and the fact that the ratio $N^{14}:C^{12}$ indicated by the $CN$-cycle cross-sections is larger than 2:1. However, these two effects tend to cancel each other.) This amount of $C^{13}$ produces 2.4 neutrons per metal atom; of these, about half are reconverted into protons and eventually alpha-particles by the $N^{14}(n, p)$ reaction and subsequent $CN$-cycle reactions. Thus only 1 in 20 of the necessary neutrons can be produced in this way.

Inspection of Table 1 would seem to indicate that $O^{17}$, $Ne^{21}$, and $Mg^{25}$ are also not sufficiently abundant. However, we must consider the possible occurrence of a resonance in the cross-section in the proton-capture reactions in which these nuclei are produced in hydrogen-burning. The most interesting possibility in this connection is $Ne^{20}(p, \gamma)Na^{21}(\beta^{+})Ne^{21}$. We have been informed by Dr. R. Middleton (1955) that he has found an excited state in $Na^{21}$ produced in $Ne^{20}(d, n')Na^{21*}$ with a $Q$-value of $-2.17$ mev, with a probable error of approximately $\pm 0.1$ mev. Coupled with $n + p = d + 2.22$ mev, this yields

$$Ne^{20} + p = Na^{21*} + 0.05 \pm 0.1 \text{ mev} . \qquad (6)$$

## TABLE 1

ABUNDANCE RELATIVE TO METAL GROUP AND CAPTURE CROSS-SECTIONS IN MILLIBARNS AT 15 KEV FOR INTERMEDIATE NUCLEI

| Isotope | Abundance | $\sigma(n, \gamma)$ | Product | Remarks |
|---|---|---|---|---|
| $C^{12}$ | 10.2 | 0.047 | 0.48 | |
| $C^{13}$ | 0.11 | 0.009 | 0.001 | |
| $N^{14}$ | 20.5 | 1.0 | 20.5 | |
| $N^{15}$ | 0.075 | 0.00024 | 0.00002 | |
| $O^{16}$ | 28.2 | 0.01 | 0.3 | |
| $O^{17}$ | 0.010 | ..... | ..... | |
| $O^{18}$ | 0.058 | 0.0021 | 0.0001 | |
| $F^{19}$ | 0.012 | 0.094 | 0.001 | |
| $Ne^{20}$ | 20.3* | ..... | ..... | |
| $Ne^{21}$ | 0.057 | ..... | ..... | |
| $Ne^{22}$ | 1.97 | 0.36 | 0.71 | |
| $Na^{23}$ | 0.059 | 2.6† | 0.15 | |
| $Mg^{24}$ | 0.90 | 0.33 | 0.30 | |
| $Mg^{25}$ | 0.12 | 2.7 | 0.32 | |
| $Mg^{26}$ | 0.13 | 6.0† | 0.78 | |
| $Al^{27}$ | 0.11 | 5.3‡ | 0.58 | |
| $Si^{28}$ | 1.19 | 0.81 | 0.96 | |
| $Si^{29}$ | 0.060 | 2.7 | 0.16 | |
| $Si^{30}$ | 0.039 | 11† | 0.43 | |
| $P^{31}$ | 0.012 | 1.93 | 0.023 | Estimated $\sigma$ probably too low |
| $S^{32}$ | 0.22 | 4.9 | ~0.55 | |
| $S^{33}$ | 0.0017 | | ~0.55 | Could contribute to $S(n,\gamma)$. $\sigma(n,\alpha)$ may be large. $\sigma(n, p) = 2.3$ mb thermal (small) |
| $S^{34}$ | 0.0097 | 2.6 | 0.026 | |
| $S^{36}$ | 0.00004 | 1.4 | 0.000056 | By-passed |
| $Cl^{35}$ | 0.016 | <313 | <5 | $\sigma$ estimate uncertain |
| $Cl^{37}$ | 0.0054 | 7.4† | 0.040 | |
| $A^{36}$ | 0.12 | < 65 | (0.043) | Produced by $Cl^{36}$ decay; $\sigma(Cl^{36})$ assumed to be 0.36 mb |
| $A^{38}$ | 0.02 | 8 | 0.16 | High but assumes all cosmic $A$ is $A^{36}$ and $A^{38}$; $N = 20$ magic |
| $A^{40}$ | ..... | 9.3† | ..... | Produced by $K^{40}$ decay |
| $K^{39}$ | 0.0083 | <18.7 | <0.16 | $\sigma$ estimate uncertain; $N = 20$ magic |
| $K^{40}$ | 0.000013* | <660 | <0.01 | $\sigma$ estimate uncertain |
| $K^{41}$ | 0.00061 | 29† | 0.018 | |
| $Ca^{40}$ | 0.082 | 2.2 | 0.18 | By-passed but doubly magic |
| $Ca^{42}$ | 0.00054 | <397 | <0.21 | $\sigma$ estimate uncertain |
| $Ca^{43}$ | 0.00012 | ..... | ..... | $\sigma$ should be large, ~100 mb |
| $Ca^{44}$ | 0.0017 | 6.3 | 0.011 | |
| $Ca^{46}$ | 0.000002 | 2.5 | 0.000005 | By-passed |
| $Ca^{48}$ | 0.00016 | 19† | 0.003 | By-passed but doubly magic |
| $Sc^{45}$ | 0.000023 | <230 | <0.0053 | $\sigma$ estimate uncertain |
| $Ti^{46}$ | 0.00028 | 5.7 | 0.0016 | |
| $Ti^{47}$ | 0.00027 | 16.2 | 0.0044 | |
| $Ti^{48}$ | 0.0025 | <80 | <0.20 | Equilibrium production |
| $Ti^{49}$ | 0.00019 | 18 | 0.0034 | |
| $Ti^{50}$ | 0.00019 | 19† | 0.0037 | |
| $V^{50}$ | 0.0000007 | 2.5 | 0.0000018 | By-passed (long-lived isobar) |
| $V^{51}$ | 0.00031 | 75‡ | 0.023 | Equilbrium production |
| $Cr^{50}$ | 0.00052 | <163 | <0.085 | Equilibrium production; by-passed in neutron capture |
| $Cr^{52}$ | 0.010 | 7.3 | 0.073 | Equilibrium production |
| $Cr^{53}$ | 0.0011 | <175 | <0.19 | Equilibrium production |
| $Cr^{54}$ | 0.00029 | ..... | ..... | No equilibrium production expected |
| $Mn^{55}$ | 0.0096 | 50‡ | 0.48 | Equilibrium production |
| $Fe^{54}$ | 0.054 | 21 | 1.1 | Equilibrium production; by-passed in neutron capture |
| $Fe^{56}$ | 0.85 | 31 | 26 | Equilibrium production |

* Abundance determination given by Aller (1953).

† Ten times the fast-neutron cross-section (~1 mev). ‡ Measured.

All other values of $\sigma(n, \gamma)$ are 1 per cent of the thermal neutron cross-sections.

Thus $Na^{21}$* "probably" falls within 50 kev above $Ne^{20} + p$ and 150 kev below it. If it is actually above $Ne^{20} + p$, then it will occur as a stellar thermal resonance in $Ne^{20}(p, \gamma)$ and will give a very large increase (by a factor of $10^3$–$10^6$) in the reaction rate for $Ne^{20}(p, \gamma)$ over the estimate previously quoted (Salpeter 1955), which neglects resonance. On the basis of Middleton's angular distribution measurements, the state has spin and parity of $\frac{1}{2}^+$, $\frac{1}{2}^-$, or $\frac{3}{2}^-$ and most probably corresponds to the well-known excited state at 2.79 mev, with $\frac{1}{2}^+$, in the mirror nucleus $Ne^{21}$. (Actually, we require only that $Ne^{21}/Ne^{20} \sim 1$ in the *Ne–Na* proton cycle. This might be the case even without the effect of a resonance, e.g., favorable selection rules or variations in matrix elements might be sufficient. In any case the $Ne^{21}$ must always be consumed in the subsequent helium-burning.)

On the basis of a resonance, all of the $Ne^{20}$ will be converted into $Ne^{21}$ by resonant *s*-wave (or *p*-wave) proton radiative capture followed by beta-decay, and it will be apparent from Table 1 that this will be just sufficient to produce the required number of neutrons. This argument assumes, of course, that there are no resonance effects in $Ne^{21}(p, \gamma)$. Here we can only note the experimental result of Broström *et al.* (1947) that only one resonance, at 0.765 mev, has been found in the bombarding energy range 0.6–1.3 mev, so that the level density is probably not too large and the chance of a level occurring between 30 and 200 kev is small. If the factor of increase is on the lower side indicated earlier, some $Ne^{22}$ will be produced even without resonance in $Ne^{21}(p, \gamma)$, and this may well be the case. The relatively large abundance of $Ne^{22}$ noted previously is in itself an indication of an anomalous $Ne^{20}(p, \gamma)$ cross-section.

We also assume that the final hydrogen-burning in the shell surrounding the helium core of a star occurs at a high enough temperature for the $Ne^{20}$ to be converted into $Ne^{21}$ before the hydrogen is completely consumed. Even with the resonance, we estimate that this temperature must be at least $40 \times 10^{6}$°, which is not unreasonable for a thin shell of hydrogen which is essentially supplying all the star's energy (Hoyle and Schwarzschild 1955). It should also be noted that $N^{14}(n, p)$ will not constitute a difficulty in absorbing part of the neutrons produced in $Ne^{21}(\alpha, n)$. Before the temperature is reached at which this latter reaction takes place, the $N^{14}$ will have been consumed by the $N^{14}(\alpha, \gamma)O^{18}$ reaction. It is assumed, however, that all the helium is not consumed before this temperature is reached. The $Ne^{21}(\alpha, n)$ reaction produces $Mg^{24}$ even before the $Ne^{20}(\alpha, \gamma)$ reaction, and the cosmic abundance of $Mg^{24}$ indicates that neon is consumed, at least partly, in helium-burning.

### E. AN ALTERNATIVE MODE OF PRODUCTION OF INTERMEDIATE ELEMENTS

It is of interest to consider the situation when neutrons are produced in a star having the normal cosmic abundance of the light elements up to neon but deficient in the heavier elements and, in particular, the metal group. At the temperature reached just before helium and neon begin to interact, the core of the star will consist of *He*, $Ne^{20}$, $Ne^{21}$, and $Ne^{22}$ in the ratios 300:60:1:1, where we assume that half the helium has been converted into $Ne^{20}$ in the helium reactions through $C^{12}$ and $O^{16}$; all the original abundance of $Ne^{20}$ condensed in the material of the core has been converted into $Ne^{21}$ at the end of the hydrogen-burning; and all the $N^{14}$ remaining from the hydrogen-burning has been converted into $Ne^{22}$ by successive alpha-particle captures. As the temperature increases, the first helium-neon process to occur will be the $Ne^{21}(\alpha, n)Mg^{24}$ reaction in which neutrons are produced. These neutrons will now be captured by the $Ne^{22}$ in the absence of the metal group, and a synthesis of $Na^{23}$ and other nuclei just above $Ne^{22}$ will begin. The extent of the synthesis will depend on the ratio of $Ne^{21}$ to $Ne^{22}$ and will be quite limited if this ratio is one to one, as indicated earlier on the basis of a one-to-one ratio for $Ne^{20}$ to $N^{14}$ in the universal cosmic abundance. However, fluctuations in this ratio can certainly occur for individual stars, and in those cases where the ratio $Ne^{20}$: $N^{14} = Ne^{21}$:$Ne^{22}$ is larger than 1, perhaps 3, there will be considerable synthesis of the intermediate nuclei.

To investigate this point of view, we have attempted to estimate the neutron-capture cross-sections at 15 kev for the nuclei listed in Table 1. This energy was chosen because it corresponds to $T = 1.7 \times 10^{8}$°, at which the $Ne^{21}(\alpha, n)$ reaction will proceed at a reasonable rate. The product of these cross-sections *times* the abundances ought to be a constant, if neutron capture has synthesized these nuclei and equilibrium has been reached. The cross-section estimates have been made in two ways, using data given by Endt and Kluyver (1954) and by Ajzenberg and Lauritsen (1955). Where the fast-neutron ($\sim$1-mev) cross-section has been measured, we have used this value multiplied by a factor of 10 to take into account the $1/v$ law, which holds at least roughly in this energy range. In cases where the fast cross-section has not been measured, we have taken 1 per cent of the thermal cross-section. This factor is indicated on an empirical basis where both measurements have been made and is consistent with a $1/v$ law over a factor of $10^4$ in energy above the thermal region and with a very much slower variation through the kilovolt range. The cross-sections are given in Table 1. We have rounded off our extrapolation factors to powers of 10 ($10^1$ and $10^{-2}$), in order not to alter the significant figures of the actual measurements. In cases where the thermal cross-sections are very large, the estimates made as indicated are not at all valid; these are noted in Table 1.

The products of the cross-sections *times* the abundances are also given in Table 1 and are plotted in Figure 1 between $Ne^{22}$ and $Ti^{50}$. The wide variations for the nuclei from $C^{12}$ to $F^{19}$ are consistent with the point of view that other mechanisms than neutron capture have synthesized these nuclei. On the other hand, from $Ne^{22}$ to $S^{32}$ the products are reasonably constant, with the exception of $P^{31}$. Beyond $S^{32}$ the products decrease markedly, indicating that insufficient neutrons have been available to build these elements up to their saturation or equilibrium values. We have investigated this point in more detail in the manner now to be described.

The synthesis of a particular element of atomic weight $A$ will be governed by the equation

$$\frac{dN_A}{dn} = \frac{-\sigma_A N_A + \sigma_{A-1} N_{A-1}}{\sum_A \sigma_A N_A},$$

where $n$ is the number of neutrons captured, $N_A$ is the number of nuclei of atomic weight $A$, and $\sigma_A$ is the neutron-capture cross-section. The equilibrium abundance of a given element is reached when $dN_A/dn = 0$ and

$$\frac{N_A}{N_{A-1}} = \frac{\sigma_{A-1}}{\sigma_A}.$$

However, if insufficient neutrons are available, the last of the elements in the synthesis chain will not attain the full value for $N_A$ given by this equation. We have carried out numerical integrations of the equations for $N_A$ in the range $A = 22$–$50$, as a function of the number of neutrons captured. In Figure 1 the computed curves of the quantity $\sigma_A N_A$ as a function of $A$ have been plotted for the following ratios of neutrons captured to the original number of $Ne^{22}$ nuclei: 2.6, 2.8, 3.0, and 3.2. The products of the cosmic abundances *times* the cross-sections for each element are plotted as points. It will be noted that the synthesis up to equilibrium values for $Ne^{22}$ to $S^{32}$ and the decreasing values up to $Ti^{50}$ are fairly well reproduced for $n/Ne^{22} \simeq 2.8$. The adjustment of the calculated curves to fit the observed products from $Ne^{22}$ to $S^{32}$ indicates that 5.6 original $Ne^{22}$ nuclei (on the scale of Table 1) are required to synthesize all the elements up to $Ti^{50}$. Thus the 20.5 $Ne^{22}$ nuclei available from the reactions $N^{14}(\alpha, \gamma)O^{18}(\alpha, \gamma)Ne^{22}$ are sufficient to build an overabundance of these elements by about a factor of 4. Since the normal abundance of $Ne^{20}$ is 20.3, the number of $Ne^{20}$ nuclei required to form $Ne^{21}$ and the requisite number of neutrons is only 2.8 times the normal abundance, an amount well within the errors in

the relative abundances or in possible fluctuations about them. These results do indicate that a substantial fraction of the $N^{14}$ and $Ne^{20}$ in the universe has been subjected to helium-burning processes if the elements from $Ne^{22}$ to $Ti^{50}$ have been synthesized in this manner.

Several additional points are of interest. An inspection of Table 1 shows that for $Ti^{48}$ and the elements beyond $V^{51}$ the product $\sigma_A N_A$ rises sharply, showing that these metals

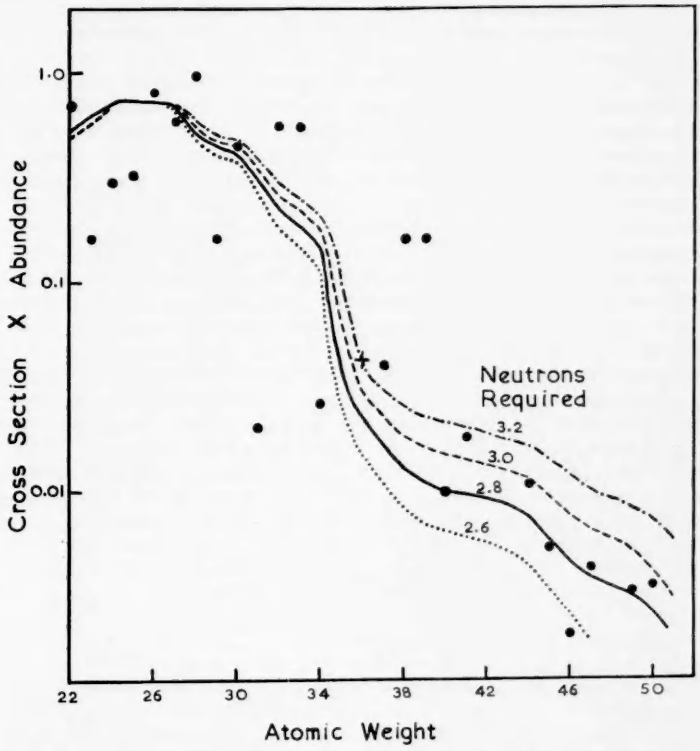


FIG. 1.—Curves showing the neutron-capture cross-section *times* the computed abundance, as a function of atomic weight, for four different ratios of the number of neutrons supplied to the number of original $Ne^{22}$ nuclei. The dots give the neutron-capture cross-section *times* the observed abundance. The cross is the point for $Cl^{36}$ (decays to $A^{36}$), whose cross-section was arbitrarily assumed to be 0.36 mb (see Table 1).

have not been synthesized by neutron-capture processes. Their large abundances must be attributed to another process, and Hoyle (1954) has shown that there is convincing quantitative agreement between the observed values and those obtained from the equilibrium theory of nuclear reactions at $T = 5 \times 10^{9}$°.

Another point involves the nuclei which are by-passed in the neutron-capture process. Of these, $S^{36}$, $Ca^{46}$, and $V^{50}$ are indeed very rare in nature, as indicated in Table 1. On the other hand, $Ca^{48}$ has a $\sigma_A N_A$ product similar to those of the neighboring nuclei produced by neutron capture, and $Ca^{40}$ has an even larger product. Both these nuclei are doubly magic, and this may be significant in view of their large abundances.

The three isobars $Ti_{22}^{50}$, $V_{23}^{50}$, and $Cr_{24}^{50}$ are very illuminating in regard to the synthesizing processes. $Ti^{50}$ is produced in neutron capture, and its abundance is consistent with its neutron-capture cross-section, as shown in Table 1 and Figure 1. $V^{50}$ is by-passed and is very rare. From the standpoint of nuclear structure, it exists at all only because its spin is greater than 6 and its beta-decay and $K$-capture lifetimes are presumably very great. On the other hand, $Cr^{50}$, which is by-passed, is more abundant than $Ti^{50}$. Using the methods of Hoyle, we find that, of the three isobars, $Cr^{50}$ is the one which will be synthesized in the equilibrium process at high temperatures. This is essentially because $Cr^{50}$ has the highest charge of the three and the process takes place with a ratio of free protons to free neutrons of 100.

The details of the synthesis of the elements by neutron-capture processes described here will, to a certain extent, be independent of the source of neutrons. Our choice of $Ne^{21}(\alpha, n)$ to supply the neutrons and of $Ne^{22}$ from $N^{14}$ to supply the original capturing nucleus has some advantages. The curves of Figure 1, however, will be obtained for any adequate source of neutrons, so long as it is assumed that the original capturing nucleus is lighter than $Ne^{22}$.

The wide spread of the points in Figure 1 is to be attributed to the occurrence of resonances in the cross-sections, which will play an important role in the range of energies under discussion, and to uncertainties in the abundance ratios. The inverse behavior of the nuclear abundances and the 1-mev neutron-capture cross-sections has been noted many times in connection with primeval synthesis from neutrons. The smooth behavior of these cross-sections with $A$ would seem to preclude wide variations in isotopic abundance except for shell effects. Near 15 kev, however, there exists the possibility that resonance effects produce large isotopic variations, especially among the intermediate-weight elements ($Cl$ to $Ti$). The matter will not be settled until capture cross-section measurements have been extended to the 15-kev range. The possible errors in our estimates are all too obvious in view of the resonant nature of the cross-sections. High-resolution measurements are, of course, not necessary because of the great spread in energy ($\sim kT$) at thermal energies. The $(n, p)$ and $(n, \alpha)$ cross-sections must also be measured. For example, the reactions

$$S^{33}(n, p)P^{33} + 0.52 \text{ mev}$$

and

$$S^{33}(n, \alpha)Si^{30} + 3.50 \text{ mev}$$

may well increase the number of neutrons required to give synthesis beyond $S^{33}$.

We must emphasize one feature of the general point of view presented in this paper. Abundance determinations in the materials making up any cosmical body—earth, meteorite, or star—tell something about the nuclear history and evolution of these materials. As an example we can consider the evolution of the materials in the cosmic abundances given by Urey (1952) and shown in part in Table 1.

About 30 per cent of the original hydrogen has been converted to helium, and about 10 per cent of this helium has been converted to still heavier elements.[2] Only a very small amount of the original hydrogen, $\sim$0.1 per cent, has gone all the way to the metals in nuclear reactions under equilibrium conditions, and only 0.2 per cent of the metals have been transformed to the heavy elements by neutron capture. On the other hand, the products of helium-burning—$C^{12}$, $O^{16}$, and $Ne^{20}$—have experienced considerable modification by subsequent nuclear activity. On the scale of Table 1, 5.6 $N^{14}$ nuclei and 15.7 $Ne^{20}$ nuclei have been required to form the elements from $Ne^{22}$ to $Ti^{50}$. Thus the $Ne^{20}$ must

[2] This great amount of nuclear activity is consistent with the conclusion of Salpeter 1955 (*Ap. J.*, **121**, 161) that the total mass which has once been in the form of main-sequence stars, but has taken on a different form by now, is of the same order of magnitude as the total mass of present stars, and that $\sim$ 90 per cent of the mass transformed is in the form of interstellar gas, while only 10 per cent remains as white dwarf stars.

have originally numbered 20.3 + 15.7 = 36.0 on this scale, while 20.5 + 5.6 = 26.1 $N^{14}$ were produced from $C^{12}$ or $O^{16}$, which originally must have totaled 10.2 + 26.1 + 28.2 = 64.5. Thus about half the original $C^{12}$, $O^{16}$, and $Ne^{20}$ from helium have been transformed by subsequent nuclear activity. This type of analysis is typical of what may be done for any specific material on which abundance determinations have been made. Specific evolutionary details can then always be checked against the over-all balance in the economy of the elements involved. Thus $C^{13}$, $N^{14}$, and $N^{15}$ have been produced in low-temperature ($10^{7}$°) burning of $C^{12}$ or $O^{16}$, and a considerable fraction of these has not undergone subsequent helium-burning. On the other hand, $Ne^{21}$ has been produced from $Ne^{20}$ only at higher temperatures ($4 \times 10^{7}$°) in the shells surrounding helium cores and has subsequently been consumed in helium reactions.

In conclusion, there would seem to be a very general basis for the expectation that neutrons will be produced and the heavy elements and probably the intermediate elements synthesized in stellar interiors by the interaction of the products of helium- and hydrogen-burning. The synthesis of the elements discussed in this paper is shown graphically in Figure 2. It must be admitted that difficulties exist in both the nuclear and the astrophysical details of the processes of synthesis. However, the possibilities discussed here at least point to promising lines of further investigation in which a detailed solution can reasonably be expected to be found.

## III. ASTROPHYSICAL CONSIDERATIONS

A possible evolutionary model, which is consistent with the element-building processes described in the previous section of this paper, is outlined in this section.

We suppose that originally a galaxy condenses out of material with a low relative abundance of the heavier elements. The origin of this mixture is not considered, but we could, following Hoyle, suppose that it consists predominantly of hydrogen, with an admixture of other elements which have been ejected from other, older, galaxies.

Stars then condense in this galaxy, and their size and distribution will depend on the local initial conditions of density and velocity. There may be regions, in the galactic plane but away from the center, where large, massive stars can condense more easily. In these regions successive cycles of condensation and evolution of stars would take place with greater frequency than elsewhere. Away from the plane of the galaxy, where the density is rapidly falling off, and in the center, where there may be higher relative velocities, the conditions may be less favorable for large stellar condensations. Clearly, these possibilities will depend on the degree of galactic condensation when stellar condensations begin.

In the condensed stars the evolutionary processes will begin. These will depend on the original element content and the later dynamical character of the instabilities that may develop. We may outline the following possibilities:

1. Stars which originally condense out of material that is predominantly hydrogen may, toward the end of their lives, consume helium and build the lighter elements, say up to *Ne*.

2. Some stars, toward the end of their evolutionary path, may collapse until temperatures of the order of $5 \times 10^{9}$° are reached in the core, and then the metallic group will be synthesized in the way described by Hoyle, using an equilibrium theory.

When condensations occur in interstellar material which has been ejected from stars which have passed through phase 1 or 2, there are the following possibilities:

3. In stars containing only the lighter elements (up to *Ne*), toward the end of their lives, neutron-capture processes may begin. Following the discussion given in Section IIE, the production of neutrons at this stage will lead to the synthesis of the elements between *Ne* and *Ti*. The synthesis will in this case be limited by the average number of neutrons available per *Ne* nucleus.

4. Some stars will condense from material already containing some elements up to the metallic group. In these stars, after the *He* reactions have begun, neutron-capture processes may begin and build the heavy elements as outlined in Section IIC. The alternative mode of heavy-element production described in Section IID can take place in stars of this type. It is reasonable to suppose that heavy-element synthesis then takes place when these stars are in the red giant stage of their evolutionary path.

The elements built in these ways must be redistributed by explosive or steady ejection. Hoyle has shown that the observed rate of supernova outbursts can explain only about 10 per cent of the material ejection, in the synthesis of the elements up to *Fe*. The processes described in this paper demand at least two condensations and redistributions

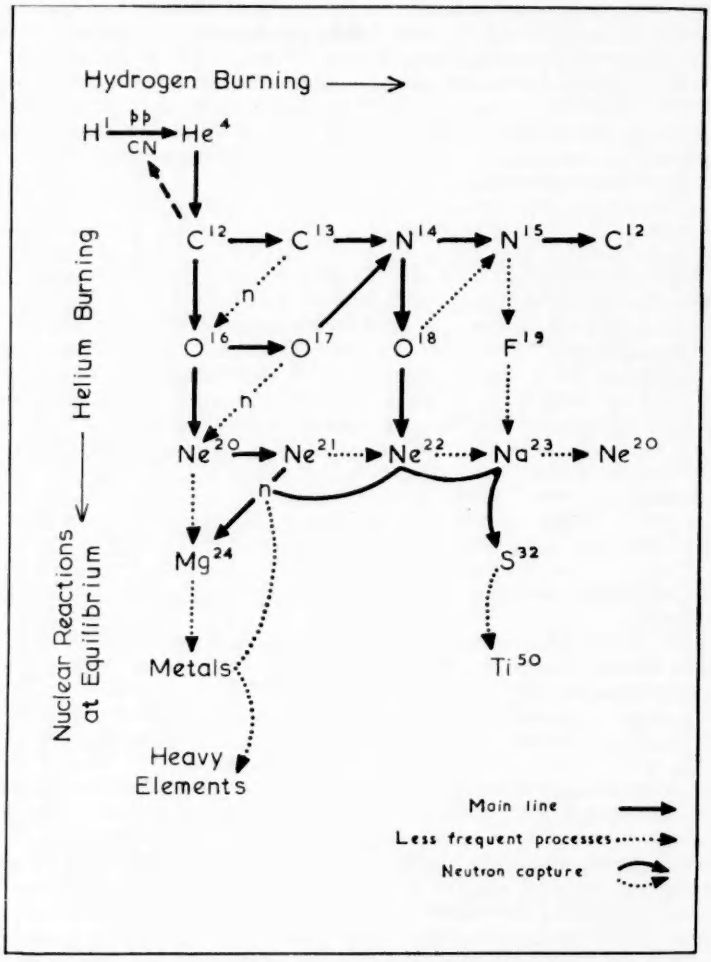


FIG. 2.—This figure shows schematically the basic processes involved in the synthesis of the elements. These are (i) hydrogen-burning, (ii) helium-burning, (iii) nuclear reactions at equilibrium at $\sim 5 \times 10^{9}$°, and (iv) neutron capture.

to explain the appearance of the heavy elements. To produce the heavy elements above the metals ($A$ = 60–209) from the metallic group, an average of about 50 neutrons per nucleus is needed. Since the cross-sections increase rapidly with $A$, the neutrons will be captured preferentially by the products of the first metal nuclei to be converted. It appears (Cameron 1955) that if, on the average, 20 neutrons per metal atom are supplied, 40 per cent of the metal atoms will be converted in this way. Since the observed meteoritic and terrestrial abundance of the heavy elements relative to the metals is about $3 \times 10^{-4}$, the proportion of stars in which the heavy elements are synthesized needs to be of the order of $10^{-3}$ of the number synthesizing the metals to produce these abundances, or $10^{-2}$ if the cosmic abundance of the heavy elements is ten times higher (cf. the following discussion). In both synthesizing processes, perhaps only 10 per cent of the stellar mass may be involved, in which case the observed supernova rate would be much too low to explain the distribution of this material. Struve (1954) has estimated that the total rate of ejection of material from stellar surfaces may be larger than the explosive ejection rate as determined from the observed novae and supernovae.

Cameron (1954) originally suggested that neutron-capture processes would take place in cool giant stars, particularly the S stars (the apparent abundance anomalies in the S, $Ba^+$, and peculiar A stars will be discussed in a forthcoming publication). In this more general scheme these stars may synthesize the heavy elements either by neutron-production processes described in Section IIC or, more probably, by the alternative neutron-producing mechanism (Sec. IID), which obviates the mixing difficulties already described. In the normal cool giants (the K and M stars) these processes may go on without any indication of abundance anomalies on the surface. This simply means that the mixing time, from the region of synthesis in the shell of energy production to the surface, is long compared to the total time for the star to travel through this part of its evolutionary path, which may be of the order of $10^7$ years. A time scale of this order is indicated by the evolutionary tracks computed by Hoyle and Schwarzschild (1955) and also observationally for population II red giants by the results described by Sandage (1954). However, we also have the observational result that the S stars apparently show anomalous excessive abundances of the heavy elements, indicated principally by the rare earths, on the stellar surface. From the apparent intensities of the spectrum lines of the rare earths in the S and the $Ba^+$ stars (the latter may represent a later evolutionary stage of the S stars), we can very roughly estimate that the abundances of the heavy elements on the surface may be $10^1$–$10^2$ times the solar abundance.

There do not exist good abundance determinations of the heavy elements beyond the metals in different types and populations of stars. The often quoted cosmic abundance-curve relies in this region on terrestrial and meteoritic data, and Greenstein (1954) has given a table showing that there is rough agreement between these and the only solar determination, by Russell (1929), which relied on scanty spectroscopic data. The mean cosmic abundance might differ by a factor of 10 from the solar abundance.

It has been shown (Cameron 1955) that when the neutron-capture processes are at their maximum efficiency, then the heavy elements are built so that they are about $10^3$ times as abundant as in the sun. On this basis we can make a rough estimate from the observed number of S stars, to see whether they are sufficient to produce the cosmic abundance of the heavy elements.

According to Keenan (1954), we may take the total number of S stars in a disk of radius 1.4 kpc centered on the sun to be $\sim 10^2$. If this is a typical sample of the distribution of these stars in the galactic disk, then the total number at the present time is approximately $10^2 \times (15/1.4)^2 \sim 10^4$. Now Keenan has also estimated that the S stars make up about 1 per cent of the M-star population, so that if we suppose that the lifetime of the M-star stage is about $10^7$ years, then the time to pass through the S-star stage would be about $10^5$ years (this time scale is in rough agreement with the upper limit on the mixing time for the S stars, as indicated by the apparently increased abun-

dance of *Tc* on the stellar surface; the most stable isotope of *Tc* so far known has a half-life of $2 \times 10^5$ years).

Let us consider a period during which a star somewhat more massive than the sun will traverse its evolutionary path and which is fairly short compared with the age of the sun, i.e., $10^9$ years. If the lifetime of an S star is $10^5$ years, then approximately $10^3$ stars will have passed through the S-star stage during $10^9$ years. The S stars may be associated with B stars, in spiral arms (Keenan 1954). If we suppose that an S star has a similar mass, say $\sim 5M_\odot$, and if the efficiency of the distribution of material into space is 10 per cent, then, remembering that the interior abundance of heavy elements is $10^3$ times the solar abundance, we shall have an amount of heavy-element material equal to the solar abundance in $10^8 \times 5 \times 10^3 \times 0.1 = 5 \times 10^{10}$ stars of solar mass. If the efficiency of distribution were 100 per cent, then we should have sufficient for ten times the solar abundance in about half the galactic mass.

Within the error due to the uncertainties in the quantities used in this estimate, it does appear, therefore, that synthesis of the heavy elements in the S-star stage alone could account for a considerable fraction of the heavy elements. A fraction of the same order would be obtained by supposing that the normal M giants were also synthesizing the heavy elements at a much slower rate. Detailed calculations of the conditions for synthesis must await the results of theoretical calculation of evolutionary tracks for a variety of stellar masses and the explanation of instabilities leading to stellar variability and explosive outbursts.

Stars which fall into category 3 may be observed as having large abundances of the elements lighter than *Ti* and low metal abundances. The identification of such characteristics depends on the mixing to the surface which makes these anomalies observable. On the other hand, stars which are not synthesizing these intermediate elements but which are condensed out of material thrown out from the stars in which they have been built will also show these characteristics.

In regions where larger, more massive, stars can condense, all the processes of element synthesis proceed more rapidly. In this connection the observed fact that population II stars appear to have only 10 per cent of the solar abundance of the metals (Chamberlain and Aller 1951; Schwarzschild and Spitzer 1953) is important. Also, the occurrence in cool giant stars in the high-velocity group of metal abundances smaller by a factor of 3 than the solar abundances (Schwarzschild, Spitzer, and Wildt 1951) indicates that intermediate abundances are also present. Much more observational work on abundance determinations in population II stars is desirable, particularly in the giant and horizontal branches, where stars analogous to the S stars in population I might be found. It is also interesting that the metal abundances may be increased by a factor of 2 or 3 in the young O and B stars relative to the sun (Strömgren 1954).

We have attempted to discuss only the general conditions under which different groups of elements may be synthesized, following the nuclear considerations of the earlier part of the paper. In nature, we cannot necessarily expect clear-cut categories of stars in which particular elements will be built, but rather a continuous distribution of configurations in which there are different abundance ratios and masses in the original condensed gas and consequently varying evolutionary paths are followed.

We are deeply indebted to F. Hoyle, A. G. W. Cameron, E. E. Salpeter, and J. L. Greenstein for helpful correspondence and discussions of the topics described in this paper. We are also indebted to R. Middleton for information concerning energy levels in $Na^{21}$.

## REFERENCES


Ajzenberg, F., and Lauritsen, T. 1955, *Rev. Mod. Phys.*

Aller, L. H. 1953, *Astrophysics* (New York: Ronald Press Co.), p. 327.

Bainbridge, K. T. 1953, *Experimental Nuclear Physics*, ed. E. Segre (New York: John Wiley & Son), Vol. **1**, Part V.

Broström, K. J., Huus, T., and Koch, J. 1947, *Nature*, **160**, 498.

Cameron, A. G. W. 1954, *Phys. Rev.*, **93**, 932.

———. 1955, *Ap. J.*, **121**, 144, and private communications.

Chackett, K. F., Fremlin, J. H., and Walker, D. 1954, *Phil. Mag.*, **45**, 173.

Chamberlain, J. W., and Aller, L. H., 1951, *Ap. J.*, **114**, 52.

Endt, P. M., and Kluyver, J. C. 1954, *Rev. Mod. Phys.*, **26**, 95.

Fowler, W. A. 1954, *Mém. Soc. R. Sci. Liège*, **14**, 88; *Communications du Colloque d'Astrophysique de Liège*, 1953; see also Bosman-Crespin, D., Fowler, W. A., and Humblet, J. 1954, *Bull. Soc. R. Liège*, **9–10**, 327.

Greenstein, J. L. 1954, *Mém. Soc. R. Sci. Liège*, **14**, 307; *Communications du Colloque d'Astrophysique de Liège*, 1953.

Hoyle, F. 1954, *Ap. J.*, Suppl., **1**, 121.

Hoyle, F., and Schwarzschild, M. 1955, in preparation.

Keenan, P. C. 1954, *Ap. J.*, **120**, 484.

McKellar, A. 1949, *Pub. Dom. Ap. Obs. Victoria*, **7**, 395.

Middleton, R. 1955, private communication.

Russell, H. N. 1929, *Ap. J.*, **70**, 11.

Salpeter, E. E. 1952, *Ap. J.*, **115**, 326.

———. 1955, *Phys. Rev.*, **97**, 1237.

Sandage, A. R. 1954, *Mém. Soc. R. Sci. Liège*, **14**, 254; *Communications du Colloque d'Astrophysique de Liège*, 1953.

Schwarzschild, M., and Spitzer, L. 1953, *Observatory*, **73**, 77.

Schwarzschild, M., Spitzer, L., and Wildt, R. 1951, *Ap. J.*, **114**, 398.

Strömgren, B. 1954, paper read at Sixième Colloque International d'Astrophysique, Liège.

Struve, O. 1954, *Sky and Telescope*, **14**, 11.

Urey, H. C. 1952, *The Planets* (New Haven: Yale University Press), p. 231.

# THE PULSATIONAL STABILITY OF MODELS FOR RED GIANT STARS*

JOHN PAUL COX†
Goethe Link Observatory, Indiana University, Bloomington, Indiana
*Received March 25, 1955*

ABSTRACT

The pulsational stability of a typical red giant star model is examined. The phase delay in energy production by the carbon cycle is found to be negligible, of the order of $10^{-3}$ radians. The nuclear reactions in the central regions are further shown to have a negligible effect on the maintenance of pulsations. The dissipation of pulsation energy by radiation losses is found, under the usual assumptions, to yield a damping time of about 10 days for the pulsations. It is therefore concluded that if the cepheids are represented by the centrally concentrated red giant models, the cause of the pulsations must be sought in the outer 15 per cent of the stellar radius, where many of the usual approximations are not valid.

## I. INTRODUCTION

The purpose of the present study is to examine the pulsational stability of recent models proposed to represent the classical cepheid variable stars. Pulsation integrations of three such highly centrally concentrated red giant models were carried out recently by I. Epstein (1950), for the purpose of examining the effect of high central-mass concentration on the pulsation properties. One of the models used was the red giant model Case 15 of Schwarzschild and Li Hen (1949). This model will hereafter be referred to simply as the "S-L model." Whenever reference is made specifically to the particular S-L model with $M = 1.34 \times 10^{35}$ gm chosen by Epstein (1950) and used for the numerical calculations here, we shall write "S-L($M$) model." The central temperature in all cases is taken as $30 \times 10^{6}$° K, and the central density appropriate to this assumed mass is 22.14 gm/cm$^3$.

The principal result of Epstein's work that is of interest here is that the relative pulsation amplitude, $\delta r/r$, for both the fundamental and the first overtone of all the models studied is about a million times smaller in the central regions than in the surface regions. Comparison with the homogeneous model (Rosseland 1949, pp. 27–29), for which $\delta r/r$ is constant throughout, indicates that the small pulsation amplitude in the central regions is a direct result of the great central-mass concentration of these models. The S-L model has been used for the numerical calculations here because pulsation integrations are available.

Although several investigators, chief among whom are Eddington (1918, 1930, 1941*a*, *b*, 1942), Cowling (1934, 1935, 1938), and Ledoux (1940, 1941), have studied the problem of the pulsational stability of stellar models, none of the models used embodied the high central-mass concentration which appears necessary, in the light of recent research, to account for the red giant character of the cepheids. The results of the present work will show that the more recent models impose even far more serious difficulties in accounting for the observed pulsations than before but, on the other hand, limit considerably the choice of possible mechanisms which might produce the phenomenon.

One of the principal purposes of this study is to investigate the amplitude and phase delay in the variation of the energy production by the carbon cycle in the central regions of a red giant model (Rosseland and Randers 1938; Rosseland 1949, chap. v). A second

* *Publications of the Goethe Link Observatory, Indiana University*, No. 16.

† Now at the Astronomy Department, Cornell University.

principal purpose is to determine the net rate of dissipation of pulsation energy by this model. Details of the calculations may be found in Cox (1954).

The results of these two parts will then permit the calculation of the damping time for the pulsations of the model, the numerical results for the S-L model being given in Section V. Although numerical calculations have been applied only to the one model, the results are expected to be valid, to an order of magnitude, for other centrally concentrated red giant models. A comparison with the observed behavior of the actual cepheids should then yield information concerning the internal structure of these stars and perhaps some insight as to the cause of the phenomenon of cepheid pulsation.

## II. THE STABILITY COEFFICIENT

The Lagrangian method of description will be used throughout in the present paper. The amplitude of the displacement of a particular element of matter from its equilibrium position $r_0$ will be denoted by $\xi$. The *relative* pulsation amplitude, $\delta r/r$, will be denoted by $\eta$. Further, $\eta_0 \equiv \delta R/R$ is the relative pulsation amplitude at the surface of the star.

The stability of a star in regard to radial pulsations is determined by the magnitude of the stability coefficient (Rosseland 1949, chap. v), which may be written as

$$\kappa = \frac{L\,(\Im_d - \Im_g)}{2\sigma^2 I}, \tag{1}$$

where $L$ is the luminosity of the star; $\sigma = 2\pi/P$ is the angular frequency of pulsation of the star, $P$ being the period of pulsation; and $I$ is the oscillatory moment of inertia of the star:

$$I = \int_0^M \xi^2\, dm \equiv MR^2\,\Im\,. \tag{2}$$

The quantities $\Im_g$ and $\Im_d$ are dimensionless numbers which are defined as follows:

$$\Im_g = \frac{1}{L}\int_0^M \theta\,\delta\epsilon\,\frac{\delta\rho}{\rho}\,dm\,, \tag{3}$$

$$\Im_d = \frac{1}{L}\int_0^M \theta\,\frac{d\,(\delta H)}{dm}\,\frac{\delta\rho}{\rho}\,dm\,. \tag{4}$$

Here $\theta = \gamma - 1$, $\gamma$ being the effective value of the ratio of specific heats; $\delta\rho$, $\delta\epsilon$, and $\delta H$ are the *amplitudes* of the Lagrangian variations in density, rate of energy production per gram, and net flux through a sphere of radius $r$, respectively. In these equations and in those that follow, all quantities not preceded by a "$\delta$" will represent equilibrium values.

The physical significance of the quantities $\Im_g$ and $\Im_d$ may be seen from the fact that the net rate at which thermonuclear heat energy is transformed into the mechanical energy of pulsations throughout the entire star is given by

$$\tfrac{1}{2}L\,\Im_g\,. \tag{5}$$

Similarly, the net rate at which the mechanical pulsation energy is transformed into heat energy throughout the entire star is given by

$$\tfrac{1}{2}L\,\Im_d\,. \tag{6}$$

The total pulsation energy of the star, on the other hand, is

$$\tfrac{1}{2}\sigma^2 I\,. \tag{7}$$

The damping time for the pulsations is then defined by $\tau = 1/|\kappa|$. In the case of a negative $\kappa$, the damping time must be interpreted as the time required for the amplitude of pulsation to increase by the factor $e$. Only the real part of $\kappa$ affects stability. The condition

$$\kappa = 0 \tag{8}$$

must be satisfied by a star which is maintaining pulsations with constant finite amplitude, as is apparently true of the cepheid variables.

## III. VARIATION IN THE RATE OF THERMONUCLEAR ENERGY PRODUCTION

The abundance variations of the constituents of the carbon cycle were computed by the use of a first-order theory. In particular, the Lagrangian variation in the abundance of the $k$th constituent was assumed to be of the form

$$\delta y_k(\mathbf{r}_0, t) = \delta y_k e^{i(\sigma t - \beta_k)}, \tag{9}$$

where $\delta y_k$ is the real amplitude of the total Lagrangian variation and $\beta_k$ is the phase delay in the abundance variation. The quantity $y_k$ is defined by

$$y_k \equiv \frac{n_k}{\sum_{j=1}^{6} n_j}, \tag{10}$$

where $n_k$ is the number of particles of type $k$ per unit volume and the summation is extended over all constituents of the carbon cycle. For the numerical calculations, the

TABLE 1

NUMERICAL VALUES OF $\delta y_k$ FOR CONVECTIVE CORE OF S-L($M$) MODEL*

| $k$ | ELEMENT | $-\delta y_k/\eta_0$ | |
|---|---|---|---|
| | | Center | Edge |
| 1 | $C^{12}$ | 4.15 (−12) | 3.43 (−14) |
| 2 | $N^{13}$ | 2.107 (−13) | 7.294 (−15) |
| 3 | $C^{13}$ | 2.27 (−13) | 9.81 (−15) |
| 4 | $N^{14}$ | 3.83 (−12) | 2.88 (−14) |
| 5 | $O^{15}$ | 5.797 (−14) | 1.501 (−15) |
| 6 | $N^{15}$ | 2.4 (−13) | 1.8 (−15) |

* The numbers in parentheses are the powers of 10 by which the corresponding entries must be multiplied.

exact analytic expressions so obtained for the $\delta y_k$ were replaced by approximate equations based on a comparison of the relative rates of reaction for the constituents of the carbon cycle.

In Table 1 are given the numerical values of the $\delta y_k$ for the convective core of the S-L($M$) model, and in Figure 1 is presented a schematic plot of the variations of the $\beta_k$ throughout the convective core of the S-L($M$) model.

As anticipated by Rosseland and Randers (1938), the phase delays for the elements that decay by collision processes ($\beta_{1,3,4,6}$) are generally large and have values ranging between $-\pi$ and $+\pi$, whereas the phase delays for the two elements which decay by spontaneous processes ($\beta_{2,5}$) are quite small, being $\lesssim 10^{-2}$ radians.

The numerical values obtained by use of the approximate equations, for the S-L($M$) model, are accurate to within better than 0.3 per cent. It turns out, further, that the first-order theory, which was the basis of the present calculation, is well justified for the centrally concentrated red giant models.

For collision processes, the contribution to the variation in energy production from the variations in the reaction rates turns out to be very much greater than that due to the variations in the abundances. Hence the variations in the reaction rates, which are in phase with the pulsations, dominate the variations in energy production. Thus the magnitude of the phase delay in energy production from the collision processes is very small—in fact, in all cases less than $10^{-5}$ radians. For spontaneous processes, on the other hand, the phase delays in the energy production are identically equal to the phase delays in the abundance variations, i.e., of the order of $\lesssim 10^{-2}$ radians. Finally, the *amplitudes* of the variations in energy production, for *all* the reactions in the carbon cycle, are of the same order of magnitude.

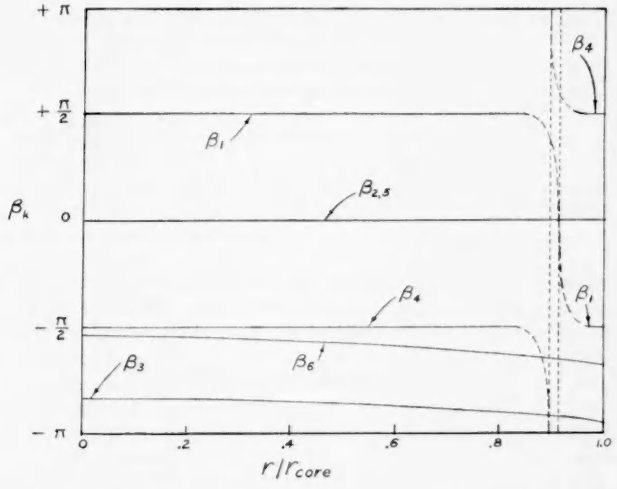


FIG. 1.—The (schematic) variation of the $\beta_k$ throughout the convective core of the S-L($M$) model. The dashed portions of the curves for $\beta_1$ and $\beta_4$ represent the two regions within which the approximate formulae break down. The indicated shapes of the curves in these regions are only estimates.

Approximate power-law expressions for the *net* variation in energy production can then be obtained by combining the results for the individual variations in energy production. These power-law expressions for the amplitude and the phase delay in the variation in energy production by the carbon cycle are given in Table 2. The ratio of specific heats here has been taken as 5/3. Further, $P$ is the pulsation period in days, $T$ is the temperature in $10^{6}$° K and $\rho$ is the density in grams per cubic centimeter. Whereas the numerical values in the second column apply specifically to the S-L($M$) model, those in the third column hold where secular equilibrium obtains. The possible existence of a resonance in the low-energy region of $N^{14}$ would have essentially no effect on the present results.

The general results of the present section may be summarized as follows: (1) the phase delay in the variation of energy production from the carbon cycle is so small ($\sim 10^{-3}$ radians) as to be negligible; (2) the small phase delay that does exist is determined es-

sentially only by the two $\beta$-processes in the carbon cycle; (3) as might be expected physically, the phase delay in the variation of energy production is inversely proportional to the period of pulsation of the star.

## IV. THE VARIATION IN THE NET FLUX OF RADIANT ENERGY

The variation in the net flux of radiant energy is expressed by the quantity $d(\delta H)/dm$ in equation (4). The following assumptions have been made throughout the star: (1) radiative transfer is the principal mechanism of energy transport, with an opacity law of the form

$$\kappa = \kappa_0 \rho^n T^{-s} , \tag{11}$$

where the constants have the values appropriate to the S-L model; (2) the pulsations are assumed to be adiabatic; (3) the ratio of specific heats $\gamma = 5/3$.

TABLE 2

POWER-LAW EXPRESSIONS FOR PHASE DELAY AND AMPLITUDE OF VARIATION IN ENERGY PRODUCTION BY CARBON CYCLE

| Quantity | In Convective Core | Outside Convective Core |
|---|---|---|
| $\delta\epsilon/\epsilon$ | $11.10\rho^{0.03}(T/30)^{0.47}(\delta\rho/\rho)$ | $10.94(\delta\rho/\rho)$ |
| $\phi$ (radians) | $4.16\times10^{-3}(T/30)^{-0.66}/P$ | $4.49\times10^{-3}/P$ |

The choice of such a simple opacity law was dictated primarily by the desire for consistency with the original S-L model, in addition to the resulting relative simplicity of the calculations. The validity of assumptions 2 and 3 is discussed in Section V.

## V. FINAL RESULTS AND CONCLUSIONS

The three dimensionless integrals $\Im$, $\Im_g$, and $\Im_d$ were evaluated numerically for the S-L model, with the following results:

$$\frac{\Im}{\eta_0^2} = 6.46 \times 10^{-6} \qquad (= \tfrac{1}{2} \text{ for the homogeneous model}) ;$$

$$\frac{\Im_g}{\eta_0^2} = 2.62 \times 10^{-9} ;$$

$$\frac{\Im_d}{\eta_0^2} = 1.69 \times 10^{2} .$$

Below are listed the physical results for the S-L($M$) model (the value $\eta_0 = 0.04$ has been used in those quantities which depend on $\eta_0$):

Oscillatory moment of inertia: $I = 1.358 \times 10^{51}$ gm cm$^2$;
Total pulsation energy $= 2.826 \times 10^{41}$ ergs;
Rate of supply of pulsation energy from the carbon cycle $= 1.12 \times 10^{25}$ ergs/sec $= 2.10 \times 10^{-11} L$;
Stability coefficient for zero dissipation of pulsation energy ($\Im_d \equiv 0$): $\kappa = -1.98 \times$ 10–17 sec$^{-1}$;

Corresponding "damping time": $\tau = 1.60 \times 10^9$ years;
Rate of dissipation of pulsation energy = $7.23 \times 10^{35}$ ergs/sec = $0.135\ L$;
Stability coefficient: $\kappa = 1.277 \times 10^{-6}$ sec$^{-1}$;
Damping time: $\tau = 7.83 \times 10^5$ sec = 9.06 days.

Perhaps the most striking feature of the foregoing numerical results is the fact that the rate of dissipation of pulsation energy is some $10^{11}$ times the rate of supply of pulsation energy from the carbon cycle. A second salient feature is the extremely short damping time ($\sim$10 days) for the model, whereas previous investigations (Rosseland 1949, p. 74; Eddington 1930, p. 200) on standard model stars have yielded damping times of the order of thousands of years.

Comparison of the figures presented here with those given by Eddington (1930, p. 199) for the standard model permits the following conclusions to be drawn: (1) the rate of dissipation of pulsation energy by the S-L model, while larger than for the standard model (by a factor of about 50), is not excessively large; (2) the oscillatory moment of inertia for the S-L model and hence the total pulsation energy are *very* much smaller than for the standard model (by a factor of about $10^{-5}$). The small amount of pulsation energy in the S-L model is accounted for by the very great central-mass concentration of this model, coupled with the attendant small relative pulsation amplitude in the central regions. It is this anomalously small amount of pulsation energy that is primarily responsible for the extremely short damping time for the pulsations of the S-L model.

The conclusion is that under the usual assumptions the highly centrally concentrated red giant models would be *excessively* stable, and any pulsations present would be damped out in a matter of days. This conclusion can apparently be traced directly back to the great central-mass concentration which appears necessary in order to account for the red giant character of the cepheids.

The requisite smallness of the rate of supply of pulsation energy from the carbon cycle yields a very important consequence. If there were no dissipation of pulsation energy whatsoever ($\mathfrak{I}_d \equiv 0$), the time required for the amplitude of the pulsations to increase by the factor $e$ as a result of the nuclear reactions in the central regions was found in the preceding section to be $1.60 \times 10^9$ years. However, the lifetime of a star such as that represented by the S-L($M$) model is almost certainly less than $2 \times 10^8$ years, or about one-eighth the "damping time" for zero dissipation of pulsation energy. Thus the amplitude of any small initial disturbance would have increased by only a few per cent during the entire lifetime of the star, and so the maximum amplitude of pulsation with which the cepheids are apparently pulsating would probably never be attained. This negative "damping time" due to the nuclear reactions would be reduced considerably if energy production were carried out in a shell source surrounding an exhausted isothermal core; however, this would at the same time automatically eliminate the possibility of an appreciable lifetime for the star.

If one assumes for the moment that the dissipative term $\mathfrak{I}_d$ is correct to an order of magnitude; that energy production is carried out by the carbon cycle in a shell source surrounding an exhausted isothermal core, with $T = 30 \times 10^6\ ^\circ$K; and that the original pulsation integrations of Epstein (1950) still hold, then, in order that $\mathfrak{I}_g \approx \mathfrak{I}_d$, the radius of the exhausted core would have to extend out to about 60 per cent of the radius of the star and contain practically the entire mass of the star. Such a large isothermal core would, however, seriously violate the natural limit established by Chandrasekhar and Schönberg (1942).

As a second possibility, again assuming $\mathfrak{I}_d$ to be correct to an order of magnitude, one might assume that energy production is carried out in a shell source surrounding an exhausted isothermal core containing, say, 30 per cent of the total mass, with $T = 30 \times 10^6\ ^\circ$K, and that the Epstein pulsation integrations still hold. Now, however, assume that energy production is by some nuclear mechanism with a higher temperature sensi-

tivity than the carbon cycle, and let the temperature exponent be determined by the condition that $\Im_d \approx \Im_g$. If no phase delays in energy production are assumed, one obtains

$$\epsilon \propto T^{108}$$

as the *minimum* temperature sensitivity of the thermonuclear reactions. Such a result would, of course, be entirely out of the question.

Several other possibilities have been examined, but they all lead to equally unacceptable consequences. The assumptions underlying the computation of $\Im_g$ appear to be justified, so that the order of magnitude of this quantity is fairly reliable. The value of the dissipative term $\Im_d$ is therefore evidently grossly in error and, in fact, must actually be zero, or perhaps slightly negative, since, even for $\Im_d \equiv 0$, nuclear reactions are apparently inadequate to sustain the pulsations. It thus appears that Eddington's "negative dissipation" (Eddington 1941*b*) may in some manner be responsible for the pulsations, if the cepheids are built according to the highly centrally concentrated red giant models.

It can be shown that the assumption of adiabatic oscillations is an excellent approximation interior to about $0.85R$; beyond this point, however, the adiabatic assumption breaks down rapidly. Assuming the opacity law to be approximately correct, then the calculation of the contribution to the dissipation from the "adiabatic" region should be fairly reliable. The dissipation in this region is definitely positive and corresponds to a damping time due to this region alone of about 160 days. Then, in order to have sustained pulsations, i.e., for $\Im_d$ to vanish, it appears to be a necessary condition that the contribution to $\Im_d$ from the outlying "nonadiabatic" region must be sufficiently negative to balance exactly the positive contribution from the adiabatic region. This implies that whatever is the cause of the pulsation phenomenon, it must lie in the regions occupying, roughly, the outer 15 per cent of the stellar radius.

It remains to be seen whether models with extensive hydrogen convection zones or different boundary conditions will remove these difficulties.

The author wishes to express his sincere gratitude to Dr. Marshal H. Wrubel for suggesting this problem, as well as for offering continued encouragement and advice throughout the work. Thanks are also extended to Dr. Martin Schwarzschild for his interest in this problem and for his valuable suggestions at critical stages in the investigation.

## REFERENCES

Chandrasekhar, S., and Schönberg, M. 1942, *Ap. J.*, **96**, 161.
Cowling, T. G. 1934, *M.N.*, **94**, 768.
———. 1935, *ibid.*, **96**, 42.
———. 1938, *ibid.*, **98**, 528.
Cox, J. P. 1954, "The Pulsational Stability of Models for Red Giant Stars" (Ph.D. Diss., Indiana University) (available through University Microfilms, Ann Arbor, Michigan).
Eddington, A. S. 1918, *M.N.*, **79**, 177.
———. 1930, *The Internal Constitution of the Stars* (Cambridge: At the University Press).
———. 1941*a*, *M.N.*, **101**, 177.
———. 1941*b*, *ibid.*, p. 182.
Epstein, I. 1950, *Ap. J.*, **112**, 6.
Ledoux, P. 1940, *Astrophysica Norvegica*, **3**, 193.
———. 1941, *Ap. J.*, **94**, 537.
Rosseland, S. 1949, *The Pulsation Theory of Variable Stars* (Oxford: Clarendon Press).
Rosseland, S., and Randers, G. 1938, *Astrophysica Norvegica*, **3**, 71.
Schwarzschild, M., and Li Hen. 1949, *M.N.*, **109**, 631.

# HYDROMAGNETIC DYNAMO MODELS

EUGENE N. PARKER
Department of Physics, University of Utah, Salt Lake City, Utah
*Received October 18, 1954; revised May 11, 1955*

## ABSTRACT

The purpose of this paper is to investigate the steady-state amplification of magnetic fields in a fluid. It is shown that a rotating sphere of conducting fluid can regenerate a dipole magnetic field. It is sufficient for the angular velocity of rotation to vary with distance from the axis of rotation and for cyclonic fluid motions to be present. The nonuniform rotation generates a toroidal field from the dipole field; the cyclones generate, from the toroidal field, loops of flux in the meridional plane which coalesce to amplify the dipole field. The rotating sphere is discussed in relation to the liquid core of the earth and the geomagnetic dipole field. If, instead of a rotating sphere, one has a prismatic volume of fluid, it is possible to construct migratory dynamo waves. The dynamo waves are discussed in relation to the solar convective zone; it is shown that such waves can account for many of the principal features of the observed solar magnetic activity.

## I. INTRODUCTION

The generation of magnetic fields $\boldsymbol{B}$ by a fluid with velocity $\boldsymbol{v}$ and conductivity $\sigma$ is described by

$$\frac{\partial \boldsymbol{B}}{\partial t} = \nabla \times (\boldsymbol{v} \times \boldsymbol{B}) + \frac{1}{\mu\sigma} \nabla^2 \boldsymbol{B}. \tag{1}$$

Elsasser (1950)[1] has suggested that there may exist fluid motions capable of regenerating various magnetic-field configurations, such as the magnetic field of the earth. Such a device has been called a "hydromagnetic dynamo." Formally, from the kinematical point of view, the question is whether there exists a $\boldsymbol{v}$ such that a solution of equation (1) can be a magnetic field $\boldsymbol{B}$ which is maintained for an indefinite period of time. The problem is sufficiently difficult that we shall consider a specific model for the fluid motion rather than inquire in a general mathematical way into sufficient conditions on $\boldsymbol{v}$ for maintaining a field $\boldsymbol{B}$. The first model we consider is based on the geometry found in the earth. In the last section we will consider another model, that of dynamo waves, which may be of interest in connection with the sunspot cycle.

Observed at the surface of the planet, the magnetic field of the earth is primarily a (poloidal) dipole. However, the existence of nonuniform rotation in the liquid core indicates that within the core the field cannot be entirely poloidal (Elsasser 1950). We shall assume, as a model from which to begin our discussion of equation (1), that the primary large-scale components of the terrestrial magnetic field are a (poloidal) dipole field, which we observe directly, and a toroidal field within the conducting core. The boundary conditions require that the toroidal field vanish outside the region of electrical conductivity (Elsasser 1947; Bullard and Gellman 1954). The toroidal field consists of lines of force circling about the axis of the earth, parallel to lines of latitude. The toroidal field is generated from the poloidal field by the nonuniform rotation of the core.

Both the poloidal and the toroidal fields have rotational symmetry about the axis of the earth. Cowling's theorem (Cowling 1933) then tells us that they cannot be maintained through equation (1) by a single direct interaction with the fluid velocity $\boldsymbol{v}$. It is possible to generate the toroidal field directly from the poloidal field, as will be shown presently, but not vice versa.

To demonstrate the generation of the toroidal field $\boldsymbol{B}_t$ from the poloidal field $\boldsymbol{B}_p$, we

[1] The fundamentals of hydromagnetic theory may be found in Elsasser's (1950) review article and are not repeated here for reasons of economy.

shall use the cylindrical co-ordinates $(\rho', \phi, z)$ about the axis of the earth. We take the nonuniform rotation to be

$$\boldsymbol{v} = \boldsymbol{e}_\phi v(\rho'), \tag{2}$$

and the poloidal field to be

$$\boldsymbol{B}_p = \boldsymbol{e}_\rho B_{p\rho} + \boldsymbol{e}_z B_{pz}, \tag{3}$$

where $\boldsymbol{e}_\rho$, $\boldsymbol{e}_\phi$, and $\boldsymbol{e}_z$ represent unit vectors in the $\rho'$-, $\phi$-, and $z$-directions, repectively. Then it is readily shown that

$$\nabla \times (\boldsymbol{v} \times \boldsymbol{B}_p) = \boldsymbol{e}_\phi B_{p\rho} \rho' \frac{\partial}{\partial \rho'}\left(\frac{v}{\rho'}\right). \tag{4}$$

We see from equation (1) that $\nabla^2 \boldsymbol{B}_t$ is in the $\phi$-direction. Since $\boldsymbol{B}_t$ is independent of $\phi$, the $\phi$-component of $\nabla^2 \boldsymbol{B}_t$ reduces to $\nabla^2 B_{t\phi} - B_{t\phi}/(\rho')^2$. Thus $\boldsymbol{B}_t$ has only a $\phi$-component, which we denote by $B$. From equations (1) and (4) we see that, for steady-state conditions, $B$ obeys

$$\nabla^2 B - \frac{B^2}{(\rho')^2} = -\mu\sigma B_{p\rho} \rho' \frac{\partial}{\partial \rho'}\left(\frac{v}{\rho'}\right). \tag{5}$$

Since $\boldsymbol{B}_t$ is parallel to $\boldsymbol{v}$, it follows that the nonuniform rotation does not interact with $\boldsymbol{B}_t$. The net result, then, is that the nonuniform rotation does not alter $\boldsymbol{B}_p$ and has as its only effect the generation of an axially symmetric toroidal field, with opposite senses in the northern and southern hemispheres. Bullard (1954) has computed $B$ resulting from various poloidal-field configurations.

## II. GENERATION OF LOOPS

We must now demonstrate a fluid motion which, by interacting with the toroidal field $\boldsymbol{B}_t$, regenerates the poloidal field. Let us fix our attention on a region of the toroidal field sufficiently small in extent that we may regard the field as uniform throughout. We define a local Cartesian co-ordinate system $(\xi, \eta, \zeta)$ where the $\eta$-axis is parallel to the toroidal field and points toward the east; the $\zeta$-axis is directed radially outward; and the $\xi$-axis points south and is tangent to the circle of longitude through the local origin. Hence, locally, the meridional planes are parallel to the $\zeta\xi$-plane. We denote the intensity of the toroidal field by $B$ and the distance from the $\zeta$-axis by $\rho$. Then

$$\boldsymbol{B}_t = \boldsymbol{e}_\phi B = \boldsymbol{e}_\eta B, \qquad \rho = \sqrt{(\xi^2 + \eta^2)}. \tag{6}$$

Now suppose that there is a body of fluid moving along the $\zeta$-axis through the toroidal field. We will further suppose that the moving fluid is rotating about the $\zeta$-axis. Dynamically, such a fluid motion is related to the cyclones and anticyclones observed in the atmosphere, in which the primary driving force is radial convection and the rotation results from the Coriolis deflection of the influx and efflux of fluid at the ends of the vertically moving column.

An elementary consideration of Coriolis forces suggests that in the northern hemisphere fluid flowing into the base of a rising convective column is deflected to the right as it approaches the column. The result is a counterclockwise rotation about the axis of the column. Opposite rotational forces apply to the efflux at the top of the convecting column. This is just the conventional elementary explanation for cyclones in the atmosphere and is not intended as a proof of the existence of cyclonic motions in the core; we wish only to suggest that it is not unreasonable to *postulate* cyclonic motions.

Unfortunately, if we include the influx and efflux in the fluid motion, the mathematics of a rigorous analytical solution becomes extremely complicated. We shall, therefore, idealize the problem. We shall simply constrain the fluid to rotate around the $\zeta$-axis and consider a fluid column of infinite length along the $\zeta$-axis. In order to restrict to finite

extent the region of interaction between the magnetic field and the fluid motion, we assume that the toroidal field is initially a slab with a thickness of the order of $a$ in the $\zeta$-direction. With these simplifications, the interaction of our idealized fluid motion and toroidal field may be computed rigorously in the limit of infinite electrical conductivity of the fluid.

To demonstrate that nothing essential has been altered by the idealization, the problem has been recomputed in the appendix for fluid motion of finite extent in the $\zeta$-direction, involving influx and efflux of fluid. A perturbation approximation is used, and it is easily shown that we obtain the same results as from the idealized model.

Consider, then, the idealized fluid motion,

$$v_\xi = -w_0\left(\frac{\eta}{a}\right) S(\rho), \qquad v_\eta = +w_0\left(\frac{\xi}{a}\right) S(\rho), \qquad v_\zeta = v_0 R(\rho), \tag{7}$$

where $w_0$, $v_0$, and $a$ are constants. We assume that $S(\rho)$ and $R(\rho)$ vanish for large $\rho$ and have a maximum at $\rho = 0$. The Gaussian exp $(-\rho^2/a^2)$ would be typical of their behavior. Here $v_\xi$ and $v_\eta$ represent a rotation about the vertical $\zeta$-axis.

The result of the interaction of the fluid given by equation (7) may be understood if we first consider the effect of $v_\zeta$. The vertical motion $v_\zeta$ will bulge up the toroidal field so that the lines of force in the vicinity of the bulge have the shape of a capital omega, $\Omega$, and $v_\zeta$ and $v_\eta$, which represent a rotation about the vertical axis, will rotate the loop of the omega about a vertical axis, so that its projection on the meridional plane (the plane perpendicular to the initial $\boldsymbol{B}_t$) will form a closed loop. Assuming many cyclones distributed throughout the core, we obtain many such meridional loops. It will be shown in Section III that these loops may coalesce to form a poloidal dipole field.

Let us now consider quantitatively the formation of meridional loops. For infinite conductivity, equation (1) reduces to

$$\frac{\partial \boldsymbol{B}}{\partial t} = \nabla \times (\boldsymbol{v} \times \boldsymbol{B}). \tag{8}$$

If we replace $\boldsymbol{B}$ by $\boldsymbol{\omega}$, we note that we have just the usual Helmholtz equation for vorticity. Cauchy's integral (Brand 1947) of this equation may be applied (Lundquist 1952), giving the Lagrangian solution,

$$\boldsymbol{B}[\boldsymbol{r}(\boldsymbol{r}_0, t)] = [\boldsymbol{B}(\boldsymbol{r}_0, 0) \cdot \nabla_0]\, \boldsymbol{r}(\boldsymbol{r}_0, t), \tag{9}$$

where $\boldsymbol{r}(\boldsymbol{r}_0, t)$ represents the position at time $t$ of an element of fluid initially at $\boldsymbol{r}_0$, and $\nabla_0$ represents differentiation with respect to $\boldsymbol{r}_0$.

By equation (7) the distance of an element of fluid from the $\zeta$-axis is independent of time. Thus $\rho$ is constant for a given element of fluid,

$$\rho = \lambda. \tag{10}$$

Then, at a time $t$, the co-ordinates of an element of fluid initially at $(\xi_0, \eta_0, \zeta_0)$ will be

$$\xi = \xi_0 \cos\left[\frac{S(\lambda) w_0 t}{a}\right] - \eta_0 \sin\left[\frac{S(\lambda) w_0 t}{a}\right], \tag{11}$$

$$\eta = \xi_0 \sin\left[\frac{S(\lambda) w_0 t}{a}\right] + \eta_0 \cos\left[\frac{S(\lambda) w_0 t}{a}\right], \tag{12}$$

$$\zeta = v_0 R(\lambda)\, t + \zeta_0, \qquad \lambda = (\xi_0^2 + \eta_0^2)^{1/2}. \tag{13}$$

Defining the functions

$$Z(\lambda) \equiv R(\lambda)\, v_0 t\,, \qquad \Psi(\lambda) \equiv \frac{S(\lambda)\, w_0 t}{a}, \tag{14}$$

equations (11), (12), and (13) may be solved for $(\xi_0, \eta_0, \zeta_0)$ to give

$$\xi_0 = +\xi \cos\Psi + \eta \sin\Psi\,, \tag{15}$$

$$\eta_0 = -\xi \sin\Psi + \eta \cos\Psi\,, \tag{16}$$

$$\zeta_0 = \zeta - Z\,. \tag{17}$$

The initial toroidal field has only an $\eta$-component. Thus, of $\nabla_0 \boldsymbol{r}$, we need only $\partial \boldsymbol{r}/\partial\eta_0$. From equations (11), (12), and (13) it is readily shown that

$$\frac{\partial\xi}{\partial\eta_0} = \frac{\eta_0\xi - \xi_0\eta}{\lambda^2} - \Psi' \frac{\eta_0\eta}{\lambda}, \tag{18}$$

$$\frac{\partial\eta}{\partial\eta_0} = \frac{\xi_0\xi + \eta_0\eta}{\lambda^2} + \Psi' \frac{\eta_0\xi}{\lambda}, \tag{19}$$

$$\frac{\partial\zeta}{\partial\eta_0} = Z' \frac{\eta_0}{\lambda}. \tag{20}$$

The primes denote differentiation with respect to $\lambda$. Introducing the azimuthal angle $\psi$ measured from the $\xi$-axis about the $\zeta$-axis, we have

$$\xi = \lambda\cos\psi\,, \qquad \eta = \lambda\sin\psi\,. \tag{21}$$

Equations (15) through (20) may be considerably simplified. Substituting equations (18), (19), and (20) in equation (9), and using equation (21), we obtain the field at $(\lambda, \psi, \zeta)$ after a time $t$ as follows:

$$B_\xi = -B(\zeta - Z)\,[\sin\Psi + \lambda\Psi' \sin\psi \sin(\psi - \Psi)]\,, \tag{22}$$

$$B_\eta = +B(\zeta - Z)\,[\cos\Psi + \lambda\Psi' \cos\psi \sin(\psi - \Psi)]\,, \tag{23}$$

$$B_\zeta = +B(\zeta - Z)\, Z \sin(\psi - \Psi)\,. \tag{24}$$

The magnetic field $\boldsymbol{B}$, given by equations (22), (23), and (24), is shown in Figure 1 by the continuous ribbons. To consider the decay of $\boldsymbol{B}$ we decompose it into two parts, $\boldsymbol{\alpha}$ and $\boldsymbol{\beta}$. Here $\boldsymbol{\beta}$ is the magnetic field that would result if $v_\zeta$ were zero, i.e., $Z = 0$, and is shown in Figure 2; and $\boldsymbol{\alpha}$ is $\boldsymbol{B} - \boldsymbol{\beta}$.

Putting $Z = 0$ in equations (22), (23), and (24), we have

$$\beta_\xi = -B(\zeta)\,[\sin\Psi + \lambda\Psi' \sin\psi \sin(\psi - \Psi)]\,, \tag{25}$$

$$\beta_\eta = +B(\zeta)\,[\cos\Psi + \lambda\Psi' \cos\psi \sin(\psi - \Psi)]\,, \tag{26}$$

$$\beta_\zeta = 0\,. \tag{27}$$

Then, since

$$\boldsymbol{B} = \boldsymbol{\alpha} + \boldsymbol{\beta}\,, \tag{28}$$

$\boldsymbol{\alpha}$ is given by

$$\alpha_\xi = -\,[B(\zeta - Z) - B(\zeta)]\,[\sin\Psi + \lambda\Psi' \sin\psi \sin(\psi - \Psi)]\,, \tag{29}$$

$$\alpha_\eta = +\,[B(\zeta - Z) - B(\zeta)]\,[\cos\Psi + \lambda\Psi' \cos\psi \sin(\psi - \Psi)]\,, \tag{30}$$

$$\alpha_\zeta = +B(\zeta - Z)\, Z' \sin(\psi - \Psi)\,. \tag{31}$$

Now suppose that the fluid motion comes to a halt after having rotated through $\pi/2$ in the vicinity of the $\zeta$-axis. Then, in the vicinity of the $\zeta$-axis, the field has been rotated to the $\xi$-direction. Assuming $Z(\lambda)$ and $\Psi(\lambda)$ to be Gaussian functions, we put

$$Z(\lambda) = a\Psi(\lambda) = a\frac{\pi}{2}\exp\left(-\frac{\lambda^2}{a^2}\right). \tag{32}$$

For this case, $\boldsymbol{B}$ is shown by the solid lines in Figure 1; $\boldsymbol{\beta}$ is shown by the continuous ribbons in Figure 2. The intermittent ribbons in Figure 1 represent $-\boldsymbol{\beta}$. The lines of force of $\boldsymbol{\alpha}$, which is $\boldsymbol{B} - \boldsymbol{\beta}$, form the closed curves obtained by combining the solid and the broken ribbons in Figure 1. Since $\boldsymbol{\beta}$ is just the projection of $\boldsymbol{B}$ on the $\xi\eta$-plane, the closed curves lie on cylindrical surfaces which are parallel to the $\zeta$-axis. Figure 3, *a*, shows the surface inclosed by the lines through $P$ and $Q$ in Figure 1. Figure 3, *b*, shows

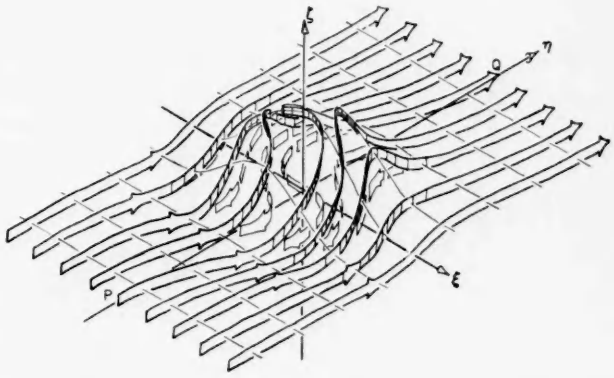


FIG. 1.—The deformation of a slab of toroidal field by cyclonic fluid motion. The ribbons underneath represent $-\boldsymbol{\beta}$.

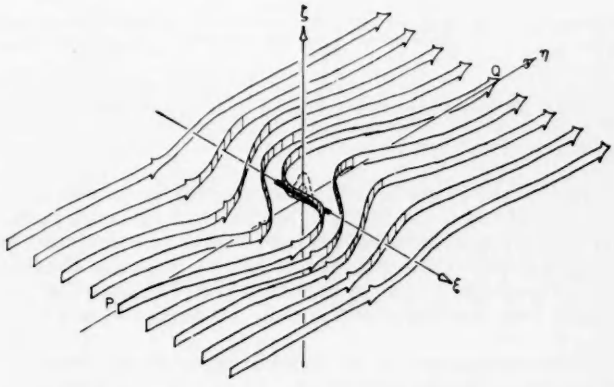


FIG. 2.—The deformation of a slab of toroidal field by a cyclonic fluid motion in the absence of vertical motion. This is the field $+\boldsymbol{\beta}$.

the same surface tipped down so that we see only the projection on the $\zeta\xi$-plane. In this projection the sign of the lines of force encircling *PDB* and *CEQ* is clockwise, whereas the lines encircling *DECB* have a counterclockwise sign. We see that the net result is a counterclockwise sign for *PDE*. We note, in fact, that so long as $Z(\lambda)$ and $\Psi(\lambda)$ are positive quantities and monotonically decreasing functions of $\lambda$, the central portion *DECB* will always predominate, with *PDE* representing a net counterclockwise rotation.

Projecting $\mathbf{a}$ on the $\eta\zeta$-plane in the same manner as on the $\zeta\xi$-plane demonstrates a circulation of flux about the $\xi$-direction, in a clockwise direction as viewed from a point on the positive $\xi$-axis. Thus we see that $\mathbf{a}$ is composed of loops of flux circulating about the $\eta$-direction plus loops circulating about the $\xi$-direction.

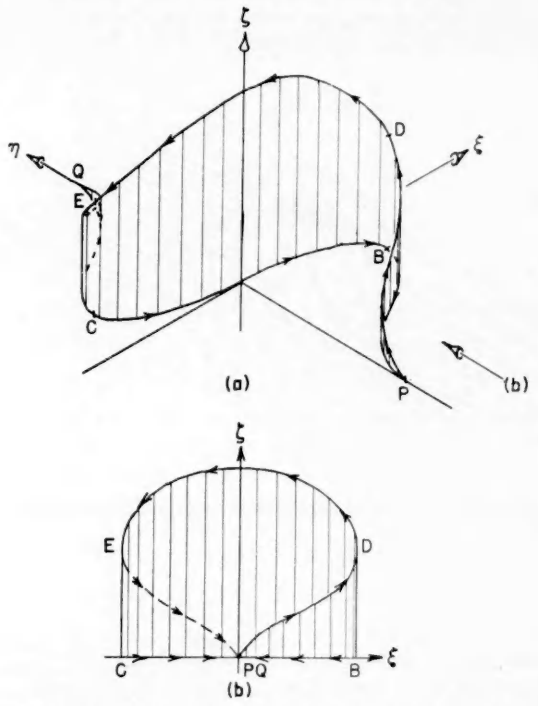


FIG. 3.—*a*, Isometric drawing of the surface inclosed by the closed line of force of $\mathbf{a}$ which passes through *P* and *Q*. *b*, The projection of the surface onto the $\zeta\xi$-plane. The arrow in *a* indicates the direction in which the projection is viewed (from the negative $\eta$-axis).

By subtracting the initial toroidal field from $\mathfrak{B}$, it may be seen from Figure 2 that $\mathfrak{B}$ consists of two loops of flux in the $\xi\eta$-plane, in addition to the initial toriodal field. The two loops have opposite directions: Viewed from a point on the positive $\zeta$-axis, the loop for $\eta > 0$ circulates in a clockwise direction. It follows, then, that the field $\boldsymbol{B}$, shown by the solid lines in Figure 1 and given by equations (22), (23), and (24), is equivalent to the initial toroidal field plus the three mutually perpendicular sets of loops shown in Figure 4*a*.

The perturbation computation in the appendix separates the sets of loops in quite a natural way: It is a second-order perturbation calculation; the terms of first and second order in the rotation $\Psi$ give the two loops of opposite direction with axes parallel to the $\zeta$-axis; the terms of first and second order in the vertical motion $Z$ give the loop circulat-

ing about the $\xi$-direction; the cross-product term $\Psi Z$ results in the loop circulating about the $\eta$-direction.

It is interesting, though not essential, to note that the three sets of loops with mutually perpendicular axes may be reduced to two sets of loops by further idealization, eliminating the loop circulating about the $\xi$-axis. If, instead of equation (32), we write

$$Z = b\,\frac{\pi}{2}\exp\left(-\frac{\lambda^2}{b^2}\right), \qquad \Psi = \frac{\pi}{2}\exp\left(-\frac{\lambda^2}{a^2}\right), \tag{33}$$

and make $a \gg b$, then in the region surrounding the $\zeta$-axis, where $Z$ is nonvanishing, $\Psi$ is essentially constant and equal to $\pi/2$. As a result of the rotation $\Psi$, then, we have,

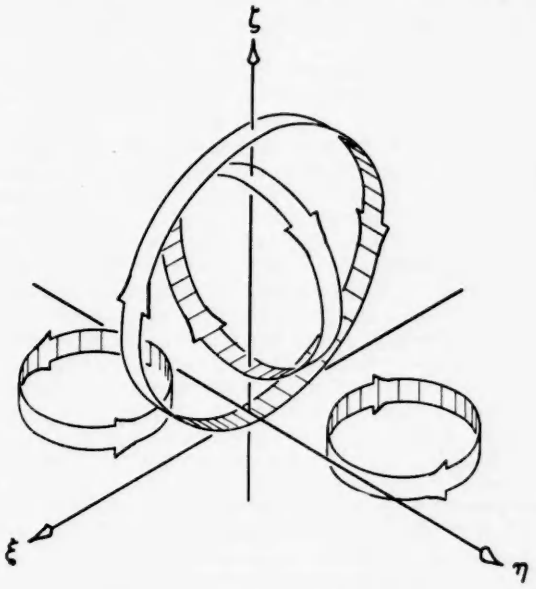


FIG. 4*a*.—Schematic drawing of the three sets of mutually perpendicular loops into which each closed line of force of $\boldsymbol{a}$ may be resolved.

in the region of nonvanishing $Z$, a uniform field in the $\xi$-direction. The vertical motion produces a hump in this uniform field, as shown by the broken line in Figure 2.

Noting that

$$\Psi(\lambda) = \frac{\pi}{2} + O^2\left(\frac{\lambda}{a}\right), \qquad \Psi'(\lambda) = O\left(\frac{\lambda}{a}\right), \tag{34}$$

we obtain, from equations (22), (23), and (24), the components of $\boldsymbol{B}$:

$$B_\xi = -B(\zeta - Z)\left[1 + O^2\left(\frac{\lambda}{a}\right)\right], \tag{35}$$

$$B_\eta = +B(\zeta - Z)\,O^2\left(\frac{\lambda}{a}\right), \tag{36}$$

$$B_\zeta = -B(\zeta - Z)\,Z'\cos\psi + O^2\left(\frac{\lambda}{a}\right)\exp\left(-\frac{\lambda^2}{b^2}\right). \tag{37}$$

Then

$$\beta_\xi = -B(\zeta)\left[1+O^2\left(\frac{\lambda}{a}\right)\right], \tag{38}$$

$$\beta_\eta = +B(\zeta)\,O^2\left(\frac{\lambda}{a}\right), \tag{39}$$

$$\beta_\zeta = 0, \tag{40}$$

and

$$\alpha_\xi = -\left[B(\zeta - Z) - B(\zeta)\right]\left[1+O^2\left(\frac{\lambda}{a}\right)\right], \tag{41}$$

$$\alpha_\eta = +\left[B(\zeta - Z) - B(\zeta)\right]O^2\left(\frac{\lambda}{a}\right), \tag{42}$$

$$\alpha_\zeta = -B(\zeta - Z)\,Z'\cos\psi + O^2\left(\frac{\lambda}{a}\right)\exp\left(-\frac{\lambda^2}{b^2}\right). \tag{43}$$

We see that the $\eta$-component of $\mathbf{a}$ may be neglected, eliminating the loop circulating about the $\xi$-direction. Figure 4*b* shows the two sets of loops into which the idealized field may be resolved.

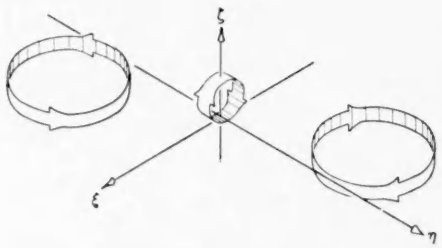


FIG. 4*b*.—Schematic drawing of the two sets of loops into which each line of $\alpha$ may be resolved when the vertical fluid motion is confined to a small neighborhood of the $\zeta$-axis.

## III. CANCELLATION OF LOOPS

Having demonstrated how loops of magnetic flux may be produced locally from the toroidal field, let us now consider what happens when a large number of cyclones appear near one another. In this section we shall demonstrate that all loops except those circulating about the $\eta$-direction can be made to vanish.

To begin with, consider a large number of groups of loops (each group as shown in Fig. 4*a*) distributed throughout the core of the earth. If $(r, \theta, \phi)$ represent spherical co-ordinates with the axis of the earth at $\theta = 0$, then the $\zeta$-axis of each local co-ordinate system is in the $r$-direction, the $\xi$-axis is in the $\theta$-direction, and the $\eta$-axis is in the $\phi$-direction.

Let us assume that all the loops in the meridional or local $\zeta\xi$-planes have the same direction of field. So far, we have discussed explicitly only the loops produced by an upwelling of fluid. There may, of course, be sinking regions. In order for a sinking region to produce a loop with the same direction as an upwelling, it may be seen from equations (29) and (31) or from Figure 1 that the direction of rotation of the fluid must be reversed. We shall assume, therefore, that sinking regions all have the opposite direction of rotation from that of upwelling regions and are distributed throughout the core in equal number with the upwelling regions.

Considering equations (30) and (31) or Figure 1, we can readily see that the loop circuating about the local $\xi$-direction ($\theta$-direction) produced by an upwelling has a direction opposite to a similar loop produced by a sinking region. Let $l$ represent the average separation of groups of loops, and let $P$ represent the radius of the core. Then, upon expanding the loops circulating about the local $\xi$-directions in a series of spherical harmonics over the core, the alternation of sign of neighboring loops results in the leading term in the series being $P_n^m(\cos\theta)\cos(m\phi + \delta_m)$, where $n$ and $m$ are both of the order of $P/l$.

The two loops in each group circulating about the local $\zeta$-direction ($r$-direction) have opposite directions and, upon expansion over the core, also contribute as the leading term, $n, m \approx P/l$.

The loop in each group circulating about the local $\eta$-direction ($\phi$-direction) will have the same direction in every case and, hence, will contribute a dipole $P_1(\cos\theta)$ as the leading term.

The decay rate of a mode is proportional to $n^2 + m^2$. Thus the ratio of the rate of decay of the superposed loops with axes in the $\phi$-direction to either of the other two sets of loops is of the order of $(l/P)^2$. In the limit, as we consider more and smaller cyclones, $(l/P) \to 0$, and only the loops with axes in the $\phi$-direction remain. To put the matter differently, unless there is a predominant direction, the loops cancel one another.

There are other circumstances under which the only loops to survive are those circulating about the $\phi$-direction. For instance, if there were not so many loops produced by sinking as by upwelling fluid, then the loops with axes in the $\theta$-direction would not vanish in the limit as $(l/P) \to 0$, since the loops produced by sinking fluid would not entirely cancel the loops generated by upwelling fluid. However, if the region of vertical motion is confined to a small neighborhood of the local $\zeta$-axis, then we obtain a set of loops, as described in equations (35)–(43), in which the loops with axes in the $\theta$-direction are not generated. Thus the problem of their cancellation does not arise.

It is easily demonstrated in this case that the loops with axes in the $\phi$-direction will predominate. The dipole moment of a loop is of the order of the total flux circulating about the axis of the loop multiplied by the radius of the loop. Thus, initially, the moment of each individual loop with axis in the $r$-direction is $Ba^3$. For the $\phi$-direction the moment of each loop is $Bb^3$. The loops circulating about the $\theta$-direction arise from the $\mathbf{a}$ given in equations (41), (42), and (43). The field intensity is of the order of $B(b/a)^2$, so that the total moment is $B(b/a)^2b^3$. If a dipole field throughout the core decays according to $\exp(-kt)$, then, upon superposition, the loops with axes in the $r$-, $\theta$-, and $\phi$-directions contribute to the over-all field, according to

$$M_r \approx Ba^3 \exp\left[\frac{-ktP}{l^2}\right], \tag{44}$$

$$M_\theta \approx Ba^3\left(\frac{b}{a}\right)^5 \exp(-kt), \tag{45}$$

$$M_\phi \approx Ba^3\left(\frac{b}{a}\right)^3 \exp(-kt), \tag{46}$$

respectively. For $t > 0$ we find, in the limit as $l \to 0$, that

$$M_r : M_\theta : M_\phi \approx 0 : \left(\frac{b}{a}\right)^2 : 1. \tag{47}$$

Thus, in the limit as $(b/a) \to 0$, there remain only the loops circulating about the $\phi$-direction.

We have demonstrated that one result of the interaction of cyclonic fluid motions with the toroidal field is to generate loops of flux in meridional planes. In the limit as the number of cyclones becomes large, this produces no fields other than these meridional loops. We note that the reduction of the cyclone fields to meridional loops depends on the fluid having finite, rather than infinite, conductivity. Ideally, we produce loops by violent small-scale, short-lived cyclones in a time so short that the effects of finite conductivity may be neglected. We allow the loops to decay for a brief period of time following their formation, in order to eliminate all but those in the meridional plane. Thus, microscopically, the process will not be a steady state, even though the gross dipole field resulting from a steady production of the loops will not vary with time.

Now we should notice that the same microscopic cyclones that generate the meridional loops from the toroidal field will also generate loops from the poloidal field. The loops generated from the poloidal field will be of the same general nature as those generated from the toroidal field, except that they will circulate about the $\theta$-direction (local $\xi$-axis) instead of the $\phi$-direction, the reason being that the initial poloidal field from which they are formed is at right angles to the toroidal field.

If the cyclones have a sense of rotation such that the loops they produce from the toroidal field regenerate the dipole field—and in any dynamo found in nature, they must have the regenerative sense—it may be seen that the loops they produce from the poloidal field have the same direction as the toroidal field. Hence they serve only to regenerate the toroidal field. However, because we are considering an idealized model, it is possible to get around this harmless complication by assuming that the nonuniform rotation greatly exceeds the cyclonic motion, so that the intensity of the poloidal field becomes vanishingly small as compared to the toroidal field. Then the loops generated from the poloidal field vanish in comparison to the loops generated from the toroidal field, and the only effect of the cyclonic motions is to produce the meridional loops.

## IV. COALESCENCE OF LOOPS

Having demonstrated that through cancellation the only effect of a large number of cyclonic motions is to produce loops of flux in the meridional planes, let us now investigate analytically the over-all effects of a large number of meridional loops.

We let $(R, \Theta, \Phi)$ represent the spherical co-ordinates of the center of a meridional loop and $(\rho, \vartheta, \varphi)$ the co-ordinates relative to the center of the loop, so that the co-ordinates $(r, \theta, \phi)$ of a point are related to the center of the loop by

$$r = R + \rho\,, \qquad \theta = \Theta + \vartheta\,, \qquad \phi = \Phi + \varphi\,. \tag{48}$$

The linear dimensions of a given loop are of the order of $a$, which has been taken as small compared to the radius $P$ of the core. Thus $\rho$, $\vartheta$, and $\varphi$ will be small quantities, of the order of $a/P$ times $r$, $\theta$, and $\phi$, respectively.

In the limit as $a \to 0$, the details of the individual loop become irrelevant: The individual details contribute to modes of the order of $P/l$ or $P/a$ and vanish in the limit as $l/P \to 0$ because of their large decay rate, just as did the pairs of loops formed in the local $\xi\eta$-planes. Thus, for convenience, we choose loops described by a Gaussian symmetrical about the loop center. We put

$$B_\rho \equiv B_\zeta = -B_0 \frac{R}{a}\,\vartheta \exp\left[-\frac{\rho^2 + R^2\vartheta^2 + R^2 \sin^2\Theta\varphi^2}{a^2}\right], \tag{49}$$

$$B_\vartheta \equiv B_\xi = +B_0 \frac{\rho}{a} \exp\left[-\frac{\rho^2 + R^2\vartheta^2 + R^2 \sin^2\Theta\varphi^2}{a^2}\right], \tag{50}$$

$$B_\varphi \equiv B_\eta = 0\,. \tag{51}$$

The lines of force are circles with centers on the $\phi$- or local $\eta$-axis.

The analysis is more conveniently carried out if we work with the curl of the magnetic field, since this is a toroidal rather than a poloidal vector. We shall need only the $\phi$-component of the curl, for reasons that will appear presently:

$$(\nabla \times \boldsymbol{B})_\phi = \frac{2B_0}{a}\left(1 - \frac{\rho^2}{a^2} - \frac{R^2}{a^2}\vartheta^2\right)\exp\left[-\frac{1}{a^2}(\rho^2 + R^2\vartheta^2 + R^2\sin^2\Theta\varphi^2)\right]. \tag{52}$$

We now expand equation (52) in terms of vector modes, whereupon we average the amplitude of each mode over all possible positions of the loop centers. If the distribution of the loops is independent of $\Phi$, only the rotationally symmetric toroidal modes will survive the averaging process. The toroidal zonal modes are

$$T_{r(ns)} = T_{\theta(ns)} = 0\,, \qquad T_{\phi(ns)} = c_{ns}\, j_n(k_{sn}r)\frac{dP_n(\cos\theta)}{d\theta}, \tag{53}$$

where $j_n(x)$ is a spherical Bessel function defined (Stratton 1941) as $(\pi/2x)^{1/2}J_{n+1/2}(x)$. The boundary conditions require (Elsasser 1947) the $k_{sn}$ to be the roots of

$$j_{n-1}(k_{sn}P) = 0\,, \tag{54}$$

where $P$ is the radius of the core.

We now develop equations (53) in ascending powers of the small quantities $\rho$ and $\vartheta$ defined in equations (48). We write

$$T_{\phi(ns)} = c_{ns}[A_{ns} + B_{ns}\rho + C_{ns}\vartheta + D_{ns}\rho^2 + E_{ns}\rho\vartheta + F_{ns}\vartheta^2 + O^3(\rho, \vartheta)]\,. \tag{55}$$

We note that

$$D_{ns} = \frac{1}{2}\frac{d^2 j_n(k_{sn}R)}{dR^2}\frac{dP_n(\cos\Theta)}{d\Theta}, \tag{56}$$

$$F_{ns} = \tfrac{1}{2}\, j_n(k_{sn}R)\frac{d^3P_n(\cos\Theta)}{d\Theta^3}. \tag{57}$$

The modes $\boldsymbol{T}_{(ns)}$ are orthogonal, so that if we write that the toroidal part of $\nabla \times \boldsymbol{B}$ is

$$(\nabla \times \boldsymbol{B})_t = \sum_{n,s} \boldsymbol{T}_{(ns)}\,, \tag{58}$$

multiply by $\boldsymbol{T}_{(pq)}$, and integrate over the volume of the core, we obtain

$$\int dV\,(\nabla \times \boldsymbol{B}) \cdot \boldsymbol{T}_{(pq)} = \int dV\,(\boldsymbol{T}_{(pq)})^2\,. \tag{59}$$

Noting that

$$\int_0^\pi d\theta \sin\theta\left[\frac{dP_n(\cos\theta)}{d\theta}\right]^2 = \int_{-1}^{+1} d\mu\,(1-\mu^2)[P_n'(\mu)]^2 = \frac{2n(n+1)}{2n+1}, \tag{60}$$

(MacRobert 1947) and that

$$\int_0^P dr\, r^2 j_n(k_{sn}r) = \frac{\pi}{2k_{sn}}\int_0^P dr\, r J_{n+1/2}^2(k_{sn}r) = \tfrac{1}{2}P^3 j_n'^2(k_{sn}P)\,, \tag{61}$$

from equation (54) and Jahnke and Emde (1945), we obtain

$$\int dV\,(\boldsymbol{T}_{(ns)})^2 = (c_{ns})^2 P^3 j_n'^2(k_{sn}P)\,\pi\frac{2n(n+1)}{2n+1}. \tag{62}$$

From equations (52) and (55) we find that

$$\int dV\ (\nabla \times \boldsymbol{B}) \cdot \boldsymbol{T}_{(ns)} = -\pi^{3/2} B_0 c_{ns} a^4 \left[ D_{ns} + \frac{F_{ns}}{R^2} + O^2\left(\frac{a}{R}\right)\right]. \tag{63}$$

Substituting equations (62) and (63) in equation (59), we obtain, finally,

$$c_{ns} = -\frac{B_0 \sqrt{\pi} a^4 (2n+1)(D_{ns} + F_{ns}/R^2)}{P^3 j_n^2 (k_{sn} P)\, 2n(n+1)}. \tag{64}$$

We next consider the time dependence of the loops. They will appear in some random fashion and decay subsequently. Consider the amplitude $\gamma_{ns}(t)$ of the $ns$-mode due to loops appearing randomly in time at $(R, \Theta, \Phi)$. If their appearance is described by the random source function, $f_{ns}(t)$, then (Elsasser 1946–1947)

$$\Lambda_{ns}\gamma_{ns}(t) + \frac{d}{dt}\gamma_{ns}(t) = f_{ns}(t), \qquad \Lambda_{ns} = \frac{k_{sn}^2}{\mu\sigma}.$$

The solution is

$$\gamma_{ns}(t) = \int_{-\infty}^{t} dt' f_{ns}(t') \exp\left[\Lambda_{ns}(t'-t)\right]. \tag{65}$$

Let us assume that the loops appear suddenly at the random times $t_i$; thereafter they spread out by diffusion. Since $c_{ns}$ is the contribution of a loop to the $ns$-mode, we put

$$f_{ns}(t) = c_{ns} \sum_i \delta(t - t_i), \tag{66}$$

where $\delta(t - t_i)$ is a Dirac delta function. Then

$$\gamma_{ns}(t) = c_{ns} \sum_i \exp\left[\Lambda_{ns}(t - t_i)\right], \tag{67}$$

where the summation is over all $i$ for which $t_i \leq t$.

The average of $\gamma_{ns}(t)$ over time is

$$\langle \gamma_{ns}(t) \rangle = \lim_{T\to\infty} \frac{1}{2T} \int_{-T}^{+T} dt \gamma_{ns}(t),$$

which gives

$$\langle \gamma_{ns}(t) \rangle = c_{ns} \lim_{T\to\infty} \frac{1}{2T} \sum_i \frac{1}{\Lambda_{ns}} = \frac{\nu c_{ns}}{\Lambda_{ns}}, \tag{68}$$

where $\nu$ is the mean number of loops appearing per unit time.

We let $h(R, \Theta)$ represent the rate at which loops are generated at $R, \Theta$, normalized to give unity upon integration over the core. The expectation value over both space and time of the amplitude $\gamma_{ns}$ is

$$\langle\langle \gamma_{ns} \rangle\rangle = 2\pi \int_0^P dR \int_0^\pi d\Theta R^2 \sin\Theta h(R, \Theta) \langle \gamma_{ns} \rangle. \tag{69}$$

Then, from equations (53), it follows that the curl of the poloidal field resulting from the superposition of the meridional loops is the toroidal vector,

$$\nabla \times \boldsymbol{B}_p = \sum_{n,s} \boldsymbol{T}_{(ns)} = -\boldsymbol{e}_\phi \sum_{n,s} \frac{\partial \Psi_{ns}}{\partial \theta}, \tag{70}$$

where

$$\Psi_{ns} = \langle\langle \gamma_{ns} \rangle\rangle j_n(k_{sn} r) P_n(\cos\theta). \tag{71}$$

$\boldsymbol{B}_p$ itself may be expressed in terms of the poloidal modes, $\boldsymbol{S}_{(ns)}$, by noting that $\boldsymbol{T}_{(ns)}$ must be related to them by

$$\boldsymbol{T}_{(ns)} = \nabla \times \boldsymbol{S}_{(ns)} .$$

Then

$$\nabla \times \boldsymbol{T}_{(ns)} = \nabla \times \nabla \times \boldsymbol{S}_{(ns)} = -\nabla^2 \boldsymbol{S}_{(ns)} = k_{sn}^2 \boldsymbol{S}_{(ns)} ,$$

and

$$\boldsymbol{S}_{(ns)} = (k_{sn})^{-2} \nabla \times \boldsymbol{T}_{(ns)} . \tag{72}$$

Using equation (70) and Legendre's equation, we find that

$$S_{r(ns)} = n(n+1) \frac{\Psi_{ns}}{k_{sn}^2 r} , \tag{73}$$

$$S_{\theta(ns)} = \frac{1}{k_{sn}^2 r} \frac{\partial^2 (k_{sn} r \Psi_{ns})}{\partial \theta \partial (k_{sn} r)} , \tag{74}$$

$$S_{\phi(ns)} = 0 , \tag{75}$$

where, now,

$$\boldsymbol{B}_p = \sum_{n,\, s} \boldsymbol{S}_{(ns)} . \tag{76}$$

## V. HOMOGENEOUS MODEL

Now let the loops be distributed with a density $h(R, \Theta)$ over the interior of a sphere of radius $R_0 \leq P$. We shall, in particular, consider a uniform distribution, $h =$ Constant. Then, with proper normalization, we take

$$h = \frac{3}{4\pi R_0^3} . \tag{77}$$

From equations (56), (57), (64), (68), and (69) we have

$$\langle\langle \gamma_{ns} \rangle\rangle = \frac{3}{2R_0^3} \int_0^{R_0} dR \int_0^{\pi} d\Theta R^2 \sin\Theta \langle \gamma_{ns}(R, \Theta) \rangle$$

$$= \frac{3(2n+1) A}{2n(n+1)(k_{sn}R_0)^3 p\, j_n^2(k_{sn}P)} \tag{78}$$

$$\times [A_1(n, s) B_1(n) + A_2(n, s) B_2(n)] ,$$

where

$$A = \frac{B_0 \sqrt{\pi a^4 \nu \mu \sigma}}{4P^2} , \tag{79}$$

and

$$A_1(n, s) = \int_0^{k_{sn}R_0} du\, u^2 j_n''(u) , \tag{80}$$

$$A_2(n, s) = \int_0^{k_{sn}R_0} du\, j_n(u) , \tag{81}$$

$$B_1(n) = \int_0^{\pi} d\theta \sin\theta \frac{dP_n(\cos\theta)}{d\theta} , \tag{82}$$

$$B_2(n) = \int_0^{\pi} d\theta \sin\theta \frac{d^3P_n(\cos\theta)}{d\theta^3} . \tag{83}$$

To evaluate $B_1(n)$, we integrate by parts and obtain

$$B_1(n) = -\int_0^\pi d\theta \cos\theta P_n(\cos\theta) .$$

This may be evaluated (MacRobert 1947) to give

$$B_1(2n) = 0 \qquad B_1(2n+1) = \frac{\Gamma(n+\frac{1}{2})\,\Gamma(n+\frac{3}{2})}{\Gamma(n+1)\,\Gamma(n+2)} . \tag{84}$$

To evaluate $B_2(n)$, we note that

$$\frac{dP_n(\cos\theta)}{d\theta} = -\sin\theta \frac{dP_n(\cos\theta)}{d(\cos\theta)}$$

vanishes at $\theta = 0$ and $\pi$. Thus, upon integrating twice by parts, we obtain

$$B_2(n) = -B_1(n) . \tag{85}$$

Since both $B_1(n)$ and $B_2(n)$ vanish for even $n$, we need compute $A_1(n, s)$ and $A_2(n, s)$ only for odd $n$. To evaluate $A_1(n, s)$ we integrate by parts and apply the identity

$$j_n'(x) = j_{n-1}(x) - \frac{n+1}{x} j_n(x) , \tag{86}$$

obtaining

$$A_1(n, s) = 2A_2(n, s) + A_3(n, s) , \tag{87}$$

where

$$A_3(n, s) = (k_{sn}R_0)^2 j_{n-1}(k_{sn}R_0) - (n+3)(k_{sn}R_0) j_n(k_{sn}R_0) . \tag{88}$$

To compute $A_2(n, s)$ we use the identity

$$j_n(x) = -x^{n-1}\frac{d}{dx}[x^{1-n} j_{n-1}(x)] , \tag{89}$$

and integrate by parts. Repeating the process $n$ times gives

$$\int dx\, j_{2n+1}(x) = -\sum_{m=0}^{n} \frac{2^m n!}{(n-m)!} \frac{j_{2n-m}(x)}{x^m} . \tag{90}$$

Noting that, for small $x$,

$$j_n(x) \sim \frac{x^n}{(2n+1)!!} , \tag{91}$$

where

$$(2n+1)!! = (2n+1)(2n-1)\ldots 3\times 1 , \tag{92}$$

we have

$$A_2(2n+1, s) = \frac{2^n n!}{(2n+1)!!} - \sum_{m=0}^{n} \frac{2^m n!}{(n-m)!} \frac{j_{2n-m}[k_{s(2n+1)}R_0]}{[k_{s(2n+1)}R_0]^m} . \tag{93}$$

Using equations (85) and (87), we rewrite equation (78) as follows:

$$\langle\langle \gamma_{ns} \rangle\rangle = -\frac{3(2n+1)\, AB_1(n)[A_2(n, s) + A_3(n, s)]}{2n(n+1)(k_{sn}R_0)^5 P j_n^2(k_{sn}P)} . \tag{94}$$

From equations (73), (74), and (75) we find the components of the poloidal mode $\boldsymbol{S}_{(ns)}$:

$$S_{r(2n)s} = S_{\theta(2n)s} = S_{\phi ns} = 0\,, \tag{95}$$

$$S_{r(2n+1)s} = \frac{3\,(4n+3)\;AB_1\,(2n+1)\,[\,A_2\,(2n+1,s) + A_3\,(2n+1\;s)\,]}{2\,(k_{s(2n+1)}P)\,(k_{s(2n+1)}R_0)^{\,3}\,j^2_{2n+1}(k_{s(2n+1)}P)} \times \frac{j_{2n+1}\,(k_{s(2n+1)}r)}{(k_{s(2n+1)}r)}\,P_{2n+1}\,(\cos\theta)\,, \tag{96}$$

$$S_{\theta(2n+1)s} = \frac{3\,(4n+3)\;AB_1\,(2n+1)\,[\,A_2\,(2n+1,s) + A_3\,(2n+1,s)\,]}{4\,(n+1)\,(2n+1)\,(k_{s(2n+1)}P)\,(k_{s(2n+1)}R_0)^{\,3}\,j^2_{2n+1}\,(k_{s(2n+1)}P)} \times \frac{1}{(k_{s(2n+1)}r)}\,\frac{d}{d\,(k_{s(2n+1)}r)}\,[\,(k_{s(2n+1)}r)\;j_{2n+1}\,(k_{s(2n+1)}r)\,]\,\frac{dP_{2n+1}\,(\cos\theta)}{d\theta}\,. \tag{97}$$

It may be shown that the double sum (76) is absolutely convergent, but the proof has been omitted here to save space. The dipole field is composed of the sum, over $s$, of the terms $\boldsymbol{S}_{(1s)}$; the quadrupole field vanishes identically; the octupole field is given by the sum of the terms $\boldsymbol{S}_{(3s)}$; etc. Numerical calculation gives the $r$-components as

$$\sum_{s=1}^{\infty} S_{r1s} = 0.24P_1\,(\cos\theta)\,,$$

$$\sum_{s=1}^{\infty} S_{r3s} = -\,0.038P_3\,(\cos\theta)\,,$$

for the special case $R_0 = P$.

It may be expected that the field will reduce to a poloidal dipole in the limit as $R_0$ becomes small. This is readily demonstrated by noting from equations (81) and (91) that

$$A_2\,(n,s) \cong \int_0^{k_{sn}R_0} du\;\frac{u^n}{(2n+1)\;!!} \cong \frac{(k_{sn}R_0)^{\,n+1}}{(n+1)\,(2n+1)\;!!} \tag{98}$$

for small $k_{sn}R_0$. Similarly, from equation (88),

$$A_3\,(n,s) \cong \frac{n-2}{(2n+1)\;!!}\,(k_{sn}R_0)^{\,n+1}\,. \tag{99}$$

Hence

$$A_2\,(n,s) + A_3\,(n,s) \cong \frac{(n^2-n-1)\,(k_{sn}R_0)^{\,n+1}}{(n+1)\,(2n+1)\;!!}\,. \tag{100}$$

From equation (96) we see that $S_{r(2n+1)s}$ is porportional to $(k_{s(2n+1)}R_0)^{2n-1}$. Thus, if we require that

$$\lim_{R_0\to 0}\frac{A}{k_{s1}R_0} = M\,, \tag{101}$$

then only the dipole terms survive, and equations (96) and (97) reduce to

$$S_{r1s} = \frac{3MP\,j_1\,(s\pi r/P)}{8\pi\,s^2\,j_1^2\,(s\pi)\,r}\cos\theta\,, \tag{102}$$

$$S_{\theta 1s} = -\,\frac{3MP}{16\pi\,s^2\,j_1^2\,(s\pi)}\,\frac{1}{r}\,\frac{d}{dr}\left[\,r\,j_1\left(s\pi\,\frac{r}{P}\right)\right]\sin\theta\,, \tag{103}$$

since $k_{s1}P = s\pi$.

It should be noted from equation (79) that $A$ is proportional to $Ba^4$. Thus, in taking the limit in equation (101), we keep constant the dipole moment $Ba^3$ of the loop. Then

$$\lim_{R_0 \to 0} \frac{A}{k_{s1} R_0} = \text{Constant} \times \lim_{R_0 \to 0} \frac{a}{R_0} = \text{Constant},$$

which maintains the relative size of the loop and $R_0$, as $R_0$ becomes small.

From the rapid convergence of expansion (76), as well as from numerical calculations, we conclude that the gross result of the meridional loops is a dipole field with relatively small octupole and higher-order components. This completes the problem, posed at the beginning of Section II, of the generation of the poloidal field from the toroidal field. Thus, combining the generation of the toroidal field from the dipole field with the generation of the dipole field, we have demonstrated that a conducting fluid sphere in which the fluid is moving in a certain way, viz., nonuniform rotation and cyclonic motion, will form a regenerative hydromagnetic dynamo. The external field of the dynamo is primarily a poloidal dipole. The next step of the problem would be, of course, the very difficult dynamical question as to the actual structure of cyclones in the rotating convecting fluid body forming the core of the earth or the central convective zones of some stars.

## VI. MIGRATORY DYNAMO

Now that we know the results of the coalescence of the loops formed by cyclonic fluid motions, it is possible to reformulate in a simpler way the development of the coalescence of loops. First, we note that in the local Cartesian co-ordinate system $(\xi, \eta, \zeta)$ the magnetic loop given by equations (49), (50), and (51) may be represented by the vector potential

$$A_\zeta = A_\xi = 0, \tag{104}$$

$$A_\eta = \tfrac{1}{2} B_0 a \exp\left[ -\frac{\xi^2 + \eta^2 + \zeta^2}{a^2} \right], \tag{105}$$

where $\xi = R\vartheta$, $\eta = R \sin \Theta\varphi$, and $\zeta = \rho$. Thus $\boldsymbol{A}$ is a vector in the $\eta$-direction and is nonvanishing only within distances of the order of $a$ from the center of the loop at $(R, \Theta, \Phi)$. If the cyclonic motions are given, the rate of generation of $\boldsymbol{A}$ is simply proportional to the toroidal field $\boldsymbol{e}_\eta B$. Assuming the cyclones to be small and numerous, the average effect is to generate $\boldsymbol{A}$ so that, writing $A$ for the $\eta$-component of $\boldsymbol{A}$,

$$\frac{\partial A}{\partial t} = \Gamma B, \tag{106}$$

where $\Gamma$ is a measure of the violence of the cyclones and may be a function of position. From equation (1) we see that, in order to include the dissipation, we should write equation (106) as

$$\frac{\partial A}{\partial t} = \Gamma B + \frac{1}{\mu\sigma} \nabla^2 A. \tag{107}$$

If there is present a fluid motion,

$$\boldsymbol{v} = \boldsymbol{e}_\eta v, \tag{108}$$

representing the nonuniform rotation, then from equation (1) the toroidal field $\boldsymbol{B}$ is generated from $\boldsymbol{A}$ according to

$$\frac{\partial \boldsymbol{B}}{\partial t} = \nabla \times [\boldsymbol{v} \times (\nabla \times \boldsymbol{A})] + \frac{1}{\mu\sigma} \nabla^2 \boldsymbol{B}. \tag{109}$$

Since $\boldsymbol{A}$ and $\boldsymbol{v}$ are independent of $\eta$ and have only $\eta$-components, $\partial \boldsymbol{B}/\partial t$ is in the $\eta$-direction, as required, and equation (109) reduces to

$$\frac{\partial B}{\partial t} = \left(\frac{\partial v}{\partial \zeta}\frac{\partial A}{\partial \xi} - \frac{\partial v}{\partial \xi}\frac{\partial A}{\partial \zeta}\right) + \frac{1}{\mu\sigma}\nabla^2 B . \tag{110}$$

It is interesting to solve the dynamo equations (107) and (110) subject to rectangular, rather than spherical, boundary conditions. Thus, instead of $(\xi, \eta, \zeta)$ representing local Cartesian co-ordinates in the spherical core of the earth, consider a rectangular volume of fluid with the Cartesian co-ordinates $(\xi, \eta, \zeta)$ throughout. Instead of nonuniform rotation, we introduce uniform shearing. We make $v$ vary linearly with $\zeta$, so that

$$\frac{\partial v}{\partial \zeta} = H = \text{Constant} , \qquad \frac{\partial v}{\partial \xi} = 0 . \tag{111}$$

Then equation (110) reduces to

$$\frac{\partial B}{\partial t} = H\frac{\partial A}{\partial \xi} + \frac{1}{\mu\sigma}\nabla^2 B . \tag{112}$$

If we distribute the cyclones uniformly throughout the space, then $\Gamma$ is a constant, and the dynamo equations reduce to two simultaneous linear equations with constant coefficients.

As a solution to equations (107) and (111) we let

$$A = A_0 \exp\left[i\left(\omega t + k\xi\right)\right] , \qquad B = B_0 \exp\left[i\left(\omega t + k\xi\right)\right] . \tag{113}$$

Substituting in equations (107) and (111), we obtain

$$A_0\left(i\omega + \frac{k^2}{\mu\sigma}\right) - B_0\Gamma = 0 , \tag{114}$$

$$-A_0 ikH + B_0\left(i\omega + \frac{k^2}{\mu\sigma}\right) = 0 . \tag{115}$$

Setting the determinant of the coefficients equal to zero, we find that

$$\left(i\omega + \frac{k^2}{\mu\sigma}\right)^2 - ikH\Gamma = 0 . \tag{116}$$

We are interested only in the solutions which survive to large values of $t$, viz., those for which the real part of $i\omega$ is positive. Thus we are interested only in the roots

$$i\omega = \left(\Omega - \frac{k^2}{\mu\sigma}\right) \pm i\Omega , \tag{117}$$

yielding

$$A_0 = -B_0\frac{(1 \pm i)\,\Omega}{kH} , \tag{118}$$

where

$$\Omega = \left(\frac{|kH\Gamma|}{2}\right)^{1/2} , \tag{119}$$

and the $\pm$ has the same sign as the product $kH\Gamma$.

Solutions (113) of the dynamo equations become the migratory *dynamo waves*,

$$B = B_0 \exp\left[\left(\Omega - \frac{k^2}{\mu\sigma}\right)t\right] \exp\left[i\,(k\xi \pm \Omega t)\,\right], \tag{120}$$

$$A = -B_0 \frac{\Omega}{kH}(1 \mp i) \exp\left[\left(\Omega - \frac{k^2}{\mu\sigma}\right)t\right] \exp\left[i\,(k\xi \pm \Omega t)\,\right]. \tag{121}$$

If $kH\Gamma > 0$, we have a dynamo wave traveling in the negative $\xi$-direction; if $kH\Gamma < 0$, the wave travels in the positive $\xi$-direction. The vector potential is $\pi/4$ out of phase with $B$. Assuming that $\Omega > k^2/\mu\sigma$, the amplitude increases exponentially with time. If the conductivity is large enough that $\Omega \gg k^2/\mu\sigma$, the amplitude increases by a factor of exp $2\pi$, or about a factor of 500, for every $2\pi/k$ (one wave length) the wave propagates. The velocity of propagation $\Omega/k$ varies as $k^{-1/2}$ and hence increases as the square root of the wave length.

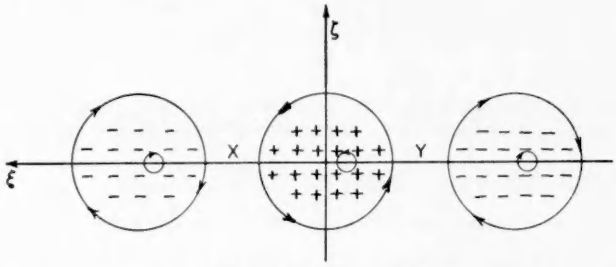


FIG. 5.—Schematic drawing of a section along a train of migratory dynamo waves. The + signs represent flux coming out of the paper, and − signs into the paper.

To understand physically the operation of the dynamo wave, consider Figure 5, which represents a section through the dynamo along the $\zeta\xi$-plane, as seen from a point on the positive $\eta$-axis. The + signs represent regions where $B > 0$, so that $\boldsymbol{B}$ is directed out of the paper; the − signs, into the paper. If $\Gamma > 0$, the loops of flux produced by the individual cyclones have the direction shown by the small circles. The individual loops coalesce to form the large loops of flux.

If $\partial v/\partial\zeta$ and hence $H$ is positive, then the fluid in the upper part of the figure is moving out of the paper relative to the fluid in the lower part. The loops are being sheared so that, for instance, in region $X$ a field in the negative $\eta$-direction is being generated. In region $Y$ a field in the positive $\eta$-direction is being generated. It is readily seen that this regenerates the right-hand side of each of the bands of flux of $B$ and degenerates the left side. The result is a migration to the right, the negative $\xi$-direction.

The migratory dynamo may be of interest in stellar magnetic activity. The magnetic fields of the sun show little or none of the steady dipole component observed for the earth. The sunspots (Kuiper 1953) and some of the prominence activity (Menzel and Bell 1953), which may be basically hydromagnetic in character, definitely exhibit migration from high toward low latitudes. The corona undergoes over-all changes in step with the magnetic activity, suggesting that sunspots and prominences are not just individual isolated magnetic phenomena but are secondary effects of a general solar magnetic cycle.

If we inquire into the geometry of the solar convective zone, where a dynamo should be located if it exists, we find this zone to be a shell sufficiently thin ($\approx 10^5$ km) that we may neglect its curvature. The dynamo equations in such a flattened space give just a migratory dynamo, as we have shown.

Finally, we note that if cyclones exist in the solar convective zone, we would expect their rotation to be strongest near the poles and to vanish at the equator. The shearing due to nonuniform rotation, on the other hand, should vanish at the poles and be strongest near the equator. Hence the toroidal field $B$, produced by the shearing $H$, will be strongest in low latitudes, and the poloidal loops (derived from $A$), produced by the cyclonic motions $\Gamma$, will predominate near the poles. If, as has been suggested elsewhere (Parker 1955), sunspots result from the magnetic buoyancy of the solar toroidal field, then we would expect sunspots where the toroidal field is strongest. We may thus obtain an explanation for the fact that sunspots appear only in low latitudes, as well as for the migration toward the equator of the region of formation of sunspots, and for the reversal of spot polarity between cycles. Fluid velocities of the order of 1 m/sec are sufficient to produce dynamo waves migrating from the pole to the equator of the sun in 22 years.

Altogether, it would seem that a migratory dynamo of some sort is strongly suggested for the sun. It is interesting to note that a high rate of rotation, together with cyclonic velocities of 1 km/sec, might produce a migratory dynamo giving the vigorous magnetic activity observed by Babcock in some magnetic stars.

I should like to express my gratitude to Dr. W. M. Elsasser for the many suggestions and helpful criticism which have contributed to the development of this paper. I should also like to thank Sir Edward Bullard for a stimulating discussion of the geomagnetic problem and Dr. S. Chandrasekhar for several valuable suggestions in the presentation of the dynamo models.

## APPENDIX

Consider the interaction with the toroidal magnetic field of a localized cyclonic fluid motion. We include the return flow of the cyclone, so that the velocity can be made to vanish identically outside the cyclonic region. As was stated earlier, the influx and efflux of fluid at the ends of the cyclonic column, together with the return flow, complicate the calculation of the trajectories of the fluid elements to such an extent that a rigorous calculation of the resulting magnetic field is difficult. Therefore, having computed rigorously in the text the field generated by an idealized cyclone, without influx and efflux or return flow, we now compute by perturbation methods an approximate expression for the field generated by a cyclone with a return flow.

We shall investigate, then, a localized cyclonic fluid motion in a large-scale magnetic field. We take the axis of the cyclone perpendicular to the magnetic field. Using the local Cartesian system $(\xi, \eta, \zeta)$, we assume that the large-scale field is of the form

$$\boldsymbol{B} = \boldsymbol{e}_\eta B(\zeta) . \tag{122}$$

Let the velocity field of the fluid be $\boldsymbol{v} = \boldsymbol{u} + \boldsymbol{w}$; then $\boldsymbol{u}$ represents the convection along the $\zeta$-axis, together with the associated influx and efflux and the necessary return flow, and $\boldsymbol{w}$ represents the rotation of the fluid about the $\zeta$-axis.

Without much loss of generality, we may take $u_\xi = 0$ and set

$$u_\eta = -u_0(t)\, X(\xi)\, Y(\eta) Z'(\zeta) , \qquad u_\zeta = u_0(t)\, X(\xi)\, Y'(\eta) Z(\zeta) , \tag{123}$$

where the primes denote derivatives. We represent $\boldsymbol{w}$ by $w_\zeta = 0$ and

$$w_\xi = -\Omega(t)\, \eta R(\rho) S(\zeta) , \qquad w_\eta = \Omega(t)\, \xi R(\rho) S(\zeta) , \tag{124}$$

where $u_0(t)$ and $\Omega(t)$ are representative of the corresponding magnitudes, provided that all the other functions are suitably normalized. Formulae (123) and (124) guarantee that $\nabla \cdot \boldsymbol{u}$ and $\nabla \cdot \boldsymbol{w}$ vanish.

From equation (1) we have for the first-order perturbation of the magnetic field

$$\mathfrak{B}(t) = \int_0^t dt \nabla \times [(\boldsymbol{u} + \boldsymbol{w}) \times \boldsymbol{B}] . \tag{125}$$

The second-order perturbation field is

$$\boldsymbol{\gamma}(t) = \int_0^t dt \nabla \times [(\boldsymbol{u}+\boldsymbol{w}) \times \boldsymbol{\beta}(t)]. \tag{126}$$

This field consists of the sum of four terms which arise, depending on whether the first step of the interaction is taken to involve either $\boldsymbol{u}$ or $\boldsymbol{w}$ and whether the second step involves either $\boldsymbol{u}$ or $\boldsymbol{w}$. Two of these terms are quadratic, in $\boldsymbol{u}$ alone and in $\boldsymbol{w}$ alone; it is physically obvious that they will not contribute to loops in the meridional or $\zeta\xi$-planes. This may be demonstrated quantitatively by noting that the $\xi$-component of the term of second order in $u_0(t)$ and the $\zeta$-component of the term of second order in $\Omega(t)$ are zero. Thus the terms cannot contribute individually. If we combine the nonzero $\zeta$-component of the former and the nonzero $\xi$-component of the latter, we obtain a field which can be shown to have no net circulation about the $\eta$-axis. We therefore omit these quadratic terms and keep only the two mixed terms which involve $\boldsymbol{u}$ in one step of the interaction and $\boldsymbol{w}$ in the other. After somewhat lengthy but straightforward calculations, this part of the second-order field, say $\boldsymbol{\delta}(t)$, is found to have the following components in the meridional planes:

$$\begin{aligned}\delta_\xi(t) = f(t) X(\xi) \Big\{ &-\left[\frac{\partial}{\partial\eta} Y(\eta) \frac{\partial}{\partial\eta} \eta R(\rho)\right] Z'(\zeta) S(\zeta) B(\zeta) \\ &+\left(\left[\frac{\partial}{\partial\eta}\eta R(\rho)\right] Y'(\eta) - R(\rho)\,\eta\, Y''(\eta)\right)\left[\frac{\partial}{\partial\zeta} Z(\zeta) S(\zeta) B(\zeta)\right] \\ &+\left[\frac{\partial}{\partial\eta} Y'(\eta)\,\eta R(\rho)\right] S(\zeta)\left[\frac{\partial}{\partial\zeta} Z(\zeta) B(\zeta)\right]\Big\};\end{aligned} \tag{127}$$

$$\begin{aligned}\delta_\zeta(t) = f(t) \Big\{ &-\left[\frac{\partial}{\partial\xi} X(\xi) \frac{\partial}{\partial\eta}\eta R(\rho)\right] Y'(\eta) + X(\xi) \\ &\times\left[\frac{\partial}{\partial\eta}\eta Y'(\eta)\frac{\partial}{\partial\xi} R(\rho)\right] + \left[\frac{\partial}{\partial\xi} X(\xi) R(\rho)\right]\eta Y''(\eta) - \xi X(\xi) \\ &\times\left[\frac{\partial}{\partial\eta} R(\rho)\, Y''(\eta)\right]\Big\} Z(\zeta) S(\zeta) B(\zeta),\end{aligned} \tag{128}$$

where

$$f(t) = \int_0^t dt' u_0(t') \int_0^{t'} dt'' \Omega(t'') = \int_0^t dt' \Omega(t') \int_0^{t'} dt'' u_0(t''). \tag{129}$$

The field lines of $\boldsymbol{u}$, $\boldsymbol{w}$, and $\boldsymbol{\delta}$ are given by

$$\frac{d\eta}{u_\eta} = \frac{d\zeta}{u_\zeta}, \qquad \frac{d\xi}{w_\xi} = \frac{d\eta}{w_\eta}, \qquad \frac{d\xi}{\delta_\xi} = \frac{d\eta}{\delta_\eta} = \frac{d\zeta}{\delta_\zeta}. \tag{130}$$

For $\boldsymbol{u}$ we obtain the family of curves

$$Y(\eta) Z(\zeta) = C_1; \tag{131}$$

for $\boldsymbol{w}$,

$$\xi^2 + \eta^2 = C_2, \tag{132}$$

where $C_1$ and $C_2$ are the parameters of each family. The differential equation for the field lines of $\boldsymbol{\delta}$ is not readily integrated except in special cases. We therefore consider the case of a Gaussian distribution:

$$X(\xi) = \exp\left(-\frac{\xi^2}{a^2}\right), \qquad Y(\eta) = \eta \exp\left(-\frac{\eta^2}{a^2}\right), \qquad Z(\zeta) = \exp\left(-\frac{\zeta^2}{a^2}\right); \tag{133}$$

$$R(\rho) = \exp\left(-\frac{\rho^2}{a^2}\right), \quad S(\zeta) = \exp\left(-\frac{\zeta^2}{a^2}\right), \quad B(\zeta) = B_0 \exp\left[-\frac{(\zeta-b)^2}{c^2}\right]. \tag{134}$$

Then equation (131) becomes

$$\eta \exp\left[-\frac{1}{a^2}(\eta^2+\zeta^2)\right]=C_1 \qquad \text{or} \qquad \eta^2+\zeta^2=a^2\ln\frac{\eta}{C_1}, \tag{135}$$

and equations (127) and (128) become

$$\delta_\xi(t)=f(t)B_0 2\left[-\zeta\pi(\eta)+\nu(\eta)\right]\exp\left[-\frac{2}{a^2}(\xi^2+\eta^2+\zeta^2)-\frac{(\zeta-b)^2}{c^2}\right], \tag{136}$$

$$\delta_\zeta(t)=f(t)B_0 2\,\xi\omega(\eta)\exp\left[-\frac{2}{a^2}(\xi^2+\eta^2+\zeta^2)-\frac{(\zeta-b)^2}{c^2}\right], \tag{137}$$

where

$$\pi(\eta)=\frac{2}{a^2}\left(1+2\frac{\eta^2}{a^2}\right)+\frac{2}{c^2}\left(1-2\frac{\eta^2}{a^2}\right)^2, \qquad \nu(\eta)=\frac{2b}{c^2}\left(1-2\frac{\eta^2}{a^2}\right)^2,$$
$$\omega(\eta)=\frac{4}{a^2}\left(1-\frac{\eta^2}{a^2}\right). \tag{138}$$

The neutral line where $\delta_\xi(t)$ and $\delta_\zeta(t)$ vanish simultaneously will be denoted by $\xi_0(\eta)$ and $\zeta_0(\eta)$. We see from equation (136) that

$$\xi_0(\eta)=0, \qquad \zeta_0(\eta)=\frac{\nu(\eta)}{\pi(\eta)}. \tag{139}$$

Substituting equations (136) and (137) in equation (130), we obtain for the field lines of $\tilde{\boldsymbol{\delta}}(t)$ the family of curves

$$[\zeta-\zeta_0(\eta)]^2+\frac{\omega(\eta)}{\pi(\eta)}\xi^2=C_3. \tag{140}$$

These are ellipses for $\eta^2<a^2$ with centers on the neutral line. For $\eta^2>a^2$ the lines form hyperbolas.

The problem of defining the "strength" of the magnetic loop generated offers some difficulty. The $\eta$-component of curl $\tilde{\boldsymbol{\delta}}$ vanishes on integration over the volume, but this does not mean that there is no net circulation of magnetic flux about the neutral line. Perhaps the simplest way to demonstrate that such a circulation has been generated is the following: We compute the flux across the $\eta\zeta$-plane above $\zeta_0(\eta)$ and show that at least some of it bends around so as to penetrate the surface $\zeta=\zeta_0(\eta)$, $\xi>0$. The fluxes are

$$\Phi_\xi=+\int_{-\infty}^{+\infty}d\eta\int_{\zeta_0(\eta)}^{+\infty}d\zeta\,\delta_\xi\big|^{\xi=0}, \qquad \Phi_\zeta=-\int_{-\infty}^{+\infty}d\eta\int_0^{\infty}d\xi\,\delta_\zeta\big|^{\zeta=\zeta_0(\eta)}. \tag{141}$$

Using equations (136) and (137), we find

$$\Phi_\xi=-2f(t)B_0\int_{-\infty}^{+\infty}d\eta\int_{\zeta_0(\eta)}^{\infty}d\zeta\left[\zeta\pi(\eta)-\nu(\eta)\right]\exp\left[-\frac{2}{a^2}(\eta^2+\zeta^2)-\frac{1}{c^2}(\zeta-b)^2\right], \tag{142}$$

$$\Phi_\zeta=-2f(t)B_0\int_{-\infty}^{+\infty}d\eta\,\omega(\eta)\exp\left\{-\frac{2}{a^2}[\eta^2+\zeta_0^2(\eta)]-\frac{1}{c^2}[\zeta_0(\eta)-b]^2\right\}\times\int_0^{\infty}d\xi\,\xi\exp\left(-\frac{2}{a^2}\xi^2\right). \tag{143}$$

In the integrand of the expression for $\Phi_\xi$, we have $\zeta\geq\zeta_0(\eta)$. From equations (139) it follows that the integrand is always positive. In the expression for $\Phi_\zeta$ the sign of the integrand is the same as

the sign of $\omega(\eta)$. From equation (138) we see that $\omega(\eta)$ is positive if $\eta^2 < a^2$, otherwise negative. But for $\eta^2 > a^2$ the Gaussian factor is very small, so small in fact that the integration over $\eta^2 > a^2$ constitutes only a small percentage of the total value. Thus the integrals are positive, and $\Phi_\xi$ and $\Phi_\zeta$ have the same sign; hence there is a net circulation of flux about the neutral line independent of the relative magnitudes of parameters $a$, $b$, and $c$.

Since the existence of a net circulation is independent of $a$, $b$, and $c$, we shall limit the evaluation of the fluxes to the special case $b = 0$, $c = \infty$. Then $\zeta_0(\eta) = 0$, and

$$\Phi_\xi = \Phi_\zeta = -\frac{3\sqrt{\pi}}{2\sqrt{2}} f(l) B_0 a . \tag{144}$$

## REFERENCES


Brand, L. 1947, *Vector and Tensor Analysis* (New York: John Wiley & Sons).
Bullard, E., and Gellman, H. 1954, *Phil. Trans. R. Soc. London*, **247**, 213.
Cowling, T. G. 1933, *M.N.*, **94**, 39.
Elsasser, W. M. 1946–1947, *Phys. Rev.*, **69**, 106; **70**, 202; **72**, 821.
———. 1950, *Rev. Mod. Phys.*, **22**, 1.
Jahnke, E., and Emde, F. 1945, *Tables of Functions with Formulae and Curves* (New York: Dover Publications).
Kuiper, G. P. 1953, *The Sun* (Chicago: University of Chicago Press).
Lundquist, S. 1952, *Ark. f. Fysik*, **5**, 297.
MacRobert, T. M. 1947, *Spherical Harmonics* (2d ed.; New York: Dover Publications), pp. 105, 106.
Menzel, D. H., and Bell, B. 1953, *Trans. 11th Volta Cong., 1952* (Rome: Acad. Lincei).
Parker, E. N. 1955, *Ap. J.*, **121**, 491.
Stratton, J. A. 1941, *Electromagnetic Theory* (1st ed.; New York: McGraw-Hill Book Co.).
Watson, G. N. 1944, *Theory of Bessel Functions* (2d ed.; Cambridge: At the University Press), p. 521.

# HYDROMAGNETIC DISTURBANCES IN A FLUID OF FINITE CONDUCTIVITY

P. H. ROBERTS
Yerkes Observatory
*Received April 16, 1955*

ABSTRACT

A study is made of the equation governing the propagation of Alfvén waves in an unbounded fluid of finite electrical conductivity. Periodic and aperiodic solutions are derived, the latter of which are obtained by operational methods.

## I. INTRODUCTION

In the study of hydromagnetics it is generally supposed that the disturbances take place in a fluid of infinite electrical conductivity. Under these circumstances they suffer no energy losses and are consequently unattenuated. Alfvén (1950) has shown that, in a fluid of finite conductivity, disturbances are damped exponentially. He has derived an approximate expression for the decay of purely periodic solutions which is valid if the attenutation is small. Walén (1944) has considered the propagation of aperiodic disturbances in a fluid of finite conductivity. He made a Fourier analysis of an arbitrarily specified initial state of motion and found the subsequent behavior of each component separately. He then recombined the components but could evaluate the resulting integrals only by assuming that the electrical conductivity was large. It will be shown in Section IV that he effectively replaced the basic hydromagnetic equation by an equation asymptotic to it in the limit of infinite conductivity.

In this paper the nature of the periodic waves will be discussed in detail. It will also be shown that the behavior of aperiodic disturbances may be found without approximation by the use of Heaviside's operational calculus.

## II. BASIC EQUATIONS

On the usual hydromagnetic approximations, it is easily verified that the velocity $\boldsymbol{u}$ of an incompressible inviscid fluid of density $\rho$ and conductivity $\sigma$ is related to the prevailing magnetic field $\boldsymbol{H}$ by the equations

$$\frac{\partial \boldsymbol{u}}{\partial t} + \boldsymbol{u} \cdot \operatorname{grad} \boldsymbol{u} = -\operatorname{grad} \frac{p}{\rho} + \frac{1}{\rho}\, j \times \boldsymbol{H}, \tag{1}$$

$$\frac{\partial \boldsymbol{H}}{\partial t} - \frac{1}{4\pi\sigma} \nabla^2 \boldsymbol{H} = \operatorname{curl}\ (\boldsymbol{u} \times \boldsymbol{H}), \tag{2}$$

where $p$ is the hydrostatic pressure in the fluid. The electrical quantities have been measured in electromagnetic units.

Suppose that the fluid is initially at rest in a uniform magnetic field $\boldsymbol{H}_0$. Suppose that this equilibrium configuration is perturbed by a small field $\boldsymbol{h}$, where

$$|\boldsymbol{h}| \ll |\boldsymbol{H}_0|. \tag{3}$$

On making the substitution

$$\boldsymbol{H} = \boldsymbol{H}_0 + \boldsymbol{h} \tag{4}$$

and neglecting squares and products of $\boldsymbol{h}$ and $\boldsymbol{u}$, we find that equations (1) and (2) assume the forms

$$\left[\frac{\partial}{\partial t}-\frac{1}{4\pi\sigma}\nabla^2\right]\boldsymbol{h}=H_0\frac{\partial \boldsymbol{u}}{\partial z}, \tag{5}$$

$$\frac{\partial \boldsymbol{u}}{\partial t}=\frac{H_0}{4\pi\rho}\frac{\partial \boldsymbol{h}}{\partial z}-\frac{1}{\rho}\operatorname{grad}\left[p+\frac{1}{8\pi}(\boldsymbol{H}_0+\boldsymbol{h})^2\right], \tag{6}$$

where $z$ is a co-ordinate measured in the direction of $\boldsymbol{H}_0$. On taking the divergence of equation (6) and remembering that $\boldsymbol{h}$ and $\boldsymbol{u}$ are solenoidal vectors, it is found that

$$\nabla^2\left[p+\frac{1}{8\pi}(\boldsymbol{H}_0+\boldsymbol{h})^2\right]=0. \tag{7}$$

If the fluid fills an unbounded region, this equation implies that

$$p+\frac{1}{8\pi}(\boldsymbol{H}_0+\boldsymbol{h})^2=p_0, \tag{8}$$

where $p_0$ is a constant. Under such circumstances, equation (6) assumes the simplified form

$$\frac{\partial \boldsymbol{u}}{\partial t}=\frac{H_0}{4\pi\rho}\frac{\partial \boldsymbol{h}}{\partial z}. \tag{9}$$

Equations (5) and (9) now show that $\boldsymbol{h}$, $\boldsymbol{u}$, curl $\boldsymbol{h}$, and curl $\boldsymbol{u}$ all satisfy the fundamental equation

$$\frac{\partial}{\partial t}\left[\frac{\partial \boldsymbol{a}}{\partial t}-\frac{1}{4\pi\sigma}\nabla^2\boldsymbol{a}\right]=V^2\frac{\partial^2\boldsymbol{a}}{\partial z^2}, \tag{10}$$

where

$$V^2=\frac{H_0^2}{4\pi\rho}. \tag{11}$$

Displayed in this form, the equation clearly shows the combination of wavelike and diffusion-like properties characteristic of hydromagnetics in a fluid of finite conductivity. In the limit of infinite $\rho$ the fluid solidifies, and the right-hand side of equation (10) becomes zero. It is then seen that $\boldsymbol{a}$ satisfies the law of electromagnetic induction in a solid conductor; namely,

$$\frac{\partial \boldsymbol{a}}{\partial t}=\frac{1}{4\pi\sigma}\nabla^2\boldsymbol{a}. \tag{12}$$

Under these circumstances a disturbance in a region characterized by a length $L$ will decay exponentially with a half-life of $4\pi\sigma L^2$. In the limit of infinite $\sigma$, equation (10) reduces to the form

$$\frac{\partial^2\boldsymbol{a}}{\partial t^2}=V^2\frac{\partial^2\boldsymbol{a}}{\partial z^2}. \tag{13}$$

This is the equation of pure wave motion familiar in the hydromagnetics of infinitely conducting fluids. Under these circumstances a disturbance crosses a region of diameter $L$ in a time of $L/V$. It is therefore clear that the condition that the wavelike properties of equation (10) shall predominate over the dissipative terms is simply

$$4\pi\sigma L^2\gg\frac{L}{V}. \tag{14}$$

Substitution of typical numerical values in this criterion shows that the difficulty of directly demonstrating hydromagnetic phenomena in the laboratory is that of producing a large enough exciting field $\boldsymbol{H}_0$ over a sufficiently large volume of fluid. However, it is worth mentioning that convincing hydromagnetic effects have recently been predicted by Chandrasekhar and Elbert (1955) for the behavior of a layer of fluid lying in a magnetic field and heated from below. Experiments by Nakagawa (1955) have verified these predictions in a striking manner.

In the remainder of this paper it will be supposed that $\boldsymbol{h}$ and $\boldsymbol{u}$ depend on $z$ and $t$ only. Under these circumstances equation (8) is valid even if the fluid is of finite extent. Thus, quite generally, the fundamental equation governing the phenomena is

$$\frac{\partial}{\partial t}\left[\frac{\partial \boldsymbol{a}}{\partial t} - \frac{1}{4\pi\sigma}\frac{\partial^2 \boldsymbol{a}}{\partial z^2}\right] = V^2 \frac{\partial^2 \boldsymbol{a}}{\partial z^2}. \tag{15}$$

In the next section simple periodic solutions of this equation will be discussed.

## III. PERIODIC SOLUTIONS

Suppose that $\boldsymbol{a}$ has a time dependence of $e^{-i\omega t}$. Define $\omega_0$, $\chi$, $a$, $\beta$, and $k$ by the following equations:

$$\omega_0 = \frac{\sigma H_0^2}{\rho}, \tag{16}$$

$$\chi = \tan^{-1}\frac{\omega}{\omega_0}, \tag{17}$$

$$a = \frac{\omega}{V}\cos\tfrac{1}{2}\chi\sqrt{\cos\chi}, \tag{18}$$

$$\beta = \frac{\omega}{V}\sin\tfrac{1}{2}\chi\sqrt{\cos\chi}, \tag{19}$$

and

$$k = a + i\beta. \tag{20}$$

As a consequence of these definitions, $k^2$ may be expressed in the form

$$k^2 = \frac{4\pi\sigma i\omega}{1 + i\omega_0/\omega}, \tag{21}$$

and equation (15) becomes

$$\frac{\partial^2 \boldsymbol{a}}{\partial z^2} + k^2 \boldsymbol{a} = 0. \tag{22}$$

Suppose that on the plane $z = 0$ the disturbance is specified in the form

$$\boldsymbol{a} = \boldsymbol{a}_0 e^{-i\omega t}, \tag{23}$$

where $\boldsymbol{a}_0$ is a constant vector. Equation (22) now shows that the behavior of $\boldsymbol{a}$ at arbitrary $z$ and $t$ is given by

$$\boldsymbol{a} = \boldsymbol{a}_0 \exp\{-\beta|z| + i(a|z| - \omega t)\}. \tag{24}$$

The phase velocity $c$ of the wave is therefore given by

$$c = \frac{\omega}{a} = \frac{V}{\cos\tfrac{1}{2}\chi\sqrt{\cos\chi}}. \tag{25}$$

It is interesting to notice that $c$ always exceeds $V$. This is also true of the group velocity $G$, which is easily shown to be

$$G = \frac{d\omega}{da} = \frac{V}{\cos \tfrac{1}{2}\chi \,(1 - \sin \tfrac{1}{2}\chi \, \sin \tfrac{3}{2}\chi) \, \sqrt{} \cos \chi} . \tag{26}$$

The skin depth $d$ of the wave (i.e., that distance in which the amplitude of the disturbance is reduced by a factor of $e$) is shown from equation (24) to be

$$d = \frac{d_0}{\sin \tfrac{1}{2}\chi \, \sqrt{(2 \sin \chi)}} , \tag{27}$$

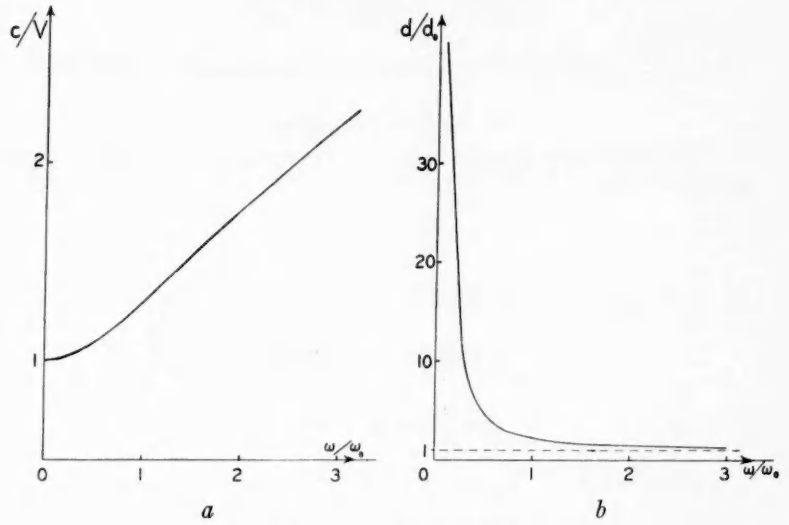


FIG. 1.—The figures show (*a*) the phase velocity and (*b*) the skin depth of a periodic disturbance plotted as functions of the frequency of the waves.

where $d_0$ is the skin depth of a *solid* conductor of conductivity $\sigma$ and is given by

$$d_0 = \frac{1}{\sqrt{(2\pi\sigma\omega)}} . \tag{28}$$

It is interesting to note that $d$ always exceeds $d_0$ and that in most cosmical applications it does so by an extremely large factor. This is shown in Figure 1, *b*.

This important fact refutes the often stated belief that magnetic disturbances taking place inside large masses of fluid are shielded from observers outside by the "skin-effect." This would be true if the prevailing field in the fluid were entirely toroidal, with no component toward the surface. However, in the case of the sun or of the earth's core, the poloidal components of $\boldsymbol{H}_0$ are sufficiently strong to insure that, for all frequencies of interest, the skin depth as defined by equation (27) greatly exceeds the diameter of the fluid mass.

Another interesting consequence of equations (25) and (26) has been called the "streak effect" by Walén, who notices that the higher-frequency components travel

faster but decay more rapidly. He points out that a disturbance initiated at a certain time will at first carry a "streak" of higher frequencies, which soon decays. The main body of the wave will become increasingly composed of low frequencies, and, since these are less dissipated, the wave motion will become increasingly pure in form.

The complex quantity $k$, defined by equation (20), has many of the properties of its counterpart in optics. For example, when a wave encounters a change in material, Fresnel's laws govern the reflection and refraction, so that

$$\frac{\text{Amplitude transmitted}}{\text{Amplitude incident}} = \frac{2k_1}{k_1 + k_2}, \tag{29}$$

$$\frac{\text{Amplitude reflected}}{\text{Amplitude incident}} = \frac{k_1 - k_2}{k_1 + k_2}. \tag{30}$$

For a perfect conductor, $k = \omega/V$, while for a solid, $k = (1 + i)d_0$.

Another way of generating a periodic solution to equation (15) is by supposing that $\boldsymbol{a}$ has a spatial dependence of $e^{-iKz}$. In this case it is found that $\boldsymbol{a}$ satisfies the equation

$$\frac{\partial^2 \boldsymbol{a}}{\partial t^2} + \frac{K^2}{4\pi\sigma}\frac{\partial \boldsymbol{a}}{\partial t} + V^2K^2\boldsymbol{a} = 0. \tag{31}$$

If $K < 2\omega_0/V$, the solutions to this equation are damped oscillations with a decay time of $8\pi\sigma K^{-2}$. If, however, $K > 2\omega_0/V$, the solutions represent exponential decay only. If $L$ is a typical length associated with the size of the fluid container, it is clear that $K > 2\pi/L$. Thus wavelike characteristics can predominate only if

$$\frac{2\omega_0}{V} \gg \frac{2\pi}{L}. \tag{32}$$

This, apart from a numerical factor of $\pi$, is just criterion (14).

## IV. APERIODIC DISTURBANCES

Walén (1944) has used the method of Fourier transforms in discussing the problem of the propagation of aperiodic disturbances. He represents $\boldsymbol{a}$ by the integral relation

$$\boldsymbol{a}(z, t) = \frac{1}{\sqrt{2\pi}} \int_{-\infty}^{\infty} \boldsymbol{A}(k, t)\, e^{-iKz} dK. \tag{33}$$

The vector $\boldsymbol{A}$ satisfies equation (31) and must therefore have the form

$$\boldsymbol{A}(K, t) = \boldsymbol{A}(K, 0)\, e^{-K^2t/8\pi\sigma} \cos\left\{ VKt \sqrt{\left[1 - \left(\frac{K}{8\pi\sigma V}\right)^2\right]} \right\}. \tag{34}$$

This shows that equation (33) may be written in the form

$$\boldsymbol{a}(z, t) = \frac{1}{\sqrt{(2\pi)}} \int_{-\infty}^{\infty} \boldsymbol{A}(K, 0) \exp\left\{ -\frac{K^2t}{8\pi\sigma} - iKz \right\} \times \cos\left\{ VKt \sqrt{\left[1 - \left(\frac{K}{8\pi\sigma V}\right)^2\right]} \right\} dK. \tag{35}$$

Walén now assumes that the initial state of the system is so deficient in harmonics of large $K$ that, to a high degree of approximation, equation (35) may be replaced by

$$\boldsymbol{a}(z, t) = \frac{1}{\sqrt{(2\pi)}} \int_{-\infty}^{\infty} \boldsymbol{A}(K, 0) \exp\left\{ -\frac{K^2t}{8\pi\sigma} - iKz \right\} \cos(VKt)\, dK. \tag{36}$$

Using the results that

$$\frac{1}{\sqrt{(2\pi)}}\int_{-\infty}^{\infty}\exp\left\{-\frac{K^2 t}{8\pi\sigma}-iKz\right\}\cos(VKt)\,dK$$
$$=\sqrt{\left(\frac{\sigma}{\pi t}\right)}\left\{\exp\left[-\frac{2\pi\sigma(z-Vt)^2}{t}\right]+\exp\left[-\frac{2\pi\sigma(z+Vt)^2}{t}\right]\right\} \tag{37}$$

and

$$\frac{1}{\sqrt{(2\pi)}}\int_{-\infty}^{\infty}\boldsymbol{A}(K,0)\,e^{-iKz}dK=\boldsymbol{a}(z,0)=\boldsymbol{a}_0(z)\qquad\text{(say)}, \tag{38}$$

the Faltung theorem of Fourier transform theory shows that equation (36) may be rewritten in the form

$$\boldsymbol{a}(z,t)=\frac{1}{\pi}\sqrt{\left(\frac{\sigma}{2t}\right)}\int_{-\infty}^{\infty}\boldsymbol{a}_0(\lambda)\left\{\exp\left[-\frac{2\pi\sigma(z-\lambda-Vt)^2}{t}\right]\right.$$
$$\left.+\exp\left[-\frac{2\pi\sigma(z-\lambda+Vt)^2}{t}\right]\right\}d\lambda \tag{39}$$

or, by a change of variable, in the alternative form,

$$\boldsymbol{a}(z,t)=\frac{1}{2\sqrt{\pi}}\int_{-\infty}^{\infty}\left[\boldsymbol{a}_0\left\{z-Vt+\xi\sqrt{\left(\frac{t}{2\pi\sigma}\right)}\right\}\right.$$
$$\left.+\boldsymbol{a}_0\left\{z+Vt+\xi\sqrt{\left(\frac{t}{2\pi\sigma}\right)}\right\}\right]e^{-\xi^2}d\xi\,. \tag{40}$$

This expression for $\boldsymbol{a}$ gives a simple picture of the behavior of the disturbance. It shows that, to the first approximation, an initial state splits up into two parts which travel with velocity $V$ in the positive and negative $z$-directions. An observer moving with either wave finds that the disturbance, relative to his moving frame, obeys the familiar laws of electromagnetic diffusion given by equation (12). The approximation made by Walén amounted to replacing the fundamental equation (15) by an equation which is asymptotic to it in the limit of infinite $\sigma$. This equation is

$$\left[\frac{\partial}{\partial t}-\frac{1}{8\pi\sigma}\frac{\partial^2}{\partial z^2}\right]^2\boldsymbol{a}=V^2\frac{\partial^2\boldsymbol{a}}{\partial z^2}. \tag{41}$$

It will be readily verified that expression (39) satisfies this equation.

Equation (15) may be solved directly by operational methods. It is convenient to introduce new variables $z'$ and $t'$ which replace $z$ and $t$ and are related to them by

$$z'=\frac{\omega_0 z}{V}\qquad\text{and}\qquad t'=\omega_0 t\,. \tag{42}$$

Henceforward the primes will be omitted. Define a new dependent variable $\boldsymbol{b}$ related to $\boldsymbol{a}$ by

$$\boldsymbol{a}=e^{-t}\boldsymbol{b}\,. \tag{43}$$

Equation (15) shows that $\boldsymbol{b}$ satisfies the equation

$$\left(\frac{\partial}{\partial t}-1\right)^2\boldsymbol{b}=\frac{\partial^3\boldsymbol{b}}{\partial t\,\partial z^2}. \tag{44}$$

The problem has now been brought into a form that is suitable for the application of operational calculus.

Suppose that at time $t = 0$ the state of the system is specified by

$$\boldsymbol{a} = \boldsymbol{a}_0(z), \qquad \frac{\partial \boldsymbol{a}}{\partial t} = \boldsymbol{a}_1(z). \tag{45}$$

Multiply each side of equation (44) by $pe^{-pt}$ and integrate from $t = 0$ to $t = \infty$. Denote by $\bar{\boldsymbol{b}}$ the Heaviside transform of $\boldsymbol{b}$, which may be defined by

$$\bar{\boldsymbol{b}}(z, p) \equiv p\int_0^\infty \boldsymbol{b}(z, t)\, e^{-pt}dt. \tag{46}$$

The operational equivalent of equation (44) is then found to be

$$\frac{\partial^2 \bar{\boldsymbol{b}}}{\partial z^2} - \mu^2 \bar{\boldsymbol{b}} = \boldsymbol{g}(z), \tag{47}$$

where

$$\mu = \sqrt{p} - \frac{1}{\sqrt{p}} \tag{48}$$

and

$$\boldsymbol{g}(z) = \boldsymbol{a}_0'^{p}(z) - \boldsymbol{a}_1(z) - (p-1)\,\boldsymbol{a}_0(z). \tag{49}$$

The most general solution to equation (15) may conveniently be considered as the superposition of two parts: (*a*) the effect of a sudden disturbing source upon an initially undisturbed system (this may be derived from the "complementary function" of eq. [47] and will be discussed in the next two sections) and (*b*) the effect of the natural decay of an arbitrarily specified initial configuration (this may be derived from the "particular integral" of eq. [47] and will be discussed in Sec. VII).

## V. THE EFFECT OF A DISTURBING SOURCE

In this section it will be supposed that, before the instant $t = 0$, the system was in an undisturbed state in which $\boldsymbol{a}$ and therefore $\boldsymbol{g}$ were zero. At the instant $t = 0$, a disturbance is initiated on the plane $z = 0$ which at later times is defined by

$$\boldsymbol{a}(0, t) = \boldsymbol{f}(t). \tag{50}$$

The relevant solution to equation (47) is

$$\bar{\boldsymbol{b}} = \bar{\boldsymbol{c}}\, e^{-\mu|z|}, \tag{51}$$

where $\boldsymbol{c}(p)$ is the transform of $\boldsymbol{c}(t) = e^t\boldsymbol{f}(t)$. In order to simplify the appearance of the algebra, the modulus signs about $z$ will henceforth be omitted.

The simplest way of inverting equation (51) is to employ a technique which is well known in the operational calculus and which is discussed, for example, in chapter 12 of a book by Carslaw and Jaeger (1941) on operational methods. It is first necessary to establish the result that the inverse transform of $e^{z/p}$ is $I_0(2\sqrt{zt})$ (where $I_0$ is the modified Bessel function of the first kind of zero order). This may be proved most easily by expanding $e^{z/p}$ in series and by inverting each term by means of Heaviside's result that

$$\overline{t^\nu} = \frac{\Gamma(\nu+1)}{p^\nu} \qquad (\nu > -1). \tag{52}$$

Thus equation (52) and the result that

$$e^{z/p} = \sum_{n=0}^{\infty} \frac{1}{n!} \left(\frac{z}{p}\right)^n \tag{53}$$

show that the inverse of $e^{z/p}$ is

$$\sum_{n=0}^{\infty} \frac{(zt)^n}{n!n!} = I_0 [2 \sqrt{(zt)}]. \tag{54}$$

Definition (46) of the Heaviside transform now shows that

$$e^{z/p} = p \int_0^{\infty} e^{-pt} I_0 [2 \sqrt{(zt)}] \, dt. \tag{55}$$

On writing $\sqrt{p}$ in place of $p$ in this result and by then multiplying by $e^{-z\sqrt{p}}$, it is found that

$$e^{-\mu z} = p \int_0^{\infty} \left[\frac{1}{\sqrt{p}} \, e^{-(x+z)\sqrt{p}}\right] I_0 [2 \sqrt{(xz)}] \, dx. \tag{56}$$

Now it can be shown that

$$\frac{1}{\sqrt{p}} \, e^{-(x+z)\sqrt{p}} = \frac{1}{\sqrt{(\pi t)}} \int_0^{\infty} e^{-(x+z)^2/4t} e^{-pt} dt \tag{57}$$

(see, for example, Carslaw and Jaeger's book). On combining results (56) and (57), it is found that

$$e^{-\mu z} = p \int_0^{\infty} e^{-pt} \left\{\frac{1}{\sqrt{(\pi t)}} \int_0^{\infty} e^{-(x+z)^2/4t} I_0 [2 \sqrt{(xz)}] \, dx\right\} dt, \tag{58}$$

where the change in the order of integration is justified by the absolute convergence of the integral in the brackets. Equation (58) shows that the operational inverse of $e^{-\mu z}$ is $\psi(z, t)$, where

$$\psi(z, t) = \frac{1}{\sqrt{(\pi t)}} \int_0^{\infty} e^{-(x+z)^2/4t} I_0 [2 \sqrt{(xz)}] \, dx. \tag{59}$$

On applying the Faltung theorem for the Heaviside transform, equations (43) and (51) show that the required solution is

$$\boldsymbol{a}(z, t) = e^{-t} \frac{\partial}{\partial t} \int_0^t e^{(t-\tau)} \boldsymbol{f}(t - \tau) \, \psi(z, \tau) \, d\tau. \tag{60}$$

Since $\psi(0)$ is zero, equation (60) may be written in the form

$$\boldsymbol{a}(z, t) = \int_0^t \boldsymbol{f}(t - \tau) \, \phi(z, \tau) \, d\tau, \tag{61}$$

where

$$\phi(z, t) = \frac{\partial \psi}{\partial t} \, e^{-t} = \frac{e^{-t}}{2 \sqrt{(\pi t^3)}} \int_0^{\infty} \left[\frac{(x+z)^2}{2t} - 1\right] e^{-(x+z)^2/4t} I_0 [2 \sqrt{(xz)}] \, dx. \tag{62}$$

As a particular example of this result, choose $\boldsymbol{f}$ to represent the disturbance set up when a thin slab of fluid is suddenly displaced by an amount $A\mathbf{1}_y$, where $\mathbf{1}_y$ is a unit vector perpendicular to $\boldsymbol{H}_0$. The slab is held rigidly in its new position. Thus, on $z = 0$, $\boldsymbol{u}$ is given by

$$\boldsymbol{u}(0, t) = A \mathbf{1}_y \delta(t), \tag{63}$$

where $\delta(t)$ is the Dirac $\delta$-function. Equation (61) now shows that at other points in the fluid the value of $\boldsymbol{u}$ is

$$\boldsymbol{u}(z, t) = A\mathbf{1}_y\phi(z, t). \tag{64}$$

In Figure 2, $A\phi(z, t)$ is plotted as a function of $z$ for the particular case in which $t = 1$. The main body of the curve was derived from equation (62) by numerical integration. The dotted lines represent the approximate expansions developed in the next section. An interesting feature of the figure is that the peak of the wave is farther advanced than point $z = t$. This is a reflection of the fact, discussed earlier, that the higher frequencies travel faster than the lower ones and that, at time $t = 1$, the disturbance is still rich in high frequencies. Later, when these have been largely damped out, the peak occurs much nearer to point $z = t$.

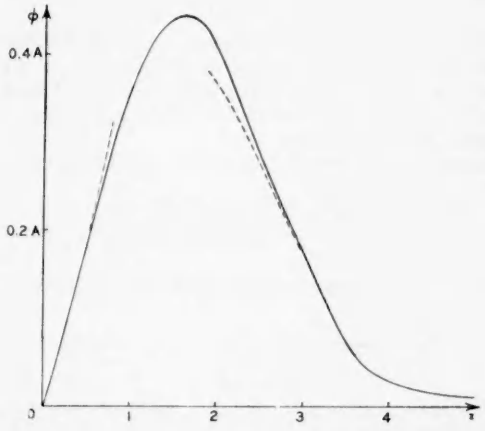


FIG. 2.—The figure shows the fluid velocity in the $y$-direction plotted as a function of $z$ at unit time after a thin slab of fluid at $z = 0$ has been impulsively displaced at distance $A\mathbf{1}_y$.

## VI. APPROXIMATE EXPANSIONS

When calculating the form of $\phi$ given by equation (62), it is desirable to have expansions available which approximate closely to $\phi$ for large and small values of $t$. An expansion suitable for large $t$ may be obtained by a saddle-point method. It is convenient to introduce the parameter $\eta$ defined by

$$\eta = \frac{z}{t}. \tag{65}$$

Change the variable of integration in equation (62) by writing

$$x = zy = \eta t y. \tag{66}$$

It is easily verified that

$$\phi = \frac{\eta e^{-t}}{2\sqrt{(\pi t)}} \int_0^\infty \left[\frac{\eta^2(1+y)^2 t}{2} - 1\right] e^{-\eta^2(1+y)^2 t/4} I_0(2\eta t\sqrt{y})\, dy. \tag{67}$$

The theory of the asymptotic expansion of Bessel functions shows that $I_0(2\eta t\sqrt{y})$ may be written in the form

$$I_0(2\eta t\sqrt{y}) = e^{2\eta t\sqrt{y}}\zeta(2\eta t\sqrt{y}), \tag{68}$$

where $\zeta(x)$ remains finite as $x$ approaches infinity. Equations (67) and (68) show that

$$\phi = \frac{\eta}{2\sqrt{(\pi t)}} \int_0^\infty e^{-t\theta(y)} \left[ \frac{\eta^2 (1+y)^2 t}{2} - 1 \right] \zeta(2\eta t \sqrt{y})\, dy, \tag{69}$$

where

$$\theta(y) = 1 - 2\eta\sqrt{y} + \tfrac{1}{4}\eta^2 (1+y)^2 \tag{70}$$

and is positive if $y$ is positive.

The function $\theta'(y)$ has just one zero at the point $y'$, defined by

$$(1+y')\sqrt{y'} = \frac{2}{\eta}. \tag{71}$$

At this point $\theta(y)$ assumes its smallest value, and, for large values of $t$, most of the integral (69) is contributed from the immediate neighborhood of $y'$. Considered as a function of $\eta$, $\theta(y')$ attains its minimum value of zero when $\eta = 1$ and hence $z = t$. Thus, as $t$ approaches infinity, the greatest value of $\phi$ occurs at the point $z = t$, at which the peak of the wave must therefore occur.

Near the saddle point $y'$, $\theta(y)$ may be expanded in a Taylor series. If

$$t \gg \frac{y'^2 (1+y')^2}{1+3y'}, \tag{72}$$

the Taylor series may be terminated after its second term with little loss of accuracy, i.e.,

$$\theta(y) = \theta(y') + \frac{1}{2!}(y-y')^2 \theta''(y'). \tag{73}$$

Substitute expansion (73) in expression (69) and, with the exception of the exponential term, represent the integrand by its value at $y'$. It is then found that the desired asymptotic expansion for $\phi$ is

$$\phi = \frac{2 - y'/t}{\sqrt{[y'(1+3y')]}}\, e^{-t(1+1/y')} I_0\left(\frac{4t}{1+y'}\right) [1 + \operatorname{erf} y']. \tag{74}$$

It is interesting to notice that, for large $t$, the maximum value of $\phi$ is approximately $(2\pi z)^{-1/2}$. If, however, the same type of disturbance had been initiated in a solid conductor, the maximum value of $\phi$ would have been $\kappa z^{-2}$, where $\kappa$ is a small constant of the order of unity. Thus, for aperiodic disturbances also, the skin depth is greatly increased if the conductor is a fluid.

An expression for $\phi$ suitable for computation, provided that $z$ is small, may be derived from the Taylor expansion for $\phi$ at $z = 0$. The successive derivatives of $\phi$ at $z = 0$ may be calculated directly from equation (62). They may also be computed by differentiating the operational equivalent $pe^{-\mu z}$ of $e^t \phi(z, t)$ and subsequently inverting these derivatives. The expansion provided by this method is found to be

$$\phi(z, t) = \frac{z e^{-t}}{\sqrt{(\pi t)}} \left[ 1 + \frac{1}{2t} + \frac{z^2}{24t^2} (8t^3 - 12t^2 - 6t - 3) + \ldots \right] + \frac{z^2 e^{-t}}{2} \left[ 1 + \frac{(t-4)}{12} z^2 + \ldots \right]. \tag{75}$$

## VII. DECAY OF AN INITIAL STATE

It will now be supposed that there are no disturbing sources in the fluid and that the system is allowed to decay freely from an arbitrarily specified initial state, in which $\boldsymbol{g}(z)$ is continuous and bounded. The solution of equation (47), which is continuous and bounded at infinity may be found by the method of variation of parameters or otherwise. It is

$$\boldsymbol{b}(z, p) = -\frac{1}{2\mu}\int_{-\infty}^{\infty} e^{-\mu|z'|}\boldsymbol{g}(z - z')\,dz'. \tag{76}$$

To invert this result, it is again useful to appeal to equation (55), which shows that

$$\frac{1}{\mu}\,e^{-\mu z} = p\int_0^{\infty}\left[\frac{e^{-(x+z)\sqrt{p}}}{p-1}\right] I_0[2\sqrt{(xz)}]\,dx. \tag{77}$$

Now it can be demonstrated that

$$\frac{e^{-(x+z)\sqrt{p}}}{p-1} = p\int_0^{\infty} e^{(1-p)t}\left\{\tfrac{1}{2}\,e^{-(x+z)}\operatorname{erfc}\left(\frac{x+z}{2\sqrt{t}} - \sqrt{t}\right) + \tfrac{1}{2}\,e^{(x+z)}\operatorname{erfc}\left(\frac{x+z}{2\sqrt{t}} + \sqrt{t}\right)\right\} dt \tag{78}$$

(this result is stated by Carslaw and Jaeger). Equations (77) and (78) show that the operational inverse of $e^{-\mu z}/\mu$ is $2e^{t}\Psi(z, t)$, where

$$\Psi(z, t) = \frac{1}{4}\int_0^{\infty}\left\{e^{-(x+z)}\operatorname{erfc}\left(\frac{x+z}{2\sqrt{t}} - \sqrt{t}\right) + e^{(x+z)}\operatorname{erfc}\left(\frac{x+z}{2\sqrt{t}} + \sqrt{t}\right)\right\} I_0[2\sqrt{(xz)}]\,dx. \tag{79}$$

The inverse of expression (76) therefore gives

$$\boldsymbol{a}(z, t) = \int_{-\infty}^{\infty}\left\{\Psi(t, |z'|)\left[\frac{\partial \boldsymbol{a}_1}{\partial z} - \frac{\partial^2 \boldsymbol{a}_0}{\partial z^2}\right]_{z-z'} + \frac{\partial \Psi(t, |z'|)}{\partial t}\,\boldsymbol{a}_0(z - z')\right\} dz'. \tag{80}$$

As a particular example of this result, suppose that the initial state of the system is specified to be

$$\boldsymbol{a}_0 = A\,\mathbf{1}_y\,\delta(z), \qquad \boldsymbol{a}_1 = 0. \tag{81}$$

Then equation (80) shows that, at subsequent times, $\boldsymbol{\phi}$ is given by

$$\boldsymbol{a} = A\,\mathbf{1}_y\,\frac{\partial \Psi}{\partial t}, \tag{82}$$

where

$$\frac{\partial \Psi}{\partial t} = \frac{e^{-t}}{4\sqrt{(\pi t^3)}}\int_0^{\infty}(x + z)\,e^{-(x+z)^2/4t} I_0[2\sqrt{(xz)}]\,dx. \tag{83}$$

The behavior of $\partial\Psi/\partial t$ is very similar to that of $\boldsymbol{\phi}$, and expansions analogous to those developed in Section VI may easily be derived for it.

Most of the work in this paper was completed during my tenure of the George Green Studentship at Gonville and Caius College, Cambridge, England. I would like to thank

Dr. S. K. Runcorn for the interest he has taken in this work. The numerical integration of expression (62) was undertaken while I was at the Yerkes Observatory and was supported by the Geophysics Research Directorate of the Air Force Cambridge Research Center, Air Research and Development Command, under contract AF 19(604)-299 with the University of Chicago.

## REFERENCES

Alfvén, H. 1950, *Cosmical Electrodynamics* (Oxford: Clarendon Press).
Carslaw, H. S., and Jaeger, J. C. 1941, *Operational Methods in Applied Mathematics* (Oxford: Oxford University Press).
Chandrasekhar, S., and Elbert, D. 1955, *Proc. R. Soc. London A* (in press).
Nakagawa, Y. 1955, *Nature*, **175**, 417.
Walén, C. 1944, *Ark. f. Mat., Astr. o. Fys.*, Vol. **30A**, No. 15.

# ON THE $X$- AND $Y$-FUNCTIONS OF S. CHANDRASEKHAR

I. W. BUSBRIDGE
St. Hugh's College, Oxford, England
*Received April 19, 1955*

ABSTRACT

The dual integral equations for the $X$- and $Y$-functions are first reduced to separate singular integral equations for the functions $\xi(\mu) = X(\mu) + Y(\mu)$ and $\eta(\mu) = X(\mu) - Y(\mu)$. These are then reduced to Fredholm equations, and the resulting Neumann series are shown to converge for all sufficiently large "optical depth" $\tau$, thus establishing the existence of $X(\mu)$ and $Y(\mu)$ for all sufficiently large $\tau$.

**1.** *Introduction.*—The existence of the $H$-function[1] satisfying the integral equation

$$H(\mu) = 1 + \mu H(\mu) \int_0^1 \frac{\Psi(u)}{u+\mu} H(u)\, du \tag{1.1}$$

was first established by Crum (1947), and another rigorous treatment for the case $\Psi(u) = \frac{1}{2}$ is given by Kourganoff and Busbridge (1952). In equation (1.1) the "characteristic function" $\Psi(u)$ is an even function which is nonnegative for $0 \leq u \leq 1$ and is such that

$$\int_0^1 \Psi(u)\, du \leq \tfrac{1}{2}. \tag{1.2}$$

When there is equality, we have the so-called "conservative" case. Usually $\Psi(u)$ is a polynomial, and, for simplicity, we shall assume that this is the case.

Crum showed that, in the nonconservative case, the solution of equation (1.1) is not unique, but that, if $H(\mu)$ is given by Chandrasekhar's integral

$$H(\mu) = \exp\left\{\frac{1}{2\pi i}\int_{-i\infty}^{i\infty} \log \Im(z)\, \frac{\mu\, dz}{z^2-\mu^2}\right\}, \tag{1.3}$$

where[2]

$$\Im(z) = 1 - \int_0^1 \Psi(u)\left\{\frac{z}{z+u} + \frac{z}{z-u}\right\} du, \tag{1.4}$$

and if $\Im(z)$ has simple zeros at $z = \pm 1/k$ $(0 < k < 1)$,[3] then $H(z)$ ($z$ complex) has a simple pole at $z = -1/k$ and there is then a further solution,

$$H_1(\mu) = \frac{H(\mu)(1+k\mu)}{1-k\mu}.$$

For this reason we shall always use $H(\mu)$ to denote the solution given by equation (1.3).

The integral equations for the $X$- and $Y$-functions, which arise in problems connected

[1] This was first introduced by Chandrasekhar (1947).

[2] If $\Psi(u)$ is a polynomial, $\Im(z)$ behaves like $\log(z-1)$ near $z = 1$.

[3] See Chandrasekhar (1950) or Chandrasekhar and Elbert (1952). It is shown that $\Im(z)$ may have such a pair of zeros in the nonconservative case but that it has no such zeros in the conservative case.

with finite atmospheres of optical thickness, $\tau$,[4] were first found by Chandrasekhar (1948; 1950, chap. viii). These are

$$X(\mu) = 1 + \mu \int_0^1 \frac{\Psi(u)}{\mu + u} [X(\mu) X(u) - Y(\mu) Y(u)] \, du, \tag{1.5}$$

$$Y(\mu) = e^{-\tau/\mu} + \mu \int_0^1 \frac{\Psi(u)}{\mu - u} [Y(\mu) X(u) - X(\mu) Y(u)] \, du. \tag{1.6}$$

Using the method of "discrete ordinates," Chandrasekhar obtained approximate solutions, but the existence of $X(\mu)$ and $Y(\mu)$, except for $\tau = 0$ and $\infty$, has never been proved mathematically. When $\tau = 0$, equations (1.5) and (1.6) have these solutions:

$$X(\mu) = 1, \qquad Y(\mu) = 1;$$

for $\tau = \infty$ they have these solutions:

$$X(\mu) = H(\mu), \qquad Y(\mu) = 0.$$

The solutions which are of astrophysical interest are bounded for $0 \leq \mu \leq 1$.

In the conservative case, Chandrasekhar has shown that the solutions (if they exist) are not unique, for if $X(\mu) = X^*(\mu)$ and $Y(\mu) = Y^*(\mu)$ are solutions, then so are

$$X(\mu) = X^*(\mu) + C\mu [X^*(\mu) + Y^*(\mu)],$$

$$Y(\mu) = Y^*(\mu) - C\mu [X^*(\mu) + Y^*(\mu)],$$

for any value of the constant $C$. Again no rigorous investigation has been made.

The object of the present paper is to establish the existence of $X(\mu)$ and $Y(\mu)$. Assuming their existence, one is led to consider the functions

$$\xi(z) = X(z) + Y(z), \qquad \eta(z) = X(z) - Y(z). \tag{1.7}$$

The analytic properties of $X(z)$ and $Y(z)$ and therefore of $\xi(z)$ and $\eta(z)$, which are given in the following theorem, are ones which we shall need either in the reduction of equations (1.5) and (1.6) to singular integral equations for $\xi(z)$ and $\eta(z)$ or in the subsequent reduction of these to Fredholm equations. Ultimately it will be verified that the solutions so obtained have these properties.

THEOREM IA.—*(Conservative case.) Analytic functions $X(z)$ and $Y(z)$ exist which have the properties:*

(i) *$X(z)$ and $Y(z)$ are regular for $|z| > 0$;*
(ii) *$X(z)$ and $Y(z)$ are bounded as $|z| \to 0$ in the angle $|\arg z| \leq \delta$, where $0 < \delta < \frac{1}{2}\pi$;*
(iii) *$zX'(z)$ and $zY'(z)$ tend to zero as $|z| \to 0$ for $|\arg z| \leq \delta$;*
(iv) *$X(z)$ and $Y(z)$ are $O(z)$ as $z \to \infty$,*

*which satisfy equations (1.5) and (1.6), if and only if functions $\xi(z)$ and $\eta(z)$ exist, which are related to $X(z)$ and $Y(z)$ by equation (1.7), which have the same analytic properties as $X(z)$ and $Y(z)$, and which, when $z$ does not lie on the real axis between $-1$ and $1$, satisfy the equations*

$$\xi(z)\, \Im(z) = 1 + e^{-\tau/z} + \int_0^1 \frac{z\Psi(u)}{u - z} \xi(u) \, du - e^{-\tau/z} \int_0^1 \frac{z\Psi(u)}{u + z} \xi(u) \, du, \tag{1.8}$$

$$\eta(z)\, \Im(z) = 1 - e^{-\tau/z} + \int_0^1 \frac{z\Psi(u)}{u - z} \eta(u) \, du + e^{-\tau/z} \int_0^1 \frac{z\Psi(u)}{u + z} \eta(u) \, du, \tag{1.9}$$

*$\Im(z)$ being given by equation (1.4).*

[4] We shall assume that $0 < \tau < \infty$ except where we state specifically that $\tau = 0$ or $\tau = \infty$.

THEOREM IB.—(*Nonconservative case.*) *The same is true except that* i *and* iv *are replaced by*

(i) $X(z)$ *and* $Y(z)$ *are regular for* $|z| > 0$ *except for simple poles at* $z = \pm 1/k$ *when* $\Im(z)$ *has zeros at these points;*

(iv) $X(z)$ *and* $Y(z)$ *are bounded as* $z \to \infty$.

We shall frequently say that $\xi(z)$ and $\eta(z)$ satisfy the conditions of Theorem I when they satisfy conditions i–iv with $X$ and $Y$ replaced by $\xi$ and $\eta$.

Theorem I is proved in section 2. In section 3 it is shown that, when $z = \mu$ $(0 < \mu < 1)$, equations (1.8) and (1.9) become

$$\xi(\mu)T(\mu) = 1 + e^{-\tau/\mu} + \int_0^1 \frac{\mu\Psi(u)}{u-\mu}\,\xi(u)\,du - e^{-\tau/\mu}\int_0^1 \frac{\mu\Psi(u)}{u+\mu}\,\xi(u)\,du, \tag{1.10}$$

$$\eta(\mu)T(\mu) = 1 - e^{-\tau/\mu} + \int_0^1 \frac{\mu\Psi(u)}{u-\mu}\,\eta(u)\,du + e^{-\tau/\mu}\int_0^1 \frac{\mu\Psi(u)}{u+\mu}\,\eta(u)\,du, \tag{1.11}$$

where

$$T(\mu) = 1 - \int_0^1 \frac{\mu\Psi(u)}{\mu-u}\,du - \int_0^1 \frac{\mu\Psi(u)}{\mu+u}\,du, \tag{1.12}$$

the first integrals in equations (1.10), (1.11), and (1.12) being Cauchy principal values.

Before proceeding, a word must be said about notation. We shall use the notation of Chandrasekhar (1950, chaps. v and viii) throughout, with one exception. Chandrasekhar uses $T(z)$ for the function $\Im(z)$ of equation (1.4). It is regular in the $z$-plane cut from $-1$ to 1, or (as we shall say in the interests of brevity) "outside the interval $(-1, 1)$." In sections 4–7 we need to use the fact that, as $z \to \mu$ $(0 < \mu < 1)$ from above and below the real axis, $\Im(z)$ tends, respectively, to

$$\Im^+(\mu) = T(\mu) + \pi i \mu \Psi(\mu),$$

$$\Im^-(\mu) = T(\mu) - \pi i \mu \Psi(\mu),$$

where $T(\mu)$ is given by formula (1.12), the first integral being a Cauchy principal value. Hence it is essential to have a notation which distinguishes $T(\mu)$ from $\Im(z)$.

We shall define, for any function $F(\mu)$,

$$f_n = \int_0^1 u^n \Psi(u) F(u)\,du \qquad (n = 0, 1, 2, \ldots). \tag{1.13}$$

Hence, corresponding to functions $H(\mu)$, $X(\mu)$, $Y(\mu)$, $\xi(\mu)$, and $\eta(\mu)$, we have the moments $h_n$, $x_n$, $y_n$, $\xi_n$, and $\eta_n$ $(n = 0, 1, 2, \ldots)$.

In the conservative case, by the corollary to Chandrasekhar's theorem 1 (1950, chap. viii), $x_0 + y_0 = 1$ and so $\xi_0 = 1$, but $\eta_0$ is indeterminate because equation (1.11) has the family of solutions

$$\eta(\mu) = \eta^*(\mu) + C\mu\xi(\mu),$$

where $\eta^*(\mu)$ is one particular solution. We therefore define $\eta(\mu)$ as the *standard solution* for which the moment $\eta_0 = 1$. This agrees with Chandrasekhar's definition of the standard $X$- and $Y$-functions as those for which $x_0 = 1$ and $y_0 = 0$. In the conservative case, $\eta(\mu)$ will always have this special meaning.

In sections 4–7 we prove the following theorems:

THEOREM IIA.—(*Conservative case.*) *If* $\xi(z)$ *and* $\eta(z)$ *satisfy conditions* i–iv *of Theorem*

*IA and equations (1.8) and (1.9), then $\xi(\mu)$ and $\eta(\mu)$ $(0 \leq \mu \leq 1)$ are solutions of the Fredholm equations*

$$\xi(\mu) = \frac{\xi_1}{h_1} H(\mu) + \int_0^1 n(u, \mu)\, \xi(u)\, du, \tag{1.14}$$

$$\eta(\mu) = \frac{\eta_1}{h_1} H(\mu) - \int_0^1 n(u, \mu)\, \eta(u)\, du, \tag{1.15}$$

*such that $\xi_0 = 1$, $\eta_0 = 1$. The kernel $n(u, \mu)$ is given by*

$$n(u, \mu) = u\Psi(u) H(\mu) \left\{ \frac{e^{-\tau/\mu}}{u+\mu} \frac{T(\mu)}{H(\mu) Z(\mu)} + \int_0^1 \frac{t\Psi(t)\, e^{-\tau/t}}{H(t) Z(t)} \frac{dt}{(t-\mu)(t+u)} \right\}, \tag{1.16}$$

*where*

$$Z(\mu) = \{T(\mu)\}^2 + \pi^2\mu^2 \{\Psi(\mu)\}^2, \tag{1.17}$$

*or equivalently by*

$$\begin{aligned} n(u, \mu) = {} & \left\{ \frac{u}{u+\mu} \Psi(u) H(u) H(\mu) - \frac{u}{h_1} \Psi(u) H(\mu) \right\} e^{-\tau/\mu} \\ & + u\Psi(u) H(\mu) \int_0^1 \frac{t\Psi(t)}{H(t) Z(t)} \frac{e^{-\tau/t} - e^{-\tau/\mu}}{t-\mu} \frac{dt}{t+u}, \end{aligned} \tag{1.18}$$

*and it is bounded for $0 \leq \mu \leq 1$ and $0 \leq u \leq 1$. For sufficiently large $\tau$, the two Neumann series, obtained from equations (1.14) and (1.15) by iteration, converge to bounded functions in (0, 1). These functions satisfy equations (1.10) and (1.11). In equations (1.14), (1.15), and (1.18), $\mu$ may be replaced by the complex variable $z$, provided that $z$ does not lie between $-1$ and 0 of the real axis, and the corresponding functions $\xi(z)$ and $\eta(z)$ satisfy the conditions of Theorem IA and equations (1.8) and (1.9).*

THEOREM IIB.—*(Nonconservative case.) Theorem IIA remains true if the following alterations are made: Theorem IA must be replaced by Theorem IB; equations (1.14) and (1.15) must be replaced by*

$$\xi(\mu) = g(\mu) + \int_0^1 n(u, \mu)\, \xi(u)\, du, \tag{1.19}$$

$$\eta(\mu) = h(\mu) - \int_0^1 n(u, \mu)\, \eta(u)\, du, \tag{1.20}$$

*where $n(u, \mu)$ is given by equation (1.16) and*

$$\begin{aligned} g(\mu) = {} & (1+e^{-\tau/\mu}) \frac{1-\xi_0}{1-h_0} H(\mu) + (1-\xi_0) H(\mu) \int_0^1 \frac{t\Psi(t)}{H(t) Z(t)} \\ & \times \frac{e^{-\tau/t} - e^{-\tau/\mu}}{t-\mu} dt + A_0 \left\{ k \int_0^1 \frac{u\Psi(u)\, \xi(u)}{ku-1} du + (1-\xi_0)(1+e^{-\tau/\mu}) \right\} \frac{H(\mu)}{k\mu - 1}, \end{aligned} \tag{1.21}$$

$$\begin{aligned} h(\mu) = {} & (1-e^{-\tau/\mu}) \frac{1-\eta_0}{1-h_0} H(\mu) - (1-\eta_0) H(\mu) \int_0^1 \frac{t\Psi(t)}{H(t) Z(t)} \\ & \times \frac{e^{-\tau/t} - e^{-\tau/\mu}}{t-\mu} dt + A_0 \left\{ k \int_0^1 \frac{u\Psi(u)\, \eta(u)}{ku-1} du + (1-\eta_0)(1-e^{-\tau/\mu}) \right\} \frac{H(\mu)}{k\mu - 1}, \end{aligned} \tag{1.22}$$

*where $A_0 = 0$ when $\Im(z)$ has no zeros and*

$$A_0 = \frac{k}{H(1/k)\, \Im'(1/k)}, \tag{1.23}$$

*when $\Im(z)$ has zeros at $z = \pm 1/k$. The kernel $n(u, \mu)$ can be put in the form (corresponding to eq. [1.18])*

$$n(u,\mu) = \left\{\frac{u\Psi(u)\,H(u)\,H(\mu)}{u+\mu} + \frac{A_0 k u\Psi(u)\,H(\mu)}{(ku+1)(k\mu-1)}\right\} e^{-\tau/\mu} + u\Psi(u)\,H(\mu)\int_0^1 \frac{t\Psi(t)}{H(t)\,Z(t)}\,\frac{e^{-\tau/t}-e^{-\tau/\mu}}{t-\mu}\,\frac{dt}{t+u}, \tag{1.24}$$

*and, in equations (1.19)–(1.22) and (1.24), $\mu$ can be replaced by $z$, provided that $z$ does not lie between $-1$ and 0 on the real axis.*

The solution obtained by iteration of equation (1.14) in Theorem IIA will be multiplied by the constant $\xi_1/h_1$, and this is determined by the condition $\xi_0 = 1$, where

$$\xi_0 = \int_0^1 \Psi(u)\,\xi(u)\,du, \tag{1.25}$$

and similarly for $\eta(\mu)$.[5] The constant $\xi_0$, which appears in the solution of equation (1.19), is similarly determined by equation (1.25) (see sec. 7).

**2.** *The proof of Theorem I.*—We first deduce equations (1.8) and (1.9) from equations (1.5) and (1.6). In the latter we can replace $\mu$ by $z$; then, provided that the $z$-plane is cut from $-1$ to 1, equations (1.5) and (1.6) may be written (except at zeros of $X[z]$ and $Y[z]$) in the forms

$$\frac{1}{X(z)} - 1 + \int_0^1 \frac{z\Psi(u)}{z+u}\,X(u)\,du = \frac{Y(z)}{X(z)}\int_0^1 \frac{z\Psi(u)}{z+u}\,Y(u)\,du, \tag{2.1}$$

$$\frac{e^{-\tau/z}}{Y(z)} - 1 + \int_0^1 \frac{z\Psi(v)}{z-v}\,X(v)\,dv = \frac{X(z)}{Y(z)}\int_0^1 \frac{z\Psi(v)}{z-v}\,Y(v)\,dv. \tag{2.2}$$

In the following reduction we shall suppose that $z$ lies in the cut plane. Then if $X(z)$ and $Y(z)$ satisfy the conditions of Theorem I, all the following processes are justified.

We multiply equations (2.1) and (2.2) vertically, using the identity

$$\frac{z}{(z+u)(z-v)} = \frac{u}{(u+v)(z+u)} + \frac{v}{(u+v)(z-v)}. \tag{2.3}$$

Then we have

$$\left\{\frac{1}{X(z)} - 1 + \int_0^1 \frac{z\Psi(u)}{z+u}\,X(u)\,du\right\}\left\{\frac{e^{-\tau/z}}{Y(z)} - 1 + \int_0^1 \frac{z\Psi(v)}{z-v}\,X(v)\,dv\right\}$$

$$= z\int_0^1\int_0^1 \Psi(u)\Psi(v)\,Y(u)\,Y(v)\left\{\frac{u}{(u+v)(z+u)} + \frac{v}{(u+v)(z-v)}\right\}du\,dv$$

$$= \int_0^1 \frac{z\Psi(u)}{z+u}\,Y(u)\,du\int_0^1 \frac{u\Psi(v)}{u+v}\,Y(v)\,dv + \int_0^1 \frac{z\Psi(v)}{z-v}\,Y(v)\,dv \times \int_0^1 \frac{v\Psi(u)}{v+u}\,Y(u)\,du$$

$$= \int_0^1 \frac{z\Psi(u)}{z+u}\left\{1 - X(u) + X(u)\int_0^1 \frac{u\Psi(v)}{u+v}\,X(v)\,dv\right\}du$$

[5] If eq. (1.14) is multiplied by $\mu\Psi(\mu)$ and integrated over (0, 1), the left-hand side is $\xi_1$, and the right-hand side, after considerable labor, reduces to $\xi_1$, so no information about $\xi_1$ is gained.

$$+\int_0^1 \frac{z\Psi(v)}{z-v}\left\{1-X(v)+X(v)\int_0^1 \frac{v\Psi(u)}{v+u}X(u)\,du\right\}dv \qquad \text{(by eq. [1.5])}$$

$$=\int_0^1 \Psi(u)\left\{\frac{z}{z+u}+\frac{z}{z-u}\right\}du-\int_0^1 \frac{z\Psi(u)}{z+u}X(u)\,du-\int_0^1 \frac{z\Psi(v)}{z-v}X(v)\,dv$$

$$+\int_0^1\int_0^1 z\Psi(u)\Psi(v)X(u)X(v)\left\{\frac{u}{(u+v)(z+u)}+\frac{v}{(u+v)(z-v)}\right\}du\,dv.$$

On using equation (2.3) again, together with the definition (eq. [1.4]) of $\Im(z)$, we get

$$\frac{1}{X(z)}\frac{e^{-\tau/z}}{Y(z)}+1-\frac{1}{X(z)}\left\{1-\int_0^1 \frac{z\Psi(v)}{z-v}X(v)\,dv\right\}$$

$$-\frac{e^{-\tau/z}}{Y(z)}\left\{1-\int_0^1 \frac{z\Psi(u)}{z+u}X(u)\,du\right\}=1-\Im(z)$$

whence

$$\frac{1}{X(z)}\left\{1-\int_0^1 \frac{z\Psi(v)}{z-v}X(v)\,dv\right\}+\frac{e^{-\tau/z}}{Y(z)}\left\{1-\int_0^1 \frac{z\Psi(u)}{z+u}X(u)\,du\right\}$$

$$-\frac{e^{-\tau/z}}{X(z)\,Y(z)}=\Im(z). \tag{2.4}$$

This relation corresponds to the relation

$$\frac{1}{H(z)\,H(-z)}=\Im(z) \tag{2.5}$$

for the $H$-function, and the method of deriving it is similar (cf. Chandrasekhar, 1950, chap. v).

On using equation (2.4), equation (2.1) becomes

$$X(z)\,\Im(z)=1-\int_0^1 \frac{z\Psi(u)}{z-u}X(u)\,du-e^{-\tau/z}\int_0^1 \frac{z\Psi(u)}{z+u}Y(u)\,du, \tag{2.6}$$

and equation (2.2) becomes

$$Y(z)\,\Im(z)=e^{-\tau/z}-\int_0^1 \frac{z\Psi(u)}{z-u}Y(u)\,du-e^{-\tau/z}\int_0^1 \frac{z\Psi(u)}{z+u}X(u)\,du. \tag{2.7}$$

Adding and subtracting and introducing the functions $\xi(z)$ and $\eta(z)$ defined by equation (1.7), we have equations (1.8) and (1.9).

It is worth noting at this point that the corresponding equation for $H(z)$ is

$$H(z)\,\Im(z)=1+\int_0^1 \frac{z\Psi(u)}{u-z}H(u)\,du. \tag{2.8}$$

We now have to prove, conversely, that if $\xi(z)$ and $\eta(z)$ satisfy the conditions of Theorem I and are solutions of equations (1.8) and (1.9), then the functions $X(z)$ and $Y(z)$, defined by equation (1.7), satisfy equations (2.1) and (2.2), and hence equations (1.5) and (1.6).

From equations (1.8) and (1.9) we obtain equations (2.6) and (2.7), and these, to-

gether with equation (2.4), imply equations (2.1) and (2.2). Hence it is only necessary to deduce equation (2.4) from equations (2.6) and (2.7); i.e., to prove that $\Sigma(z) = 0$, where

$$\Sigma(z) \equiv e^{\tau/z}X(z)\,Y(z)\,\Im(z) + 1 - X(z)\left\{1 - \int_0^1 \frac{z\Psi(u)}{u+z}\,X(u)\,du\right\} - e^{\tau/z}Y(z)\left\{1 - \int_0^1 \frac{z\Psi(v)}{z-v}\,X(v)\,dv\right\}. \tag{2.9}$$

From equations (1.8) and (1.9) we have the relations

$$\xi(-z) = e^{\tau/z}\xi(z), \tag{2.10}$$

$$\eta(-z) = -e^{\tau/z}\eta(z), \tag{2.11}$$

from which it follows that[6]

$$Y(z) = e^{-\tau/z}X(-z). \tag{2.12}$$

Since $\Im(z)$ is an even function of $z$, it follows that

$$\Sigma(-z) = \Sigma(z). \tag{2.13}$$

Equation (2.6), after multiplying by $e^{\tau/z}Y(z)$, can be written

$$\Sigma(z) - 1 + X(z)\left\{1 - \int_0^1 \frac{z\Psi(v)}{z+v}\,X(v)\,dv\right\} = -Y(z)\int_0^1 \frac{z\Psi(v)}{z+v}\,Y(v)\,dv, \tag{2.14}$$

and from this it follows that $\Sigma(z)$ is regular outside the interval $(-1, 0)$ except, perhaps, for simple poles at $z = \pm 1/k$ in the nonconservative case. Hence, by equation (2.13), $\Sigma(z)$ has at most an isolated singularity at $z = 0$ and, in the nonconservative case, simple poles at $z = \pm 1/k$.

We next obtain an integral equation for $\Sigma(z)$. Let $z$ lie outside the interval $(-1, 1)$. From equations (2.6) and (2.7), using the identity (2.3), we have

$$\left\{X(z)\,\Im(z) - \left[1 - \int_0^1 \frac{z\Psi(v)}{z-v}\,X(v)\,dv\right]\right\}\left\{Y(z)\,\Im(z) - e^{-\tau/z} \times \left[1 - \int_0^1 \frac{z\Psi(u)}{z+u}\,X(u)\,du\right]\right\}$$

$$= e^{-\tau/z}\int_0^1\int_0^1 z\Psi(u)\Psi(v)\,Y(u)\,Y(v)\left\{\frac{u}{(u+v)(z+u)} + \frac{v}{(u+v)(z-v)}\right\}du\,dv \tag{2.15}$$

$$= e^{-\tau/z}\int_0^1 \frac{z\Psi(u)}{z+u}\,Y(u)\,du\int_0^1 \frac{u\Psi(v)}{u+v}\,Y(v)\,dv + e^{-\tau/z}\int_0^1 \frac{z\Psi(v)}{z-v}\,Y(v)\,dv\int_0^1 \frac{v\Psi(u)}{v+u}\,Y(u)\,du.$$

On the right-hand side of equation (2.15) we use equation (2.14) with $z = u$ $(0 \le u \le 1)$;

[6] I find that this relation is known to Chandrasekhar, though not given (1948, 1950).

we expand the left-hand side of equation (2.15) and use equation (2.9) and the identity (2.3). After multiplying by $e^{r/z}$, we have

$$\Im(z)\Sigma(z)+1-\Im(z)-\int_0^1\frac{z\Psi(v)}{z-v}X(v)\,dv-\int_0^1\frac{z\Psi(u)}{z+u}X(u)\,du$$
$$+\int_0^1\int_0^1 z\Psi(u)\Psi(v)X(u)X(v)\left\{\frac{u}{(u+v)(z+u)}+\frac{v}{(u+v)(z-v)}\right\}du\,dv$$
$$=-\int_0^1\frac{z\Psi(u)}{z+u}\left\{\Sigma(u)-1+X(u)-X(u)\int_0^1\frac{u\Psi(v)}{u+v}X(v)\,dv\right\}du$$
$$-\int_0^1\frac{z\Psi(v)}{z-v}\left\{\Sigma(v)-1+X(v)-X(v)\int_0^1\frac{v\Psi(u)}{v+u}X(u)\,du\right\}dv.$$

By definition (1.4) of $\Im(z)$, this reduces to

$$\Im(z)\Sigma(z)=-\int_0^1\frac{z\Psi(u)}{z+u}\Sigma(u)\,du-\int_0^1\frac{z\Psi(v)}{z-v}\Sigma(v)\,dv,$$

and, since $\Sigma(z)$ is an even function, this can be written

$$\Im(z)\Sigma(z)=-\int_{-1}^1\frac{z\Psi(u)\Sigma(u)}{z-u}\,du. \tag{2.16}$$

We shall now show that $\Sigma(z)$ is bounded as $z\to 0$ and therefore regular at $z=0$, since this is an isolated singularity. We shall also show that $\Sigma(0)=0$.

Let $z=re^{i\theta}$. If $|\theta|\le\delta$ $(0<\delta<\frac{1}{2}\pi)$, then $X(z)$ and $Y(z)$ are bounded as $r\to 0$. Also, if $0\le v\le 1$, then

$$\left|\frac{z}{z+v}\right|\le 1.$$

Hence it follows at once from equation (2.14) that $\Sigma(z)$ is bounded as $r\to 0$ for $|\theta|\le\delta$. Since $\Sigma(-z)=\Sigma(z)$, it is also bounded for $\pi-\delta\le\theta\le\pi+\delta$. In particular, $\Sigma(u)$ is bounded for $-1\le u\le 1$.

We shall deduce the boundedness as $r\to 0$ for $\delta\le|\theta|\le\pi-\delta$ from the following lemma, which is of considerable importance in later sections. The proof will be given at the end of this section.[7]

LEMMA I.—*If $\psi(t)$ is bounded and integrable over $(a, b)$ and if $a\le\mu\le b$, then, as $z\to\mu$,*

$$\int_a^b\psi(t)\frac{z-\mu}{z-t}\,dt\to 0$$

*uniformly with respect to arg $(z-\mu)$ within any sector $\delta\le|\arg(z-\mu)|\le\pi-\delta$ $(0<\delta<\frac{1}{2}\pi)$. A similar result holds if $\mu=a$ or $b$ for the sectors $|\arg(z-a)|\le\delta$ and $|\arg(z-b)|\le\pi-\delta$, respectively. The lemma is also true if $\psi(t)$ depends on $\mu$ and $z$, provided that $\psi(t)$ is uniformly bounded for $a\le t\le b$, $a\le\mu\le b$, and arg $(z-\mu)$ in the appropriate sector.*

Taking $a=-1$, $b=1$, $\mu=0$, and $\psi(t)=\Psi(t)\Sigma(t)$, it follows at once from equation (2.16) that $\Im(z)\Sigma(z)\to 0$ as $r\to 0$ for $\delta\le|\theta|\le\pi-\delta$. Again, since $\Psi(u)$ is an even function, equation (1.4) can be written

$$\Im(z)=1-\int_{-1}^1\Psi(u)\frac{z}{z-u}\,du;$$

[7] I am indebted to a referee for pointing out that the insertion of Lemma I would save the repetition of very similar analysis.

and it therefore follows from the lemma that $\Im(z) \to 1$ as $r \to 0$ for $\delta \leq |\theta| \leq \pi - \delta$. Hence $\Sigma(z) \to 0$ as $r \to 0$ within this sector. Thus $\Sigma(z)$ is bounded near $z = 0$ for all arg $z$, and it is therefore regular at $z = 0$. Moreover, $\Sigma(0) = 0$.

In the conservative case, since $X(z)$ and $Y(z)$ are $O(z)$ for large $z$, it follows from equation (2.14) that $\Sigma(z)$ is $O(z)$. Since it is regular for all finite $z$,

$$\Sigma(z) = Az + B .$$

But $\Sigma(-z) = \Sigma(z)$ and $\Sigma(0) = 0$; hence $A = 0$, $B = 0$, and

$$\Sigma(z) = 0 .$$

In the nonconservative case $X(z)$ and $Y(z)$ are bounded for large $z$, and therefore, from equation (2.14), $\Sigma(z)$ is bounded. If $\Sigma(z)$ has no poles at finite points, then

$$\Sigma(z) = \Sigma(0) = 0 .$$

If $\Sigma(z)$ has simple poles at $z = \pm 1/k$, then

$$\Sigma(z) = \frac{A}{k^2 z^2 - 1},$$

since it is an even function. Putting $z = 0$, we have $A = 0$ and hence again $\Sigma(z) = 0$. This completes the proof of the theorem.

*The proof of Lemma I.*—If $a < \mu < b$, let $z - \mu = re^{i\theta}$, where $\delta \leq |\theta| \leq \pi - \delta$. Then

$$\begin{aligned} |z - t| &= |z - \mu + \mu - t| \\ &= \{r^2 + 2r(\mu - t)\cos\theta + (\mu - t)^2\}^{1/2} \\ &\geq \{r^2 - 2r|\mu - t|\cos\delta + (\mu - t)^2\}^{1/2} . \end{aligned}$$

From this it follows that

$$|z - t| \geq r \sin\delta \quad \text{and} \quad |z - t| \geq |\mu - t| \sin\delta . \tag{2.17}$$

Let $\rho > 0$. Since $\psi(t)$ is bounded in $(a, b)$, we have, by the first inequality in formula (2.17),

$$\left| \int_a^b \frac{z - \mu}{z - t} \psi(t)\, dt \right| = O\left( \int_a^{\mu - \rho} \frac{r}{|z - t|}\, dt + \int_{\mu + \rho}^b \frac{r}{|z - t|}\, dt \right) + O\left( \int_{\mu - \rho}^{\mu + \rho} \operatorname{cosec}\delta\, dt \right).$$

In the first two integrals on the right, $|\mu - t| \geq \rho$, and so, by inequality (2.17), $|z - t| \geq \rho \sin\delta$. Hence

$$\begin{aligned} \left| \int_a^b \frac{z - \mu}{z - t} \psi(t)\, dt \right| &= O\left( \frac{r}{\rho} \operatorname{cosec}\delta \right) + O(\rho \operatorname{cosec}\delta) \\ &= O(r^{1/2}) \quad \text{if} \quad \rho = r^{1/2} \\ &= o(1) \quad \text{as} \quad r \to 0 , \end{aligned}$$

and this is uniform with respect to $\theta$. A similar proof holds when $\mu = a$ or $b$.

**3.** *The form of equations (1.8) and (1.9) when $z = \mu$ $(0 < \mu < 1)$.*—In this and the subsequent sections we shall make frequent use of the Plemelj formulae of Muskhelishvili (1953, sec. 17). The conditions which our functions will satisfy are not included in those given by him, and we therefore prove the following lemma:

LEMMA II.—*If $\phi(t)$ has a continuous derivative for $0 < t < 1$ and is bounded for $0 \leq t \leq 1$, and if*

$$\Phi(z) = \int_0^1 \frac{\phi(t)}{t-z}\,dt, \tag{3.1}$$

*then, for $0 < \mu < 1$, $\Phi(z) \to \Phi^+(\mu)$ as $z \to \mu$ from above the real axis, $\Phi(z) \to \Phi^-(\mu)$ as $z \to \mu$ from below the real axis, where*

$$\Phi^+(\mu) = \pi i\phi(\mu) + \int_0^1 \frac{\phi(t)}{t-\mu}\,dt, \tag{3.2}$$

$$\Phi^-(\mu) = -\pi i\phi(\mu) + \int_0^1 \frac{\phi(t)}{t-\mu}\,dt, \tag{3.3}$$

*and the integrals are Cauchy principal values.*

We can write

$$\Phi(z) = \int_0^1 \frac{\phi(t)-\phi(\mu)}{t-z}\,dt + \phi(\mu)\log\frac{z-1}{z}, \tag{3.4}$$

where $\log\{(z-1)/z\}$ is real for $z$ real and greater than unity. Let $0 < \eta \leq \mu \leq 1-\eta$. Then $\phi'(t)$ is bounded in the interval $(\eta, 1-\eta)$, and

$$\psi(t, \mu) = \frac{\phi(t)-\phi(\mu)}{t-\mu} \tag{3.5}$$

is uniformly bounded in $(0, 1)$.

From equations (3.4) and (3.5) we have

$$\Phi(z) - \int_0^1 \frac{\phi(t)-\phi(\mu)}{t-\mu}\,dt = \int_0^1 \psi(t, \mu)\frac{z-\mu}{t-z}\,dt + \phi(\mu)\log\frac{z-1}{z}.$$

But, by Lemma I,

$$\int_0^1 \psi(t, \mu)\frac{z-\mu}{t-z}\,dt \to 0$$

as $z \to \mu$ within the sector $\delta \leq |\arg(z-\mu)| \leq \pi - \delta$ $(0 < \delta < \frac{1}{2}\pi)$, and the convergence is uniform for $\eta \leq \mu \leq 1-\eta$ when $\delta$ is fixed. Also, as $z \to \mu$ from above the real axis,

$$\log\frac{z-1}{z} \to \log\frac{1-\mu}{\mu} + i\pi;$$

as $z \to \mu$ from below the real axis,

$$\log\frac{z-1}{z} \to \log\frac{1-\mu}{\mu} - i\pi.$$

Hence

$$\Phi^+(\mu) = \int_0^1 \frac{\phi(t)-\phi(\mu)}{t-\mu}\,dt + \left\{\log\frac{1-\mu}{\mu} + i\pi\right\}\phi(\mu),$$

$$\Phi^-(\mu) = \int_0^1 \frac{\phi(t)-\phi(\mu)}{t-\mu}\,dt + \left\{\log\frac{1-\mu}{\mu} - i\pi\right\}\phi(\mu),$$

whence equations (3.2) and (3.3) follow. Finally, from the uniformity of the convergence for $\eta \leq \mu \leq 1-\eta$ when $z \to \mu$ within the sector $\delta \leq |\arg(z-\mu)| \leq \pi - \delta$, it follows that $\Phi(z)$ is continuous at $z = \mu$ from above and below the real axis (see Muskhelishvili 1953, sec. 14) and hence that equations (3.2) and (3.3) hold when $z \to \mu$ in any manner.

Since $\Psi(u)$ is a polynomial, when $\xi(z)$ and $\eta(z)$ satisfy the conditions of Theorem I, then $\xi(u)\Psi(u)$ and $\eta(u)\Psi(u)$ satisfy the conditions of Lemma II. Hence the Plemelj formulae can be applied to the right-hand sides of equations (1.8) and (1.9) and also to equation (1.4). The latter gives

$$\begin{aligned} \mathfrak{Z}^+(\mu) &= T(\mu) + \pi i \mu \Psi(\mu), \\ \mathfrak{Z}^-(\mu) &= T(\mu) - \pi i \mu \Psi(\mu), \end{aligned} \tag{3.6}$$

where $T(\mu)$ is given by equation (1.12). These are, in fact, true for $-1 < \mu < 1$. If we now let $z \to \mu$ $(0 < \mu < 1)$ from above and below the real axis in equations (1.8) and (1.9) and add the resulting equations, we get equations (1.10) and (1.11).

Conversely, suppose that $\xi(z)$ satisfies conditions i–iv of Theorem I and equation (1.10). By means of equation (1.12), the latter can be written

$$\xi(\mu) = 1 + e^{-\tau/\mu} + \int_0^1 \mu\Psi(u) \frac{[\xi(u) - \xi(\mu)]}{u - \mu}\, du - e^{-\tau/\mu} \int_0^1 \frac{\mu\Psi(u)}{u + \mu}\, \xi(u)\, du + \xi(\mu) \int_0^1 \frac{\Psi(u)}{u + \mu}\, du. \tag{3.7}$$

The function obtained by replacing $\mu$ on the right-hand side of equation (3.7) by $z$ is regular (except for possible poles in the nonconservative case) outside the interval $(-1, 0)$. It equals $\xi(\mu)$ for $0 < \mu < 1$, and hence, by analytic continuation, it equals $\xi(z)$ for all $z$ outside $(-1, 0)$. Rearranging, we have equation (1.8). Similarly for $\eta(z)$.

Formulae (3.6) play an important role in the subsequent reduction of equations (1.8) and (1.9) to Fredholm equations. We shall write[8]

$$Z(\mu) = \mathfrak{Z}^+(\mu)\, \mathfrak{Z}^-(\mu) = \{T(\mu)\}^2 + \pi^2\mu^2\{\Psi(\mu)\}^2. \tag{3.8}$$

In general, $T(\mu)$ and $\mu\Psi(\mu)$ do not vanish together, and we shall assume that this is the case. Then there is a positive constant $K$ such that

$$Z(\mu) \geq K \qquad \text{for} \qquad 0 \leq \mu \leq 1. \tag{3.9}$$

**4.** *The reduction to Fredholm equations; preliminaries.*—Consider the singular integral equation

$$\phi(\mu) T(\mu) - \mu\Psi(\mu) \int_0^1 \frac{\phi(u)}{u - \mu}\, du = f(\mu), \tag{4.1}$$

where $f(\mu)$ is a known function and $\phi(\mu)$ is unknown. *We shall assume that $f(\mu)$ and $\phi(\mu)$ are bounded for $0 \leq \mu \leq 1$, have continuous derivatives for $0 < \mu \leq 1$, and that $\mu\phi'(\mu)$ and $\mu f'(\mu)$ tend to finite limits as $\mu \to +0$.*

Let

$$\Phi(z) \int_0^1 \frac{\phi(u)}{u - z}\, du. \tag{4.2}$$

By the Plemelj formulae (3.2) and (3.3), equation (4.1) can be written

$$[\Phi^+(\mu) - \Phi^-(\mu)] T(\mu) - \pi i \mu \Psi(\mu) [\Phi^+(\mu) + \Phi^-(\mu)] = 2\pi i f(\mu),$$

[8] When $\Psi(\mu) = \frac{1}{2}$,

$$Z(\mu) = \left(1 - \tfrac{1}{2}\mu \log \frac{1+\mu}{1-\mu}\right)^2 + \tfrac{1}{4}\pi^2\mu^2,$$

This function is denoted by $Z(\mu)$ in Kourganoff and Busbridge (1953), formula (29.67). The formula given there is really the Laplace transformation of equation (5.4) below.

or, by formulae (3.6),

$$\Phi^+(\mu)\,\mathfrak{J}^-(\mu) - \Phi^-(\mu)\,\mathfrak{J}^+(\mu) = 2\pi i f(\mu)\,. \tag{4.3}$$

Now let (see eqs. [2.5] and [2.8])

$$\chi(z) = \frac{1}{H(-z)} = H(z)\,\mathfrak{J}(z) = 1 + z\int_0^1 \frac{\Psi(u)\,H(u)}{u-z}\,du\,. \tag{4.4}$$

From this we see that $\chi(z)$ is regular outside the interval $(0, 1)$. Also, if $0 < \mu < 1$,[9]

$$\chi^+(\mu) = H(\mu)\,\mathfrak{J}^+(\mu)\,, \qquad \chi^-(\mu) = H(\mu)\,\mathfrak{J}^-(\mu)\,. \tag{4.5}$$

Since $1/H(z)$ is regular outside the interval $(-1, 0)$, $H(z) \neq 0$ in this domain, and we can divide equation (4.3) by $H(\mu)Z(\mu)$ (see eqs. [3.8] and [3.9]). Then we have, by equation (4.5),

$$\frac{\Phi^+(\mu)}{\chi^+(\mu)} - \frac{\Phi^-(\mu)}{\chi^-(\mu)} = \frac{2\pi i f(\mu)}{H(\mu)\,Z(\mu)}\,. \tag{4.6}$$

Let

$$F(z) = \int_0^1 \frac{f(u)}{H(u)\,Z(u)}\,\frac{du}{u-z} - \frac{\Phi(z)}{\chi(z)}\,. \tag{4.7}$$

Then again applying the Plemelj formulae, it follows from equation (4.6) that

$$F^+(\mu) = F^-(\mu) \qquad (0 < \mu < 1)\,. \tag{4.8}$$

Now $F(z)$ is regular outside the interval $(0, 1)$, except for possible poles at zeros of $\chi(z)$; and, by equation (4.8), it is continuous across the interval $(0, 1)$. Hence it is regular everywhere except, perhaps, for isolated singularities at $z = 0$, $1$, $\infty$ and at the zeros of $\chi(z)$.

We shall now prove that $F(z)$ is regular at 0 and 1. For this we need two lemmas.

LEMMA III.—*Let $g(u)$ be bounded for $0 \leq u \leq 1$, have a continuous derivative for $0 < u < 1$, and let $ug'(u)$ and $(1-u)g'(u)$ tend to finite limits as $u \to +0$ and $u \to 1-0$, respectively. Let*

$$G(z) = \int_0^1 \frac{g(u)}{u-z}\,du\,. \tag{4.9}$$

*Then $zG(z)$ is bounded in the neighborhood of $z = 0$, and $(z-1)G(z)$ is bounded near $z = 1$. Also, if $\alpha > 0$, $z^\alpha G(z) \to 0$ as $|z| \to 0$ for fixed $\arg z \neq 0, \pm 2\pi, \ldots$, and $(z-1)^\alpha G(z) \to 0$ as $|z-1| \to 0$ for fixed $\arg(z-1) \neq \pm\pi, \pm 3\pi, \ldots$.*

It will be sufficient to prove the lemma for the end $z = 0$. When $z \neq 0$ and $0 < \arg z < 2\pi$,

$$zG(z) = \int_0^1 \frac{u\,g(u)}{u-z}\,du - \int_0^1 g(u)\,du\,. \tag{4.10}$$

The derivative of $ug(u)$ tends to a finite limit as $u \to +0$, and therefore $ug(u)$ satisfies the Hölder condition near $u = 0$. Hence (see Muskhelishvili 1953, sec. 16), the first integral is bounded near $z = 0$. Hence $zG(z)$ is bounded near $z = 0$.

Now let $z = re^{i\theta}$, where $0 < \theta < 2\pi$. Then

$$|G(z)| = O\left\{\int_0^1 [(u - r\cos\theta)^2 + r^2\sin^2\theta]^{-1/2}\,du\right\}$$

$$= O\{|\log[r(1-\cos\theta)]|\}\,.$$

[9] $H(z)$ is regular for $\mathrm{R}z < 0$.

Hence for fixed $\theta \neq 0, \pm 2\pi, \ldots,$

$$| z^{a} G(z) | = O(r^{a} | \log r |)$$
$$= o(1) \quad \text{as} \quad r \to 0 .$$

LEMMA IV.—*If* $| \arg z | \leq \pi - \delta < \pi$, *then*

$$H(z) \to 1 \quad \text{as} \quad | z | \to 0 ,$$
$$z H'(z) \to 0 \quad \text{as} \quad | z | \to 0 ,$$

*the convergence being uniform with respect to arg* $z$.

By equation (1.1), with $\mu$ replaced by $z$ ($-\pi < \arg z < \pi$) and with $u$ replaced by $-u$, we obtain

$$\frac{1}{H(z)} - 1 = z \int_{-1}^{0} \frac{\Psi(u) H(-u)}{u - z} \, du . \tag{4.11}$$

Since $\Psi(u)H(-u)$ is bounded in $(-1, 0)$,[10] it follows from the second part of Lemma I that the right-hand side of equation (4.11) tends uniformly to zero as $|z| \to 0$ for $|\arg z| \leq \pi - \delta$.

From equation (4.11), if $| \arg z | < \pi$, we obtain

$$\frac{z H'(z)}{\{H(z)\}^{2}} = - \int_{-1}^{0} \Psi(u) H(-u) \frac{zu}{(u - z)^{2}} \, du . \tag{4.12}$$

But if $|\arg z| \leq \pi - \delta$, $|u/(u - z)| \leq \operatorname{cosec} \delta$ (cf. eq. [2.17]), and so the result again follows from Lemma I.

Now consider $F(z)$ (see eq. [4.7]) near $z = 0$ and 1. By our hypotheses concerning $\phi(u)$ and $f(u)$, by Lemma IV, and from the fact that $Z(u)$ behaves like $[\log (1 - u)]^{2}$ near $u = 1$, it is easy to see that $\phi(u)$ and $f(u)/\{H(u)Z(u)\}$ satisfy the conditions imposed on $g(u)$ in Lemma III. Hence, provided that $1/\chi(z)$ is bounded near $z = 0$ and 1, $zF(z)$ is bounded near $z = 0$, $(z - 1)F(z)$ is bounded near $z = 1$, $z^{a}F(z) \to 0$ as $z \to 0$ for fixed $\arg z \neq 0, \pm 2\pi, \ldots, (z - 1)^{a}F(z) \to 0$ as $z \to 1$ for fixed $\arg z \neq \pm \pi, \ldots,$ and we can take $0 < a < 1$. From the first two statements and the fact that the singularities are isolated, it follows that $F(z)$ has, at most, simple poles at 0 and 1; and from the last two statements it follows that $F(z)$ is, in fact, regular at 0 and 1.

To complete the proof, we have to show that $1/\chi(z)$ is bounded near 0 and 1, where $\chi(z)$ is given by equation (4.4). Since $\Im(z) \to 1$ as $z \to 0$, by Lemma IV $1/\{H(z)\Im(z)\} \to 1$ as $|z| \to 0$ for $|\arg z| \leq \frac{1}{2}\pi$, and $H(-z) \to 1$ as $|z| \to 0$ for $\frac{1}{2}\pi \leq \arg z \leq \frac{3}{2}\pi$. Hence $1/\chi(z)$ is bounded near $z = 0$. Near $z = 1$, $H(z)$ is regular and $H(1) \neq 0$; also $|\Im(z)| \to \infty$ (like $|\log [z - 1]|$) and so $|1/\chi(z)| \to 0$ as $z \to 1$. Thus $1/\chi(z)$ is also bounded near $z = 1$.

We next have to consider the behavior of $F(z)$ for large $z$. From equation (4.2) we have

$$\Phi(z) = - z^{-1} \int_{0}^{1} \phi(u) \, du + O(z^{-2}) . \tag{4.13}$$

Also, from equation (4.4),

$$\{H(-z)\}^{-1} = (1 - h_0) - h_1 z^{-1} + O(z^{-2}) . \tag{4.14}$$

In the conservative case, $h_0 = 1$ (see Chandrasekhar 1950, theorem 1), and equation (4.14) gives, for large $z$,

$$H(-z) = - \frac{z}{h_1} + O(1) . \tag{4.15}$$

[10] $1 \leq H(\mu) \leq H(1)$ for $0 \leq u \leq 1$.

Hence, by equation (4.13),

$$\frac{\Phi(z)}{\chi(z)} = H(-z)\,\Phi(z) = h_1^{-1}\int_0^1 \phi(u)\,du + O(z^{-1}). \tag{4.16}$$

Also the integral in equation (4.7) is $O(z^{-1})$ for large $z$, and so $F(z)$ is bounded as $z \to \infty$.

$\Im(z)$ and, therefore, $\chi(z)$ have no zeros in the conservative case; hence $F(z)$ is regular for all finite $z$ and is therefore a constant. Hence

$$F(z) = -h_1^{-1}\int_0^1 \phi(u)\,du,$$

and, if $z$ lies outside the interval (0, 1),

$$\Phi(z) = H(z)\,\Im(z)\int_0^1 \frac{f(u)}{H(u)Z(u)}\,\frac{du}{u-z} + H(z)\,\Im(z)\,h_1^{-1}\int_0^1 \phi(u)\,du. \tag{4.17}$$

We can now let $z \to \mu$ $(0 < \mu < 1)$ from above and below the real axis. Applying the Plemelj formulae (3.2) and (3.3), taking the difference, using equation (3.6), and dividing by $2\pi i$, we get

$$\phi(\mu) = \frac{f(\mu)T(\mu)}{Z(\mu)} + \mu H(\mu)\Psi(\mu)\,h_1^{-1}\int_0^1 \phi(u)\,du + \mu\Psi(\mu)\,H(\mu)\int_0^1 \frac{f(u)}{H(u)Z(u)}\,\frac{du}{u-\mu}. \tag{4.18}$$

This gives the solution of equation (4.1).

In the nonconservative case, $h_0 \neq 1$, and hence, by equations (4.13) and (4.14),

$$\frac{\Phi(z)}{\chi(z)} = H(-z)\,\Phi(z) = O(z^{-1})$$

for large $z$. Hence $F(z)$ is $O(z^{-1})$.

If $\Im(z)$ has no zeros, $F(z)$ is regular everywhere, and $F(z) \to 0$ as $z \to \infty$; hence

$$F(z) = 0. \tag{4.19}$$

If $\Im(z)$ has simple zeros at $z = \pm 1/k$ $(0 < k < 1)$, then $H(-z)$ has a simple pole at $z = 1/k$. Hence

$$F(z) = \frac{Ak}{kz-1}, \tag{4.20}$$

where, from equation (4.7), $A$ is the residue of

$$-\frac{\Phi(z)}{H(z)\,\Im(z)}$$

at $z = 1/k$. Hence

$$A = -A_0\int_0^1 \frac{\phi(\mu)}{ku-1}\,du, \tag{4.21}$$

where $A_0$ is given by equation (1.23), viz., $k/\{H(1/k)\Im'(1/k)\}$. Equation (4.19) can be included in equation (4.20) by defining $A_0$ to be zero when $\Im(z)$ has no zeros (cf. Theorem IIB).

From equations (4.7), (4.19), and (4.20) we have

$$\Phi(z) = H(z)\,\Im(z)\left\{\int_0^1 \frac{f(u)}{H(u)Z(u)}\,\frac{du}{u-z} - \frac{Ak}{kz-1}\right\}, \tag{4.22}$$

where $A$ is given by equation (4.21). Applying the Plemelj formulae to equation (4.22) as in the conservative case, we get

$$\phi(\mu) = \frac{f(\mu)\,T(\mu)}{Z(\mu)} - \mu\Psi(\mu)\,H(\mu)\,\frac{Ak}{k\mu-1} + \mu\Psi(\mu)\,H(\mu)\int_0^1 \frac{f(u)}{H(u)\,Z(u)}\,\frac{du}{u-\mu}. \tag{4.23}$$

**5.** *Some deductions from the formulae of section 4.*—In this section we obtain some formulae for $H(z)$ which will be needed in sections 6 and 7.

If

$$f(\mu) = \Psi(\mu) \tag{5.1}$$

in equation (4.1), then

$$\phi(\mu) = \Psi(\mu)\,H(\mu)\,. \tag{5.2}$$

Since $\mu H'(\mu) \to 0$ as $\mu \to +0$, the conditions imposed on $f(\mu)$ and $\phi(\mu)$ are satisfied. From equations (4.2) and (2.8), we have

$$\Phi(z) = z^{-1}\{H(z)\,\mathfrak{Z}(z) - 1\}. \tag{5.3}$$

In the conservative case, since

$$\int_0^1 \phi(u)\,du = \int_0^1 \Psi(u)\,H(u)\,du = h_0 = 1\,,$$

therefore equation (4.17) gives

$$1 - \{H(z)\,\mathfrak{Z}(z)\}^{-1} = z\int_0^1 \frac{\Psi(u)}{H(u)\,Z(u)}\,\frac{du}{u-z} + \frac{z}{h_1}.$$

On using equation (2.5) and writing $-z$ for $z$, we have

$$H(z) = 1 + \frac{z}{h_1} + z\int_0^1 \frac{\Psi(u)}{H(u)\,Z(u)}\,\frac{du}{u+z}. \tag{5.4}$$

This holds for $z$ outside the interval $(-1, 0)$.

Equation (4.18) gives, for $0 < \mu < 1$,

$$H(\mu) = \frac{\mu}{h_1}\,H(\mu) + \frac{T(\mu)}{Z(\mu)} + \mu H(\mu)\int_0^1 \frac{\Psi(u)}{H(u)\,Z(u)}\,\frac{du}{u-\mu}. \tag{5.5}$$

In the nonconservative case, equation (4.21) gives

$$A = -A_0\int_0^1 \frac{\Psi(u)\,H(u)}{ku-1}\,du = A_0$$

by equation (2.8) with $z = 1/k$, since $\mathfrak{Z}(1/k) = 0$ in the case $A_0 \neq 0$. Hence equation (4.22) reduces to

$$H(z) = 1 + z\int_0^1 \frac{\Psi(u)}{H(u)\,Z(u)}\,\frac{du}{u+z} + \frac{kA_0 z}{kz+1}. \tag{5.6}$$

This holds for $z$ outside the interval $(-1, 0)$.

Equation (4.23) gives, for $0 < \mu < 1$,

$$H(\mu) = \frac{T(\mu)}{Z(\mu)} + \mu H(\mu)\int_0^1 \frac{\Psi(u)}{H(u)\,Z(u)}\,\frac{du}{u-\mu} - \frac{kA_0\mu}{k\mu-1}\,H(\mu)\,. \tag{5.7}$$

A further formula will be needed in section 7 (nonconservative case). In equation (4.1) take

$$f(\mu) = (1 - h_0)\,\mu\Psi(\mu)\,. \tag{5.8}$$

Equation (2.8) can be written

$$H(z)\,\mathfrak{I}(z) = 1 - h_0 + \int_0^1 \frac{u\Psi(u)\,H(u)}{u - z}\,du\,, \tag{5.9}$$

and, as in section 3, this reduces to

$$H(\mu)\,T(\mu) = 1 - h_0 + \int_0^1 \frac{u\Psi(u)\,H(u)}{u - \mu}\,du \tag{5.10}$$

as $z \to \mu$ $(0 < \mu < 1)$. Equation (4.1) becomes equation (5.10) if

$$\phi(\mu) = \mu\Psi(\mu)\,H(\mu)\,. \tag{5.11}$$

From equations (4.21) and (5.9) we obtain

$$A = -A_0 \int_0^1 \frac{u\Psi(u)\,H(u)}{ku - 1}\,du = \frac{A_0(1 - h_0)}{k}\,, \tag{5.12}$$

since $\mathfrak{I}(1/k) = 0$ when $A_0 \neq 0$. Hence equation (4.23) gives

$$\frac{H(\mu)}{1 - h_0} = \frac{T(\mu)}{Z(\mu)} + H(\mu) \int_0^1 \frac{u\Psi(u)}{H(u)\,Z(u)} \frac{du}{u - \mu} - \frac{A_0}{k\mu - 1}\,H(\mu)\,. \tag{5.13}$$

**6.** *The proof of Theorem IIA.*—In the conservative case, $\xi(\mu)$ and the standard solution $\eta(\mu)$ are such that

$$\xi_0 = 1\,, \qquad \eta_0 = 1\,. \tag{6.1}$$

Then equations (1.10) and (1.11) can be written

$$\xi(\mu)\,T(\mu) = \int_0^1 \frac{u\Psi(u)}{u - \mu}\,\xi(u)\,du + e^{-\tau/\mu} \int_0^1 \frac{u\Psi(u)}{u + \mu}\,\xi(u)\,du\,, \tag{6.2}$$

$$\eta(\mu)\,T(\mu) = \int_0^1 \frac{u\Psi(u)}{u - \mu}\,\eta(u)\,du - e^{-\tau/\mu} \int_0^1 \frac{u\Psi(u)}{u + \mu}\,\eta(u)\,du\,. \tag{6.3}$$

When $\tau = 0$, equation (6.2) has the solution

$$\xi(\mu) = 2\,, \tag{6.4}$$

and this satisfies equations (6.1). Equation (1.11) has the solution $\eta(\mu) = 0$ and therefore (see sec. 1) equation (6.3) has the solution $\eta(\mu) = C\mu$, where, from equations (6.1), we obtain

$$C = \frac{1}{\int_0^1 u\Psi(u)\,du}\,.$$

Hence the standard solution when $\tau = 0$ is

$$\eta(\mu) = \frac{\mu}{\int_0^1 u\Psi(u)\,du}\,. \tag{6.5}$$

Solutions (6.4) and (6.5) provide a useful check on our working.

Since $h_0 = 1$, on comparing equations (6.2) and (6.3) with (5.10), we see that, when $\tau = \infty$,

$$\xi(\mu) = H(\mu), \qquad \eta(\mu) = H(\mu). \tag{6.6}$$

We now show that equation (6.2) can be reduced to equation (1.14). The reduction of equation (6.3) to equation (1.15) is simply obtained by changing the sign of every exponential term. We shall therefore deal only with $\xi(\mu)$.

If $\xi(z)$ satisfies the conditions of Theorem IA, then $\mu\xi'(\mu) \to 0$ as $\mu \to +0$. Hence if in equation (4.1) we take

$$\phi(\mu) = \mu\Psi(\mu)\,\xi(\mu), \tag{6.7}$$

$$f(\mu) = \mu\Psi(\mu)\, e^{-\tau/\mu}\int_0^1 \frac{u\Psi(u)}{u+\mu}\,\xi(u)\,du, \tag{6.8}$$

then $\mu\phi'(\mu)$ tends to a finite limit as $\mu \to +0$, and it is easy to verify that the same is true of $\mu f'(\mu)$. Hence the conditions stated in italics at the beginning of section 4 are clearly satisfied. With the values (6.7) and (6.8), equation (4.1) reduces to equation (6.2).

Substituting from equations (6.7) and (6.8) in equation (4.18), we get

$$\begin{aligned}\xi(\mu) = {} & \frac{T(\mu)}{Z(\mu)}\, e^{-\tau/\mu}\int_0^1 \frac{u\Psi(u)}{u+\mu}\,\xi(u)\,du + \frac{\xi_1}{h_1}H(\mu) \\ & + H(\mu)\int_0^1 \frac{t\Psi(t)\, e^{-\tau/t}}{H(t)\,Z(t)}\,\frac{dt}{t-\mu}\int_0^1 \frac{u\Psi(u)}{t+u}\,\xi(u)\,du.\end{aligned} \tag{6.9}$$

The inversion of the order of integration in the double integral is justified (cf. Muskhelishvili 1953, sec. 23), and we have

$$\xi(\mu) = \frac{\xi_1}{h_1}H(\mu) + \int_0^1 n(u,\mu)\,\xi(u)\,du, \tag{6.10}$$

where

$$n(u,\mu) = e^{-\tau/\mu}\frac{T(\mu)\Psi(u)}{Z(\mu)}\,\frac{u}{u+\mu} + u\Psi(u)\,H(\mu)\int_0^1 \frac{t\Psi(t)\, e^{-\tau/t}}{H(t)\,Z(t)}\,\frac{dt}{(t-\mu)(t+u)}. \tag{6.11}$$

This proves equations (1.14) and (1.16) of Theorem IIA.

In order to prove equation (1.18) and hence the boundedness of $n(u,\mu)$ for $0 \le \mu \le 1$, we put $\tau = 0$ in equation (6.11). Denoting the resulting kernel by $n_0(u,\mu)$, we have

$$n_0(u,\mu) = \frac{u\Psi(u)}{u+\mu}\left\{\frac{T(\mu)}{Z(\mu)} + H(\mu)\int_0^1 \frac{\Psi(t)}{H(t)\,Z(t)}\left(\frac{\mu}{t-\mu}+\frac{u}{t+u}\right)dt\right\}. \tag{6.12}$$

By equations (5.4) and (5.5), this becomes

$$n_0(u,\mu) = \frac{u\Psi(u)}{u+\mu}\,H(\mu)\left\{H(u) - \frac{u+\mu}{h_1}\right\}. \tag{6.13}$$

Subtracting $e^{-\tau/\mu}$ times equation (6.12) from equation (6.11) and using equation (6.13), we have

$$\begin{aligned}n(u,\mu) = {} & \left\{\frac{u\Psi(u)\,H(u)\,H(\mu)}{u+\mu} - \frac{u}{h_1}\Psi(u)\,H(\mu)\right\}e^{-\tau/\mu} \\ & + u\Psi(u)\,H(\mu)\int_0^1 \frac{t\Psi(t)}{H(t)\,Z(t)}\,\frac{e^{-\tau/t} - e^{-\tau/\mu}}{t-\mu}\,\frac{dt}{t+u},\end{aligned} \tag{6.14}$$

and this is equation (1.18).

It is easy to verify from equations (6.10) and (6.14) that equation (6.4) gives a solution when $\tau = 0$ and that equation (6.5) gives a solution of equation (1.15) when $\tau = 0$.

In equations (6.10) and (6.14) we can replace $\mu$ by $z$, provided that $z$ lies outside the interval $(-1, 0)$. The quantity $H(z)$ is not defined in this interval. Consider $n(u, z)$, which is regular in this domain. We have

$$\frac{e^{-\tau/t} - e^{-\tau/z}}{t - z} = \frac{1}{t - z}\int_z^t \frac{\tau}{\zeta^2}\, e^{-\tau/\zeta} d\zeta\,, \tag{6.15}$$

where the path of integration is the straight line joining $z$ to $t$. Let $z = re^{i\theta}$, where $|\theta| \leq \delta < \frac{1}{2}\pi$, and let $\zeta = \rho e^{i\phi}$. Then $|\phi| \leq \delta$ and

$$\left|\frac{\tau}{\zeta^2} e^{-\tau/\zeta}\right| \leq \frac{\tau}{\rho^2} e^{-(\tau\cos\delta)/\rho}$$

$$\leq 4\, e^{-2}\tau^{-1}\sec^2\delta \qquad (\tau > 0)$$

for all $\rho$. Hence equation (6.15) gives

$$\left|\frac{e^{-\tau/t} - e^{-\tau/z}}{t - z}\right| \leq 4\, e^{-2}\tau^{-1}\sec^2\delta\,, \tag{6.16}$$

and this bound tends to zero as $\tau \to \infty$.

Since $H(z) \to 1$ as $r \to 0$ for $|\theta| \leq \delta$ (Lemma IV), therefore $H(z)$ is bounded for $|\theta| \leq \delta$, $0 \leq r \leq R < \infty$. Also, if $0 \leq u \leq 1$ and $0 \leq t \leq 1$, then $H(t) \geq 1$, $Z(t) \geq K$ (by eq. [3.9]), and

$$|\, e^{-\tau/z}| \leq e^{-(\tau\cos\delta)/R}\,, \qquad \left|\frac{u}{u+z}\right| \leq 1\,, \qquad \left|\frac{t}{t+u}\right| \leq 1\,.$$

Hence $n(u, z)$ is bounded, and the bound tends to zero as $\tau \to \infty$. In particular, for sufficiently large $\tau$,

$$|\, n\,(u,\, \mu)\,| \leq \lambda < 1 \qquad (0 \leq \mu \leq 1\,,\ 0 \leq u \leq 1)\,. \tag{6.17}$$

Since $H(\mu)$ is bounded in $(0, 1)$, it follows that the Neumann series obtained by iteration of equation (6.10) converges to a function $\xi(\mu)$, which is bounded in $(0, 1)$. The series will be multiplied by the constant $\xi_1/h_1$, and this is determined by the condition $\xi_0 = 1$.

Because $\xi(\mu)$ exists and is bounded for $0 \leq \mu \leq 1$, equation (6.10), with $\mu$ replaced by $z$, defines $\xi(z)$. Because of the analytic properties of $H(z)$ and $n(u, z)$, it is an analytic function regular outside the interval $(-1, 0)$, and it is bounded as $|z| \to 0$ in the angle $|\arg z| \leq \delta$. Since $H(z)$ is $O(z)$ for large $z$, it is easily seen from equations (6.10) and (6.14) that $\xi(z)$ is $O(z)$ for large $z$.

When $|\arg z| < \pi$ and $0 < |z| < \infty$, differentiation under the integral sign in equations (6.10) and (6.14) (with $\mu$ replaced by $z$) is permissible. Since $zH'(z) \to 0$ as $|z| \to 0$ for $|\arg z| \leq \pi - \delta\,(\delta > 0)$, in order to prove that $z\xi'(z) \to 0$ as $|z| \to 0$ for $|\arg z| \leq \delta$ $(0 < \delta < \frac{1}{2}\pi)$, it is sufficient to prove that $z(\partial/\partial z)n(u, z) \to 0$ as $|z| \to 0$ uniformly for $0 \leq u \leq 1$ when $|\arg z| \leq \delta$. By Lemma IV, this will be the case if there is a constant $\kappa$ such that

$$\left|\frac{\partial}{\partial z}\left\{\frac{e^{-\tau/t} - e^{-\tau/z}}{t - z}\right\}\right| \leq \kappa \tag{6.18}$$

for $0 \leq t \leq 1$ and sufficiently small $|z|$. If

$$f(z) = e^{-\tau/z}\,,$$

then

$$|\, f''(z)\,| = |\, e^{-\tau/z}(\tau^2 z^{-4} - 2\tau z^{-3})\,| \qquad (|\,z\,| > 0)$$

$$\leq e^{-(\tau\cos\delta)/r}(\tau^2 r^{-4} + 2\tau r^{-3})\,.$$

When $\tau > 0$, this tends to zero as $r \to 0$, and so there is a constant $\kappa = \kappa(\tau, \delta)$ such that

$$| f''(z) | \leq \kappa \tag{6.19}$$

for $|\arg z| \leq \delta$ and sufficiently small $|z|$. Now

$$\frac{\partial}{\partial z}\left\{\frac{e^{-\tau/t} - e^{-\tau/z}}{t - z}\right\} = \frac{1}{(t-z)^2}\int_z^t d\zeta \int_z^\zeta f''(u)\, du,$$

where $\zeta$ lies on the straight line joining $z$ to $t$. From this and equation (6.19), equation (6.18) immediately follows. This proves property iii of Theorem IA.

So far we have shown only that $\xi(z)$ is regular outside the interval $(-1, 0)$. If $\xi(z)$ satisfies equation (1.8), then $\xi(-z) = e^{\tau/z}\xi(z)$, and $\xi(z)$ must, in fact, be regular for $|z| > 0$. Hence all that remains to be proved is that our solution $\xi(z)$ does satisfy equation (1.8) or that $\xi(\mu)$ satisfies equation (6.2). To do this, it is easiest to reverse the steps by which equation (6.10) was obtained from equation (6.2).

If $f(\mu)$ and $\phi(\mu)$ are defined by equations (6.7) and (6.8), then equation (6.9) is the same as equation (4.18). If we can show that equation (4.18) implies equation (4.17), where

$$\Phi(z) = \int_0^1 \frac{\phi(u)}{u - z}\, du, \tag{6.20}$$

then it will follow that

$$\frac{\Phi^+(\mu)}{H(\mu)\,\mathfrak{Z}^+(\mu)} - \frac{\Phi^-(\mu)}{H(\mu)\,\mathfrak{Z}^-(\mu)} = \frac{2\pi i f(\mu)}{H(\mu) Z(\mu)};$$

whence

$$\Phi^+(\mu)\,\mathfrak{Z}^-(\mu) - \Phi^-(\mu)\,\mathfrak{Z}^+(\mu) = 2\pi i f(\mu).$$

This is equation (4.3), which is equivalent to equation (4.1), i.e., to equation (6.2).

Thus we have only to show that, if

$$\Omega(z) = H(z)\,\mathfrak{Z}(z)\left\{\int_0^1 \frac{f(u)}{H(u) Z(u)} \frac{du}{u - z} + h_1^{-1}\int_0^1 \phi(u)\, du\right\}, \tag{6.21}$$

if $\phi(u)$ satisfies equation (4.18), and if $\Phi(z)$ is defined by equation (6.20), then

$$\Omega(z) = \Phi(z).$$

Since $H(z)\mathfrak{Z}(z) = 1/H(-z)$, $\Omega(z) - \Phi(z)$ is regular outside the interval $(0, 1)$. Also, from equations (6.20), (6.21), and (4.18), by the Plemelj formulae,

$$\Omega^+(\mu) - \Omega^-(\mu) = \Phi^+(\mu) - \Phi^-(\mu),$$

and thus

$$[\Omega(\mu) - \Phi(\mu)]^+ = [\Omega(\mu) - \Phi(\mu)]^-.$$

Hence $\Omega(z) - \Phi(z)$ is continuous across the interval $(0, 1)$, and it is therefore regular everywhere except, perhaps, at 0, 1, and $\infty$. These may be isolated singularities.

Since $\mu\xi'(\mu) \to 0$ as $\mu \to +0$, therefore, from equations (6.7) and (6.8), $\mu\phi'(\mu)$ and $\mu f'(\mu)$ tend to finite limits as $\mu \to +0$. It follows by an argument based on Lemmas III and IV and similar to that used in section 4 that $\Omega(z) - \Phi(z)$ is regular at $z = 0$. At $z = 1$, however, trouble arises from $\mathfrak{Z}(z)$, which behaves like $\log(z - 1)$.

By Lemma III (cf. sec. 4), $(z - 1)\Omega(z)/\mathfrak{Z}(z)$ and $(z - 1)\Phi(z)$ are bounded near $z = 1$. Since, for $0 < \alpha < 1$,

$$(z - 1)^\alpha \mathfrak{Z}(z) \to 0 \qquad \text{as} \qquad z \to 1$$

therefore

$$(z-1)^{1+\alpha}\,[\Omega(z)-\Phi(z)]\to 0$$

as $z\to 1$. It follows that $\Omega(z)-\Phi(z)$ has, at most, a simple pole at $z=1$.

Since, by equation (4.14),

$$H(z)\,\mathfrak{Z}(z) = -h_1 z^{-1}+O(z^{-2}) \tag{6.22}$$

for large $z$, $\Omega(z)-\Phi(z)$ tends to zero as $z\to\infty$, and it follows that

$$\Omega(z)-\Phi(z) = \frac{A}{z-1}, \tag{6.23}$$

where $A$ is a constant. For large $z$, from equations (6.20), (6.21), and (6.22) we obtain

$$\begin{aligned}\Omega(z)-\Phi(z) &= -z^{-1}\int_0^1 \phi(u)\,du + z^{-1}\int_0^1 \phi(u)\,du + O(z^{-2})\\ &= O(z^{-2}).\end{aligned}$$

Hence $A=0$ in equation (6.23) and

$$\Omega(z)=\Phi(z).$$

This completes the proof of Theorem IIA.

**7.** *Theorem IIB.*—Having proved Theorem IIA in detail, we shall only show how the formulae of Theorem IIB are obtained.

In the nonconservative case, equations (1.10) and (1.11) can be written

$$\begin{aligned}\xi(\mu)\,T(\mu) = (1+e^{-\tau/\mu})(1-\xi_0) &+ \int_0^1 \frac{u\Psi(u)}{u-\mu}\,\xi(u)\,du\\ &+ e^{-\tau/\mu}\int_0^1 \frac{u\Psi(u)}{u+\mu}\,\xi(u)\,du,\end{aligned} \tag{7.1}$$

$$\begin{aligned}\eta(\mu)\,T(\mu) = (1-e^{-\tau/\mu})(1-\eta_0) &+ \int_0^1 \frac{u\Psi(u)}{u-\mu}\,\eta(u)\,du\\ &- e^{-\tau/\mu}\int_0^1 \frac{u\Psi(u)}{u+\mu}\,\eta(u)\,du.\end{aligned} \tag{7.2}$$

Hence, as in equation (6.7), we take

$$\phi(\mu) = \mu\Psi(\mu)\,\xi(\mu), \tag{7.3}$$

but we take

$$f(\mu) = \mu\Psi(\mu)\left\{(1+e^{-\tau/\mu})(1-\xi_0) + e^{-\tau/\mu}\int_0^1 \frac{u\Psi(u)}{u+\mu}\,\xi(u)\,du\right\}. \tag{7.4}$$

Then equation (4.1) becomes equation (7.1).

Equation (4.23) gives

$$\begin{aligned}\xi(\mu) = \frac{T(\mu)}{Z(\mu)}\Big\{&(1+e^{-\tau/\mu})(1-\xi_0) + e^{-\tau/\mu}\int_0^1 \frac{u\Psi(u)}{u+\mu}\,\xi(u)\,du\Big\}\\ &+ H(\mu)\int_0^1 \frac{t\Psi(t)}{H(t)Z(t)}\,\frac{e^{-\tau/t}}{t-\mu}\,dt\int_0^1 \frac{u\Psi(u)}{u+t}\,\xi(u)\,du\\ &+ H(\mu)(1-\xi_0)\int_0^1 \frac{t\Psi(t)}{H(t)Z(t)}\,(1+e^{-\tau/t})\,\frac{dt}{t-\mu} - \frac{Ak}{k\mu-1}\,H(\mu),\end{aligned} \tag{7.5}$$

where, by equation (4.21),

$$A = -A_0 \int_0^1 \frac{u\Psi(u)\,\xi(u)}{ku-1}\,du. \tag{7.6}$$

On inverting the double integral in equation (7.5), we get

$$\xi(\mu) = g(\mu) + \int_0^1 n(u,\mu)\,\xi(u)\,du, \tag{7.7}$$

where $n(u, \mu)$ is given by equation (6.11) (or by eq. [1.16]) and

$$\begin{aligned} g(\mu) = (1-\xi_0)(1+e^{-\tau/\mu})\frac{T(\mu)}{Z(\mu)} - \frac{Ak}{k\mu-1}H(\mu) \\ + (1-\xi_0)H(\mu)\int_0^1 \frac{t\Psi(t)}{H(t)Z(t)}(1+e^{-\tau/t})\frac{dt}{t-\mu}. \end{aligned} \tag{7.8}$$

On subtracting from this $(1-\xi_0)(1+e^{-\tau/\mu})$ times equation (5.13), we get

$$\begin{aligned} g(\mu) = (1+e^{-\tau/\mu})\frac{1-\xi_0}{1-h_0}H(\mu) + \{A_0(1-\xi_0)(1+e^{-\tau/\mu}) - Ak\}\frac{H(\mu)}{k\mu-1} \\ + (1-\xi_0)H(\mu)\int_0^1 \frac{t\Psi(t)}{H(t)Z(t)}\frac{e^{-\tau/t}-e^{-\tau/\mu}}{t-\mu}\,dt, \end{aligned} \tag{7.9}$$

and this becomes equation (1.21) on using equation (7.6).

To get the second form for $n(u, \mu)$, we again put $\tau = 0$ in equation (6.11), giving equation (6.12), and this, by equations (5.6) and (5.7), is

$$\eta_0(u,\mu) = \frac{u\Psi(u)\,H(u)\,H(\mu)}{u+\mu} + \frac{A_0 ku\Psi(u)\,H(\mu)}{(k\mu-1)(ku+1)}. \tag{7.10}$$

Hence we get the form (1.24) for $n(u, \mu)$.

When $\Im(1/k) = 0$, it follows from equation (1.4) with $z = 1/k$ that

$$k\int_0^1 \frac{u\Psi(u)}{ku+1}\,du + k\int_0^1 \frac{u\Psi(u)}{ku-1}\,du = 2\int_0^1 \Psi(u)\,du - 1. \tag{7.11}$$

From equations (7.10) and (7.11), with the aid of the relation

$$(1-h_0)^2 = 1 - 2\int_0^1 \Psi(u)\,du \tag{7.12}$$

(see Chandrasekhar 1950, theorem 1), it is easy to verify that $\xi(\mu) = 2$ is a solution of equation (7.7) when $\tau = 0$.

The solution obtained from equation (7.7) by iteration when $|n(u, \mu)| \leq \lambda < 1$ (i.e., for sufficiently large $\tau$) will be of the form

$$\xi(\mu) = (1-\xi_0)\,\xi_1(\mu) + A\,\xi_2(\mu),$$

and the constants $\xi_0$ and $A$ are uniquely determined by equation (7.6) and

$$\xi_0 = \int_0^1 \Psi(u)\,\xi(u)\,du.$$

In equations (1.21) and (1.24), $\mu$ can be replaced by $z$, provided that $z$ lies outside the interval $(-1, 0)$. When $\Im(z)$ has zeros (so that $A_0 \neq 0$), $H(z)$ has a simple pole at $z = -1/k$, and it is easily seen that $\xi(z)$must therefore have simple poles at $z = \pm 1/k$.

**8.** *Concluding remarks.*—In section 6 we have proved the existence of $\xi(\mu)$ only for sufficiently large $\tau$, but it can be verified that equations (1.14) and (1.15) have solutions (6.4) and (6.5) when $\tau = 0$. Hence the existence of solutions for small $\tau$ seems probable, and this point needs further investigation.

Assuming their existence, Chandrasekhar and Elbert have published tables of $X$- and $Y$-functions for $\Psi(u) = \frac{1}{2}\hat{\omega}_0$ $(0 < \hat{\omega}_0 \leq 1)$ and $0 < \tau \leq 1$ (see Chandrasekhar and Elbert 1952). These were obtained by iterating equations (1.5) and (1.6), starting from a first approximation given by Chandrasekhar (1950, chap. viii). Some trouble, however, was found with the convergence of the iterations, especially for the larger values of $\tau$.

When $|n(u, \mu)| \leq \lambda < 1$, the homogeneous equation

$$\phi(\mu) = \int_0^1 n(u, \mu)\, \phi(u)\, du$$

has no solution other than $\phi(\mu) = 0$, and so the solutions found for sufficiently large $\tau$ are unique, but for small $\tau$ further investigation is necessary.

## REFERENCES

Chandrasekhar, S. 1947, "The Transfer of Radiation in Stellar Atmospheres," *Bull. Amer. Math. Soc.*, **53**, 641.

———. 1948, "On the Radiative Equilibrium of a Stellar Atmosphere. XXII," *Ap. J.*, **107**, 48.

———. 1950, *Radiative Transfer* (London: Oxford University Press), chaps. v and viii.

Chandrasekhar, S., and Elbert, Donna. 1952, "The $X$- and $Y$-Functions for Isotropic Scattering. I and II," *Ap. J.*, **115**, 244.

Crum, M. M. 1947, "An Integral Equation of Chandrasekhar," *Quart. J. Math.* (Oxford), **18**, 244.

Kourganoff, V., and Busbridge, I. W. 1952, *Basic Methods in Transfer Problems* (London: Oxford University Press), sec. 29.

Muskhelishvili, N. I. 1953, *Singular Integral Equations*, trans. J. R. M. Radok (Leiden: Noordhoff).

# NOTES

## AURORAL RAYS AS ELECTRIC-DISCHARGE PHENOMENA

Although auroral arcs appear to be associated with incident protons (Meinel 1951) and, in fact, are probably produced by these protons (and possibly other particles), auroral rays have not yet been satisfactorily explained. Actually, there is a number of indications that rays are not produced directly by incident particles but rather by some other form of excitation.

The most remarkable feature about rays is their nearly constant luminosity over a very large range in altitude and atmospheric density. It seems likely, however, from qualitative considerations that an ionospheric discharge might produce just such a luminosity-curve, if the electric field does not change too rapidly with height. Thus, if the atoms and molecules are excited by inelastic collisions with electrons, the luminosity will tend to decrease with height because of the decrease in atmospheric density; but, on the other hand, the greater mean free path at higher altitudes would allow more electrons to reach the threshold energy for excitation. It is conceivable that under certain conditions these two effects would just compensate each other. Hence a quantitative but provisional investigation of this problem has been undertaken, and some of the results are summarized in this note.

To ascertain the amount of excitation occurring within a given electric field, we need, first, to derive the energy distribution of the electrons. For the case wherein electrons lose much of their energy by inelastic collisions, accurate distribution-curves are not easily computed, but I have obtained approximate curves by numerical solutions of an integrodifferential equation derived by Smit (1936). These energy distributions have also been used to derive the mean drift velocity along the field by a method originated by Lorentz, and the condition has been adopted that the electron current density in a ray is constant with height.

Application of these computations to the auroral problem indicates that a very long ray with nearly constant luminosity in the green [O I] line can, in fact, be expected under certain conditions: (1) There must, of course, be some means of creating and maintaining a field (and current) of sufficient strength. It is found that the current density necessary to produce the observed brightness of an average ray is about $6 \times 10^{12}$ electrons/cm$^2$ sec, if the ray is $10^4$ cm in diameter. (2) Since at any point the field and drift velocity depend on the electron density, the latter must have a particular distribution with height in order to produce a constant-luminosity ray. The calculations indicate that $N_e$ is about $10^6$ cm$^{-3}$ in the lower part of the ray and slowly decreases with height. This electron density is somewhat higher than we would encounter in the undisturbed ionosphere, although the theory does indicate values much lower than the $10^8$ electrons/cm$^3$ that are thought by many auroral physicists to exist in *arcs*. Moreover, an examination of ionization and recombination in the ray indicates that an electron density of the correct order of magnitude would be maintained by such a discharge.

The electron current density stated earlier is rather uncertain, largely because of the uncertainty in the cross-sectional area of the rays. The particle flux required to produce an arc has been estimated at between $10^7$ and $10^8$ protons/cm$^2$ sec (Chamberlain 1954), but again the data used were necessarily very approximate. Hence we can state only that a comparison of the arc and the ray theories indicates electron current *densities* several orders of magnitude greater than those for protons. Since rays occupy only a small

fraction of the horizontal area covered by an arc, however, the *total* electron and proton currents may well be equal. Thus it is reasonable to think that ionospheric electrons may be accelerated downward by the pull of the protons (which would penetrate much deeper into the atmosphere than electrons entering with, say, the same velocity). A constriction of the electron flow along narrow paths is observed in laboratory discharges under certain conditions, but it is hypothetical whether it would occur in aurorae. Since the region of the arc is likely to have a comparatively high conductivity, the arc (i.e., the region of proton influx) might recede and leave rays in the same position as that in which they were originally formed in the atmosphere.

A more complete paper, giving details of the theory and computations, is in preparation for publication elsewhere.[1] The research reported in this note has been supported in part by the Geophysical Research Directorate of the Air Force Cambridge Research Center, Air Research and Development Command, under Contract AF 19(122)-480 with the University of Chicago.

JOSEPH W. CHAMBERLAIN

YERKES OBSERVATORY
June 15, 1955

REFERENCES

Chamberlain, J. W. 1954, *Ap. J.*, **120**, 360.
Meinel, A. B. 1951, *Ap. J.*, **113**, 50.
Smit, J. A. 1936, *Physica*, **3**, 543.

[1] To be published in *J. Atmos. Terr. Phys. Supplement 3: The Airglow and Aurora*, ed. A. Dalgarno and E. Armstrong (London: Pergamon Press). In this paper the variations in ray spectra with height and collisional de-excitation of [*O* I] are also discussed quantitatively.

---

## IS HELIUM A COMPONENT OF AURORAL PARTICLES?*

Spectroscopic studies of the optical emission of air bombarded by high-energy protons, $He^+$ ions, and $Ne^+$ ions, with the purpose of investigating the excitation mechanisms of the aurora borealis, have been previously reported (Fan and Meinel 1953). It was found that, with the spectrograph aligned along the direction of the incident beam, a proton-induced spectrum invariably showed Doppler-shifted hydrogen lines, resulting from electron capture by the incident protons. A similar blueward shift has been observed for $H\alpha$ in the spectrum of an auroral arc (Meinel 1954). It seemed puzzling, however, that no Doppler-shifted *He* and *Ne* lines were found in the $He^+$- and $Ne^+$-induced spectra, respectively.

The experiments to which reference has been made were done with the kevatron of the Institute for Nuclear Studies of the University of Chicago. Because of the limited beam intensity available then, the pressures of the air sample used in these experiments were about $10^{-1}$ mm *Hg* or higher, so that the exposure time of each spectrum would not be intolerably long. It then became apparent that the pressures were too high for the spectroscopic studies of charge-exchange phenomena because of the effect of collisional de-excitation. Indeed, the recent measurement by Krasner (1955) gives $7 \times 10^{-16}$ cm$^2$ as the average electron-loss cross-section for *He* atoms (120–450 kev) in air. At an air pressure of $10^{-1}$ mm *Hg*, the mean life of the first bound electron of an *He* atom is only $10^{-9}$ second. Therefore, an excited *He* atom would have lost its electron before the optical transition could occur. This explains the failure to detect Doppler-shifted *He* lines in our earlier experiments.

* The research reported in this paper was supported in part by the Geophysics Research Directorate of the Air Force Cambridge Research Center, Air Research and Development Command, under Contract AF 19(122)-480.

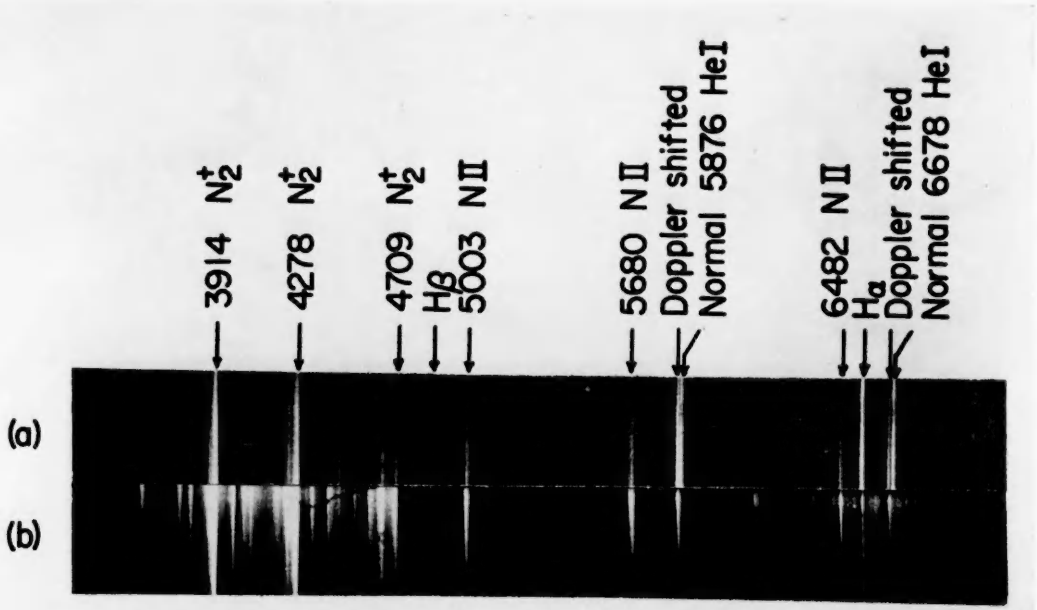


Fig. 1 Spectra excited by 10 Kev. $He^+$ ions
(a) Air pressure about $10^{-4}$ mm-Hg
(b) Air pressure about $10^{-3}$ mm-Hg

FIG. 1.—Emission spectra of air by 10-kev $He^+$ ion bombardment

A 30-kv ion accelerator has recently been constructed at the Yerkes Observatory. It produces protons or $He^+$ ions with a total beam intensity of several hundred microamperes. With this accelerator, the experiments of $He^+$ ion excitation were repeated at much lower pressures, spectra being obtained with the nebular grating-spectrograph of the McDonald Observatory on Eastman 103*a*-F(3) film, as in the earlier experiments. Figure 1 shows two of the spectra produced by 10-kev $He^+$ ions; Doppler-shifted *He* lines are now clearly shown in the spectra.

The first spectrum in Figure 1 was taken at an air pressure of about $10^{-4}$ mm *Hg*. The pressure was so low that there was a sufficient amount of helium gas collected in the absorption chamber to produce stationary *He* lines under the bombardment of $He^+$ ions. These lines have served as a wave-length scale to indicate the amount of Doppler shift of the *He* lines produced by the impinging particles. The second spectrum was taken at a pressure of $10^{-3}$ mm *Hg*. The absence of the stationary lines indicates that the process of charge exchange occurs indeed between $He^+$ ions and air molecules. If the Doppler-shifted helium emission were produced by charge exchange between $He^+$ and *He* collected in the chamber, the relative intensity of the Doppler-shifted and the stationary lines would not change with gas pressure. The difference between the two intensity ratios "Doppler-shifted 5876/Doppler-shifted 6678" and "stationary 5876/stationary 6678" is rather interesting. The difference in the decrements apparently reflects a difference in the dominant excitation processes operating: electron capture from air molecules for the shifted lines and direct excitation from the ground state for the stationary lines.

In an auroral spectrum, the position of λ 6678 blends with the intense λ 6705 band of the first positive system of $N_2$. On the other hand, the position of λ 5876 is relatively unobscured. Furthermore, for an equal amount of $He^+$ ions and protons at the same velocity, the $He^+$ ions will produce more than twice the luminosity in air than will the protons. This can be inferred from the ratio of the total available energies, as well as from the ratio of the ionization cross-sections (Fan and Meinel 1953). In view of the high relative intensity of λ 5876 in the $He^+$-induced spectrum, this line is likely to be detectable in an auroral spectrum, should auroral particles be composed of 5 per cent or more of helium ions. There is no conclusive evidence in the literature that this line has ever been observed. It appears that high-dispersion spectra of quiet arcs are needed to decide whether the line is truly missing or has been overlooked because of obscuration by the weak but complicated first positive bands in this region.

C. Y. Fan

Yerkes Observatory
Williams Bay, Wisconsin
May 24, 1955

REFERENCES

Fan, C. Y., and Meinel, A. B. 1953, *Ap. J.*, **118**, 205.
Krasner, S. 1955, to be published in *Phys. Rev.*
Meinel, A. B. 1951, *Ap. J.*, **113**, 50.

## ON CERTAIN REGULARITIES IN THE STRUCTURE OF COMPLEX TERM SPECTRA*

Catalan, Rohrlich, and Shenstone (1954) have recently discovered certain "astonishing and unexplained regularities" in the term spectra of atoms belonging to the first two long periods. The present note offers a qualitative, theoretical interpretation of these regularities.

* The research reported in this paper has been supported by the Geophysics Research Directorate, Air Force Cambridge Research Center, under Contract AF19(604)-146 with Harvard University.

Let $E(C, T; Z)$ denote the energy of a term $T$ of the configuration $C$ in an atom of atomic number $Z$. We are concerned mainly with the ground terms $T_g$ of the configurations $d^n$ and $d^{n-1}s$ ($n = 1, 2, \ldots, 10$) in the first two long periods. Let $D_1(n; Z)$ denote the interval between the ground term of $d^n$ and the ground term of $d^{n-1}s$ in an atom belonging to the first long period:

$$D_1(n; Z) = E(3d^n T_g; Z) - E(3d^{n-1}4sT_g; Z); \tag{1a}$$

and let $D_2(n; Z)$ denote the same interval in an atom belonging to the second long period:

$$D_2(n; Z) = E(4d^n T_g; Z) - E(4d^{n-1}5sT_g; Z). \tag{1b}$$

Catalan *et al.* plotted the intervals $D_1$ and $D_2$ against $n$ for the successive spectra: I (arc), II (spark), etc. For any given spectrum (i.e., stage of ionization) the functions $D_1$ and $D_2$

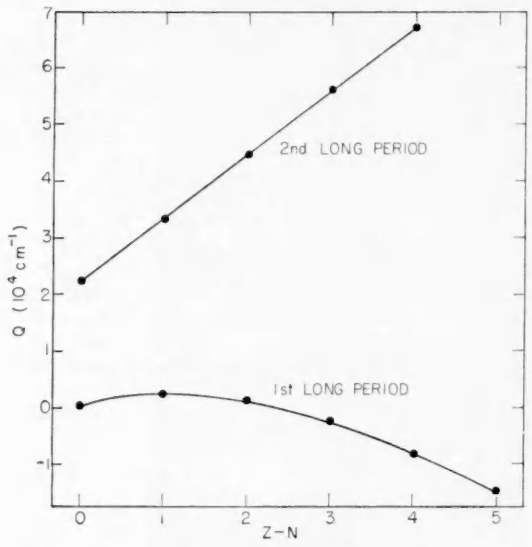


FIG. 1.—Variation of $Q$ with $Z$ in the first two long periods

vary with $n$ in a way that is nearly independent of the stage of ionization. They were able to account theoretically for the main features of this variation. But they also found that $D_1$ and $D_2$ varied in a surprisingly systematic way from one spectrum to the next. Let $Q_i(Z)$ denote the difference between the first interval $D_i(1; Z)$ in a given spectrum and the last interval $D_i(10; Z - 1 + 9)$ in the preceding spectrum:

$$Q_i(Z) = D_i(1; Z+1) - D_i(10; Z+8). \tag{2}$$

Figure 1, which is adapted from Figure 9 of the paper cited previously, shows how $Q$ varies with $Z$ in the first two long periods.

Catalan *et al.* emphasized the linearity of $Q_2$ and the small numerical values of $Q_1$.

To predict how $Q_1$ and $Q_2$ depend on $Z$, we use the following formula (Layzer 1955):

$$E(C, T; Z) = R(E_2Z^2 + E_1Z + E_0 + E_{-1}Z^{-1} + \ldots), \tag{3}$$

where

$$E_2 = -\sum_{i=1}^{N} n_i^{-2}. \tag{4}$$

In equation (3) $R$ is the Rydberg constant, which varies slowly with $Z$, but may be set equal to $R_\infty$ in the present discussion. In equation (4), $n_i$ is the principal quantum number of the $i$th electron, and the summation extends over all $N$ electrons. Formula (4) for $E_2$ is rigorous.

Evaluating the right-hand side of definition (2), with the help of definitions (1*a*)and (1*b*) and formulae (3) and (4), we obtain

$$Q_i(Z) = A_i Z + B_i + O(Z^{-1}), \tag{5}$$

where $A_i$ and $B_i$ are constants whose explicit dependence on the coefficients $E_i$ we need not write down. The most significant feature of equation (5) is the absence of a quadratic term. Thus $Q_1$ and $Q_2$ should be asymptotically linear in $Z$. Figure 1 shows that, in fact, they are.

Do any other features of the experimental curves $Q_1$ and $Q_2$ admit a simple theoretical explanation? The asymptotic slope of the curve $Q_i$ is given by the coefficient $A_i$, which, in turn, depends only on coefficients $E_2$ and $E_1$ in the expansions of the term energies concerned. But $E_2$ is given explicitly by equation (4), and the writer has shown elsewhere (Layzer 1955) that, to calculate $E_1$ for a particular term, one need take into account the effects of configuration mixing for only a finite (and usually small) number of configurations. Using a variational technique, the writer has calculated $E_1$ for the terms of the configurations $1s^22s^2$ and $1s^22p^2$ (Layzer 1951). The same technique should apply to other configurations as well. In principle, then, one can accurately predict the coefficient $A_i$ and hence the asymptotic slope of the curve $Q_i$.

But to predict the shapes of the curves $Q_1$ and $Q_2$ for small values of $Z - N$, one needs to know the coefficients $E_i$ ($i \leq 0$) for the terms concerned. The task of evaluating these coefficients differs qualitatively from that of evaluating $E_1$, since the effects of configuration mixing for infinitely many configurations must be taken into account. This fact suggests that the small numerical values of $Q_1$ for small values of $Z - N$ and the remarkably linear variation of $Q_2$ with $Z$ for small values of $Z - N$ have no simple theoretical interpretation. They merely reflect accidental numerical coincidences.

I am indebted to Professor Fritz Rohrlich for calling my attention to the paper by Catalan, Rohrlich, and Shenstone and for helpful comments on an earlier version of the present note.

DAVID LAYZER

HARVARD COLLEGE OBSERVATORY

REFERENCES

Catalan, M. A., Rohrlich, F., and Shenstone, A. G. 1954, *Proc. R. Soc. London*, *A*, **221**, 421.
Layzer, D. 1951, *A.J.*, **56**, 43.
———. 1955, *M.N.* (in press).

## ON THE COLORS OF SUBDWARFS

The main spectroscopic difference observed between subdwarfs and dwarfs consists in the fact that, for a given absolute magnitude, the subdwarfs have an earlier spectral type and bluer color than the ordinary dwarfs. This difference is presumably caused in part by actual differences in the stellar radii (i.e., in the effective temperature) and in part by modifications in the atmospheric radiation arising from the large differences in

chemical composition. In discussing the relative importance of these effects, it seems best to use observed colors rather than spectral types, since the latter appear greatly affected by differences in chemical composition in a manner which does not easily lend itself to analysis. However, even the color is not a pure function of the effective temperature; owing to low metal abundances, the subdwarfs have absorption lines generally much weaker than those of the dwarfs, and, since the absorption lines are more crowded in the blue than in the yellow, this atmospheric difference causes a subdwarf to be bluer than a dwarf of the same effective temperature. It is the purpose of this note to derive a first rough estimate of this atmospheric effect on the colors of subdwarfs.

In 1954, spectrograms for the three stars listed in Table 1 were obtained with the 100-inch coudé spectrograph,[1] one spectrum each for the F0 dwarf and the G0 subdwarf and

TABLE 1

DATA OF THREE PROGRAM STARS

| Star | Sp. | Population | $\alpha(1950)$ | $\delta(1950)$ | $m_{pv}$ | $\pi$ | $M_{pv}$ |
|---|---|---|---|---|---|---|---|
| HD 58946..... | F0 | Dwarf | $7^h\,26^m$ | $31°\,53'$ | 4.16 | $+0.059\pm0.006$ | 3.01 |
| HD 13974..... | G0 | Dwarf | 2 14 | 34 01 | 4.87 | $+ .090\pm .005$ | 4.64 |
| HD 64090..... | G0 | Subdwarf | 7 50 | 30 46 | 8.25 | $+0.042\pm0.006$ | 6.37 |

TABLE 2

RESULTS FOR BLANKETING FRACTION, $\epsilon_\lambda$

| λ REGION | HD | | | λ REGION | HD | | |
|---|---|---|---|---|---|---|---|
| | 58946 | 13974 | 64090 | | 58946 | 13974 | 64090 |
| 3850–3900.... | 0.15 | 0.23 | 0.15 | 4400–4450.... | 0.05 | 0.10 | 0.05 |
| 3900–3950.... | .17 | .32 | .28 | 4450–4500.... | .07 | .10 | .03 |
| 3950–4000.... | .21 | .26 | .21 | 4500–4550.... | .05 | .06 | .03 |
| 4000–4050.... | .04 | .12 | .09 | 4550–4600.... | .05 | .08 | .03 |
| 4050–4100.... | .11 | .14 | .08 | 4600–4650.... | .03 | .07 | .01 |
| 4100–4150.... | .14 | .14 | .10 | 4650–4700.... | .02 | .06 | .01 |
| 4150–4200.... | .06 | .12 | .07 | 4700–4750.... | .02 | .05 | .02 |
| 4200–4250.... | .05 | .14 | .11 | 4750–4800.... | .03 | .06 | .02 |
| 4250–4300.... | .05 | .18 | .16 | 4800–4850.... | .04 | .05 | .02 |
| 4300–4350.... | .19 | .22 | .19 | 4850–4900.... | 0.14 | 0.12 | 0.07 |
| 4350–4400.... | 0.07 | 0.13 | 0.11 | | | | |

two spectra for the G0 dwarf. These spectrograms had a dispersion of 10 A per millimeter and covered well the region from λ 3850 to λ 4900. The spectra were registered on the direct-intensity microphotometer of the Mount Wilson Observatory, and highly smoothed continua were drawn through the peaks of the registration-curves. The tracings were divided into 21 wave-length regions, each 50 A long. The blanketing fraction, $\epsilon_\lambda$, was determined for each wave-length region of each tracing, by planimetering the area cut out from the continuum by the absorption lines and by dividing this area by the total area under the continuum. The results are given in Table 2. Here the column for the G0 dwarf represents the means of the two spectra for this star. By comparing these two spectra, it was estimated that the probable error of the blanketing fraction determined for a 50 A region on one plate is approximately $\pm0.008$.

[1] These plates were obtained by L. Spitzer as guest investigator at the Mount Wilson and Palomar Observatories.

To describe the effect which blanketing has on the observed photoelectric colors, a weighted mean of the blanketing fractions was used. The blue filter used nowadays for photoelectric color measurements covers just about the same wave-length range as the data given in Table 2. The weighted mean for the blue, $\bar{\epsilon}_B$, was therefore obtained by weighting the $\epsilon_\lambda$'s of Table 2 with both the sensitivity function of the photoelectric measurements (Johnson 1951) and the Planck function for 6000°, which may roughly represent the stellar energy function. The resulting mean blanketing fractions were converted into magnitudes by

$$\Delta B = 2.5 \log (1 - \bar{\epsilon}_B)$$

and are given in this form in the second column of Table 3.

The same procedure could not be employed for obtaining mean blanketing fractions for the yellow, since spectrograms covering the yellow wave-length range were not available. Instead, estimates for the yellow were obtained as follows. Wempe (1937) has determined the blanketing fraction for the sun over a wide wave-length region, including the blue and the yellow. From his data (Michard 1950) the mean blanketing fraction for the blue and for the yellow was derived, weighted as before. The results, converted into magnitudes, are given in the last line of Table 3. It was then assumed that the ratio of the blanketing fraction in the yellow to that in the blue as obtained for the sun could be applied to the three program stars. Under this assumption, the yellow blanketing correction, $\Delta V$, could be computed for each star from the measured blue blanketing correction, $\Delta B$. The results are given in parentheses in the third column of Table 3; they are believed to be of sufficient accuracy for the present purpose, since the yellow blanketing corrections must be much smaller than the blue ones.

TABLE 3

BLANKETING CORRECTIONS FOR MAGNITUDES AND COLORS

| Star | $\Delta B$ | $\Delta V$ | $\Delta C$ | $C_{obs}$ | $C_{cont}$ |
|---|---|---|---|---|---|
| F0 dwarf | −0.085 | −0.028 | −0.06 | 0.31 | 0.25 |
| G0 dwarf | − .145 | − .045 | − .10 | .61 | .51 |
| G0 subdwarf | − .092 | − .028 | − .06 | .61 | .55 |
| G2 sun | − .245 (−0.190) | −0.072 | − .17 (−0.12) | 0.64 | .47 (0.52) |

The difference between the blue and the yellow blanketing corrections, then, gives the blanketing correction for the color, $\Delta C$, which is listed in the fourth column of Table 3. This column shows that the color correction for the three ordinary dwarfs increases continuously with advancing spectral type but that the subdwarf has too small a color correction for its spectral type—as was to be expected from the extraordinary weakness of the absorption lines in subdwarfs.

The actual colors of the three program stars were measured with the photoelectric photometer on the 60-inch telescope of the Mount Wilson Observatory by Dr. Arp, to whom we are most grateful. The results are given in the fifth column of Table 3. The color of the sun was taken from the data by Johnson and Morgan (1953) for G2 dwarfs. When these observed colors are corrected for the blanketing effect, $\Delta C$, one obtains the continuum colors, $C_{cont}$, which are given in the last column of Table 3. Comparing, first, the continuum colors of the three ordinary dwarfs, one finds that the continuum color of the sun is bluer than that of the G0 dwarf. This is obvioulsy an erroneous result, which is probably caused by the fact that the solar data are based on spectra of much higher quality than those of the three other stars; the continuum was very likely drawn too low in the tracings of these three stars. To make the solar data comparable with the stellar data, it was estimated that, for the present purpose, the solar continuum should

be lowered by about 5 per cent. The resulting values for the sun are given in parentheses at the bottom of Table 3 (the corresponding corrections in the yellow were estimated to be too small to be of interest). The continuum colors of the three ordinary dwarfs now present a proper sequence, and so do their $\Delta C$ values.

Comparing next the subdwarf with the ordinary dwarfs, one finds from the continuum colors that the subdwarf is certainly no hotter than the sun and is perhaps cooler. With this in mind, we may compare the $\Delta C$ value of the subdwarf with that of an ordinary dwarf somewhat cooler than the sun. Thus one finds that the blanketing correction for the color of the subdwarf is, in absolute amount, at least 0.06, and actually probably about 0.08 mag., smaller than that of an ordinary dwarf with the same effective temperature. We conclude that the color index of a subdwarf should be increased by 0.08—with an uncertainty of perhaps $\pm 0.03$—to make it equal to the color index of an ordinary dwarf of equal effective temperature.

The observed colors and magnitudes indicate that, on the average, the subdwarfs lie 1.5 mag. below the ordinary main sequence (Roman, as quoted by Reiz 1954). If the colors of the subdwarfs are corrected by the differential blanketing effect discussed here, the subdwarfs are moved closer in the Hertzsprung-Russell diagram to the ordinary main sequence and are found—accepting the foregoing estimate of the magnitude of the correction—to lie only about 1 mag. below the main sequence. This corrected position in the Hertzsprung-Russell diagram can be explained according to a recent investigation by Reiz (1954) by the assumption that the subdwarfs differ from the ordinary dwarfs—not in the helium content, but only in having, in contrast to the ordinary dwarfs, a negligible abundance of the heavier elements. (The uncorrected position could have been explained by a helium content of about 30 per cent for the subdwarfs, which would appear rather high for population II stars.) One may then conclude that the total observed difference in position in the Hertzsprung-Russell diagram between dwarfs and subdwarfs is produced by one cause, namely, a great difference in the abundance of the heavier elements, but that this one cause affects the observed colors in two ways: first, through the strength of the atmospheric absorption lines, which produces a difference in the blanketing effect, and, second, through the internal stellar structure, which produces a difference in the actual effective temperature.

This explanation is probably not applicable to all subdwarfs. Those extreme cases, lying much farther below the main sequence than the normal subdwarfs, may well be an entirely distinct class of stars. While the average subdwarfs appear to be ordinary dwarfs modified by low abundance of heavy elements and may as yet have used very little of their total stock of nuclear fuel, the extreme subdwarfs may possibly be stars which have exhausted most of their nuclear fuel and which are now on their way to the white dwarf stage.

We must emphasize the tentative character of the present investigation. To settle the questions here discussed, a more extensive program would be needed, including a larger number of stars, a larger wave-length region, and a theoretical investigation of the effects which differences in blanketing produce on the continuum colors.

M. Schwarzschild
L. Searle
R. Howard

Princeton University Observatory

REFERENCES

Johnson, H. L. 1951, *Ap. J.*, **114**, 523.
Johnson, H. L., and Morgan, W. W. 1953, *Ap. J.*, **117**, 313.
Michard, R. 1950, *B.A.N.*, **11**, 228.
Reiz, A. 1954, *Ap. J.*, **120**, 351.
Wempe, J. 1947, *A.N.*, **275**, 97.

## ON THE DETERMINATION OF THE MASS OF A SPHERICALLY SYMMETRIC CLUSTER

The exact formula for the determination of the total mass of a statistically steady, spherically symmetric cluster (Schwarzschild 1954) involves the use of a continuous function giving the number of stars counted in strips of unit width. When the cluster in case is poor in members, the determination of such a function is not very easy, however, and the following approximation may prove to be useful in such cases.

We consider the distribution of the $n(n-1)$ mutual distances (each counted twice) of the $n$ stars. We shall regard them as vectors from a common origin. According to the assumption of spherical symmetry, the distribution of their end-points will also be spherically symmetric, and a general consideration leads to a three-dimensional Gaussian distribution of them as a first approximation, because the distribution function in each rectangular co-ordinate arises in much the same way as does the distribution of accidental errors from the combinations of terms (in this case two only) of random sign. The distribution of the lengths of the distances is then approximated by the following function:

$$\phi(\rho)\, d\rho = \frac{1}{\sigma^3}\left(\frac{2}{\pi}\right)^{1/2} \rho^2 e^{-\rho^2/2\sigma^2} d\rho\,, \tag{1}$$

where we have normalized the total probability to be equal to 1.

In the relation

$$2T = -\Omega \tag{2}$$

we now express $-\Omega$ by the parameter $\sigma$:

$$-\Omega = Gm^2 \Sigma \rho_{ij}^{-1} = Gm^2 \frac{n(n-1)}{2} \frac{1}{\sigma^3}\left(\frac{2}{\pi}\right)^{1/2} \int_0^\infty \rho\, e^{-\rho^2/2\sigma^2} d\rho = \frac{Gm^2 n(n-1)}{\sigma (2\pi)^{1/2}}. \tag{3}$$

Then we express $\sigma$ by the mean-square distance of the stars from the center of gravity by Lagrange's identity,

$$\Sigma r_i^2 = \frac{1}{n} \Sigma \rho_{ij}^2\,, \tag{4}$$

that is,

$$n\langle r^2 \rangle = \frac{1}{n} \frac{n(n-1)}{2} \langle \rho^2 \rangle = \frac{n-1}{\sigma^3 (2\pi)^{1/2}} \int_0^\infty \rho^4 e^{-\rho^2/2\sigma^2} d\rho = \tfrac{3}{2}(n-1)\,\sigma^2. \tag{5}$$

Expressing $-\Omega$ by $\langle r^2 \rangle$, we now find from equation (2)

$$\langle V^2 \rangle = \frac{Gm(n-1)}{\sigma (2\pi)^{1/2}} = \frac{Gm(n-1)}{(2\pi)^{1/2}} \left[\frac{3(n-1)}{2n\langle r^2 \rangle}\right]^{1/2} = \tfrac{1}{2} Gm \left[\frac{3(n-1)^3}{\pi n \langle r^2 \rangle}\right]^{1/2}. \tag{6}$$

If we disregard the difference between $n$ and $n-1$, we find, for the total mass of the cluster,

$$GM = 2\langle V^2 \rangle \left(\frac{\pi}{3} \langle r^2 \rangle\right)^{1/2}. \tag{7}$$

Comparing with the formula (Chandrasekhar 1942)

$$GM = 2\langle V^2 \rangle \langle R \rangle, \tag{8}$$

we find that $\langle R \rangle$ in our approximation is given by $(\langle r^2 \rangle)^{1/2}$, apart from a factor which is very nearly equal to 1.

In formula (7) we may introduce a rectangular co-ordinate $x$ and the radial velocity $V_R$ by the following relations, due to the assumed spherical symmetry:

$$\langle r^2 \rangle = 3\langle x^2 \rangle, \qquad \langle V^2 \rangle = 3\langle V_R^2 \rangle. \tag{9}$$

Formula (6) holds with a comparatively small error, even in the extreme case of two bodies moving in circular orbits. With $n = 2$, we get

$$Gm = \left(\frac{8\pi}{3}\right)^{1/2} V^2 r\,, \tag{10}$$

which is 72.4 per cent of the correct value,

$$Gm = 4V^2 r\,. \tag{11}$$

MOGENS RUDKJØBING

UNIVERSITY OBSERVATORY
COPENHAGEN

REFERENCES

Chandrasekhar, S. 1942, *Principles of Stellar Dynamics* (Chicago: University of Chicago Press), pp. 198–200.
Schwarzschild, M. 1954, *A.J.*, **59**, 273, eqs. (11)–(14).

## ANNOUNCEMENT

### A MANUAL OF STYLE FOR THE *ASTROPHYSICAL JOURNAL*

In order to help authors in preparing manuscripts intended for publication in the *Astrophysical Journal*, a *Manual of Style* has been prepared. A careful study of this *Manual* and a close adherence to its recommendations would contribute toward more rapid editorial processing and publication of the papers submitted.

In the future, it may be necessary to return to the authors for revision manuscripts prepared without regard to the recommendations set forth in the *Manual*.

Copies of the *Manual* can be had by writing to the *Astrophysical Journal*, Yerkes Observatory, Williams Bay, Wisconsin. The cost of single copies is 25 cents; orders for more than ten copies will be charged at the reduced rate of 20 cents a copy. Orders must be accompanied with remittances.

## ERRATA

In *Ap. J.*, Vol. **122**, No. 1, the legends for the figures on pages 172 and 173 should be interchanged.

On page 196, two lines above "Andrew McKellar," *read* 3143.25, *instead of* 2143.25.

# ABSTRACTS OF ASTROPHYSICAL JOURNAL SUPPLEMENT SERIES

Supplement No. 14, Volume II

## STUDIES IN GALACTIC STRUCTURE. II. LUMINOSITY CLASSIFICATION FOR 1270 BLUE GIANT STARS

W. W. MORGAN
Yerkes Observatory

AND

A. D. CODE AND A. E. WHITFORD
Washburn Observatory

A catalogue is given of 1152 early-type stars of high luminosity for which spectra have been obtained at the Yerkes and McDonald Observatories. Accurate two-dimensional types on the revised system of the Yerkes *Spectral Atlas* are listed.

For a number of the same stars, photoelectric colors determined with the Mount Wilson 60-inch and the Washburn 15-inch telescopes are also given.

The observing program was made up from the early-type stars of the *Henry Draper Catalogue* and the list of early-type supergiants of Nassau and Morgan; the latter list has been essentially completely reobserved.

In addition to the above, a catalogue of 118 southern early-type stars which were observed at the Radcliffe and Cape Observatories is given. New photoelectric colors were obtained for 102 of the latter stars.

---

Supplement No. 15, Volume II

## STELLAR SPECTRA IN MILKY WAY REGIONS

## III. A REGION IN CEPHEUS-LACERTA

S. W. MCCUSKEY
Warner and Swasey Observatory

This paper presents the data on stellar spectra, colors, and apparent photographic magnitudes for a Milky Way region of 16.9 square degrees centered at R.A. $22^h22^m$; Dec. $+53°.8$ (1945); $l = 70°$, $b = -3°$. An analysis of the data for galactic structure and for changes in the general stellar luminosity function with distance has been published by McCuskey (1951).

Sectional charts covering the area, designated as LF4, and the catalogue of data contain 4222 stars. Blue-red color indices for 1764 early-type stars are given. All the observations were made with the 24–36-inch Schmidt-type telescope of the Warner and Swasey Observatory.

Four Kodak II*a*-O plates were used for determination of the blue magnitudes, and four Kodak 103*a*-E plates for the red. A Wratten No. 22 filter was used for the latter. Calibration sequences for the magnitudes were established by polar comparison, the

NPS magnitudes (slightly revised) provided by Nassau and Burger (1946) serving as standards for the red magnitudes. A subsequent photoelectric check of the sequence stars indicates that a correction of +0.02 mag. should be made to the catalogue values of $m_{pg}$. The probable error of a final blue magnitude in the case of those stars for which colors are available is ±0.04. For the balance of the blue magnitudes the probable error is ±0.07. The red magnitudes have a probable error of ±0.03, on the average, and hence the color indices have an internal probable error of ±0.05 mag. The photoelectric check mentioned earlier indicates that the catalogued red indices are too blue by 0.01 mag. but are otherwise free of serious systematic error. Details of our photocell equipment and the color system have been published elsewhere (MacRae, Harris, and Rogerson 1952).

The catalogue lists not only the spectral type for all 4222 stars but also the luminosity class for all stars brighter than $m_{pg} = 11.0$ and of spectral class F0 and later. The nomenclature for luminosity class is that of Morgan, Keenan, and Kellman (1943). High-luminosity objects of early type are designated by the class OB, following the work of Nassau and Morgan (1951).

REFERENCES

McCuskey, S. W. 1951, *Ap. J.*, **113**, 672.
MacRae, D. A., Harris, D. L., and Rogerson, J. 1952, *A.J.*, **57**, 19.
Morgan, W. W., Keenan, P. C., and Kellman, E. 1943, *An Atlas of Stellar Spectra* (Chicago: University of Chicago Press).
Nassau, J. J., and Burger, V. 1946, *Ap. J.*, **103**, 25.
Nassau, J. J., and Morgan, W. W. 1951, *Pub. U. Michigan Obs.*, **10**, 43.

---

## STELLAR SPECTRA AND COLORS IN A MILKY WAY REGION IN CASSIOPEIA

ALICE H. FARNSWORTH
John Payson Williston Observatory

This paper is essentially a catalogue of spectral types, apparent photographic magnitudes, and blue-red color indices for a thousand stars brighter than 12.4 mag. photographic in a Milky Way region centered at R.A. $1^h40^m$; Dec. +60°.2 (1945); $l = 97°$, $b = -1°$. The circular field covers 11.3 square degrees. Identification charts for the area, designated LF5, are provided. All stars for which it was possible to determine the spectral type are included.

All the plates were taken with the Schmidt-type 24–36-inch telescope at the Warner and Swasey Observatory of the Case Institute of Technology. Photometric measures were made with a graduated scale of images. Photoelectric magnitudes are listed for a sequence of standard stars which formed the basis for the catalogue. Photographic and red magnitudes were obtained, respectively, from four Kodak IIa-O plates and from four Kodak 103a-E plates used with Wratten No. 22 filter. The average probable error for both red and blue magnitudes is ±0.04.

Spectral types and luminosities were estimated by Dr. J. J. Nassau and the writer on objective-prism plates of 4° dispersion. Comparison of types with *HD* and *HDE* data is shown.

# THE ASTROPHYSICAL JOURNAL

*announces the publication of*

**A GENERAL INDEX, Volumes 76–100**

Price $5.00*

ORDERS NOW ACCEPTED

*Also available:*

GENERAL INDEX, Volumes 1–25 .....$2.50
GENERAL INDEX, Volumes 26–50 .....$2.50
GENERAL INDEX, Volumes 51–75 .....$2.50

* Postage $0.15 per copy extra to foreign addresses.

THE UNIVERSITY OF CHICAGO PRESS
5750 ELLIS AVENUE CHICAGO 37 • ILLINOIS

# THE OBSERVATORY

**FOUNDED 1877**

* * *

A Magazine presenting current developments in Astronomy by means of Articles, Correspondence, Notes on discoveries and Reviews of important astronomical books. The papers read at the Meetings (Astronomical & Geophysical) of the Royal Astronomical Spciety and the discussions which follow are also fully reported.

* * *

*Annual subscription for 6 issues, post free, £1 (U.S.A. and Canada, $3.00) should be sent to*

*The Editors,* ROYAL GREENWICH OBSERVATORY
Herstmonceux Castle, Hailsham, Sussex, England

# THE ASTROPHYSICAL JOURNAL SUPPLEMENT SERIES

These *Supplements* are intended to provide a medium for the publication of extensive investigations, such as wave-length lists of stars of special interest, photometric data, results of numerical integrations pertaining to stellar interiors, model stellar atmosphere calculations, and original memoirs. The following twelve *Supplements* are in Volume I.

1. "Chromospheric Structure of the K-type Component of Zeta Aurigae." O. C. Wilson and Helmut A. Abt. $1.25
2. "Spectroscopic Observations of Mira Ceti, 1934–1952." Alfred H. Joy. $1.25
3. "An Analysis of W Virginis." Helmut A. Abt. $1.25
4. "Photometric Investigation of the Eclipsing Binary UX Ursae Majoris." H. L. Johnson, Barbara Perkins, and W. A. Hiltner. $1.25
5. "On Nuclear Reactions Occurring in Very Hot Stars. I. The Synthesis of Elements from Carbon to Nickel." F. Hoyle. $1.25
6. "On the Dissipation of Gas and Volatilized Elements from Protoplanets." Harold C. Urey. $1.25
7. "Catalogue and Bibliography of Emission-Line Stars of Types Later than B." William P. Bidelman. $3.00
8. "The Index of Clumpiness of the Distribution of Images of Galaxies." Jerzy Neyman, Elizabeth L. Scott, and C. D. Shane. $1.25
9. "The Spectrum of the *CN* Molecule." A. E. Douglas and P. M. Routly. $1.25
10. "Numerical Integrations for the Stellar Interior." R. Härm and M. Schwarzschild. $2.50
11. "An Analysis of the Magnetic Variable $\alpha^2$ Canum Venaticorum." G. R. Burbidge and E. Margaret Burbidge. $1.25
12. "The Thermodynamic Structure of the Outer Solar Atmosphere. III, IV, V." Satoshi Matsushima; R. G. Athay and R. N. Thomas; R. G. Athay, D. H. Menzel, J-C. Pecker, and R. N. Thomas. $1.25

An abstract of each supplement is published in THE ASTROPHYSICAL JOURNAL. The *Supplements* appear irregularly, and may be purchased separately or by subscription. Each volume of *Supplements* will consist of approximately 500 pages.

*Subscriptions*

$8.00 per volume
Canada, $8.75. Foreign, $9.50.
To members of the American Astronomical Society, $6.00 per volume.

THE UNIVERSITY OF CHICAGO PRESS

5750 ELLIS AVENUE CHICAGO 37, ILLINOIS